CHARACTERIZATION OF EARLY CD8 T CELL RESPONSES AFTER BYSTANDER AND ANTIGEN-SPECIFIC ACTIVATION

by

Namit Sunil Holay

Submitted in partial fulfilment of the requirements
for the degree of Doctor of Philosophy

at

Dalhousie University
Halifax, Nova Scotia
November 2022

Dalhousie University is located in Mi'kma'ki, the
ancestral and unceded territory of the Mi'kmaq.
We are all Treaty people.

For Dada who lit the fire of curiosity and never had the opportunity to go to school.

For mummy, pappa, and aaji who inspired me to keep on going, come what may, and make my work into an offering.

For my guru who has been a burning light helping me see that one may acquire knowledge but “knowing” is of a different nature.

Shiva Shambho

TABLE OF CONTENTS

LIST OF TABLES

LIST OF FIGURES

ABSTRACT

In light of the recent COVID-19 pandemic, it has become imperative to understand how CD8 T cells, an important line of defense in the adaptive immune system, are activated in response to virus infections and other diseases. Although past work informs our understanding about the biology of CD8 T cell response at the later stages of the adaptive immunity (usually 5-7 days post initiation), only scanty information is available about the events that shape CD8 T cell activation during the early time points (0-3 days post initiation). To address this knowledge gap, this study investigated the early events that characterize CD8 T cell activation. In the first part of this work, we focused on bystander activation of CD8 T cells. Here, we studied how naïve CD8 T cells are activated in a bystander manner within 24 hours of exposure to virus. We elucidated the role of type 1 interferons and STAT1 in this bystander activation of naïve CD8 T cells and further demonstrated that metabolic reprogramming occurs in these cells at this early time point. We additionally discovered a role for NAD+ salvage metabolism in the bystander induction of naïve CD8 T cells. This study provided novel insight into the early events that impact the biology of naïve CD8 T cells after virus exposure and will serve to guide better development of anti-viral treatments and vaccines that rely on effective CD8 T cell activation.

In the second part of this study, we focused on a poorly characterized CD8 T cell subset identified as CD44lowCD62Llow CD8 T cells. We first discovered that CD44lowCD62Llow CD8 T cells are induced as early as 1 hour after antigen-specific stimulation. We demonstrated that the CD44lowCD62Llow CD8 T cells were capable of functional activity via IFN-γ production as early as 6 hours after stimulation and that type 1 interferons drove increased functional capacity of these cells. Further, we revealed that these early CD44lowCD62Llow CD8 T cells were metabolically unique when compared to the other naïve, effector and memory CD8 T cell subsets. Our analyses uncovered a role for aminoacyl tRNA biosynthesis in the metabolism of CD44lowCD62Llow T cells and overall, our studies support the model that naïve CD8 T cells differentiate to this unique phenotype-CD44lowCD62Llow-a transition state induced prior to effector or memory differentiation. This previously unreported, very early differentiation event provides invaluable insight into antigen-driven early CD8 T cell activation and will be critical for future studies aiming to study/harness CD8 T cells for treatment across multiple disease areas.

LIST OF ABBREVIATIONS AND SYMBOLS USED

α- alpha

β- beta

γ- gamma

κ- kappa

ACK- Ammonium chloride

APC- Antigen-presenting cell

ATP- Adenosine triphosphate

BCR- B cell receptor

CPT1A- Carnitine palmitoyltransferase 1A

cDC- Conventional Dendritic Cell

CoA- Coenzyme A

ConA- Concanavalin A

DC- Dendritic cell

DHAP- Dihydroxyacetone phosphate

EAE- Experimental allergic encephalomyelitis

EBV- Epstein Barr virus

FAD- Flavin Adenine Dinucleotide

FAO- Fatty acid oxidation

FAS- Fatty acid synthesis

FBS- Fetal bovine serum

GA3P: Glyceraldehyde 3-phosphate

GEF- Guanine nucleotide exchange factor

GVHD- Graft versus host disease

HAV- Hepatitis A virus

HILIC- Hydrophilic interaction liquid chromatography

HIV- Human immunodeficiency virus

IKK- IκB kinase

IL-2- Interleukin-2

IL-7- Interleukin-7

IL-15- Interleukin- 15

IL-15- Interleukin-15

IL-18- Interleukin-18

ILIS- Isotopically labeled internal standard

IFN-γ- interferon gamma

IFNAR- Interferon-α/β receptor

IRF- Interferon regulatory factors

ISGF3- Interferon-stimulated gene factor 3

ISG- Interferon-stimulated genes

ISVP- Infectious subvirion particle

JAK1- Janus kinase 1

JMEM- Joklik modified minimum essential media

KEGG- Kyoto Encyclopedia of Genes and Genomes

KI- Knock-in

KO- Knock-out

KG- ketoglutarate

LPS- Lipopolysaccharides

MAPK- mitogen-activated protein kinase

MBL- Mannose-binding lectin

MDA-5- melanoma differentiation-associated protein 5

MEM- Minimum essential media

MeV- MultiExperiment Viewer

MHC- Major Histocompatibility Complex

MPEC- Memory precursor effector cell

MSK1/2- Mitogen and stress-induced kinase

mTOR- mammalian target of rapamycin

NA- Nicotinic acid

NAD- Nicotinamide adenine dinucleotide

NADH: reduced nicotinamide adenine dinucleotide

NAR- niacinamide

NF-kB- Nuclear factor kappa B

NK- Natural killer

NLRs- NOD-like receptors

NMN- Nicotinamide mononucleotide

OAA- Oxaloacetate

P- Phosphate

PAMPs- Pathogen-associated molecular patterns

pDC- Plasmacytoid Dendritic Cell

PBS- Phosphate-buffered saline

Pfu- Plaque forming units

PI3K- Phosphoinositide 3-kinase

PRR- Pattern Recognition Receptors

Rac1- Ras-related C3 botulinum toxin substrate 1

RBC- Red blood cell

RIG-I- retinoic acid-inducible gene-I

ROS- Reactive oxygen species

SLEC- Short-lived effector cell

STAT- Signal transducers and activators of the transcription

Suc- Succinyl

T_N- Naïve T cell

T_{EM}- Effector memory T cell

T_{CM}- Central memory T cell

T_{SCM}- Stem cell memory T cell

T_{EFF}- Effector T cell

TCA- Tricarboxylic acid cycle

TCR- T cell receptor

TLR – Toll-like receptors

TSCM- Stem cell memory T cell

TEFF- Effector T cell

TYK2- Tyrosine kinase 2

UMAP- Uniform Manifold Approximation and Projection

ACKNOWLEDGEMENTS

This work would not have been possible without the collective support of many people. First, I would like to thank my Ph.D. supervisor, Dr. Shashi Gujar, who accepted me into the program and allowed me to pursue my curiosity to the fullest. Thank you for teaching me valuable lessons over the years including the importance of organization and of time. I will carry these lessons with me wherever I go.

Next, I would like to thank my parents- Chhaya and Sunil Holay. They have always supported me no matter what I have chosen to do in my life. Moving across the world to pursue a Ph.D. was a no different matter. My grandmother, aaji- Sushila Harishchandra Holay- is a constant source of inspiration in my life. My sister, Neha Bhongale, has been with me through thick and thin every step of the way. Satyan Bhongale, thank you for your encouragement, advice and inspiration on this road to becoming a scientist. A big thank you to my extended family- the Raskar and Yadav families- for their support over all these years. I feel blessed to be born into a family that has always supported me in everything I have done and gone beyond their means to ensure I always have a conducive atmosphere to grow and prosper.

I would also like to extend sincere thanks to my committee- Dr. Jean Marshall, Dr. Carman Giacomantonio, and Dr. Beata Derfalvi. They have been there to support me in this graduate school journey along every step. A special thank you to Dr. Jean Marshall for going out of her way to help me when I was struggling, for providing guidance, for sharing her enormous experience with me, and for helping me find a way forward when there seemed to be none. I would not be where I am today without your continued guidance and support and for that, I am eternally grateful.

The work that I have done over the past 7 years in this lab would not be possible without an enormous team of people who have helped me along the way. I am so grateful to have come across every one of them and feel lucky to be able to call them my friends. Dr. Yura Kim, thank you for training me when I first joined the lab, and thank you for your friendship over the years. Dr. Prathyusha Konda, we started in the lab together, learned together and your friendship has meant a lot to me. Vishnu, thank you for all the help you have provided over the last couple of years, and it has been very enriching working with you. Dr. Derek

Clements, thank you for teaching me about mouse work and immunology, Dr. Barry Kennedy, thank you for introducing me to metabolism, always being there to bounce ideas off, and for being a great friend inside and outside the lab. Dr. Patrick Murphy and Michael Giacomantonio, thank you for all your help with proteomics and metabolomics and for creating a fun environment in the lab to be in. Dr. Gopal Pathak, your support and guidance have meant a lot to me over the years. Mariam Elaghil- thank you for your help with the experiments you conducted while you were here.

I also wish to thank our collaborators- Joao Paulo and Steve Gygi at Harvard University- for running the proteomics experiment, and Gary Sisson as well as Chris Richardson at CCfV for all their help with mouse work.

A big thank you to Derek Rowter, Renee Raudonis, and Tatjana Brauer-Chapin with whom I have spent a lot of time learning and performing flow cytometry over the years. Tatjana, thank you for taking the time to help out with data analysis and visualization of data.

This work would not be possible without all the lovely staff in animal care. A big thank you to you all.

Next, I would also like to acknowledge Karen Bedard and Eileen Donavan Wright for their support over the years during the testing times of the program.

I could not be where I am today without incredible support outside the lab. A big thank you to all my friends for being an incredible support system over the years. Andra Sterea and Moamen Bydoun, discussions about lab, science, and life with you over the years are something that I cherish deeply. George Woodhouse and Sherise Jones, thank you for your incredible friendship and support over these years. To the many other friends that I have lived with (Steve, Charlotte, Mark, and Joss) or have met in Halifax after I moved here, thank you for your patience, encouragement, and support over the years.

A big thank you to Denise and Fred Cox and the Cox family who have treated me like family and have been so supportive in helping me cross the finish line on this long journey. Finally, Autumn Cox, thank you for your incredible support. Your patience, kindness, and support have meant the world to me.

Chapter 1. Introduction

The immune system plays an important role in our bodies by protecting us from external and internal challenges. For example, it protects us from infectious agents such as bacteria, viruses, protozoa, and parasites. It also protects us from diseases like cancer that can arise spontaneously within the body. The immune system also interacts with commensal microorganisms that are non-pathogenic and co-exist with other cells in the human body (Wiertsema et al., 2021). These interactions allow our immune system to become tolerant to the indigenous microbiome (Yoo et al., 2020). Together, this complex interplay between immune cells, microorganisms, and non-immune cells allows the immune system to mount an appropriate immune response.

Dysregulation of the immune system is at the core of most diseases in the human body. In the case of external infections and internal threats like cancer, if a robust immune response is not induced it can lead to life-threatening disease (Fridman et al., 2017; Oshi et al., 2022). This phenomenon is quite evident in the recent SARS-Cov2 pandemic, wherein many individuals are asymptomatic or have mild disease, and some have severe, life-threatening disease based on the individuals' capacities to mount an immune response to the virus (Blanco-Melo et al., 2020; Lewis et al., 2021; Merad et al., 2022). On the other hand, autoimmune diseases like lupus, type 1 diabetes, and others occur due to the overactivity of the immune system against the body's cells. Treatments for such conditions involve strategically subduing the immune response to protect the body from itself (Burt et al., 1998). Hence, regulation of immunity is at the core of health and well-being. Several factors determine whether an individual will induce an appropriate immune response to the

threat, including age, sex, diet, genetics, and lifestyle (Zimmermann and Curtis, 2019). To better understand how the immune system works in health and disease, it is essential first to understand the two parts of the immune system- innate and adaptive immunity.

1.1. Innate Immunity

The innate arm of the immune system is the first line of defense and is responsible for the early recognition and elimination of pathogens. It consists of anatomical barriers like the skin and mucous membranes, chemical barriers like stomach acid and antimicrobial peptides, and cellular components of the myeloid and lymphoid lineages which are discussed in detail below.

1.1.1. Cellular components of innate immunity

Innate cells of the myeloid lineage, like macrophages, dendritic cells, and granulocytes, are phagocytic in nature and serve to internalize and degrade pathogens. Monocytes are immature macrophages that circulate in the blood and can migrate into tissues where they differentiate into specialized macrophages like microglial cells in the brain and alveolar macrophages in the lungs (Coillard and Segura, 2019). Macrophages perform various roles in the immune system, primarily as phagocytic cells, but also function in inducing inflammation by producing cytokines, recruiting other cells to the site of infection, and acting as scavengers to clear dead cells and cellular debris (Gordon and Martinez-Pomares, 2017). Further, depending on the pathogen and the inflammatory response induced, macrophages can be polarized to have pro-inflammatory functions or anti-inflammatory roles and exist on a spectrum (Murray, 2017).

Dendritic cells (DCs) are another type of phagocytic cell that plays a crucial role in the functioning of the innate immune system. They continually take in a large amount of

extracellular fluid via macropinocytosis. Pathogens taken up by the cells are degraded leading to the generation of antigens. Antigens derived from different parts of the pathogen are displayed by DCs on their cellular surface via major histocompatibility molecules (MHC). These are recognized by T cells and lead to T cell activation (discussed later). Consequently, this leads to the activation of the adaptive arm of the immune response (Howard et al., 2004). For this reason, dendritic cells are known as professional antigen-presenting cells (APCs). Antigen presentation typically occurs via two different pathways-presentation via MHC class I or class II molecules. Cytosolic peptides derived from intracellular pathogens or cell proteins are presented via the MHC class I pathway. Endocytic peptides typically derived from extracellular sources are presented via MHC class II molecules. A unique antigen presentation pathway that occurs in DCs is cross-presentation wherein antigens derived from extracellular sources may be presented via the MHC class I pathway. This pathway is important for the presentation of antigens derived from the lysis of virus infected cells or cancer cells for example. Dendritic cells can also be of various types (Patente et al., 2019). Conventional dendritic cells (cDCs) present antigens to T cells and are responsible for producing cytokines like Interleukin-2 (IL-2) which regulate cell survival. In contrast, plasmacytoid dendritic cells (pDCs) are important for responses to viruses and produce type 1 interferons which can activate anti-viral immunity. Other types of DCs include migratory DCs that are found in lymphoid organs and can migrate to different tissues.

The final class of phagocytic cells in the innate immune system are the granulocytes which include neutrophils, eosinophils, and basophils. Neutrophils are among the most abundant cells in the innate immune response and are among the earliest responders upon exposure

to a pathogen (Aulakh, 2018). They can take up pathogens by phagocytosis and degrade them in intracellular vesicles with the help of granules and enzymes. Eosinophils and basophils play an important role in host defense against parasites and are also responsible for detrimental allergic responses (Nadif et al., 2013).

Mast cells are essential and versatile players in the innate immune system and are best known for their role in allergy and inflammation (Marshall and Jawdat, 2004). They contain large cytoplasmic granules filled with histamine released upon mast cell activation. Mast cells have important roles in protection against pathogens (Urb and Sheppard, 2012), wound healing (Trabucchi et al., 1988), and immune tolerance (Costela-Ruiz et al., 2018).

Natural killer (NK) cells are cells of the lymphoid lineage that are also regarded as a part of the innate immune system due to their ability to respond to pathogens in a non-specific manner. NK cells can recognize and kill tumor cells and cells infected with viruses or intracellular pathogens (Vivier et al., 2008).

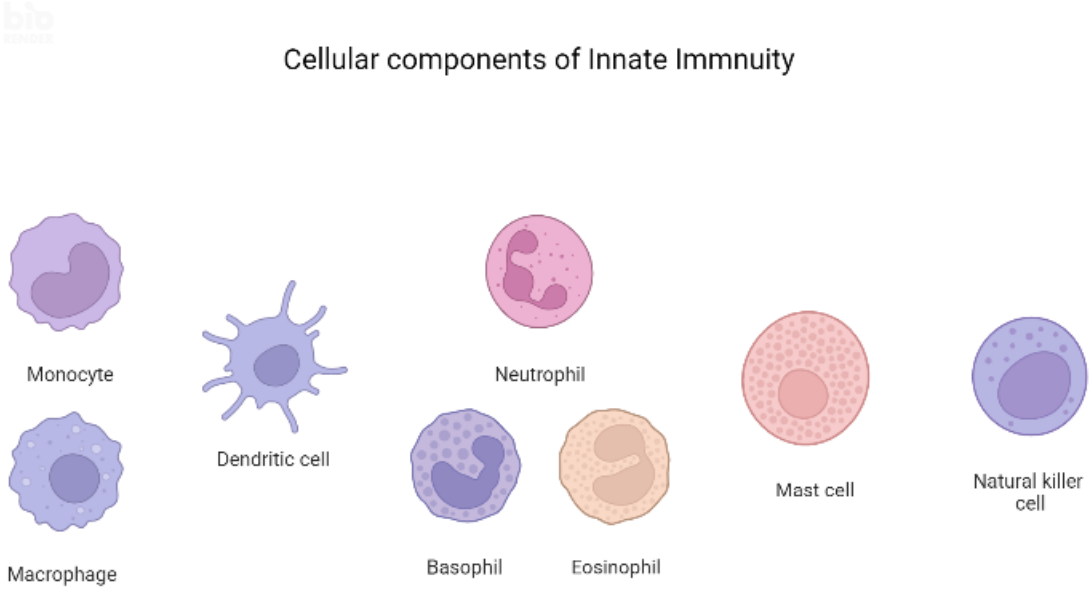

<u>Fig. 1.1:</u> Cellular components of the innate immune system. Phagocytic cells- monocytes, macrophages, dendritic cells, granulocytes (neutrophils, basophils, and eosinophils)- as well as other cells of the innate immune system- mast cells and Natural Killer (NK) cells. Image generated using Biorender.

1.1.2. Molecular sensors of innate immunity

The innate immune system is responsible for early protection upon exposure to pathogens. A key feature of this response is the ability to mount a very rapid immune response (within minutes and hours). If this immune response is not regulated, it can cause immense damage to the healthy cells of the body (Palm and Medzhitov, 2007). An important element that allows for recognizing pathogens upon exposure and initiating the immune response is the presence of highly evolved and conserved molecular pathogens sensors in the innate immune system. These sensors recognize specific elements of pathogens and damaged cells and help initiate molecular signaling networks that lead to inflammation and early regulation of the immune response (Chamy et al., 2008). Collectively, these sensors are known as pattern recognition receptors (PRRs).

PRRs can be free receptors like mannose-binding lectin (MBL) which trigger the complement response of the innate immune system, or they may be membrane-bound or cytoplasmic.

One set of PRRs, first discovered in Drosophila melanogaster, are the Toll-like receptors (TLRs). TLRs can be activated by various pathogen-associated molecular patterns (PAMPs) (Kumar and Barrett, 2022). TLR3, discussed later in this thesis, is activated by double-stranded RNA found in viruses like reovirus. Similarly, single-stranded RNA from viruses like flaviviruses can activate TLR7. TLR9 recognized unmethylated CpG dinucleotides from bacteria and viruses. Other TLRs like TLR4 and TLR5 are important for recognizing PAMPs from bacteria, e.g., Lipopolysaccharides (LPS) and flagellin, respectively. Upon binding, TLR signaling can activate transcription factors like NF-kB and AP-1, which produce pro-inflammatory cytokines (Kawai and Akira, 2007). Another

family of transcription factors activated is the IRF family (Honda and Taniguchi, 2006), which is also discussed later in this thesis. These lead to the production of type 1 interferons, which are important early mediators of anti-viral immunity.

TLRs such as TLR3, 7, and 9 are important for the identification of PAMPs from viruses. However, since they are primarily located in the endosomes within cells, they can only recognize PAMPs from extracellular material that has entered the endocytic pathway. RIG-I-like helicases are another important set of proteins that can recognize viral RNA in the cytoplasm. These include proteins like retinoic acid-inducible gene-I (RIG-I) and melanoma differentiation-associated protein 5 (MDA-5), which can sense uncapped cytoplasmic viral RNA and dsRNA, respectively. This leads to the activation of downstream signaling molecules like MAVS, TRAF6, and TBK1 (Thoresen et al., 2021). The consequence of this recognition and activation is the production of type 1 interferons. Other PRRs, like NOD-like receptors (NLRs) are cytoplasmic sensors responsible for sensing bacterial infections. Most TLRs that recognize bacterial PAMPs are located on the cell surface and serve to identify extracellular bacteria. NLRs are important for the recognition of intracellular bacteria and lead to the activation of the nuclear factor kappa-light-chain-enhancer of activated B cells (NF-κB) pathway and initiation of a pro-inflammatory response (Kim et al., 2016). A summary of molecular sensing of the innate immune system can be found in Fig. 1.2.

Overall, the innate immune system is a critical, early component of the immune system that mounts a rapid response to pathogens. This rapid, non-specific response helps control pathogens and allows time for the adaptive immune response to develop.

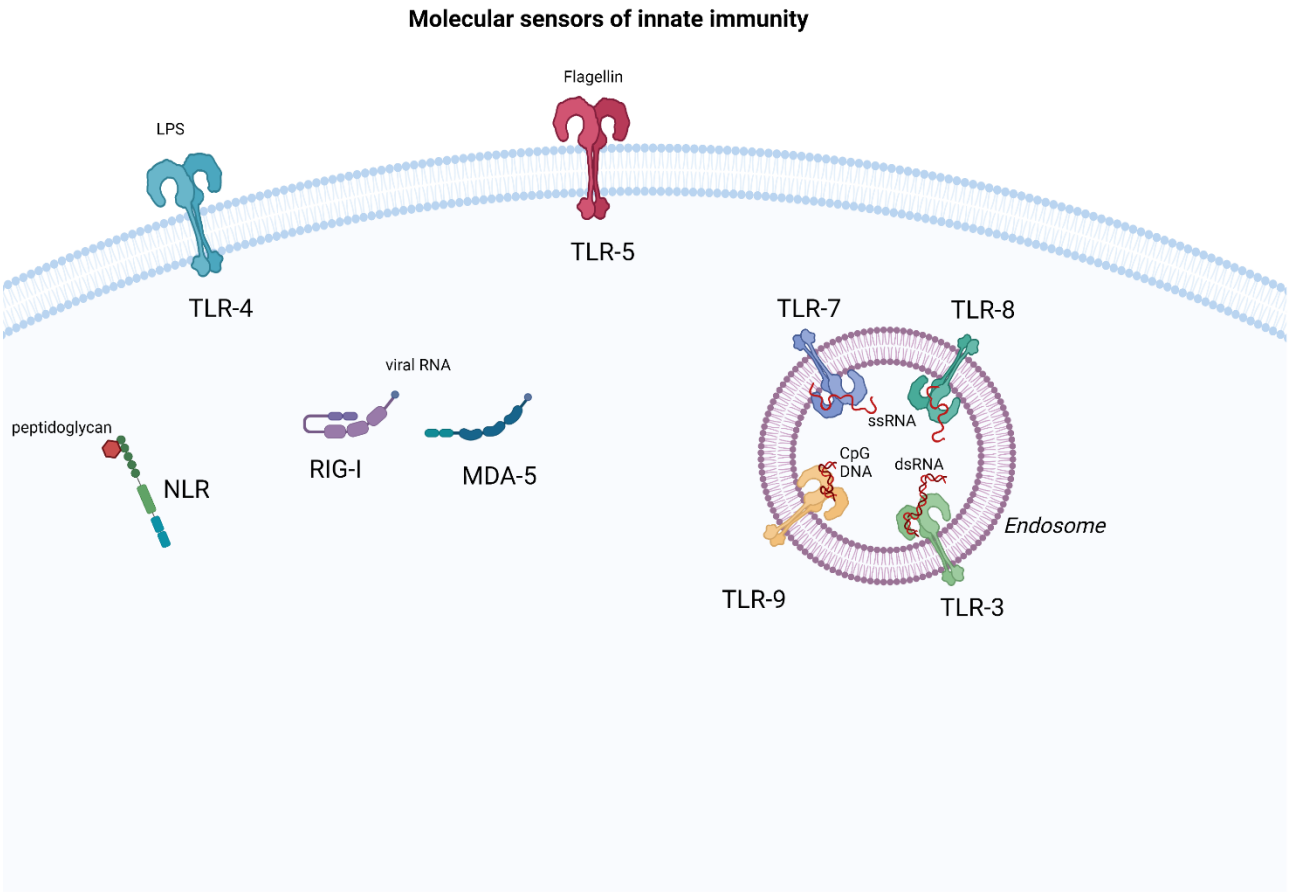

Fig. 1.2: Molecular sensors of innate immunity. Pattern Recognition Receptors including Toll-like receptors (TLR), NOD-like receptors (NLR), retinoic acid-inducible gene- I (RIG-I), and RIG-I-like receptor melanoma differentiation-associated protein 5 (MDA-5). Adapted from "TLR Signaling pathway", by BioRender.com (2022). Retrieved from https://app.biorender.com/biorender-templates.

1.2. Adaptive immunity

The adaptive immune response is the second arm of the immune response. It is characterized by the activation of an antigen-specific immune response that develops slowly over time (days to weeks). The main cells that mediate adaptive immunity are B cells and T cells.

1.2.1 B cells

B cells are important cellular components of the adaptive immune response. They mature in the bone marrow and have B cell receptors (BCR) capable of recognizing antigens. Upon antigen binding by BCRs, B cells are activated and differentiate into plasma cells capable of producing antibodies. Antibodies are soluble forms of the respective membrane-bound BCR that can circulate in plasma and bind free antigens directly. Most B cells require "help" from T cells for further antibody production (Crotty, 2015). B cells can also act as APCs and present antigen to T cells leading to T cell activation.

1.2.2. T cells

T cells are another type of lymphoid cell that mature in the thymus and form an important component of the adaptive immune response. Broadly, they can be of 2 types- CD4 and CD8 T cells. CD4 T cells are commonly known as helper T cells as they provide "help" signals to a myriad of cells, including B cells for antibody production. CD8 T cells are known as cytotoxic T cells because they are primarily responsible for killing virus-infected and tumor cells. It is important to note that these classifications are being updated with recent literature on the discovery of cytotoxic CD4 T cells (Cenerenti et al., 2022) and CD8 T cells with more regulatory functions (Levescot and Cerf-Bensussan, 2022). Since this

thesis focuses on T cell responses to virus exposure, we dive deeper into the biology of T cells.

1.2.2.1 T cell activation

T cell activation requires 3 signals (Fig.1.3). The first signal is provided by peptide-bound MHC molecules present on the surface of APCs. These peptide-MHC complexes are recognized by the T cell receptor (TCR) on the surface of T cells. Recognition of antigen by TCR in conjunction with CD3 leads to activation of downstream TCR signaling and initiates the process of T cell activation (Courtney et al., 2018). T cell signal strength has important consequences for the activation and differentiation of T cells (Shakiba et al., 2022) (discussed later). The next signal required for T cell activation is co-stimulation. Upon activation of APCs, costimulatory molecules like CD80 and CD86 are upregulated on their cell surface. These are recognized by corresponding receptors like CD28 on the surface of T cells and constitute the second signal of T cell activation. Co-stimulation reduces the signal threshold for stimulation, increasing the survival and proliferation of T cells (Pardigon et al., 1998). The next and final signal required for T cell activation is the presence of cytokines. Cytokines like IL-2, Interleukin-7 (IL-7), Interleukin- 15 (IL-15), and type 1 interferons are soluble molecules that bind to corresponding receptors on T cells and provide signal 3 of T cell activation required for enhanced survival, proliferation, or differentiation (Curtsinger and Mescher, 2010).

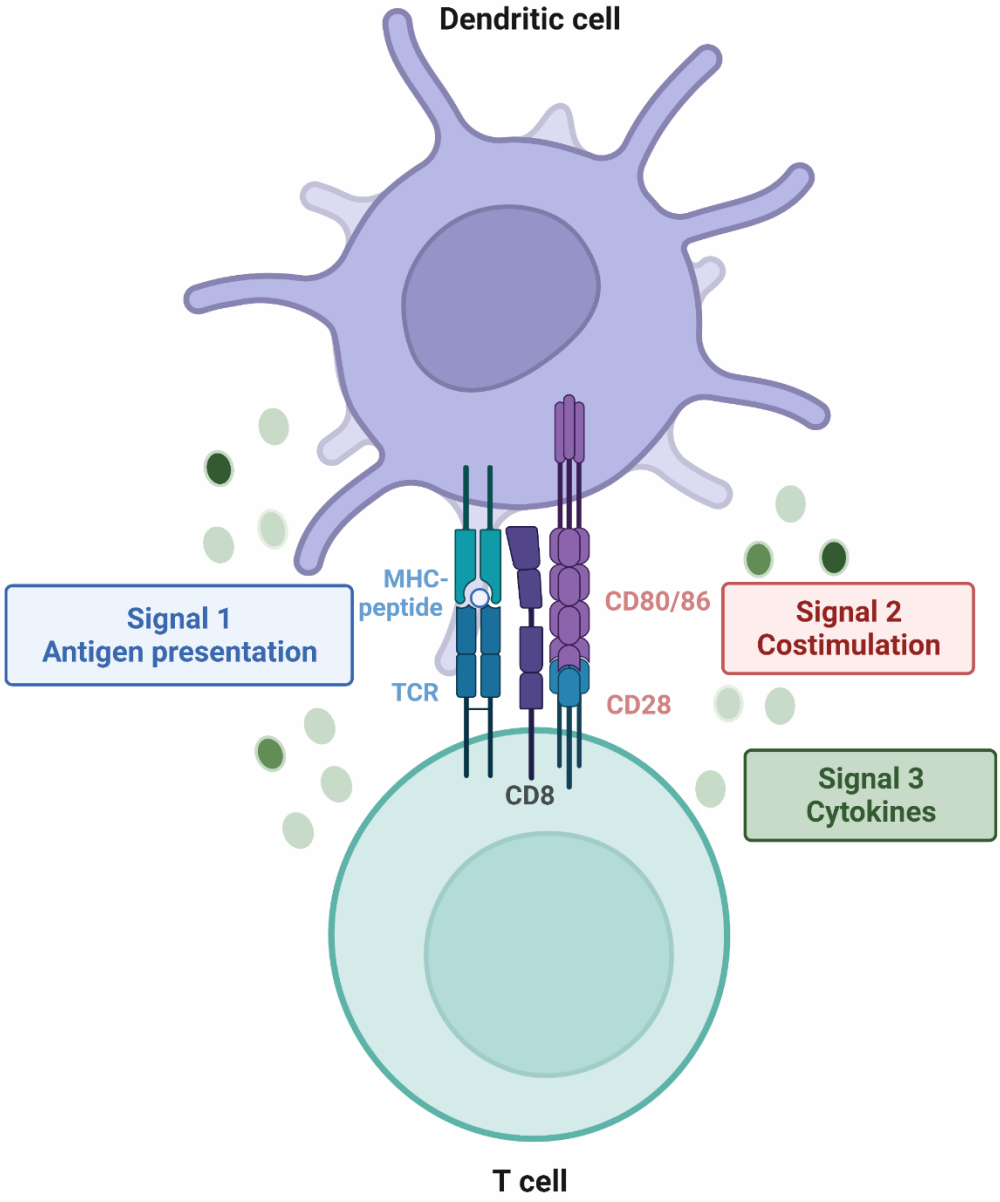

Fig. 1.3: T cell activation. The three signals of T cell activation for a CD8 T cell are depicted above. These include- antigen presentation by an antigen presenting cell (APC), in this case, a dendritic cell, via major histocompatibility (MHC) I molecule to the T cell receptor (TCR), co-stimulatory signals via CD80/CD86 binding to CD28 on the T cell, and cytokines. Created with BioRender.com (2022).

1.3. CD8 T cell responses to virus infection

1.3.1. Phases of T cell response

Before antigen stimulation, T cells exist as naïve T cells (T_N). These are characterized by low expression of CD44 adhesion molecule and high expression of CD62L (CD44lowCD62L+). Upon priming with antigen, T cells can differentiate into effector memory (T_{EM}) and central memory (T_{CM}) T cells (CD44hi) (Kaech et al., 2002). T_{EM} cells are characterized by loss of CD62L expression (CD44hiCD62L-) whereas T_{CM} cells retain CD62L expression (CD44hiCD62L+). T cell responses occur after exposure to viruses in 3 different phases (Fig.4). The first phase is ***clonal expansion***. Upon activation of T cells by APCs, T cells undergo clonal expansion over time to produce a large number of effector T cells (Denizot et al., 1986; Kaech et al., 2002). These effector T cells migrate to the site of infection and are responsible for the direct killing of cells infected with the virus. Upon clearance of the virus, effector T cells undergo a ***contraction phase*** wherein many effector T cells die by apoptosis (Badovinac et al., 2004), and a small percentage of cells remain behind in the final phase of ***memory formation,*** which leads to the generation of long-lived memory T cells that provide long-term protection against reinfection (Omilusik and Goldrath, 2017). Studies thus far have demonstrated that the generation of memory T cells is not random, and effector T cells with different memory potentials exist (Kaech and Cui, 2012). These cells have variable long-term persistence and memory formation capabilities. For example, populations like memory precursor effector cells (MPECs) and short-lived effector cells (SLECs) have been identified within T_{EM} cells with differential persistence (Joshi et al., 2007). MPECs are characterized by increased expression of IL-7R or CD127 and reduced expression of KLRG1, whereas SLECs have the opposite phenotype.

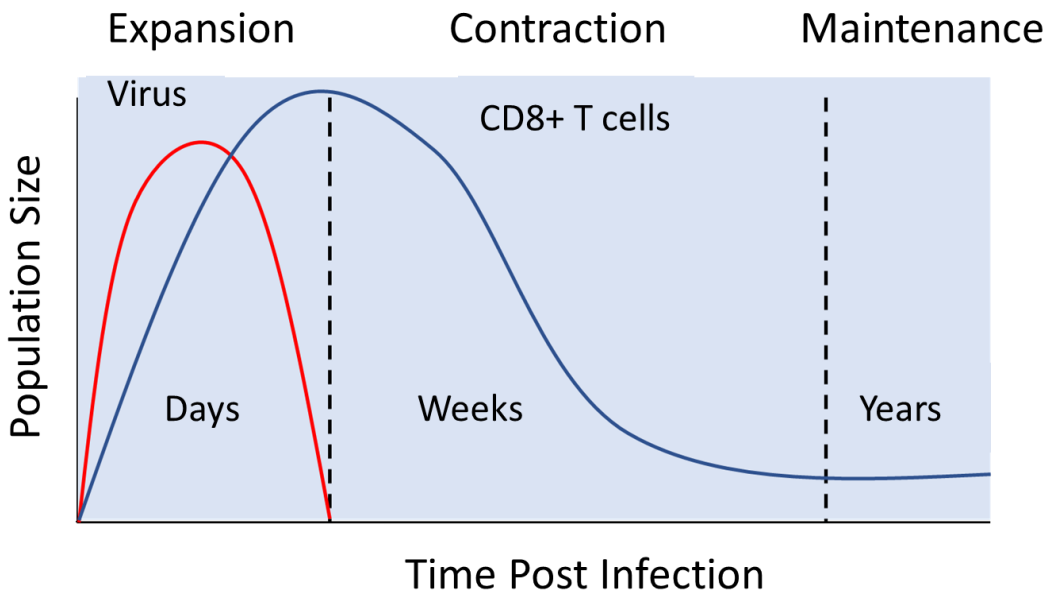

Fig. 1.4: Phases of a T cell response to acute virus infection. Expansion occurs over days, leading to the formation of effector T cells with cytotoxic functions. The virus is cleared over the course of this phase. Contraction follows expansion wherein most effector T cells die off over a period of weeks. The maintenance phase involves memory T cells that are left behind after the contraction for the secondary immune response in case of reinfection.

[Adapted from Kaech and Cui, 2012, Nature Reviews Immunology]

1.3.2. Models of T cell differentiation

Various models have been proposed for explaining the dynamics of effector and memory T cell generation after acute virus infection. The decreasing potential model or the linear model suggests that naïve T cells transition into less differentiated memory T cells called stem cell memory T cells and progressively into central memory, effector memory, and effector T cells (Durek et al., 2016; Restifo and Gattinoni, 2013). The memory potential of the T cells is progressively reduced, and the model suggests a linear transition based on certain factors like TCR signal strength, duration, or extent of stimulation during T cell activation (Gattinoni et al., 2017; Kaech et al., 2002). Strong TCR signaling leads to the generation of more differentiated effector subsets, whereas lower antigenic stimulation leads to the selection of memory T cells. A contradictory model, the circular model or the "on-off-on" model, suggests that naïve T cells differentiate into effector T cells that can dedifferentiate into memory T cells and re-differentiate into effectors upon reinfection (Henning et al., 2018). The asymmetric division model is another model that suggests that T cells with effector and memory potentials arise as early as after the 1st cell division (Arsenio et al., 2015; Flossdorf et al., 2015). In this case, the fate of the T cells is determined by the asymmetric division of transcription factors and epigenetic regulators between the daughter cells that, in turn, dictates whether the daughter T cells will have effector or memory capabilities.

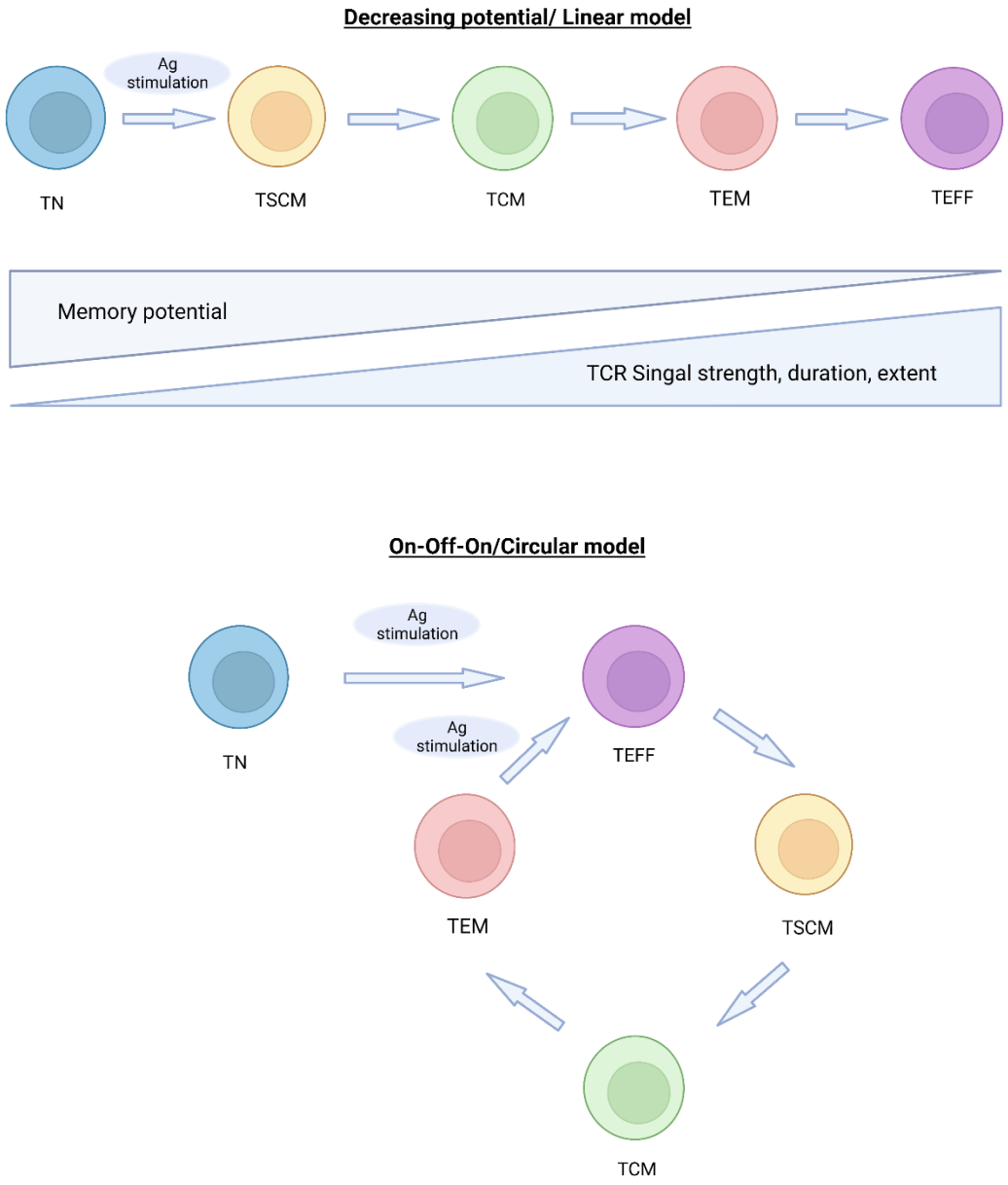

Fig. 1.5: Models of T cell differentiation. Decreasing potential/Linear model is characterized by progressively reduced memory potential depending on TCR signal strength, duration, and extent. On-Off-On/Circular model. On-Off-On refers to the pattern in which transcription factors related to effector and memory T cells need to be switched off or on for the progression of this model. This circular model suggests that effector T

cells dedifferentiate into memory T cells. TN- Naïve T cell, TSCM- Stem cell memory T cell, TCM- Central memory T cell, TEM- Effector memory T cell, TEFF- Effector T cell Created with BioRender.com (2022).

[Adapted from Henning et al., 2018, Nature Reviews Immunology]

1.3.3. Bystander T cell responses in virus infection

With lessons from SARS-Cov-2, H7N9, MERS, and SARS, it has become clear that activation of heterologous immunity is an important factor for protection against viral infections that can otherwise prove to be severe and life-threatening (Channappanavar et al., 2014; Lee et al., 2020; Moss, 2022; Veit et al., 2018). Heterologous immunity may be a consequence of cross-reactive T cell activation or bystander activation. Cross-reactive T cells are T cells specific for other viruses that are activated by antigenic peptides because of sequence homology between the infecting virus and other viruses to which the individual has been previously exposed (Lee et al., 2020). Cross-reactive T cell activation occurs in a TCR-dependent manner, and this type of T cell activation has been discussed in detail in an earlier section. Bystander activation is TCR-independent T cell activation and occurs when T cells, typically pre-existing memory T cells from other virus infections, are activated by cytokines and lead to cytotoxicity (Lee et al., 2022). Bystander activation is important during virus infection that can be beneficial by conferring rapid early protection or may be involved in contributing to immunopathology and host damage (Kim and Shin, 2019; Lee et al., 2022). The following section discusses bystander activation of T cells in the context of different viruses and the mechanisms that drive bystander activation.

In acute hepatitis A virus (HAV) infection, severe liver injury may occur (Shin et al., 2016), and it is debated whether this is due to hepatitis A virus-specific T cells. Although virus-

specific T cells are detected in the liver, studies have shown that their numbers do not increase until after both viremia and injury are reduced (Zhou et al., 2012). On the other hand, bystander-activated T cells have also been detected in the liver upon acute HAV infection, and these cells are capable of innate-like cytotoxic activity (Kim et al., 2018). Unlike hepatitis A, hepatitis B and C can cause chronic infection, and virus-specific T cells become exhausted throughout infection (Shin et al., 2016). Bystander-activated T cells have been identified in both hepatitis B and C infections and are associated with severe immune pathology (Maini et al., 2000; Sandalova et al., 2010).

Bystander-activated T cells have also been identified in other infections like human immunodeficiency virus (HIV) (Dalod et al., 1999; Doisne et al., 2004), Epstein Barr virus (EBV), and influenza A virus infection. In HIV infection, it is hypothesized that both antigen-specific and non-specific T cells can drive immune activation (Haas et al., 2011). Immune activation is an important factor contributing to immunopathology and disease progression in HIV. Bystander activation of CD8 T cells occurs early during HIV infection, and a strong correlation exists between CD8 T cell activation and loss of CD4 T cells (Deeks et al., 2004). In EBV infection, the frequency of bystander-activated memory T cells was comparable before and after primary EBV infection (Odumade et al., 2012), suggesting that bystander T cell activation can prevent loss of memory T cells and have enhanced survival. Bystander CD8 T cells are also found in the lung during influenza A virus infection (Ely et al., 2003). They have cytotoxic capabilities, but the full impact of their role on disease progression or immunopathology during the infection is unclear.

Bystander activation occurs via many different mechanisms and is a cytokine-dependent phenomenon. Interleukin-15 (IL-15), interleukin-18 (IL-18), and type 1 interferons are

some of the most important cytokines responsible for bystander activation of T cells (Kim and Shin, 2019). Bystander-activated T cells can exert their protective functions via the production of interferon gamma (IFN-γ), Granzyme B, and NKG2D activation (Lee et al., 2022).

Upon exposure to IL-15, pre-existing memory T cells can undergo proliferation and exert effector capabilities (Liu et al., 2002). IL-15 drives memory T cells to upregulate NK cell receptors like NKG2D (Roberts et al., 2001). It also leads to the upregulation of granzymes and perforin (Correia et al., 2011). Upon engaging NK ligands, these bystanders activated memory T cells can exert cytotoxic effects by degranulation of perforins and granzyme B (Soudja et al., 2012). So, IL-15 is responsible for bystander activation of T cells that leads to innate-like cytotoxicity.

IL-18, on the other hand, binds to IL-18R on memory CD8 T cells. It synergizes with other cytokines like IL-12 to induce bystander activation and lead to the proliferation of T cells and the production of IFN-γ (Berg et al., 2003; Kambayashi et al., 2003). Compared to IL-15, which can cause immunopathology with its innate-like cytotoxicity, IFN-γ production via IL-18-driven bystander activation is considered to have an early protective role during infections (Lertmemongkolchai et al., 2001; Raué et al., 2013).

Type 1 interferons can also lead to bystander activation of T cells (Tough et al., 1997, 1996). Since type 1 interferons are among the earliest mediators of anti-viral immunity and form a central topic of research in this thesis, the impact of type 1 interferons on T cells, bystander or otherwise, has been discussed at length in subsequent sections.

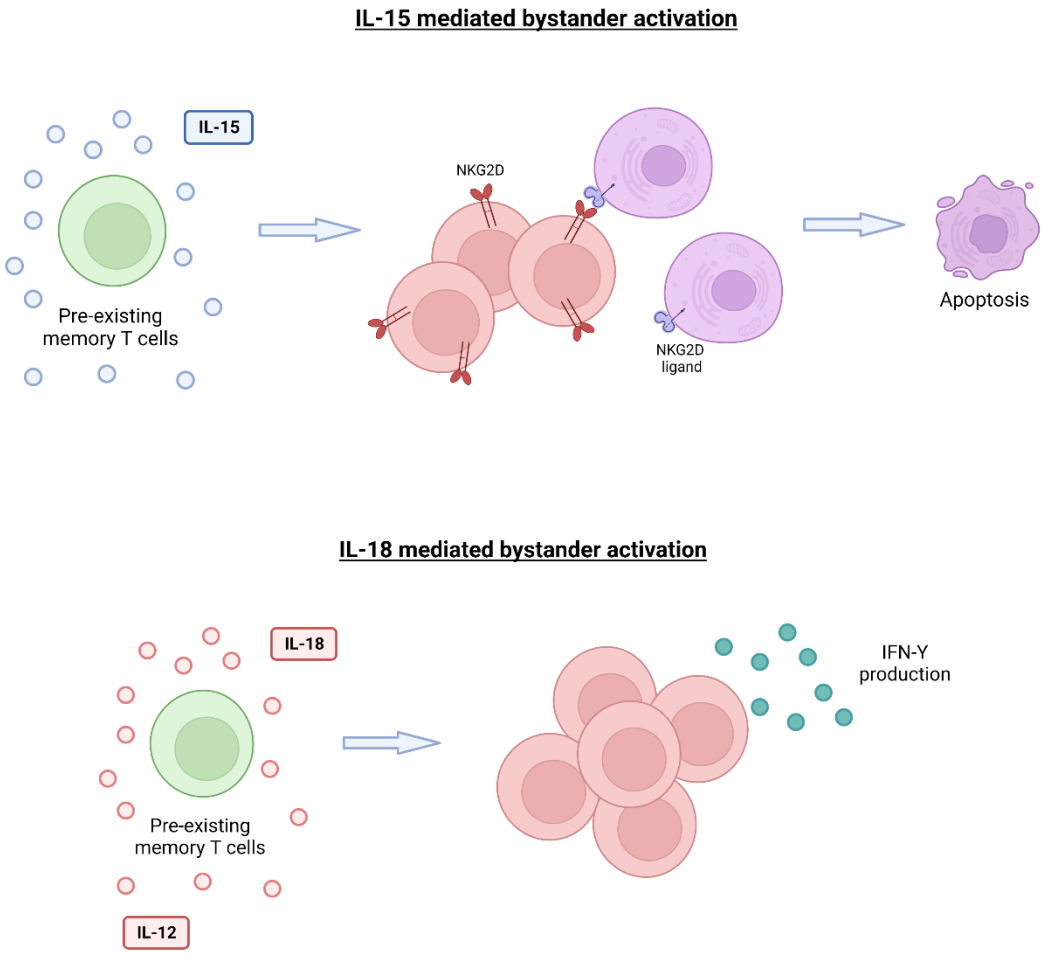

Fig. 1.6: Mechanisms of bystander activation. IL-15-mediated bystander activation of pre-existing memory T cells leads to NKG2D-dependent cytotoxicity. IL-18-mediated bystander activation leads to IFN-γ production with a synergistic effect in the presence of IL-12. Created with BioRender.com (2022).

[Adapted from Lee et al., 2022, Nature Reviews Immunology]

1.4.Type 1 interferons

1.4.1. Type 1 interferon signaling

Type 1 interferons are among the earliest responders to viruses and play an important role in controlling the infection. Type 1 interferons are induced when innate cells of the immune system recognize viral nucleic acids via sensors like TLRs. This recognition sets a complex signaling mechanism into motion, activating transcription factors like NF-κB and the interferon regulatory factors (IRF) family of transcription factors, which drives type 1 interferon production (Hiscott et al., 2003). Type 1 interferons bind to the interferon-α/β receptor (IFNAR), which is a heterodimer of IFNAR1 and IFNAR2 proteins. These are constitutively bound to tyrosine kinase 2 (TYK2) and Janus kinase 1 (JAK1). Type 1 interferon binding induces phosphorylation of both proteins via transphosphorylation. This can lead to a myriad of signaling pathways being activated that drive further transcription of important genes (Chen et al., 2017). One family of transcription factors activated because of type 1 interferon signaling is the signal transducers and activators of the transcription (STATs) family. STAT1 and 2 are one such pair of STATs that can be activated by type 1 interferons. In combination with IRF-9, STAT1 and STAT2 are collectively known as interferon-stimulated gene factor 3 (ISGF3) (Fu et al., 1990). This complex translocates into the nucleus and leads to the transcription of interferon-stimulated genes (ISGs) and anti-viral proteins (Chen et al., 2017). STAT1 can also form a homodimer that translocates in the nucleus and regulates the transcription of inflammatory genes. Other STATs like STAT3, 4, 5, and 6 can also form homo- or heterodimers and translocate to the nucleus to regulate the inflammatory response (McNab et al., 2015). STAT5 can also act

in combination with CrkL protein to translocate into the nucleus upon phosphorylation and regulate inflammatory immune responses (Fish et al., 1999).

Next, another family of proteins activated by type 1 interferon signaling is the phosphoinositide 3-kinase (PI3K) family. PI3K binds insulin receptor substrate (IRS1/2) and can lead to the activation of Protein kinase B or Akt as it is also known. Akt leads to the activation of IκB kinase (IKK) and leads to the degradation of IκB via the proteasome. This frees up NF-κB to translocate into the nucleus and drive the transcription of survival-related genes. Akt can also lead to increased protein synthesis by blocking the mammalian target of rapamycin (mTOR) and activating mRNA translation (Ivashkiv and Donlin, 2014).

Another important pathway activated by type 1 interferon signaling is the mitogen-activated protein kinase **(**MAPK) pathway. Vav, guanine nucleotide exchange factors (GEFs), and Ras-related C3 botulinum toxin substrate 1 (Rac1) lead to the activation of MAPKKK, which causes growth inhibition and chromatin remodeling via mitogen and stress-induced kinase (MSK1/2) (Ivashkiv and Donlin, 2014). Overall, type 1 interferons can lead to various signaling pathways being activated in the cell that provide a diverse range of signals from survival to the transcription of anti-viral factors. A comprehensive summary of the pathways involved in type 1 interferon signaling has been shown in Fig. 1.7.

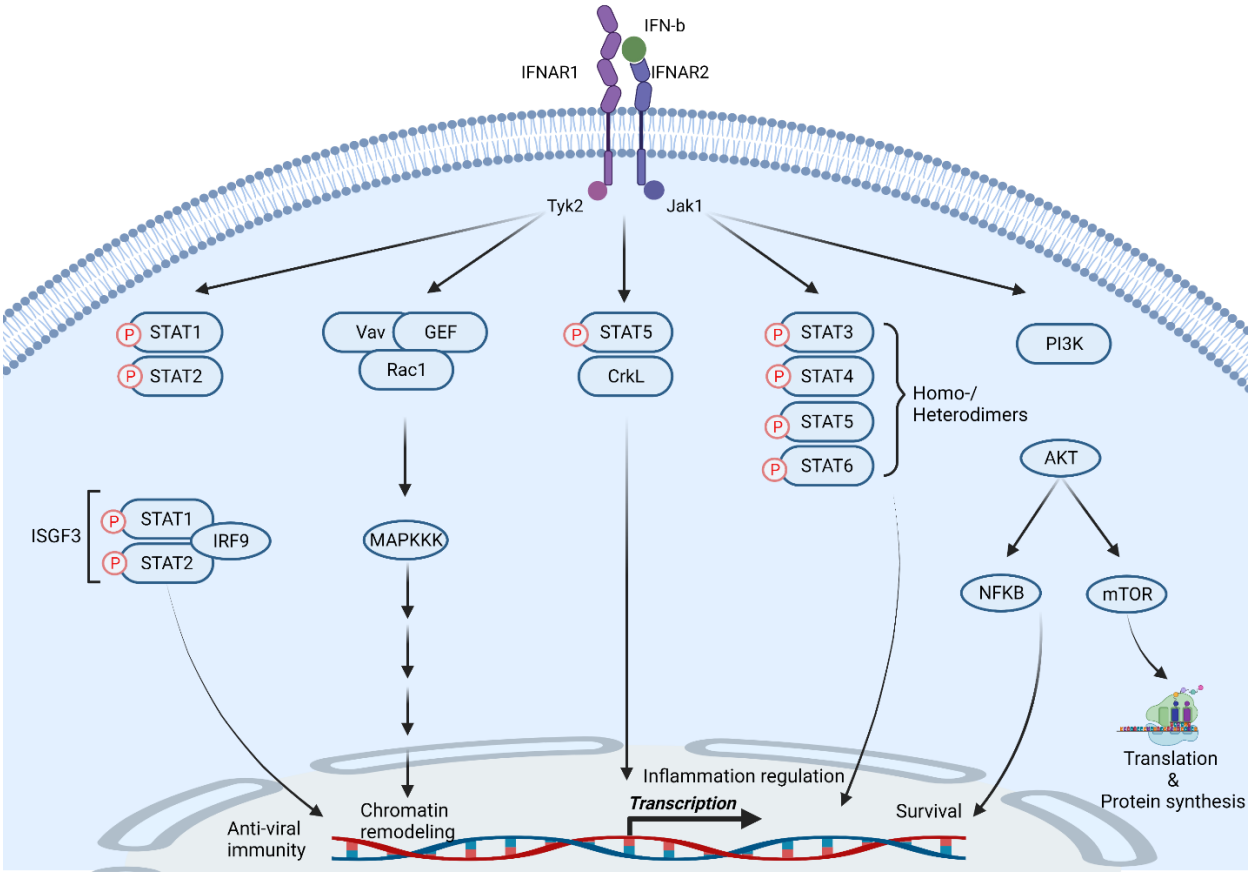

Fig. 1.7: Type 1 interferon signaling pathway. Upon binding of type 1 interferon to the interferon receptor, several different signaling pathways may be activated, including signal transducers and activators of the transcription (STAT) pathways, Vav-GEF-Rac1 pathway, and phosphoinositide 3-kinase (PI3K)-AKT pathways, typically leading to transcription of genes important for inflammation and anti-viral immunity. Created with BioRender.com (2022).

1.4.2. Type 1 interferons and CD8 T cells

Type 1 interferons can impact T cell responses in many ways. They can act on APCs that affect the development of the T cell response or act directly on T cells and have an immunoregulatory function. Upon exposure to viruses, APCs produce type 1 interferons rapidly, upregulate MHC molecules and migrate the lymphoid organs and prime T cells. In these lymphoid organs, type 1 interferons can lead to the attrition of pre-existing memory T cells and the proliferation of antigen-specific T cells (Welsh et al., 2012). The STAT family of transcription factors mentioned earlier are important regulators of proliferation in T cells. STAT1 may be upregulated upon exposure of T cells to type 1 interferon. STAT1 blocks proliferation but is downregulated upon antigen-specific stimulation of T cells (Tanabe et al., 2005; van Boxel-Dezaire et al., 2006). T cell expansion may also occur through the activity of other STATs like STAT4. STAT3 and STAT5 are particularly important in providing pro-mitogenic and anti-apoptotic signals in T cells that downregulate STAT1 after antigen priming (Durbin et al., 2006; Tanabe et al., 2005). Hence, type 1 interferon can have context-dependent roles in T cells, either limiting or causing their proliferation depending on the activation status (antigen primed or unprimed) or differentiation status (naïve versus memory) of T cells. In mixed lymphocyte cell cultures, the dose of type 1 interferon has been shown to inhibit or increase T cell proliferation, further substantiating the context-dependent roles of type 1 interferons on T cell proliferation (Welsh, 1984).

Another important factor that determines the role of type 1 interferons on T cells is the timing of interferon exposure. We have discussed that antigen-primed T cells can proliferate upon exposure to type 1 interferons; however, if T cells are exposed to type 1

interferon before antigen priming, a rapid pathway of effector differentiation may be activated upon priming (Marshall et al., 2010). This allows for rapid cytolytic activity and cytokine production (for example, IFN-γ) when naïve T cells are exposed to type 1 interferon before priming with antigen (Urban et al., 2016). This altered differentiation pathway is thought to occur due to increased self-MHC presentation via APCs to T cells due to type 1 interferons (Marshall et al., 2010). This provides a low-level signal to naïve T cells for activation as opposed to a direct effect of the exposure of T cells to type 1 interferons.

In the context of bystander T cell activation discussed earlier, studies have shown that type 1 interferons can drive the non-specific proliferation of T cells. Specifically, viral infection and LPS have been shown to drive type 1 interferon-dependent proliferation of T cells in mice (Tough et al., 1997, 1996). Type 1 interferons have also been shown to drive T cell proliferation in an LCMV model of infection (DURBIN et al., 2006). In HIV infection, type 1 interferons have been shown to drive T cell activation and disease progression (Hardy et al., 2013). The exact mechanisms of bystander activation by type 1 interferons are not known. Since bystander activation has typically been studied in the context of memory T cells and type 1 interferon can drive attrition of memory T cells, it has been suggested that type 1 interferons may be detrimental or low levels of type 1 interferons may be necessary for bystander activation of memory T cells (Kim and Shin, 2019).

In general, bystander activation is studied primarily in the context of pre-existing memory T cells. Naïve CD8 T cells are also activated in a bystander manner as a consequence of being in an inflammatory milieu after virus infection and being exposed to cytokines. The bystander activation of naïve CD8 T cells remains ill-characterized in general, and even

less is known in the context of type 1 interferons. A recent study has demonstrated that bystander activation of naïve CD8 T cells by type 1 interferons modulated T cell homeostasis and function (Jergović et al., 2021). Much remains to be understood about the role of type 1 interferons in the bystander activation of naïve CD8 T cells, and this topic forms a central theme in this thesis.

1.5. Immunometabolism

Immunometabolism is a rapidly evolving, important area in the field of immunology that helps understand the role of metabolism in the differentiation and function of immune cells. It describes the changes in metabolite levels upon activation or suppression of immune cells and the implications of such changes on immune regulation. Major pathways interrogated in the study of immunometabolism include glycolysis, tricarboxylic acid (TCA) cycle, pentose phosphate pathway, fatty acid oxidation, fatty acid synthesis, and amino acid metabolism.

T cell immunometabolism is a particularly exciting field that has helped delineate how different types of T cells, like memory and effector T cells, rely on different metabolic pathways for their functional capabilities.

1.5.1. Important metabolic pathways

1.5.1.1. Glycolysis

Glycolysis is an essential metabolic pathway that occurs in the cytoplasm of a cell. It involves glucose uptake into the cell and results in its ultimate conversion to pyruvate. Byproducts of glycolysis formed at various steps like glucose-6-phosphate and 3-phosphoglycerate are diverted to other important pathways like the pentose phosphate pathway and serine biosynthesis, respectively (Alvarez et al., 2013; Reid et al., 2018).

Glycolysis, by itself, is an anaerobic process and can be divided into energy-consuming and energy-producing stages. The 1st stage uses two molecules of adenosine triphosphate (ATP), whereas the second stage produces four molecules of ATP. Hence, glycolysis leads to the generation of two net molecules of ATP from one glucose molecule. It also leads to the reduction of nicotinamide adenine dinucleotide (NAD^+) to NADH which is an important co-factor for enzymes. Although glycolysis does not produce a large amount of ATP, it is upregulated by rapidly dividing and growing cells and is essential for driving the proliferation of immune cells like T cells (Chang et al., 2013; Menk et al., 2018).

1.5.1.2. Tricarboxylic acid cycle

The TCA cycle, also known as the citric acid cycle or Kreb's cycle, is another important cellular metabolic pathway that occurs in the mitochondrial matrix. It uses the end product of glycolysis- pyruvate-and converts it to acetyl Coenzyme A (CoA), which is then converted to citrate, the first metabolite in the cycle. Acetyl-CoA may also be synthesized from fatty acids before entering the TCA cycle (Wang et al., 2018). Although acetyl-CoA is the major starting point for the cycle, other important metabolites like glutamate also enter the cycle through conversion to α-ketoglutarate. Two important reduced products of the TCA cycle are NADH and (Flavin Adenine Dinucleotide) $FADH_2$. These reduced products transfer electrons to the electron transport chain, leading to ATP generation via oxidative phosphorylation. Combined with oxidative phosphorylation, the TCA cycle accounts for the majority of ATP production during cellular respiration. Intermediates of the TCA cycle also provide substrates for other metabolic pathways like amino acid synthesis, lipid synthesis, and heme generation. Due to the efficient ATP production via

the TCA cycle and oxidative phosphorylation, most quiescent cells rely on this pathway for their long-term energy requirements (Mohammad et al., 2019).

1.5.1.3. Pentose phosphate pathway

The pentose phosphate pathway is another important metabolic pathway that supports cellular growth and proliferation. Glucose-6 phosphate- the first metabolite generated in glycolysis by the phosphorylation of glucose- serves as the starting point of this pathway. The pentose phosphate pathway occurs in the cytosol in two distinct phases- oxidative and non-oxidative phases. In the oxidative phase, glucose-6-phosphate is converted to ribulose-5-phosphate and NADPH. NADPH is an important redox molecule that, like NADH, acts as an electron donor. It is also important for the synthesis of other metabolites like fatty acids. In the non-oxidative phase of the pentose phosphate pathway, ribulose-5-phosphate can be converted into ribose-5-phosphate, which is essential for the synthesis of nucleotides for making DNA and RNA. Ribose-5-phosphate may also be converted into a 10-carbon molecule which, over a series of steps involving interconversion, gives rise to intermediates that may feed back into glycolysis or may be involved in the synthesis of amino acids like phenylalanine, tyrosine, and tryptophan. Hence, the pentose phosphate pathway can drive growth and proliferation by allowing for nucleotide production and synthesis of many important cellular metabolites (O'Neill et al., 2016).

1.5.1.4. Fatty acid synthesis

Fatty acid synthesis involves the production of lipids from the products of various metabolic pathways discussed above, like glycolysis, the TCA cycle, and the pentose phosphate pathway. Citrate, produced in the TCA cycle, can be shuttled out of the mitochondria and converted back to acetyl CoA and oxaloacetate. Acetyl CoA can then be

converted to malonyl-CoA and fatty acids like palmitate by utilizing reducing molecules like NADPH, obtained from the pentose phosphate pathway. Other straight-chain fatty acids of different chain lengths may be synthesized from palmitic acid. The synthesis of branched-chain fatty acids requires the availability of branched-chain amino acids like leucine as starting substrates. All the enzymes for fatty acid synthesis are present in the cytoplasm, but its substrate, acetyl CoA, is made available by shuttling citrate from the mitochondria and breaking it down in the cytoplasm. Fatty acid synthesis is an important anabolic process critical for cell growth and proliferation (Li et al., 2012).

1.5.1.5. Fatty acid oxidation

The fatty acid oxidation pathway allows for the production of a large amount of energy via a process called β-oxidation of fatty acid molecules like palmitate. For this process, fatty acids in the cytoplasm are activated in an ATP-dependent manner to produce fatty acid acyl-CoA. This is the first step of fatty acid oxidation. Next, activated short-chain fatty acids (less than six carbon molecules) can diffuse into the mitochondria. Medium and long chain activated fatty acids need to be transported into the mitochondria by conjugation with carnitine before shuttling. Once in the mitochondria, the carnitine group is removed, and β-oxidation of the fatty acid acyl CoA is initiated. The mitochondrial and β-oxidation of fatty acids leads to the generation of many products like acetyl CoA, NADH, and FADH2, which can further be utilized to produce energy via the TCA cycle and oxidative phosphorylation. The shuttling of activated fatty acids from the cytoplasm into the mitochondria is a key feature of fatty acid oxidation. It is important because the enzyme involved in activating medium and long-chain fatty acids- carnitine palmitoyltransferase 1A (CPT1A)- is inhibited by malonyl-CoA, an intermediate product of fatty acid synthesis

in the cytoplasm. This is critical for regulating fatty acid oxidation and does not allow fatty acid oxidation to occur when a cell is undergoing fatty acid synthesis.

1.5.1.6. Amino acid metabolism

Amino acids are important precursors for the synthesis of proteins. Apart from this, amino acids can also serve as substrates for synthesizing nucleotides and branched-chain fatty acids. Glutamine is an important substrate for many cells as it can be directed into the TCA cycle via its breakdown into α-keto-glutarate. In this manner, glutamine can be used for ATP generation or the generation of TCA intermediates like citrate for fatty acid synthesis. Glutamine can also be used for purine and pyrimidine synthesis which is required to produce nucleotides.

Tryptophan is another substrate that can be broken down by the *de novo* pathway for the generation of NAD^+. NAD^+ is responsible for maintaining redox balance and serving as a co-factor for several cellular enzymatic reactions. Tryptophan metabolism also generates other key metabolites like kynurenine that have an emerging role in immunosuppression in tumor microenvironments (Belladonna et al., 2007).

1.5.1.7. One-carbon metabolism

One-carbon metabolism is a metabolic pathway that contributes to one-carbon metabolites via the interconversion of serine, glycine, and folate. It has emerged as an important regulator of immune function especially in early activated T cells (Kurniawan et al., 2021; Richter and Clarke, 2021). One-carbon metabolism contributes to one-carbon units required for nucleotide synthesis, NADPH generation for maintaining redox balance, and the generation of methyl groups for methylation reactions in epigenetic maintenance. One-

carbon metabolism can also contribute to energy generation in the mitochondria by regulating mitochondrial protein synthesis by mitochondrial tRNA methylation.

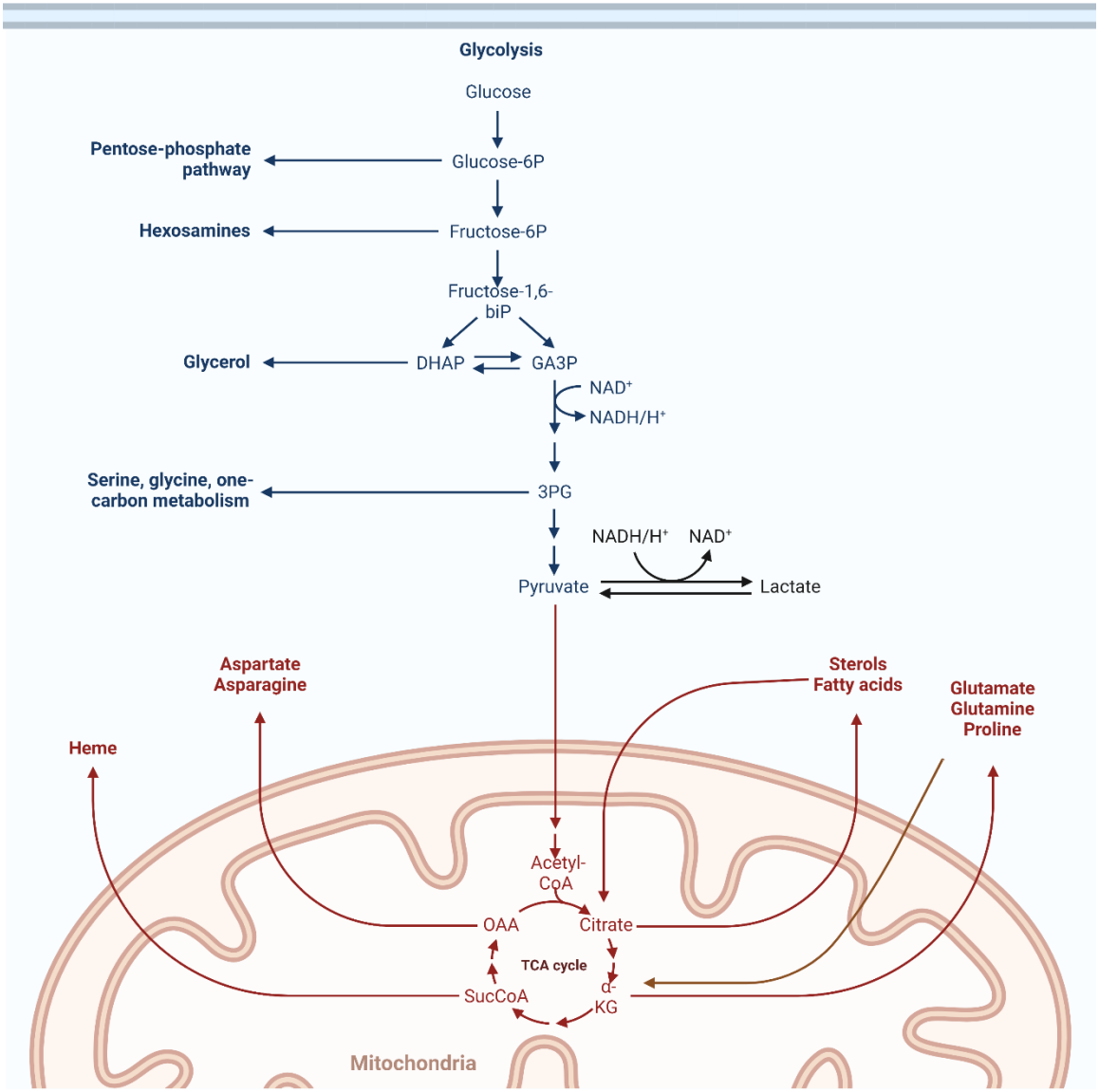

<u>Fig. 1.8:</u> Overview of metabolic pathways in the cell. Different metabolic pathways depicted above include central energy metabolism pathways- glycolysis and tricarboxylic acid (TCA) cycle- as well as the starting points for metabolic pathways like pentose-phosphate pathway, hexosamine pathway, and serine metabolism that use the products of

central energy metabolism pathways to generate a wide range of important metabolites. P: Phosphate, DHAP: Dihydroxyacetone phosphate, GA3P: Glyceraldehyde 3-phosphate, NAD+: Nicotinamide Adenine Dinucleotide, NADH+: reduced NAD, AcetylCoA: Acetyl Coenzyme A, α-KG: alpha-ketoglutarate, SucCoA: Succinyl Coenzyme A, OAA: Oxaloacetate. Adapted from "Warburg Effect", by BioRender.com (2022). Retrieved from https://app.biorender.com/biorender-templates.

1.5.1.8. NAD^+ biosynthesis

NAD^+ is an important cofactor that catalyzes several reactions in energy metabolism, including steps of glycolysis, glutaminolysis, and fatty acid oxidation. Outside of energy metabolism, NAD+ acts as an essential cofactor for many enzymes involved in cellular senescence, chromatin remodeling, and DNA repair (Belenky et al., 2007; Verdin, 2015). NAD^+ decline has been associated with many age-related diseases, and NAD^+ repletion is being explored as a strategy for targeting these diseases (Johnson and Imai, 2018; Verdin, 2015). NAD^+ can be generated via many different pathways in the cell. First, the *de novo* pathway involves the breakdown of tryptophan in a series of steps to produce NAD^+. The NAD^+ salvage pathway utilizes nicotinamide to generate NAD^+ via nicotinamide mononucleotide (NMN). Finally, the Priess Handler pathway involves the conversion of nicotinic acid to NAD^+. These pathways are critical for NAD^+ generation for supporting enzymes that serve a series of functions, as mentioned above. Different cell types rely on different NAD^+ pathways for the generation of NAD^+, and not all pathways are fully utilized in all cells.

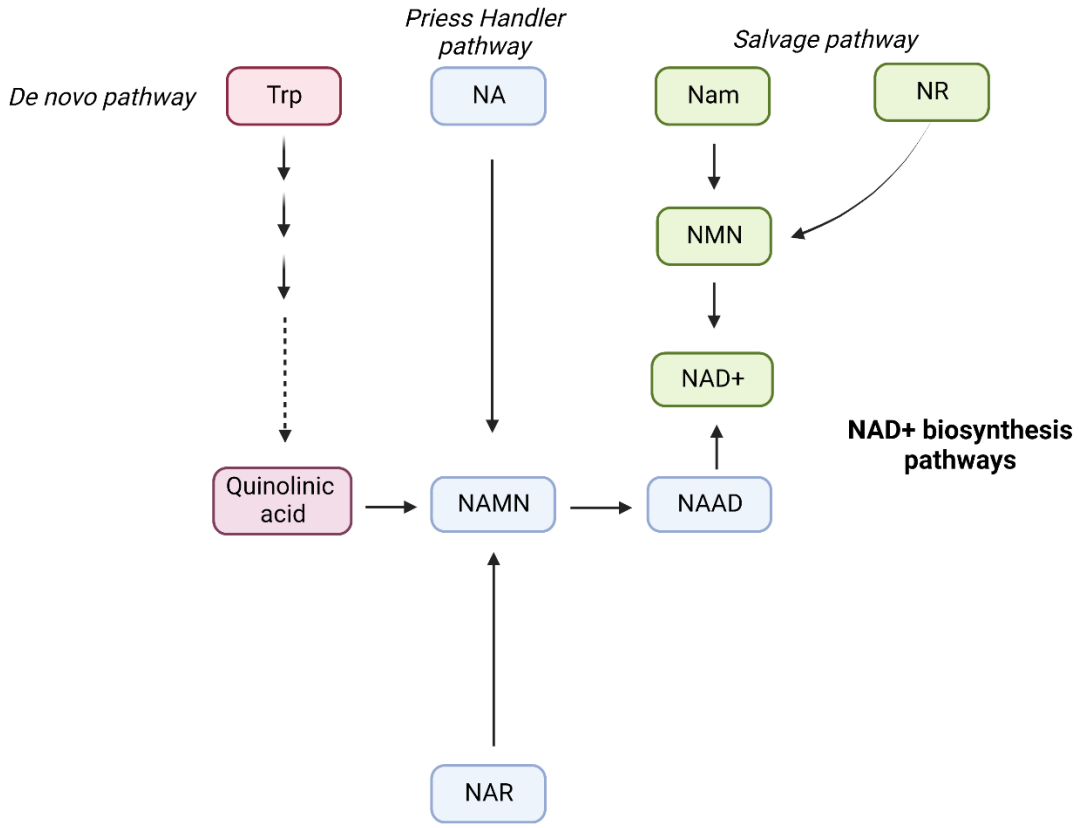

Fig. 1.9: NAD$^+$ biosynthesis pathways. NAD$^+$ can be generated in the cell from different pathways, including the de novo pathway, wherein NAD$^+$ is generated from tryptophan (Trp) broken down via a series of steps, the Priess Handler pathway, which uses nicotinic acid (NA) or niacinamide (NAR) and breaks them down to generate NAD$^+$ as well as the salvage pathway which recycles nicotinamide or nicotinamide riboside to NAD$^+$. Image generated using Biorender.

1.5.2. T cells immunometabolism

As described earlier, T cells can undergo many changes upon activation in the presence of virus infection and inflammatory stimuli. Naïve T cells become activated and, over time, proliferate into effector T cells and memory T cells. Effector T cells are responsible for the cytotoxic function, and memory T cells are responsible for providing long-term immunity and are activated again in case of re-infection. This activation leads to the acquisition of many different functions by T cells, like the production of cytokines and cytotoxic molecules, proliferation, and migration. The rapid acquisition of new functions and eventual transition into memory T cells is possible because naïve T cells can transition from their quiescent states to more active states. This transition requires them to switch to different metabolic pathways as the T cells progress from naïve to effector to memory T cells (Buck et al., 2017; Menk et al., 2018).

1.5.2.1 Effector T cell metabolism

When naïve T cells are not activated by an antigen, they are quiescent and mainly rely on oxidative phosphorylation for their energy needs (van der Windt and Pearce, 2012). Upon stimulation with antigen, naïve T cells undergo metabolic reprogramming. The resulting effector T cells are highly proliferative and, as a result, have significantly increased energy demands. The rates of glycolysis and oxidative phosphorylation are both increased in effector T cells (Buck et al., 2017; Chang et al., 2013). Although glycolysis produces fewer molecules of ATP compared to oxidative phosphorylation, effector T cells rely heavily on glycolysis to meet their immediate energetic and proliferative needs (Phan et al., 2016). This increased rate of glycolysis allows for the generation of important metabolic intermediates like glucose-6-phosphate, used in the pentose phosphate pathway for

nucleotide synthesis, and 3-phosphoglycerate, used in the serine biosynthesis pathway for the generation of amino acids (Pearce et al., 2013; Wang et al., 2011). Further, increased glycolysis helps maintain the redox balance by maintaining the NAD+/NADH ratio (Anastasiou et al., 2011; Vander Heiden et al., 2009). An increase in glycolysis can be supported easily and quickly by overexpression of the enzymes involved in the process as compared to increased oxidative phosphorylation, which would require mitochondrial biogenesis (O'Neill et al., 2016). However, effector T cells also have increased oxidative phosphorylation that helps meet their energy requirement (MacIver et al., 2013). The breakdown of pyruvate in the TCA cycle also generates metabolic intermediates like oxaloacetate, which can also be used for nucleotide synthesis. For effector T cells proliferating at a rapid rate at this stage, the generation of nucleotides is a critical process supported by this metabolic rewiring. Similarly, other anabolic processes are important for cellular growth and biomass generation at this stage, and citrate from the TCA cycle can be used to generate lipids. Further, succinate, an intermediate in the TCA cycle, has been linked with reactive oxygen species (ROS) and hypoxia-inducible factor 1α (HIF-1α) (Lukyanova et al., 2018). ROS is important for the T cell function (Belikov et al., 2015; Murphy and Siegel, 2013), and inhibition of succinate dehydrogenase has been shown to impact T cell function (Gudgeon et al., 2022; Nastasi et al., 2021).

1.5.2.2. Memory T cell metabolism

Memory T cells, like naïve T cells, are also quiescent but are antigen-experienced and can be activated to produce cytokines and proliferate at a rate that is much faster than naïve T cells. In terms of their development, it has been suggested that when naïve T cells are activated, two types of effector T cells are formed- short-lived effector cells (SLECs),

which are transient in their response, and memory precursor effector cells (MPECs) which will be long-lived and eventually generate memory T cells (Joshi et al., 2007; Youngblood et al., 2017). The differences in the three signals of T cell activation- antigenic stimulation, costimulation, and cytokines- determine the development and ratio of SLECs and MPECs (Kalia et al., 2010; Sarkar et al., 2008). Costimulation, in particular, has been shown to play an important role in the generation of memory T cells. Without CD28 costimulation, for example, primarily effector T cells are generated. Memory T cells primarily rely on catabolic processes like fatty acid oxidation and oxidative phosphorylation to sustain their energetic demands. CD28 costimulation leads to increased fatty acid oxidation via overexpression of CPT1a, which is important for the transport of long-chain fatty acids and their β-oxidation (Klein Geltink et al., 2017). CD28 costimulation also sends signals to the mitochondria for inhibition of cristae loosening and allows for the generation of memory T cells with increased spare respiratory capacity (Klein Geltink et al., 2017). Further, cytokines play an important role in the generation of memory T cells. Studies have shown that during virus infection, cytokines like IL-7 and IL-15 help drive memory T cell generation by activation of catabolic metabolic processes (Alizadeh et al., 2019; Cui et al., 2015; Hurton et al., 2016). This is achieved again by enhancing fatty acid oxidation, increasing mitochondrial biogenesis, and overexpressing the CPT1a enzyme. The increased mitochondrial mass and consequent increase in spare respiratory capacity allow the memory T cells to survive for longer and have rapid response abilities upon restimulation.

CD28 costimulation also leads to an increase in glycolysis (Frauwirth et al., 2002). Memory T cells employ a seemingly futile pathway that involves the conversion of glucose

to fatty acids and consequent fatty acid oxidation for energy production (Corrado and Pearce, 2022). There is no net gain of ATP in the process, and it is unclear why memory T cells adopt this choice of pathways. It has been suggested that doing so allows for generating metabolic intermediates that may be necessary for other pathways and maintaining redox balance. It has also been hypothesized that this might help engage glycolytic and lipogenesis machinery and maintain mitochondrial health during quiescent periods for memory T cells (Corrado and Pearce, 2022; O'Sullivan et al., 2014). The above choice of substrates is commonly seen with central memory T cells that circulate through the secondary lymphoid organs. Tissue-resident memory T cells, on the other hand, utilize fatty acids from the microenvironment for fatty acid oxidation (Pan et al., 2017). Hence, fatty acid oxidation of fatty acids derived from glucose or exogenous fatty acids leads to the production of metabolic substrates that enter the TCA cycle in the mitochondria and lead to energy production via oxidative phosphorylation.

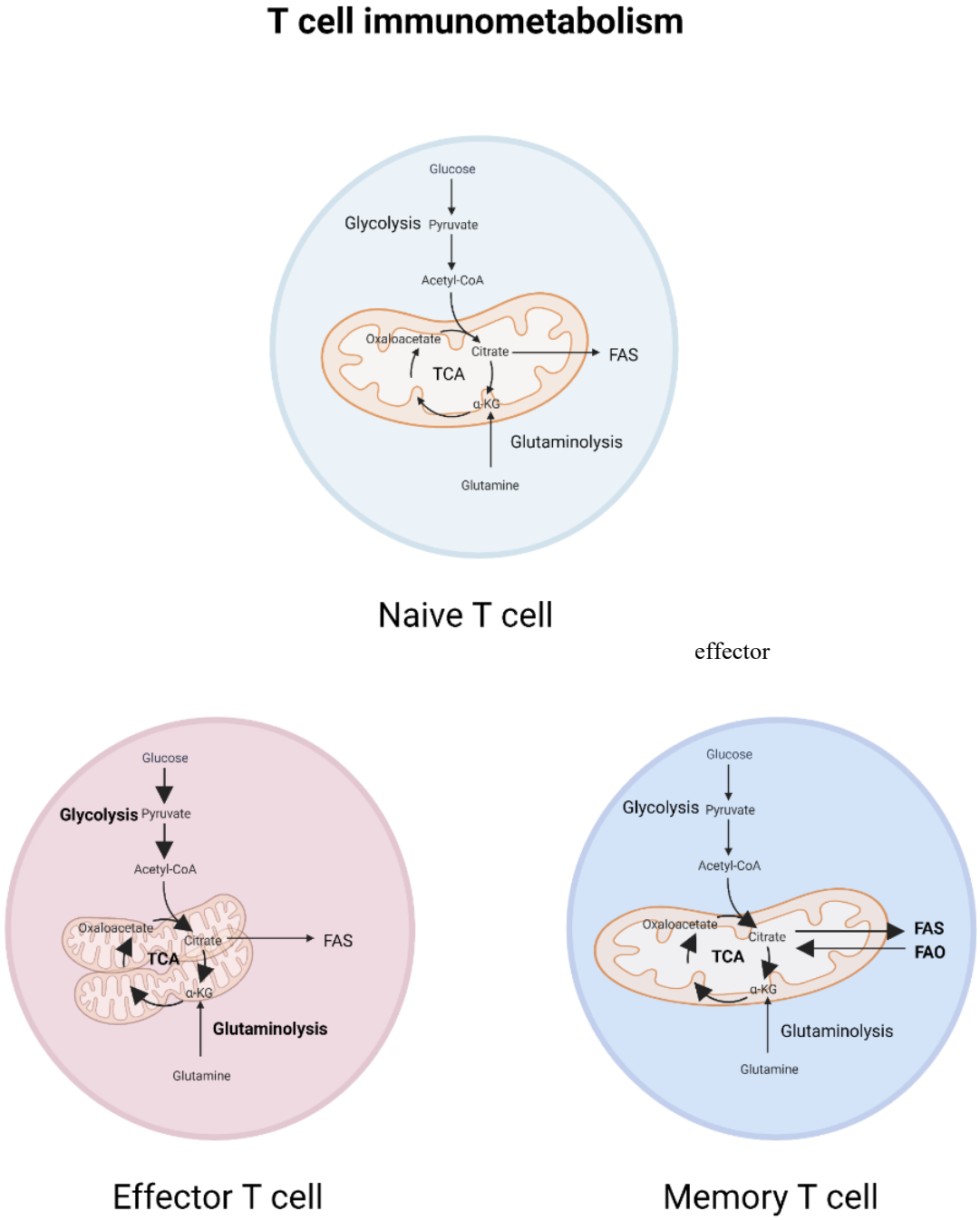

effector T

<u>Fig. 1.10:</u> T cell immunometabolism. Metabolic pathways that are active and upregulated in different T cells- Naïve, effector, and memory T cells have been depicted above. Effector T cells have increased central energy metabolism, including increased glycolytic flux and

TCA cycle. Memory T cells rely on fatty acid synthesis (FAS) and fatty acid oxidation (FAO) for their energy needs. Image generated using Biorender.

1.6. Reovirus

Reovirus is a double-stranded RNA virus that can infect a wide range of hosts. "Reo" stands for the respiratory enteric orphan virus, and reovirus can infect the respiratory and gastrointestinal systems. It is a non-enveloped virus with ten segments of dsRNA packaged into capsids (Joklik, 1981). The outer capsid consists of σ1, σ3, μ-1c, and λ-2 proteins. The inner capsid consists of λ-1, λ-3, σ-2, and μ-2 proteins. The virus also encodes σ-NS, μ-NS, and μ-NSC non-structural proteins in its genome (Coombs, 2006; Joklik, 1981).

Reovirus attaches to cells via its σ1 protein, which can bind to sialic acid and junction adhesion molecules on the cell surface (Lee and Gilmore, 1998). The virus then enters the cell via receptor-mediated endocytosis. Next, proteolysis occurs in the endolysosome leading to the formation of infectious subvirion particles (ISVPs). ISVPs may also be formed by extracellular proteolysis, allowing them to enter the cell directly. Next, viral core particles are released into the cytoplasm. Primary transcription occurs within these core particles, and primary transcripts are released into the cytoplasm. These transcripts and early translation products form complexes that allow for further transcription and translation, leading to virus assembly, replication, cell death, and release of the new virus (Silverstein et al., 1976).

In terms of its clinical presentation, most cases of reovirus infection are mild or sub-clinical in humans; however, one study in mice has implicated reovirus in celiac disease (Bouziat et al., 2017). This study suggested that reovirus infection enabled inflammatory responses

to dietary antigens and caused the development of celiac disease. However, much remains to be understood about the full immunological impact of reovirus infection.

Therapeutically, reovirus has been pioneered as an oncolytic virus for the treatment of various cancers (Coffey et al., 1998; Gujar et al., 2010; Müller et al., 2020; Thirukkumaran et al., 2010). Its clinical preparation, Reolysin, is currently in multiple clinical trials, primarily in combination with checkpoint inhibitors, for the treatment of many different tumors (Black and Morris, 2012; Gong et al., 2016).

We employ reovirus in our studies to examine how CD8 T cells are activated during acute infection with a virus that causes acute infection and is known to be easily cleared by the immune system. This will allow us to understand the early determinants of successful anti-viral T cell immunity.

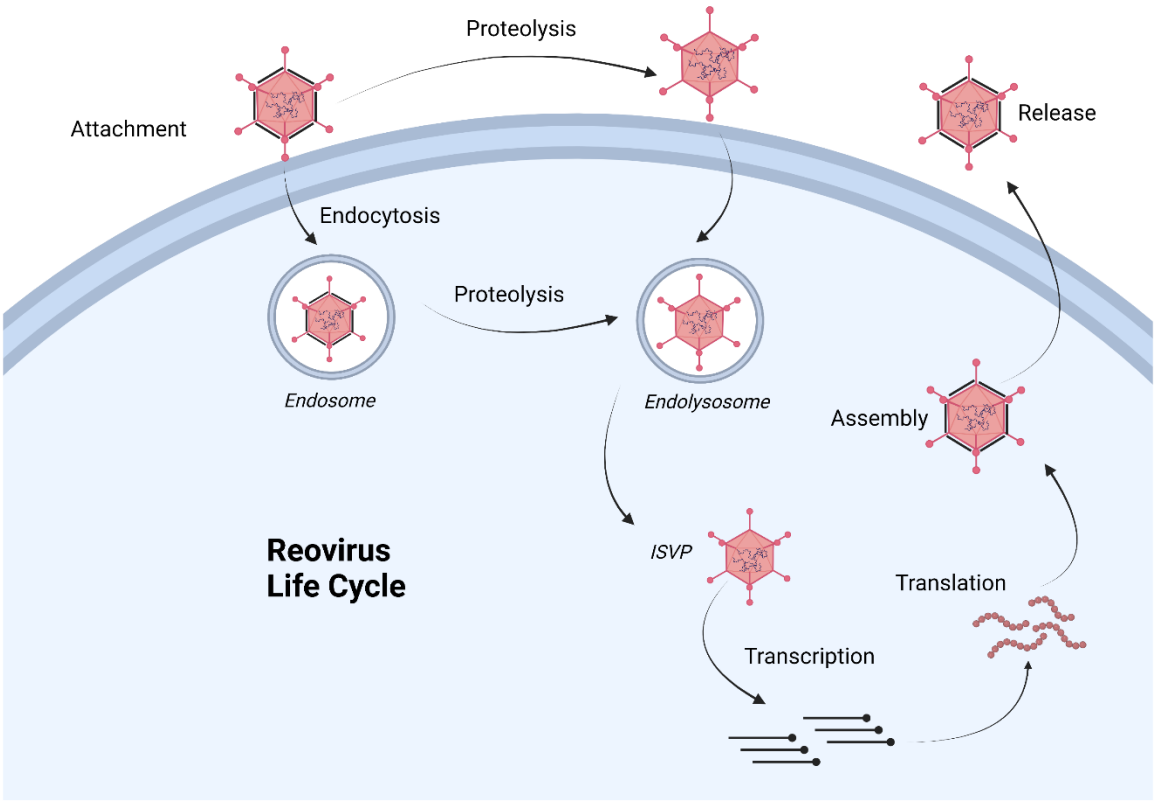

Fig. 1.11: Reovirus life cycle. The image above shows various steps involved in the attachment and entry of reovirus followed by proteolysis and generation of an infectious subvirion particle (ISVP). This is followed by transcription and translation leading to assembly of the virus and release of progeny

Chapter 2. Materials and Methods

2.1. Viruses, cell lines, and reagents.

Reovirus (serotype 3, Dearing strain) was cultured, amplified, and isolated using a previously established protocol (Coffey et al., 1998; Kennedy et al., 2022) described below. L929 cells were cultured in minimum essential media (MEM) with (5% vol/vol Glutamax, 5% fetal bovine serum (FBS), 1X sodium pyruvate, 1X nonessential amino acids, and 1X Anti-Anti [Invitrogen, Carlsbad, CA]). Measles viruses (Edmonston and IC323 strains) were obtained from Dr. Christopher Richardson at the Canadian Centre for Vaccinology, Halifax, Nova Scotia. Herpes simplex viruses (ICP0 and 1716) and vesicular stomatitis virus (Indiana strain) were obtained from Dr. Tommy Alain at the University of Ottawa.

2.2. Reovirus preparation

For titration of reovirus, L929 cells were seeded in 12-well plates and grown until they were 80-90% confluent in a complete MEM medium. Next, the original virus stock was serially diluted (1/10) in MEM incomplete. The growth medium was removed from the plate with L929 cells, the cells were washed with phosphate-buffered saline (PBS), and reovirus dilutions were then added to the 12-well plates at a total volume of 100 µL per well. Cells were infected with reovirus for 1 hour and periodic shaking every 10 minutes. Subsequently, reovirus dilutions were removed from the wells, and agar plugs were added, which were made with 2X MEM complete and 2% agar in a 1:1 ratio. Plates were then incubated at 37 degrees Celsius with 5% CO_2 for 96 hours. At this time point, virus plaque formation was observed, and individual plaques were collected with a glass pipette for reovirus expansion, or titration was done using crystal violet staining, and the concentration of the virus was calculated in plaque forming units (pfu)/mL.

Crystal violet staining was done by formaldehyde fixation (30-40% formaldehyde in PBS), manual agar plug removal, and methanol wash, followed by crystal violet stain (1% crystal violet in 50% ethanol) for 1 minute. Crystal violet stain was removed, and the cells were rinsed with water. Plates were then allowed to dry before the plaques were counted. Individual plaques were collected from the plaque assay and incubated in 1 mL of incomplete MEM for 24 hours at 4ºC. They were then added to a T75 flask with L929 cells at ~85% confluency and incubated at 37ºC at 5% CO2 until total cell death was observed, usually about 72 hours later. The dead cells and the supernatant were collected as reovirus stocks for expansion and stored at -20ºC.

For reovirus expansion, L929 cells were cultured in spin culture round-bottom flasks. The cells were cultured in a spin culture with complete Joklik modified minimum essential media (JMEM; 11.05 g/L JMEM powder, 2.2 g/L NaHCO3, 1.2 g/L, 1 g/L glucose, pH 7.2) at 37ºC until they reached a concentration of $1x10^6$ cells/mL. Reovirus stock, as prepared earlier, was thawed, and half of it was used for every liter of the cells. The temperature for spin culture conditions was reduced to 32.5ºC. Infection of cells was allowed to proceed over the next 72 hours and depending on the amount of cell death observed, temperature conditions were maintained at 30.5-32.5ºC. This was done to control the rate of replication of the virus and expand the window for collection. Upon reaching ~50% cell death, the flasks were moved to 4 degrees overnight. Cells were collected on the following day by centrifugation at 500g for 15 minutes. They were then stored at -80ºC for 1-7 days before extraction of the virus.

Cell pellet obtained after the expansion was resuspended in resuspension buffer comprising 0.25 M NaCl, 10 mM Tris-HCl (pH 8.0). 15 mL of the resuspension buffer was used for

every 1 liter of L929 cells. Reovirus was extracted using Vertrel (Dymar Chemicals Ltd., Mississauga, ON). Next, a repeating sequence of sonication, centrifugation, collection of supernatants, and an ultra-centrifugation step was done. For ultra-centrifugation cells were spun at 107000g for 1 hour at 4ºC. The supernatant was discarded, and the pellet was stored at 4ºC overnight. On the next day, the pellet containing the virus and debris was resuspended in 1 mL of SSC buffer (0.15 M NaCl, 0.015 M sodium citrate, pH 7.0). It was then homogenized and pipetted on a cesium chloride gradient ranging from 1.2-1.4 g/ml in 20 mM Tris-HCl (pH 7.4). This was centrifuged at 107000g for 2 hours at 4ºC. Next, whole and empty reovirus particles were separated within the gradient. The whole reovirus fraction was collected and placed in dialysis tubing for a 3-day dialysis process. The dialysis buffer (0.15 M NaCl, 15 mM $MgCl_2$, 10 mM Tris-HCl [pH 7.4]) was changed three times with fresh dialysis buffer. After dialysis, reovirus titration was done via a standard plaque assay, and the virus was stored at 4ºC. The particle to pfu ratio was calculated based on the optical density (OD)260 using the formula: 1 OD260 = 2.1x1012 reovirus particles.

2.3. Animal studies.

All animal work and *in vivo* experiments were conducted with prior approval from the Ethics Committee at Dalhousie University, Halifax, Nova Scotia. Wild type C57BL/6 and BALB/c mice were purchased from Charles River Laboratory (Montreal, Quebec, Canada). OT-1 transgenic and TLR3 knockout KO mice were obtained from The Jackson Laboratory, United States. Intraperitoneal injections of reovirus (5×10^8 plaque-forming units/ml) were carried out, and mice were sacrificed 1, 3, or 7 days post injection to harvest splenocytes for analysis of T cell populations. SLAM knock-in (KI) and SLAM KI, STAT1

KO mice for harvesting splenocytes and *ex vivo* virus treatment was obtained from Dr. Christopher Richardson. All animals used for experiments were between the ages of 6-10 weeks.

2.4. Flow cytometry analysis and cell sorting.

Sample processing for flow cytometry was carried out by harvesting splenocytes in 5mL PBS-EDTA. The cells were filtered using a 40micron filter and treated with RBC-lysing ammonium chloride (ACK) buffer. The cells were then incubated with CD16/32 Fc blocking antibody in FACS buffer (PBS + 1% EDTA + 1% FBS) for 25 minutes at 4°C, washed and stained with fluorophore labelled primary antibodies in BD Brilliant Stain buffer or FACS buffer for 25 minutes at 4°C. Stained cells were then washed and fixed with 4% paraformaldehyde for 15 minutes. For intracellular staining, fixation/permeabilization of the cells was carried out using the FoxP3/ Transcription Factor Staining Buffer Set after staining with extracellular antibodies. Intracellular labelling with IFN-γ antibody in permeabilization buffer was done for 25 minutes at 4°C. The cells were finally washed and resuspended in FACS buffer. Sample data acquisition was done using the BD FACS Symphony A5 or the LSR Fortessa SORP flow cytometers. Data analysis was carried out using BD FACS Diva (BD Bioscience), FCS Express 7 (DeNovo Software, Los Angeles, CA) and FlowJo version 10 (BD biosciences, Ashland, OR). Dimensionality reduction performed on total CD8 T cells and CD8 T cell subsets using the UMAP (version 2.4) FlowJo plugin. Bar graphs were generated using GraphPad (GraphPad Software Inc., San Diego, CA). Anti-mouse BV785 CD45, BV650 CD62L, BV510 CD3, PerCP-Cy5.5 CD8, and APC-H7 CD4 antibodies were purchased from BD Biosciences. FITC CD44, PerCP CD44, BV711 CD44, BV650 CD62L, PE CD62L, PerCP CD8, PE-Cy7 CD3, PE

CD3, APC IFN-γ, PE Sca-1, and AF647 Sca-1 were purchased from Biolegend. For cell sorting, splenocytes were harvested and stained via the same protocol described for flow cytometry. The paraformaldehyde fixation step was eliminated, and cells were sorted live using FACSAria III, BD Biosciences with a 95-98% purity.

2.5. *Ex vivo* treatment of splenocytes.

C57BL/6 mice and others, depending on the experiment, were sacrificed and splenocytes were harvested and prepared using the initial steps described for flow cytometry processing. After treatment with ACK buffer for RBC lysis, 3 x 10^6 cells were plated in 12-well plates for 24 hours and treated with varying MOIs of reovirus, different strains of measles or herpes simplex viruses, or vesicular stomatitis virus. For OT-1 mice experiments, splenocytes were isolated as described above and plated in 96-well plates at a concentration of 1-2 x 10^6 cells/well. These cells were then stimulated with ovalbumin peptide (SIINFIKEL) at the 18-hour timepoint for 6 hours. Other *ex vivo* treatments included the treatment of splenocytes with varying concentrations of IFN-α1 and IFN-β1. Combination treatments were also carried out such as treatment of splenocytes with reovirus/ IFN-β1 and anti-IFNAR1 antibody or isotype control or treatment of splenocytes with reovirus/ IFN-α1/ IFN-β1 in the presence of FK866 and NMN. For intracellular staining, brefeldin A (2µg/mL) was added to the cells at the 18-hour timepoint for 6 hours. After 24 hours, cells were collected, washed, and processed for analysis via flow cytometry. Anti-IFNAR1 antibody (catalog no. 127324), isotype control (catalog no. 400198), IFN-α1 (catalog no. 752802,) and IFN-β1 (catalog no. 581302) were purchased from Biolegend. FK866 (product no. F8557) and NMN (product no. N3501) and brefeldin

A (catalog no. B7651) were purchased from Sigma. Ovalbumin peptide (257-264) was purchased from Genscript (catalog no. RP10611).

2.6. Quantitative *in vivo* proteomics.

Animals were injected with reovirus as previously described, and T cell subsets were collected either from the non-treated spleen or spleens on 1 and 7 days post-infection (d.p.i.) via the cell sorting process described above. Each sample was prepared by pooling spleens of 5 animals for isolation. Isolated cells were washed with PBS, pelleted, and lysed in 6 M guanidine-HCl, 50 mM HEPES, pH 8.5, containing Roche complete mini protease inhibitor mixture (1 tablet per 10 mL) (Roche, Madison, WI). Lysis was performed via sonication and cleared by centrifugation. Cysteine residues were reduced using 5 mM dithiothreitol and then alkylated with 14 mM iodoacetamide. Aliquots containing 50 μg of protein were diluted to 1.5 M guanidine-HCl, 50 mM HEPES (pH 8.5), and digested with trypsin (Promega, Madison, WI). Digested peptides were desalted using 60 mg solid-phase C18-extraction cartridges (Waters, Milford, MA), lyophilized, and labeled using TMT 10-plex reagents as described previously (Murphy et al., 2015). Samples were then mixed equally, desalted using solid-phase C18 extraction cartridges (Waters, Milford, MA), and lyophilized. Tmt10-labeled samples were fractionated using high-pH reversed phase chromatography performed with an Onyx monolithic 100 × 4.6 mm C18 column (Phenomenex, Torrance, CA). The flow rate was 800 μL/min, and a gradient of 5−40% acetonitrile (10 mM ammonium formate, pH 8) was applied over 60 min using an Agilent 1100 pump (Agilent) from which 12 fractions were collected. Fractions were desalted using homemade Stage Tips, lyophilized, and analyzed with an Orbitrap Fusion mass spectrometer (Thermo-Fisher Scientific, Rochford, IL) using the SPS-MS3 method (Gc et

al., 2014). Protein identification was performed using a database search against a mouse proteome database (downloaded from UniProtKB in September 2014) concatenated to a mammalian orthoreovirus 3 (Dearing strain) database (downloaded from UniProtKB in September 2014). All false discovery rate (FDR) filtering and protein quantitation was performed as previously described (Murphy et al., 2015). A protein was required to have a minimum total signal-to-noise ratio of 100 in all TMT reporter channels, and the maximum number of missing channels was equal to 8. Data for heat maps and individual protein profiles are represented by relative TMT intensity, which is based on the summed signal-to-noise. The data set was subsequently analyzed via K-means clustering with Euclidean distance using MultiExperiment Viewer (MeV), followed by DAVID Bioinformatics Resources (https://48avid. Ncifcrf.gov/) to conduct GO-term analysis for biological processes, molecular functions and cellular compartments on specific clusters. Our total data set was utilized as the background for the data analysis searches. A volcano plot was generated using the R statistical analysis package, and bar graphs were generated using GraphPad

2.7. *Ex vivo* bystander T_N cell metabolomics.

For metabolomic analysis of bT_N cells, each sample was prepared by pooling spleens of 3-5 mice. Live T cell populations were sorted, washed with PBS-EDTA, and resuspended in 100 µl 80% ice-cold methanol. 20 µl of methanol extracted cells were combined with 180 µl of HPLC buffer A [95% (vol/vol) water, 5% (vol/vol) acetonitrile, 20 mM ammonium hydroxide, 20 mM ammonium acetate (pH = 9.0)]. The sample was split into triplicates and run using a triple quadrupole mass spectrometer 5500 QTRAP, and metabolite levels were analyzed. Based on known Q1 (precursor ion) and Q3 (fragment ion) transitions, the

metabolite name, the dwell time, and the appropriate collision energies (Ces) for both positive and negative ion modes were identified. Using this protocol, a selected reaction monitoring transition list of 289 (approximately 10–14 scans per metabolite peak) metabolites can be accurately identified. MultiQuant v2.0 software was used to integrate the peak areas from the Q3 TIC values across the chromatographic elution. Each metabolite from every sample was manually confirmed; typically, a single dominant peak will be present for most detectable compounds. Peak heights normalized to the sum of peak heights per sample were used to determine relative metabolite concentrations between samples. For computational analysis, the metabolomics database was analyzed using R to identify metabolites with significant fold changes and p values. Metabolite rank was obtained by comparing significantly changing metabolites in the order of decreasing fold change (bT_N / T_N). NAM, NMN, and NAD^+ were further analyzed using a targeted analysis on a Qexactive Orbitrap Mass Spectrometer. Here, a targeted selective ion monitoring (tSIM) method was employed with a resolution of 140,000. Metabolic features identified by tSIM were confirmed using Maven software, and peak heights were exported to excel. Peak heights were again normalized using cell numbers and relative peak heights calculated. Graphs were generated by GraphPad Prism. All detectable metabolites were organized into specific and general metabolic pathways based on the Kyoto Encyclopedia of Genes and Genomes (KEGG) metabolic pathways. To determine pathways that were enriched in bT_N cells, an overrepresentation analysis was completed. Metabolites that were increased or decreased by 2-fold and t-test probability less than or equal to 0.05 were selected and compared with the original list of metabolites, and then we calculated the percent of metabolites changed. We used this percent to calculate the expected number of metabolites

that would change if the metabolites were randomly distributed throughout the various metabolic pathways. We then calculated fold enrichment by dividing metabolites changed by 2-fold by the number of metabolites expected to have changed if random. Probability was calculated by the hypergeometric test.

2.8. Metabolomics analysis of CD8 T cells from OT-1 mice

Naive (P1), central memory (P2), effector memory (P3) and CD44lowCD62Llow (P4) CD8 T cells were sorted using flow cytometry with or without treatment with ova peptide in cell culture for 6h or 24h (for P2 cells). Cells obtained after cell sorting were washed with PBS and spun down at 500g for 5 minutes, and this wash was repeated one more time. The cell pellets were resuspended in 20µL of PBS and kept on ice. Next, for 10 samples, a solution with 800µL of chilled 100% methanol and 50µL of isotopically labeled internal standard (ILIS; Cambridge Isotopes Laboratories catalog no. MSK-A2-1.2) was prepared and 85µL of this solution was added to each sample. The samples were then stored at -80ºC until further sorting experiments were completed, and all samples were similarly processed on different days. After all samples were collected, samples were removed from -80ºC, vortexed, and transferred to -20ºC for 30 minutes. The samples were then centrifuged at 10,000g for 5 minutes at 4ºC. The protein-free supernatant was collected and transferred to a new tube. 10µL of each sample was transferred to a separate tube and labeled as the “pool”. Next, a 10X dilution was made by adding 25µL of the sample to 225µL of hydrophilic interaction liquid chromatography (HILIC) buffer (95% acetonitrile/5% Buffer A (5% acetonitrile, 95% water 1 mM ammonium acetate pH 9.0)) or 225µL of reverse phase buffer (5% Acetonitrile/0.1% formic acid) for reverse phase chromatography, depending on the MS protocol used. 250µL of the sample was transferred

to a labeled MS vial, and samples were kept at 4ºC until they were ready to be run. The "pool" sample was also included in the run.

LC separations were performed using an Agilent 1290 HPLC equipped with an XBridge Amide 3.5µm, 1.0x50mm column (Waters 186004871). 10µl of sample was loaded and separated using the gradient shown in Table 1 and Table 2. Samples were analyzed using an AB/Sciex 5500 QTrap mass spectrometer. Each sample was injected twice for both a positive and negative mode analysis. The positive mode method was prepared to analyze 286 metabolites (286 Q1/Q3 transitions) and the negative mode method was set to analyze 298 metabolites (298 Q1/Q3 transitions). All transitions acquired using a 3-ms dwell time (Yuan et al., 2012).

Once the sample run was completed, peak integration was performed on MS files using Skyline (version 21.2). Briefly, peak boundaries were determined by calculating the mean of the manually adjusted integration boundaries for two standard samples (or two pool samples for metabolites where a standard was not included), these boundaries were applied to all samples and peak intensities were exported. An in-house R script (R-4.2.1) was used for initial data filtering and processing. To reduce signal intensity drift, samples were normalized to pool injections. The intensity of each metabolite in a sample was normalized to (divided by) the mean intensity of that metabolite in the two pool injections flanking the sample. Metabolites with low intensity (< 10000 or < LOD) or high variability in intensity (> 30% CV) of pool replicates were excluded from further analysis. For statistical analysis, including t-tests and volcano analysis using MetaboAnalyst (version 5.0), the data was autoscaled and log 10 transformed.

Time (min)	Flow µl/min	A (%)	B (%)
0	400	99	1
0.01	200	99	1
0.5	200	99	1
0.51	400	99	1
2	400	85	15
4.5	400	2	98
6.5	400	2	98
6.6	400	99	1
10	400	99	1

Table 1. Reverse phase liquid chromatography separation. The table depicts the gradient used for reverse phase liquid chromatography separation. Reverse Phase buffers- Buffer A: Water, 0.1% formic acid; Buffer B: Acetonitrile, 0.1% formic acid.

Time (min)	Flow µl/min	A (%)	B (%)
0	400	1	99
0.05	200	1	99
0.25	200	1	99
0.26	400	1	99
4	400	20	80
4.5	400	99	1
5.5	400	99	1
6	400	1	99
10	400	1	99

Table 2. HILIC separation. The table depicts the gradient used for HILIC separation. HILIC buffers- Buffer A: 5% acetonitrile, 95% water 1 mM ammonium acetate pH 9.0; Buffer B: 99% acetonitrile/ 1% water.

2.9. Quantitative real-time PCR.

CD8 T cells were sorted from splenocytes using flow cytometry and were used for RNA extraction and qPCR. 3-5 animals were pooled for isolation of every sample, and this was repeated 2-3 times. RNA extractions were conducted using standard TRIzol methodology following the manufacturer's instructions (Qiagen). Extracted RNA was quantified, diluted to a total of 2 μg, and synthesized into cDNA using Superscript II (Invitrogen, Burlington, ON). SsoAdvanced Universal SYBR Green Supermix (Biorad catalog no. 1708882) was used for qPCR and run on the BioRad CFX96 instrument for amplification and quantification. Gene-specific primers for murine *Ifna2*, *Ifnr1*, *Ifnr2* (type I interferon genes), *Nampt, Kynu, Kyat1, Qprt, Nmrk1, Nmnat1, Nmnat2, Nmnat3* (NAD+ synthesis genes)*, Gapdh,* and *Hprt* (housekeeping genes*)* were purchased from Invitrogen (Table 3). The data from the qPCR were collected and analyzed using Livak and Schmittgen's $2^{-\Delta\Delta CT}$ method (Livak and Schmittgen, 2001). The fold change was calculated by first normalizing the quantification cycle (Cq) of the indicated gene against *Gapdh* or *Hprt,* followed by comparison against the respective controls. Bar graphs were generated using GraphPad.

Gene name	Primer sequence	NCBI Accession
Ifnα2	F: CTGTGCTTTCCTCGTGATGCT R: AAAGGGGAGCCTCCTCATCTG	NM_010503.2
Ifnr1	F: GGTCATTACTGTCACCGCCA R: ACACAGTACACAGTCAGCGG	NM_010508.2
Ifnr2	F: AGAGAACAAGTCTGGCCCAC R: CACTATGACGATGGCGACGA	NM_010509.2
Nampt	F: ATGGTCATCTCCCGATTGAAGTAAA R: TTGGATACCAGGACTGAACAAGAAT	NM_021524.2
Kynu	F: CCTGCGTTAGTGGGATGGTT R: AGACCTCTAAACTGGCGTGC	NM_027552.3
Kyat1	F: ATCTAGGGCTCGGCCTCTTT R: CCTGAGTCCCACACACAGTT	NM_172404.3
Qprt	F: ACTGTGGTGAACACACTGAC R: GTTGTAGGGGGTAACAGGAGC	BC011191.1
Nmrk1	F: GTGTGATTTCCAAAGCCAGTTATGA R: GGCTTGAAGAAGTCATCCTGAGATA	NM_145497.2
Nmnat1	F: ACAATGGCTGGGCCTTTAGA R: ACATGCAACCCTCTGACAGC	NM_001356357.1
Nmnat2	F: TGTTCGAGAGAGCCAGGGAT R: GTGTCCTGATAGCACTCCCAT	BC089007.1
Nmnat3	F: ACGACAGAGTCAGATGGCTG R: ATATTCGTGATGGGGTTGAAGGAAC	NM_144533.3
Gapdh	F: GAGAGTGTTTCCTCGTCCCG R: ATGAAGGGGTCGTTGATGGC	NM_001289726.1
Hprt	F: CAGTCCCAGCGTCGTGATTA R: TGGCCTCCCATCTCCTTCAT	NM_013556.2

Table 3. Primer sequences for quantitative real-time PCR (qPCR). The table shows the forward and reverse primer sequences synthesized and used for qPCR with the accession number of each gene from NCBI.

2.10. Statistical analysis.

Depending on the indicated experiment, two-way ANOVA with Tukey/Sidak post-test or a two-tailed Student's *t*-test with a 95% confidence interval was used for statistical analysis, and *p* values of <0.05 were considered significant. Asterisks were used to signify *p* values as follows: not significant (ns) = $p > 0.05$; *$p < 0.05$; **$p < 0.01$; ***$p < 0.001$; **** $p < 0.0001$.

Chapter 3. Early bystander naive CD8 T cell activation relies on NAD^+ salvage metabolism upon virus exposure

3.1. Abstract

CD8 T cells play a central role in antiviral immunity. Type I interferons are among the earliest responders after virus exposure and can cause extensive reprogramming and antigen-independent bystander activation of CD8 T cells. Although bystander activation of pre-existing memory CD8 T cells has been acknowledged to play an important role in host defense and immunopathology, its impact on naïve CD8 T cells remains underappreciated. Here, we report that exposure to reovirus *in vivo* promotes induction of bystander naïve CD8 T cells within 24 hours. This distinct subtype of cells displays an innate, antiviral, type I interferon sensitized signature. The induction of bystander naïve CD8 T cells was shown to be STAT1 dependent. Finally, using metabolomics, we identified a role for the NAD^+ salvage pathway in the early induction of these bystander naïve CD8 T cells.

3.2. Background

CD8 T cells are an important arm of cellular immunity to viruses and are responsible for identifying and eliminating virus-infected cells during the adaptive phase of the immune response. Following virus exposure, T cells can be activated by TCR-dependent and -independent mechanisms. Upon TCR engagement, T cells rapidly change thier phenotype, become CD44hi, and are known as differentiated T cells (Hwang et al., 2020). In TCR-independent activation, known as bystander activation, cytokines play an important role in the activation of effector functions in pre-existing memory T cells. Specifically, cytokines like IL-15 and IL-18 can drive antigen-independent IFN-γ secretion or cytolytic activity via NKG2D in non-specific, pre-existing memory T cells (Kim and Shin, 2019; Lee et al., 2022). Naïve CD8 T cells can also undergo bystander activation because of their presence in an inflammatory milieu. The impact of cytokine-driven bystander activation in naïve CD8 T cells, however, is not well understood. Notably, naïve CD8 T cells from patients with chronic HCV infection demonstrate hyperactivation and acquire a memory-like phenotype (Alanio et al., 2015). Interestingly, a recent study in mice reported that infection, as well as inflammation, driven by cohousing of laboratory mice with pet store mice can activate naïve CD8 T cells in a bystander manner and impact their homeostasis and function (Jergović et al., 2021). Type I interferons are often promptly produced after virus exposure, and some viruses, like SARS-CoV2, can drive severe disease by dysregulation and delay of host type I interferon production (Acharya et al., 2020; Lee and Shin, 2020). Exposure of naïve CD8 T cells to type I interferons can also drive rapid acquisition of effector function upon antigenic stimulation (Marshall et al., 2010; Urban et al., 2016). The

complex interplay between naïve CD8 T cells and type I interferons during bystander activation *early on* following virus exposure remains poorly understood.

Recent advances in immunometabolism have indicated that T cell function is also closely linked with metabolism (Biase et al., 2019; Menk et al., 2018). Virus exposure as well as type I interferons have been reported to cause metabolic restructuring in immune cells (Ayres, 2020; Wu et al., 2016). While most studies in the area of T cell immunometabolism have focussed on effector and memory T cell subsets (Buck et al., 2017; Klein Geltink et al., 2018), very little is known about the metabolic reprogramming that occurs within naïve CD8 T cells immediately following virus exposure. Several studies have demonstrated a connection between NAD^+, a substrate and redox cofactor for several important metabolic pathways, and the function of T cells (Yoshino et al., 2018). For example, intracellular NAD^+ acts as an essential cofactor for glycolysis, and glycolytic flux is well known to mediate effector vs memory function in T cells (Beier et al., 2018). Also, the activity of NAD^+-dependent deacetylase SIRT1 has been shown to promote the formation of memory T cells (Jeng et al., 2018). Further, extracellular NAD^+ promotes immune response through receptor-mediated downregulation of regulatory T cell populations (Hubert et al., 2010). Similarly, tumor CD38-mediated breakdown of extracellular NAD^+ promotes T cell exhaustion in tumor microenvironments (Chatterjee et al., 2018). As a result, therapeutic modulation of NAD^+ levels has been implemented to control T cell function in several disorders, including, autoimmune conditions like graft versus host disease (GVHD) (Gerner et al., 2020) and experimental allergic encephalomyelitis (EAE) (Bruzzone et al., 2009; Tullius et al., 2014). However, the implications for NAD^+ metabolism in the context of antiviral CD8 T cell immunity remain relatively unknown.

In the present study, using a combination of flow cytometry, quantitative proteomics, metabolomics, and pharmacological inhibition approaches within *in vivo* and *in vitro* settings, we report an NAD^+ salvage-dependent, type I interferon-driven induction of bystander naïve CD8 T cells (CD8 bT_N) within 24 hours of virus exposure. Given the importance of bystander activation and the early determinants of antiviral adaptive immunity, this study highlights underappreciated consequences of type I interferon-mediated metabolic reprogramming of naïve CD8 T cells immediately after exposure to viruses.

3.3. Results

3.3.1. Development of a 16-parameter flow cytometry panel to identify different CD8 T cell subsets after exposure to reovirus

To identify and characterize CD8 T cells and their different subsets, as well as various activation markers on their cell surface, we developed a flow cytometry panel as described in Table 4 and Table 5. The gating strategy (Fig. 3.1) was developed by first gating on live cells that are negative for the viability dye. Next, within live cells, doublets were gated out on forward scatter- area (FSC-A) versus forward scatter- height (FSC-H). On a sequentially gated plot for FSC-A versus side scatter-area (SSC-A), lymphocytes were gated on. Within the lymphocyte population, cells were gated for CD3+CD8+ T cells, which were further gated on CD44 and CD62L to identify different T cell subsets. CD44lowCD62L+ cells were classified as the P1 population or naïve T cells (T_N), CD44hiCD62L+ cells as the P2 population or central memory T cells (T_{CM}), and CD44hiCD62L- cells as P3 cells or effector memory T cells (T_{EM}). Finally, CD44lowCD62Llow cells were also identified as P4 cells and are discussed further in Chapter 4.

Marker	Role
Fixable viability dye	Gating for live cells
Forward Scatter	Gating according to size; doublet discrimination; gating on lymphocytes
Side Scatter	Gating according to granularity; doublet discrimination; gating on lymphocytes
CD3	Identification of T cells
CD8	Identification of T cells
CD44	Adhesion molecule
CD62L	Selectin molecule
Sca-1	Bystander activation marker
Ly6C	Bystander activation marker
CD69	TCR-mediated activation marker
KLRG1	TCR-mediated activation marker
CD25	TCR-mediated activation marker
CD49d	TCR-mediated activation marker
CD127	IL-7 Receptor
CD122	IL-2 Receptor β
PD-1	Activation molecule

Table 4. Development of T cell flow cytometry panel. A flow cytometry panel with different markers for the identification of T cell subsets as well as the role of those markers is described above.

			Fortessa	
Lasers	**Filters**	**Marker**	**Clone**	**Fluorochrome**
Violet Laser (407nm)	783/40	Ly6C		BV786
	750/20			
	710/40	CD44		BV711
	660/20	CD62L		BV650
	605/30	PD-1		BV605
	575/36			
	525/50	KLRG1		BV510
	440/40	CD122		BV421
Blue Laser (488)	710/50	CD8a		PerCP-Cy5.5
	515/20	CD3e		FITC
Green Laser (532)	780/40	CD69		PE-Cy7
	710/50			PE Cy5.5
	660/40			
	610/20	CD127		PE-CF594
	575/25	CD49d		PE
Red Laser (640)	780/60	Live/Dead		FVS780
	730/45	CD25		R718
	670/30	Sca-1		AF647

Table 5. Marker and fluorophore combination for flow cytometry instrument. The T cell flow cytometry panel with corresponding fluorochrome and the filter/detector set which captures its emission is shown above.

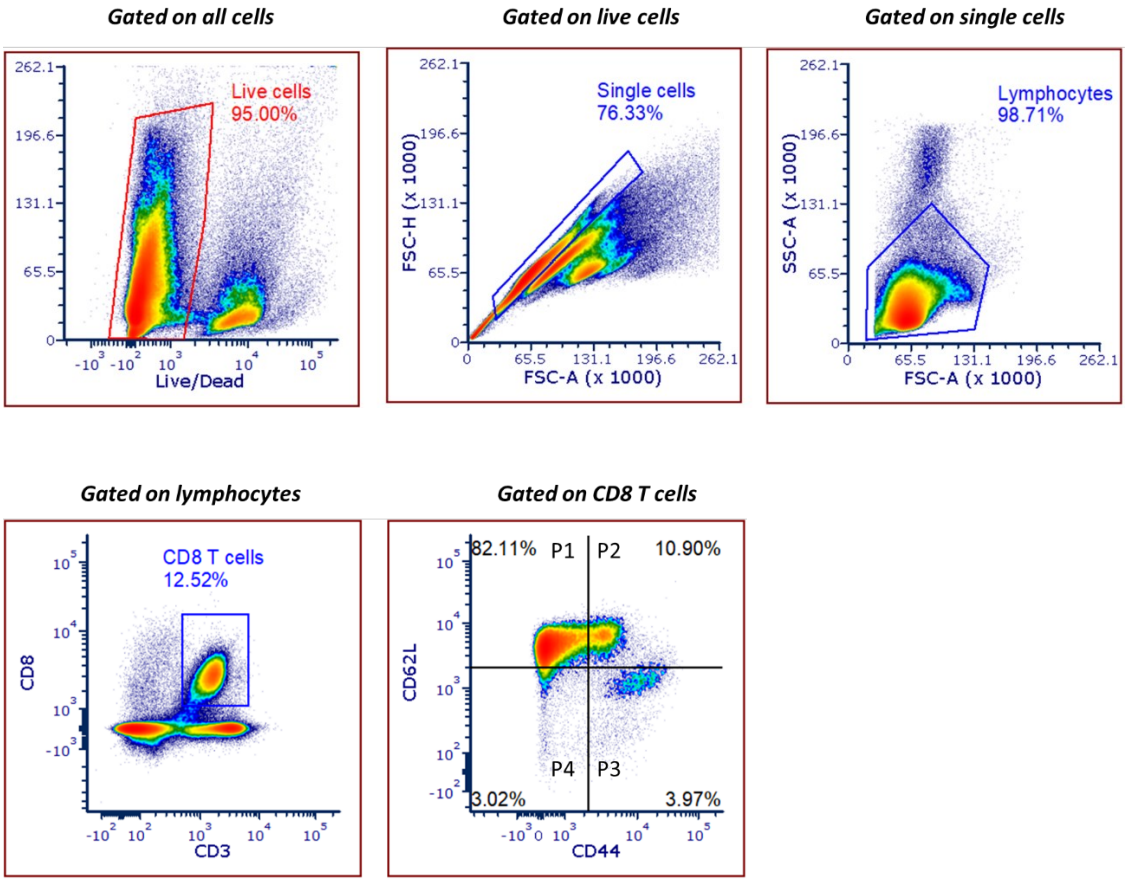

<u>Fig. 3.1:</u> Gating strategy for CD8 T cell subsets. Identification of different P1 (naïve), P2 (central memory), P3 (effector memory), and P4 populations has been shown above with prior gating on live cells, single cells, lymphocytes, and CD3+CD8+ T cells.

3.3.2. Bystander activation of naïve CD8 T cells within 24 hours of reovirus exposure *in vivo*

To identify and characterize the earliest changes in CD8 T cells upon virus exposure, we injected C57BL/6 mice with reovirus intraperitoneally and focused on an early timepoint of changes that occur 1-day post-injection with reovirus. Further, since the naïve CD8 T cell population represents unstimulated T cells and forms the majority population in non-treated C57BL/6 mice, we investigated the earliest changes within this subset of T cells after reovirus exposure. A UMAP displaying T_N cells in non-treated mice and reovirus-treated mice 1-day post-injection is shown in Fig 3.2A. One of the earliest phenotypic changes in naïve CD8 T cells that we observed upon reovirus exposure was the upregulation of markers like Ly6C and Sca-1 (Fig. 3.2B).

The Ly6 family of proteins like Ly6C and Ly6A/E (Sca-1) are important early indicators of bystander activation (DeLong et al., 2018; Jergović et al., 2021). Ly6C has been used recently to identify bystander-activated naïve CD8 T cells after microbial infection. Sca-1, as opposed to Ly6C, was observed to be *uniquely* upregulated on virus-exposed naïve CD8 T cells and not in T cells from non-treated spleens and was hence, used as a marker to identify bystander naïve CD8 T cells (CD8 bT_N cells). Since CD8 T cells still maintained naive (CD44lowCD62L+) phenotype, it was unlikely that the increase in Sca-1 and Ly6C expression was due to TCR triggering. However, to confirm this, we measured the expression of CD69, CD25, KLRG1, and CD49d. Upregulation of these markers is indicative of T cell activation via TCR triggering. Naïve CD8 T cells failed to upregulate any of these markers within 24 hours after virus exposure confirming that they were indeed activated in a bystander manner (Fig. 3.2C).

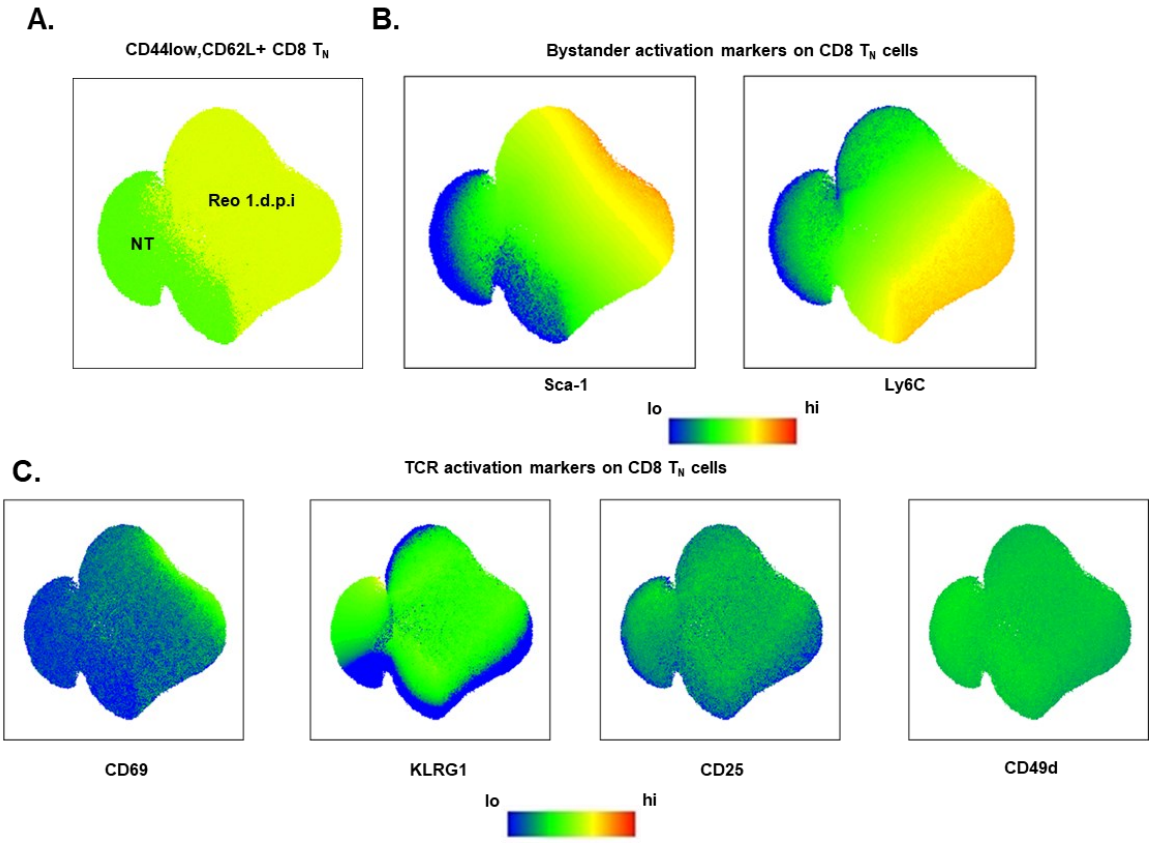

Fig. 3.2: Reovirus induces early bystander-activated naïve CD8 T cells *in vivo* **A.** UMAP showing CD8 T_N cells in non-treated (NT) and reovirus treated (Reo 1 d.p.i.) C57BL/6 splenocytes. **B.** UMAP depicting bystander activation markers Sca-1 and Ly6C in CD8 T_N cells. **C.** UMAP represents TCR activation markers CD69, KLRG1, CD25, and CD49d in CD8 T_N cells. (n=9; NT-3, Reo 1 d.p.i.-6 in all UMAP plots).

Expression of bystander markers Sca-1 and Ly6C as well as markers of TCR-dependent activation were also investigated on total CD8 T cells to compare how they differed from expression on naive CD8 T cells (Fig.3.3). Ly6C and Sca-1 were upregulated on total CD8 T cells similar to naïve CD8 T cells (Fig.3.3B). Some upregulation in KLRG1 and CD25 was also visible in the UMAP (Fig.3.4C-yellow region).

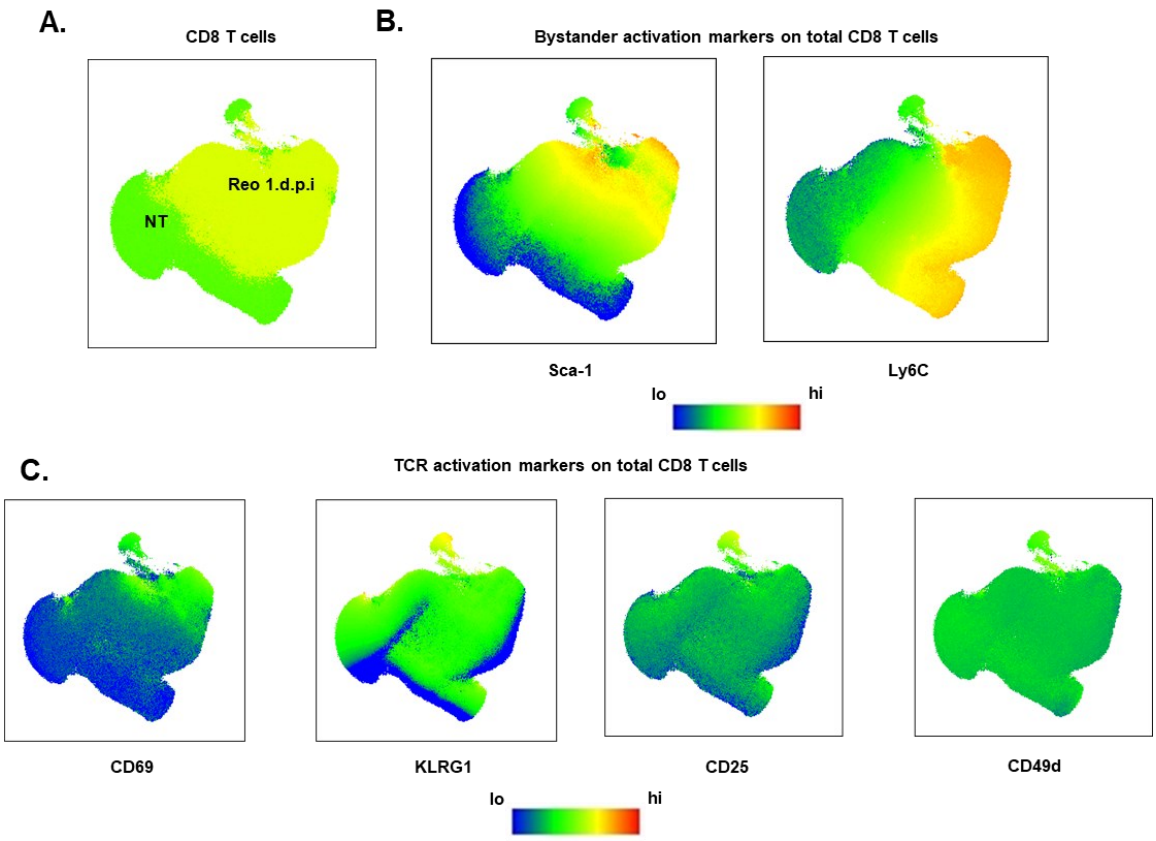

Fig. 3.3: T cell activation markers on CD8 T cells. **A.** UMAP showing total CD8 T cells in non-treated (NT) and reovirus treated (Reo 1 d.p.i.) C57BL/6 splenocytes. **B.** UMAP depicting bystander activation markers Sca-1 and Ly6C on all CD8 T cells. **C.** UMAP represents TCR activation markers CD69, KLRG1, CD25, and CD49d on all CD8 T cells. (n=9; NT-3, Reo 1 d.p.i.-6 in all UMAP plots).

3.3.3. Induction of bT_N cells at different sites over time after reovirus exposure

Next, we investigated if CD8 bT_N cells were induced at different sites after *in vivo* reovirus exposure and, if so, how long they were maintained at these different sites. We discovered that in the spleen, CD8 bT_N cells were induced on 1 d.p.i. and a significant percentage of CD8 bT_N cells was maintained on 3 d.p.i. On 7 d.p.i., the percentage of CD8 bT_N cells was reduced and a significant percentage of CD8 T_{EM} cells was observed. However, at this time point, an almost equal percentage of CD8 bT_N cells was maintained in the spleen (Fig. 3.4A).

In the mesenteric lymph nodes (MLN), CD8 bT_N cells were induced robustly on 1 d.p.i. and were maintained at high frequency on 3 d.p.i. as well as on 7 d.p.i. (Fig. 3.4B). In the peritoneal flush, which contains cells obtained from the site of infection, CD8 bT_N cells were induced on 1 d.p.i along with other cell types. The percentage of CD8 bT_N cells was not as high as at the other sites and these cells also progressively reduced in numbers at 3 d.p.i. and 7 d.p.i. (Fig. 3.5C).

Taken together, this data demonstrated that CD8 bT_N cells were induced at multiple different sites after reovirus exposure, albeit at different frequencies. They were also maintained differentially at the different sites over time following virus exposure. This suggests that their role at different sites and persistence over time may be context-dependent after virus exposure.

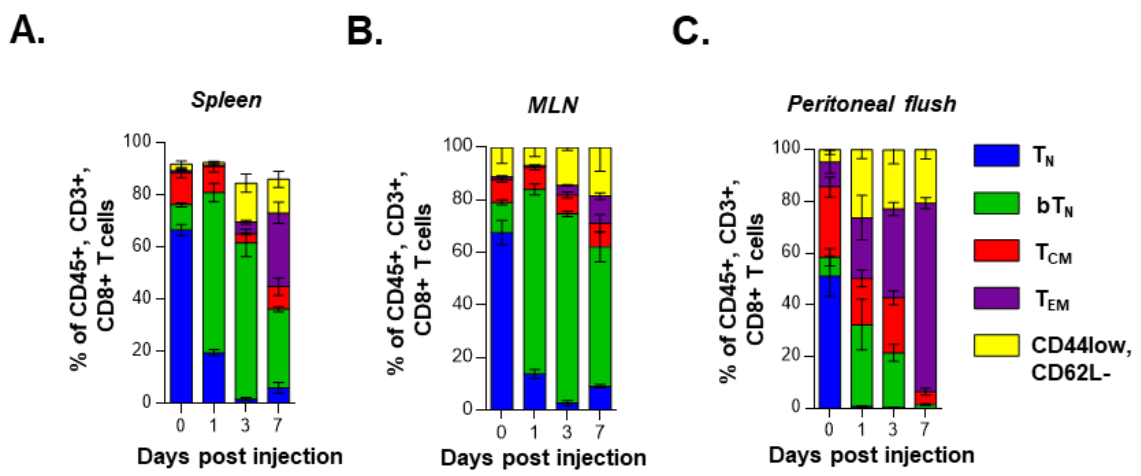

<u>Fig. 3.4:</u> Induction of CD8 bT_N cells in the spleen, and PC after reovirus exposure. Bar graphs depicting the induction of T_N, bT_N , T_{CM}, T_{EM} and CD44lowCD62Llow CD8 T cells in **A.** spleen, **B.** mesenteric lymph node (MLN), and **C.** peritoneal flush on days 1, 3, and 7 after injection of reovirus (n=3 each).

3.3.4. CD8 bT_N cells are induced in mice with different backgrounds and genotypes upon exposure to reovirus

Next, we wanted to investigate whether the induction of CD8 bT_N cells was dependent on the mouse background. For this purpose, we injected BALB/c mice with reovirus and observed that a robust CD8 bT_N cell response was induced on 1 d.p.i (Fig.3.5A). This demonstrated that the induction of CD8 bT_N cells was independent of the mouse background.

Now, since reovirus is a dsRNA virus, we sought to understand whether dsRNA sensing molecules like TLR3 have a role to play in the induction of CD8 bT_N cells. For this purpose, we injected TLR3 knockout (KO) mice with reovirus and studied the induction of CD8 bT_N cells. We observed that CD8 bT_N cells were induced robustly even in TLR3 KO mice after exposure to reovirus (Fig.3.5B). Next, we looked at whether CD8 bT_N cells were induced in CCR2 KO mice since CCR2 is an important pro-inflammatory mediator for CD8 T cells during the immune response to viruses. We discovered that CD8 bT_N cells were robustly induced in CCR2 KO mice as well on 1 d.p.i. (Fig. 3.5C).

Finally, PD-1 is an important checkpoint inhibitor that has not only been shown to be important during chronic virus exposure but also acute virus infection. We employed PD-1 KO mice to test whether the induction of CD8 bT_N cells was affected in these mice. We discovered that higher numbers of CD8 bT_N cells were present in PD-1 KO mice even without exposure to the virus (Fig. 3.5D). PD-1 KO mice have been shown to have increased immune cell infiltration in different disease models including sepsis (Keir et al., 2007, p. 1), and have also been shown to have increased susceptibility to certain pathogens

(Lázár-Molnár et al., 2010, p. 1). Previous studies have shown that even simple co-housing of mice can lead to bystander activation of naïve CD8 T cells (Jergović et al., 2021). Since these mice were not maintained in sterile conditions, they may have bystander activation because of their housing conditions which would explain the increased percentage of CD8 bT_N cells even in non-treated animals. The percentage of CD8 bT_N cells was seen to be increased further upon exposure to reovirus at 1 d.p.i. (Fig. 3.5D).

Taken together, these data suggest that the induction of CD8 bT_N cells is independent of mouse background and also occurs in a TLR3-independent manner. The absence of pro-inflammatory molecules like CCR2 does not affect CD8 bT_N cell induction and neither does PD-1.

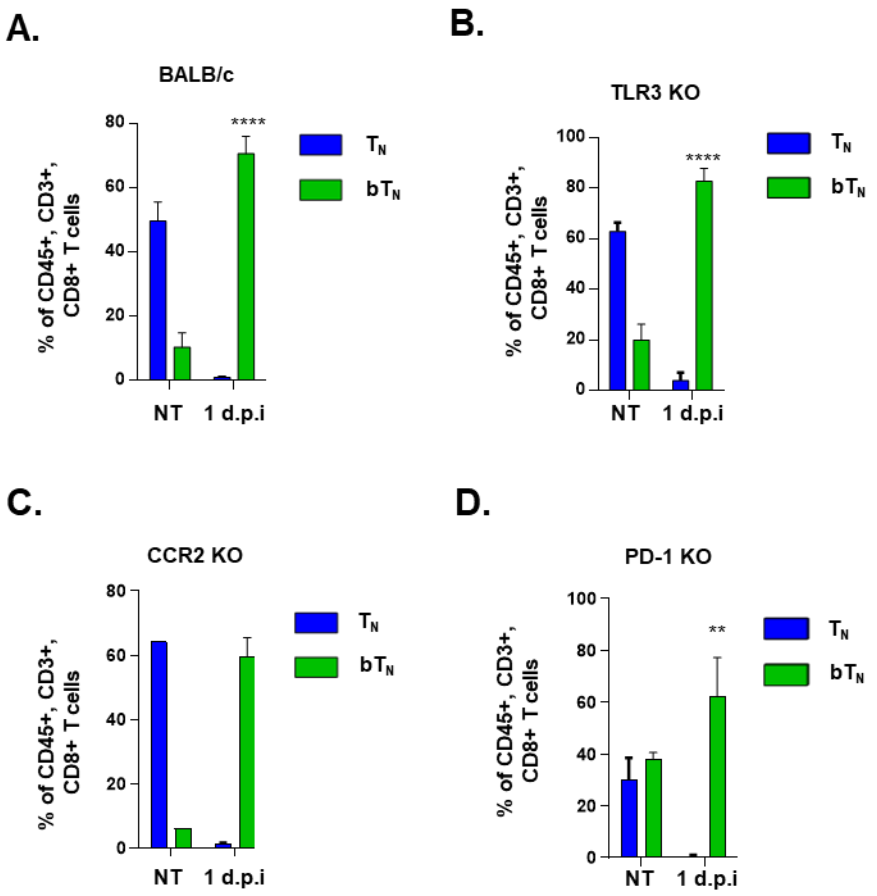

<u>Fig. 3.5:</u> Induction of CD8 bT_N cells in mice from different backgrounds or genotypes. Bar graphs depict the induction of CD8 bT_N cells upon exposure to reovirus in vivo in **A.** Balb/c mice (n=3 each) **B.** TLR3 knockout mice (NT- n=3; 1 d.p.i. n=5) **C.** CCR2 knockout mice (NT- n=1; 1 d.p.i. n=5) and **D.** PD-1 knockout mice (NT- n=3; 1 d.p.i. n=5). Two-way ANOVA with Sidak's multiple comparisons test and 95% confidence interval was used for statistical analysis. Significance has been indicated for CD8 bT_N cells in 1 d.p.i. versus non-treated conditions. Not significant (ns) = $p > 0.05$; *$p < 0.05$; **$p < 0.01$; ***$p < 0.001$; **** $p < 0.0001$.

3.3.5. Induction of CD8 bT_N cells *ex vivo* and IFN-γ production

Next, we wanted to develop a system to induce and modulate CD8 bT_N cells *ex vivo*. To this end, we isolated C57BL/6 mice splenocytes and treated them with varying concentrations of reovirus for 24 hours in cell culture *ex vivo*. We then processed the samples for flow cytometry analysis of the CD8 T cell subsets. We observed that a robust induction of bT_N cells occurred in a dose-dependent manner (Fig.3.6A).

To assess the functionality of bT_N cells, we employed the OT-1 mouse model. OT-1 splenocytes were similarly isolated and exposed to reovirus in cell culture for 18 hours, followed by priming with ova peptide for 6 hours. We then processed the samples for identification of T cells and intracellular staining for IFN-γ cytokine production. We observed that upon treatment with ova peptide an IFN-γ response was induced in the OT-1 T cells as expected (Fig. 3.6B). However, upon treatment with reovirus for 18 hours before peptide stimulation, an increase in the percentage of IFN-γ+ CD8 T cells was seen (Fig. 3.6B). This suggested that bystander activation of naïve CD8 T cells by reovirus enhanced functional capabilities via IFN-γ production upon priming with antigen.

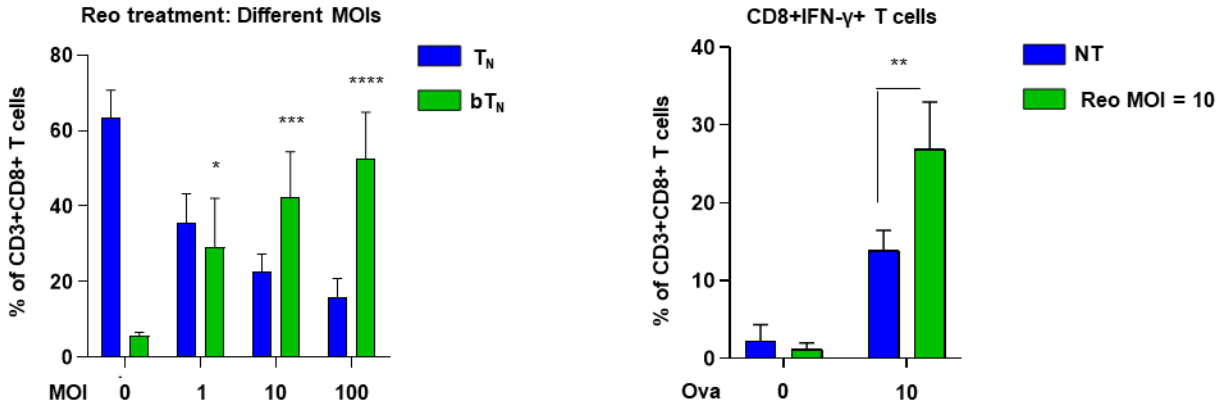

<u>Fig. 3.6:</u> Induction of CD8 bT_N cells and IFN-γ production *ex vivo*. A. Bar graphs showing the induction of CD8 bT_N cells upon *ex vivo* exposure of C57BL/6 splenocytes to varying MoIs of reovirus in cell culture (n=3). **B.** Bar graphs for % of CD8+IFN-γ+ T cells in OT-1 splenocytes after *ex vivo* treatment with reovirus for 18h followed by stimulation with ova for 6h (n=3). Two-way ANOVA with a 95% confidence interval was used for statistical analysis in bar graphs. Significance has been indicated only for CD8 bT_N cell populations induced within 24 hours in comparison with untreated control population levels. Not significant (ns) = $p > 0.05$; *$p < 0.05$; **$p < 0.01$; ***$p < 0.001$; **** $p < 0.0001$.

3.3.6. Quantitative *in vivo* multiplexed proteomic analysis of CD8 T cell subsets after reovirus exposure

To investigate the molecular networks that drive the induction of CD8 bT_N cells, we decided to perform quantitative multiplex proteomics on CD8 bT_N cells and other CD8 T cell subsets. To this end, we first sorted out the chosen CD8 T cell subsets via flow cytometry before processing for proteomics, as described in Chapter 2. Specifically, pure populations of CD8 T_N cells, bT_N cells (Day 1), bT_N cells (Day 7), and T_{EM} cells (Day 7) were isolated from C57BL/6 splenocytes using flow cytometry and were digested, labeled with TMT, pooled, and processed for mass spectrometry-based proteome profiling as depicted in the schematic (Fig. 3.7A). A heatmap representing 4718 proteins identified by the proteomic analysis shows these proteins grouped into various clusters by K-means clustering across the tested T cell types (Fig.3.7B). Clusters 1, 2, 8, 9, 10 represent proteins that appear to be upregulated in T_{EM} cells (Day 7). Cluster 3 shows proteins that are upregulated in bT_N cells (Day 1) while clusters 4 and 5 depict proteins that appear to be downregulated in T_{EM} cells (Day 7). Clusters 6 and 7 do not seem to have a noticeable trend in any one cell type. The top 2 hits from each of the clusters after GO term analysis for biological function have been listed in Table 6.

A.

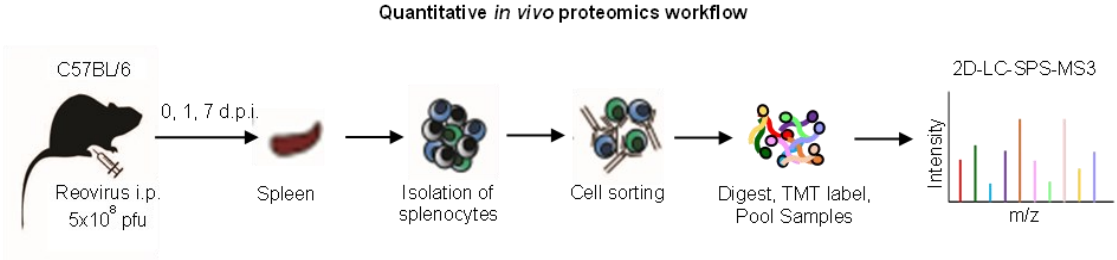
Quantitative *in vivo* proteomics workflow
C57BL/6
Reovirus i.p.
5x10^8 pfu
0, 1, 7 d.p.i.
Spleen
Isolation of splenocytes
Cell sorting
Digest, TMT label, Pool Samples
2D-LC-SPS-MS3
Intensity
m/z

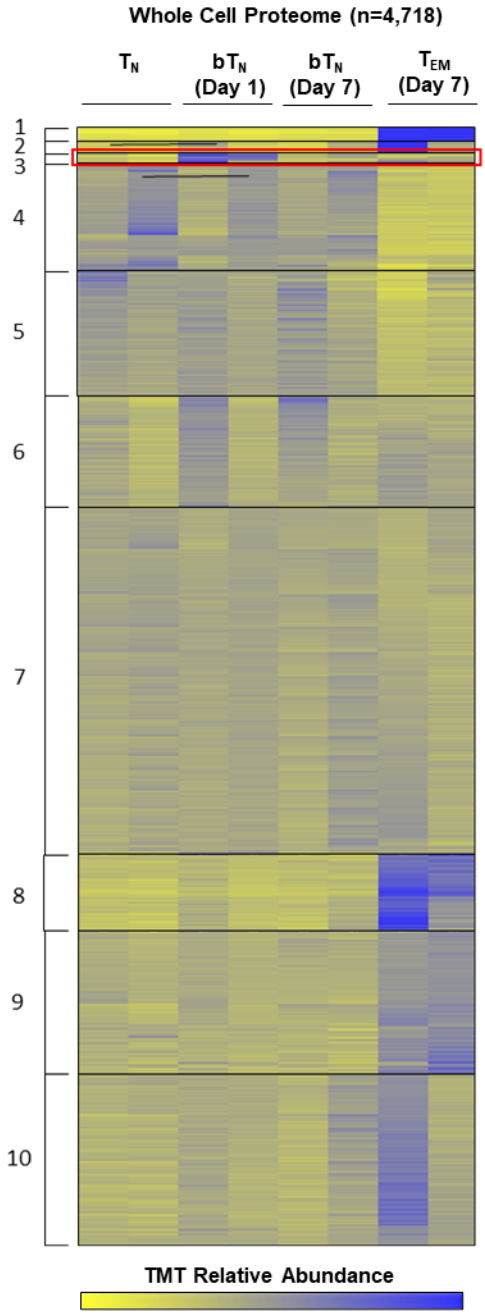
Whole Cell Proteome (n=4,718)
T_N
bT_N (Day 1)
bT_N (Day 7)
T_{EM} (Day 7)
1
2
3
4
5
6
7
8
9
10
TMT Relative Abundance

<u>Fig. 3.7:</u> Quantitative *in vivo* proteomic analysis of CD8 bT_N cells. A. Schematic for the workflow of quantitative *in vivo* proteomics with T cells isolated from spleens of C57BL/6 mice (n=5 pooled for each cell type). **B.** Heatmap for the whole cell proteome of 4 different subsets of T cells. Naïve CD8 T cells- T_N, bystander naïve CD8 T cells 1 day post injection- CD8 bT_N (1 d.p.i.), bystander naïve CD8 T cells 7 days post injection- CD8 bT_N (7 d.p.i.) and effector CD8 T cells 7 days post injection- T_{EM} (7 d.p.i.).

Cluster:	Gene-Ontology: Biological Function	Proteins/ Term	Benjamini Value:
1	DNA Replication	8	5.20E-05
	Cell Cycle	13	9.20E-05
2	Protein Transport	7	9.90E-01
	Endocytosis	4	9.80E-01
3	Defense Response to Virus	9	1.50E-07
	Innate Immune System	9	4.20E-05
4	rRNA Processing	23	4.60E-11
	Ribosome Biogenesis	17	5.00E-08
5	Oxidation-Reduction Process	51	3.10E-08
	Metabolic Process	35	3.90E-05
6	Antigen Processing and Presentation via MHC Class I	12	4.30E-08
	Proteolysis Involved in Cellular Protein Catabolism	12	4.20E-05
7	mRNA Processing	119	9.70E-51
	RNA Splicing	97	9.70E-45
8	DNA Replication	14	4.60E-05
	Cell Cycle	29	7.70E-05
9	Translation	45	4.50E-11
	Protein Folding	23	1.50E-08
10	Protein Transport	66	3.40E-14
	Translation Initiation	14	1.40E-05

Table 6. K-means clustering summary. The table depicts the different clusters, the top two hits for each cluster after Gene Ontology (GO) term analysis for biological function as well as the number of proteins in each term with the corresponding Benjamini value.

3.3.7. Proteomic analysis reveals CD8 bT_N cells have altered functional capabilities

Within the proteomic dataset, we first investigated the functional signatures of CD8 bTN cells. Upon comparing bT_N cells on Day 1 and Day 7, we discovered that bT_N cells on Day 7 had increased granzyme K expression (Fig. 3.8A). Further, compared with the other dominant population on Day 7- TEM cells- bT_N cells had increased expression of memory markers TCF7 and FOXO1 (Fig. 2.8B). Using flow cytometry, we also noted that bT_N cells on Day 7 were mostly positive for CD127 expression as compared to effector memory T cells that include distinct CD127+ and CD127- populations (Fig. 3.8C) that are known to comprise memory precursors and short-lived effectors, respectively (Chng et al., 2019; Rivadeneira et al., 2019; Youngblood et al., 2017). Taken together with our previous data indicating increased IFN-γ production in OT-1 splenocytes after exposure to reovirus (Fig. 3.6B) suggests that CD8 bT_N cells bear distinct proteome changes accompanying alerted functional capabilities.

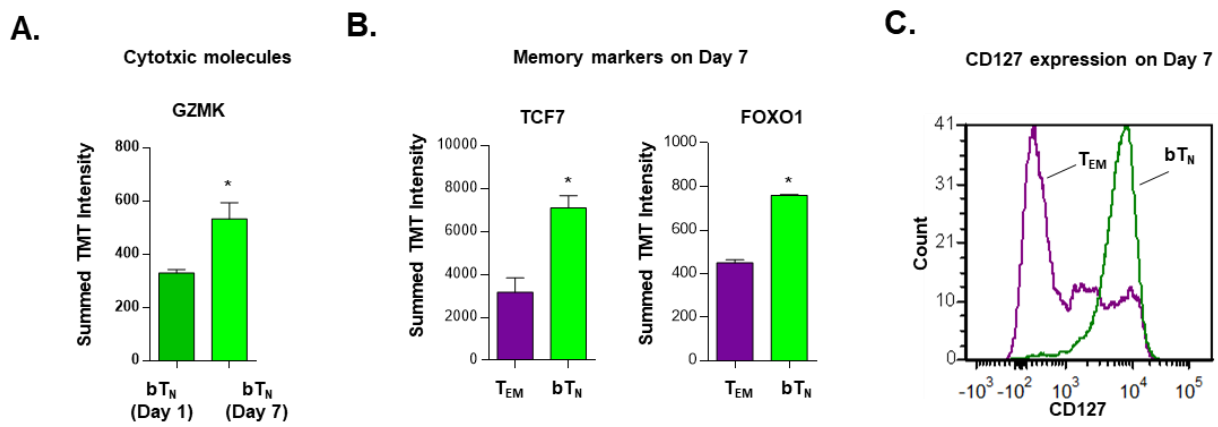

Fig. 3.8: Functional proteomic signatures in CD8 bT_N cells. A. Bar graph for protein expression from quantitative proteomics of granzyme K expression in CD8 bT_N cells (1 d.p.i. and 7 d.p.i.). **B.** Bar graphs for protein expression from quantitative proteomics of memory markers TCF7 and FOXO1 expression in T_{EM} cells (7 d.p.i.) and CD8 bT_N cells (7 d.p.i.). **C.** Histogram overlay for memory marker CD127 in T_{EM} cells (7 d.p.i.) and CD8 bT_N cells (7 d.p.i.). Two-tailed Student's *t*-test with a 95% confidence interval was used for statistical analysis. Not significant (ns) = $p > 0.05$; *$p < 0.05$; **$p < 0.01$; ***$p < 0.001$; **** $p < 0.0001$.

3.3.8. CD8 bT_N cells have an innate anti-viral proteomic signature

To get an insight into the molecular signature of early induced CD8 bT_N cells and understand how they differed from T_N cells within 24 hours of virus exposure, we next focussed our analysis of the proteomic data from these two groups of cells. We identified proteins that were significantly changed (at least 2-fold) between them (Fig. 3.9A). From among the K-means clusters described earlier, cluster 3 represents proteins that are upregulated in CD8 bT_N cells when compared to T_N cells. Gene Ontology (GO) term analysis for proteins in this cluster revealed differential expression of proteins related to defense response to the virus, innate immune response, type I interferon, and purine biosynthesis (Fig. 3.9B). The type I interferon pathway is a major pathway associated with viral defense and type I interferon sensitization in CD8 T cells has important functional and phenotypic consequences (Kolumam et al., 2005; Marshall et al., 2010; Urban et al., 2016). Hence, we focussed our attention on the molecular differences within this pathway in CD8 bT_N cells. We observed that levels of interferon-driven proteins like the IFIT family, ZBP1, BST2, ADAR, IFI35, and EIF2AK2 were upregulated in CD8 bT_N cells (Fig. 3.9C).

As mentioned previously, the induction of CD8 bT_N cells after reovirus exposure was observed to be independent of TLR3 signaling (Fig. 3.5B), however, among the proteins related to defense response to the virus and innate immune response, RIG-I-related proteins were upregulated in CD8 bT_N cells (Fig. 3.10A). Along with TLR3, RIG-I is also involved in dsRNA recognition and regulation of immune responses (Saito et al., 2007).

Taken together, these data demonstrated a clear signature of type I interferon sensitization, a characteristic event driven during virus recognition, in CD8 bT_N cells and an innate anti-viral proteomic gene signature in these cells.

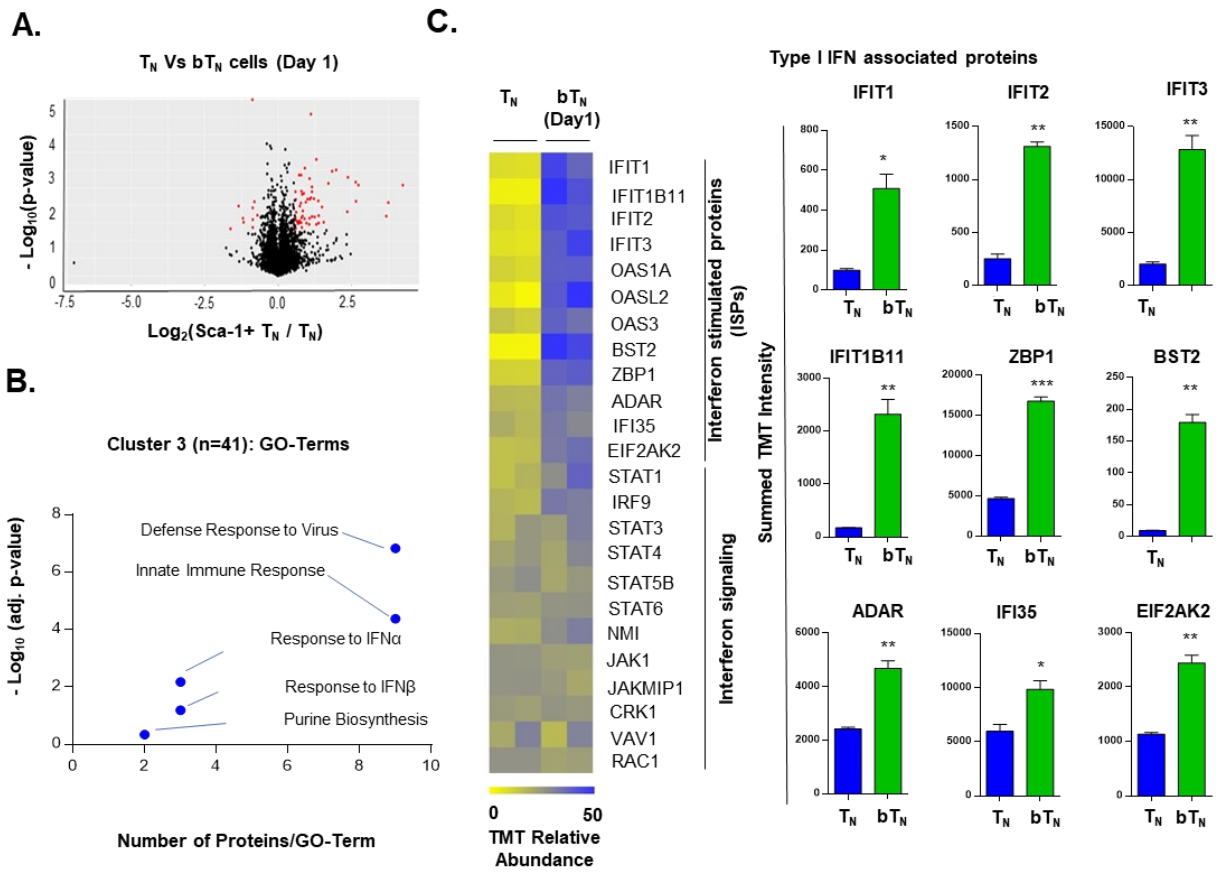

Fig. 3.9: Innate anti-viral proteomic signature of CD8 bT$_N$ after 24 hours of reovirus exposure *in vivo*. A. Volcano plot compares all identified proteins across CD8 T$_N$ and CD8 bT$_N$ cells (1 d.p.i.). **B.** Cluster 3 of GO TERM analysis of proteomics depicting differentially regulated pathways in CD8 bT$_N$ cells compared to T$_N$ cells. **C.** Heatmap for the relative levels of interferon-stimulated proteins and interferon signaling proteins identified in T$_N$ and CD8 bT$_N$ cells (1 d.p.i.). Corresponding bar graphs show the levels of several type I interferon-associated proteins in T$_N$ and CD8 bT$_N$ cells. Two-tailed Student's *t*-test with a 95% confidence interval was used for statistical analysis. Not significant (ns) = $p > 0.05$; *$p < 0.05$; **$p < 0.01$; ***$p < 0.001$; **** $p < 0.0001$.

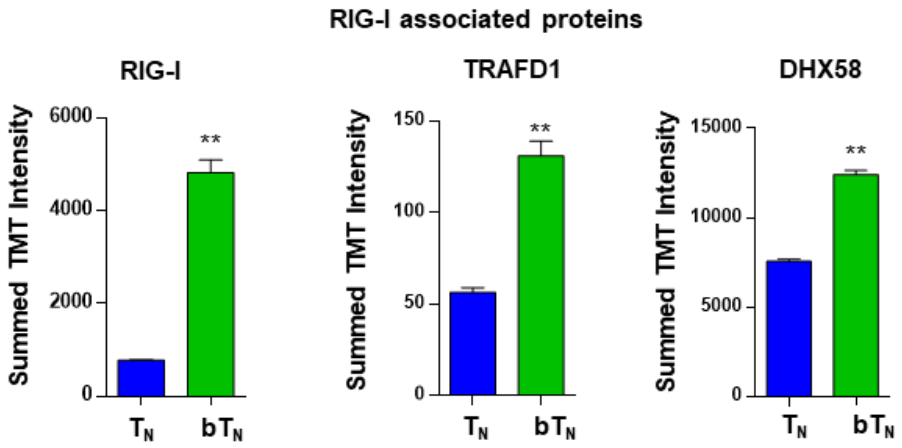

<u>Fig. 3.10:</u> RIG-I associated protein signatures in CD8 bTN cells after 24 hours of reovirus exposure *in vivo.* Bar graphs for RIG-I associated proteins in CD8 T_N and CD8 bT_N cells (1 d.p.i.). Two-tailed student t-test was used for statistical analysis. Not significant (ns) = $p > 0.05$; *$p < 0.05$; **$p < 0.01$; ***$p < 0.001$; **** $p < 0.0001$.

3.3.9. Antiviral type I interferons induce CD8 bT_N cells in a STAT1-dependent manner

Next, to further investigate the role of type I interferons in the induction of bT_N cells, we first confirmed that an increased level of type I interferon was observed in the spleen of mice exposed to reovirus (Fig. 3.12 A). Hence, we next asked if type I interferons might be able to directly drive the induction of bT_N cells without reovirus. To test this, we treated *ex vivo* isolated C57BL/6 splenocytes with exogenous IFN-α1 and IFN-β1. Both treatments induced a robust, dose-dependent induction of bT_N cells (Fig. 3.11 A, B respectively). We further tested whether type I interferon signaling had a role to play in the induction of bT_N cells. Using quantitative PCR, we noted that the levels of *Ifnar1* and *Ifnar2* remained unchanged in splenocytes on day 1 after treatment of mice with reovirus (Fig. 3.12 B). We proceeded to block the IFNAR1 receptor with a blocking antibody during the treatment of splenocytes with reovirus *ex vivo*. This led to the abolishment of bT_N cell induction (Fig. 3.11C). Within the type I interferon signaling pathway, the ISGF3 (STAT1-STAT2-IRF9) complex forms an important regulator of type I interferon signaling in cells (Fu et al., 1990). Although signaling proteins in other type I interferon signaling pathways remained unchanged (Fig. 3.12C, lower half of heatmap), IRF9 of the ISGF3 complex was significantly upregulated in bT_N cells (Fig. 3.11D). In the proteomics data, all the STATs, except STAT2, were identified and STAT1 levels were found to be increased, albeit not to significant levels (Fig. 3.12D). Nonetheless, given the importance of STATs in response to type I interferons and the upregulation of IRF9 of the ISGF3 complex in the proteomics data, we decided to test the induction of bT_N cells in STAT1 KO mice. Reovirus failed to induce bT_N cells in splenocytes isolated from STAT1 KO mice (Fig. 3.11E). Similar results

were also observed with type I interferons, wherein no induction of bT_N cells was observed with IFN-α1 and IFN-β1 (Fig. 3.11F). In addition, it should be noted that our model of STAT1 KO mice also had a SLAM knock-in. SLAM or CD150 is a receptor for the measles virus, and this model was previously designed for the study of measles infection (Hsu et al., 2001). To confirm that the lack of induction of bT_N cells in the STAT1 KO mice was not a result of SLAM knock-in, we tested splenocytes from SLAM knock-in only control mice and found robustly induced bT_N cells following treatment with reovirus and IFN-β1 (Fig. 3.12D). Altogether, these data conclusively demonstrate a role for type I interferon signaling in the induction of bT_N cells and provide evidence that this induction occurs in a STAT1-dependent manner.

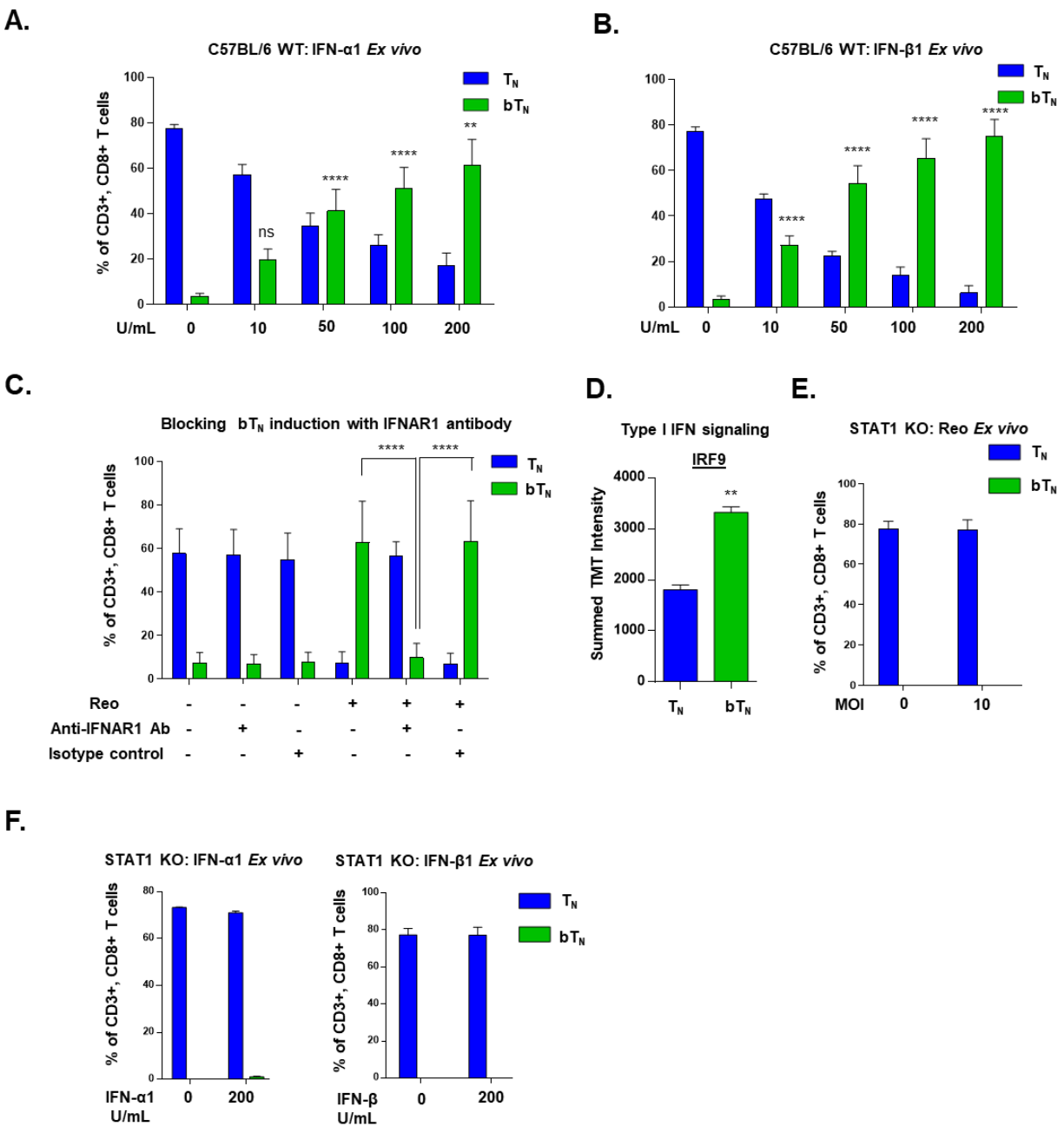

<u>Fig. 3.11:</u> Induction of CD8 bT$_N$ cells occurs in a type 1 interferon and STAT-1 dependent manner. Bar graphs showing induction of CD8 bT$_N$ cells upon *ex vivo* treatment of splenocytes from C57BL/6 mice with **A.** varying concentrations of IFN-α1 from 10 U/mL- 200 U/mL (n=3), **B.** varying concentrations of IFN-β1 from 10 U/mL- 200 U/mL (n=3) and **C.** reovirus (MOI = 10) + IFNAR1 antibody (10µg/mL, n=3; Significance

shown as indicated in the figure) or isotype control. **D.** IRF9 protein intensity (Two-tailed Student's t-test). **E & F.** Bar graphs for induction of CD8 bT_N cells upon *ex vivo* treatment of splenocytes from STAT1 KO mice withIovirus I = 10 (n=3) **(E) and**, IFN-α1 and IFNβ1 (200 units (U)/ml each) (n=2) **(F)**. Two-way ANOVA with Tukey's multiple comparisons test and 95% confidence interval was used for statistical analysis unless otherwise indicated. Significance has been indicated for CD8 bT_N cells in treatment conditions versus non-treated conditions unless otherwise indicated. Not significant (ns) = $p > 0.05$; *$p < 0.05$; **$p < 0.01$; ***$p < 0.001$; **** $p < 0.0001$.

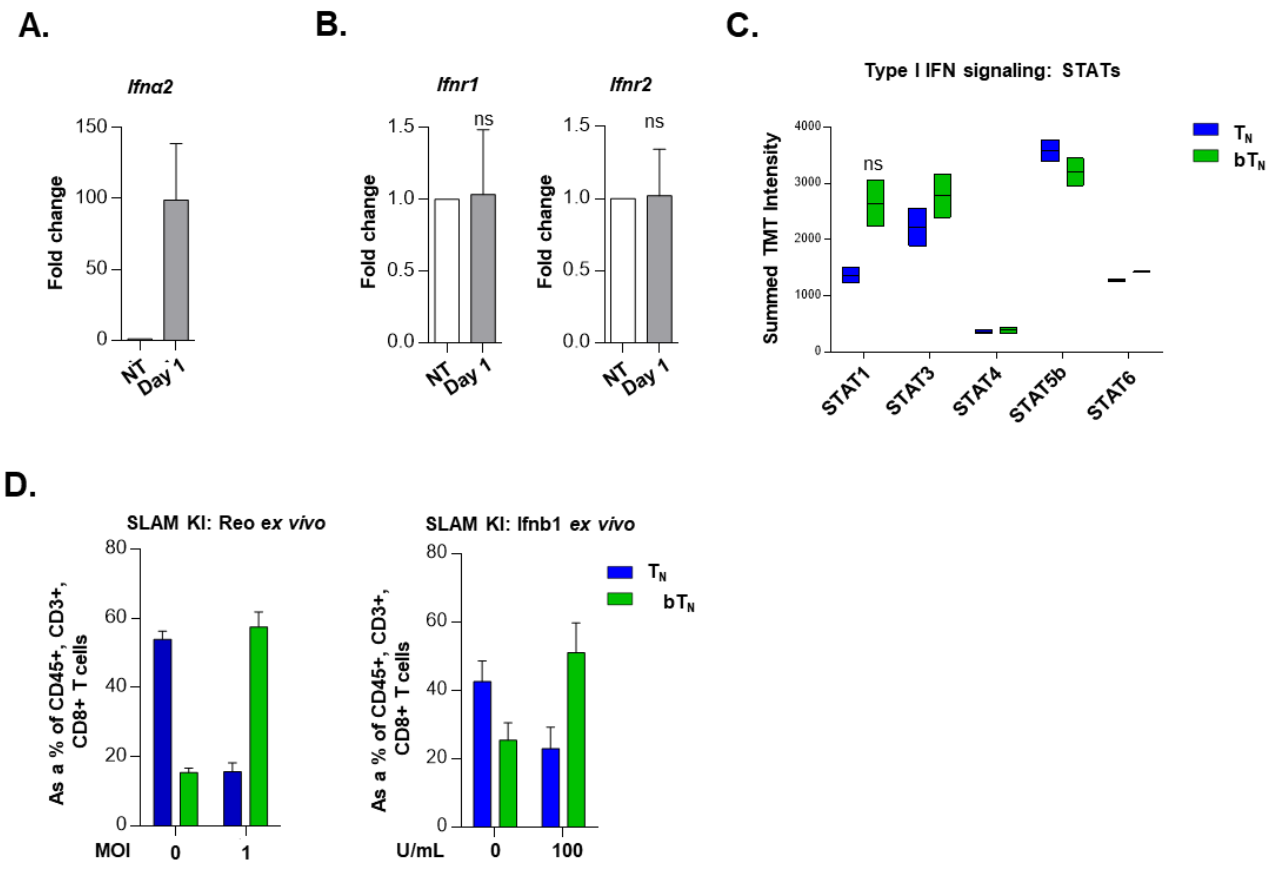

<u>Fig. 3.12:</u> Role of type I interferons in the induction of CD8 bT$_N$ cells. Quantitative PCR analysis of **C.** *Ifnα2*, **D.** *Ifnr1,* and *Ifnr2* levels in splenocytes of non-treated (NT) mice and mice treated with reovirus 1 d.p.i. **E.** Protein levels of STAT proteins in CD8 T$_N$ and CD8 bT$_N$ cells from quantitative *in vivo* proteomics analysis. **F.** Bar graphs for the induction of CD8 bT$_N$ cells upon treatment of splenocytes of SLAM knock-in (KI) mice with reovirus and IFN-β1 *ex vivo*. Two-tailed student t-test was used for statistical analysis of **A-E.** Not significant (ns) = $p > 0.05$; *$p < 0.05$; **$p < 0.01$; ***$p < 0.001$; **** $p < 0.0001$.

3.3.10. Induction of CD8 bT_N cells with different viruses depends on their interferon activating capacity

To assess whether different viruses were equally capable of inducing bystander activation of naïve CD8 T cells, we investigated the induction of CD8 bT_N cells upon *ex vivo* exposure to several different viruses. We observed that two different strains of herpes simplex virus-HSV- ICP0 (Everett, 2000) and 1716 (Valyi-Nagy et al., 1994)- robustly induced CD8 bT_N cells at a low MoI of 0.1 (Fig. 4A). Next, the Indiana strain of VSV (Freer et al., 1994) induced CD8 bT_N cells at a higher MoI (Fig. 4B). Further, we employed measles virus and discovered that the Edmonston vaccine strain of measles (Bankamp et al., 2011)- induced CD8 bT_N cells at an MoI of 0.1 (Fig. 4C) however, the IC323 strain of measles virus (Takeuchi et al., 2002)failed to induce a significant CD8 bT_N cell response (Fig. 4D). Within the array of viruses employed, IC323 strain of measles is known for its inferior capacity to stimulate type I interferons (Nguyen et al., 2016; Shingai et al., 2007) Taken together, this data suggested that CD8 bT_N cell induction occurred variably in different viruses and was a function of their interferon-activating/suppressing capabilities.

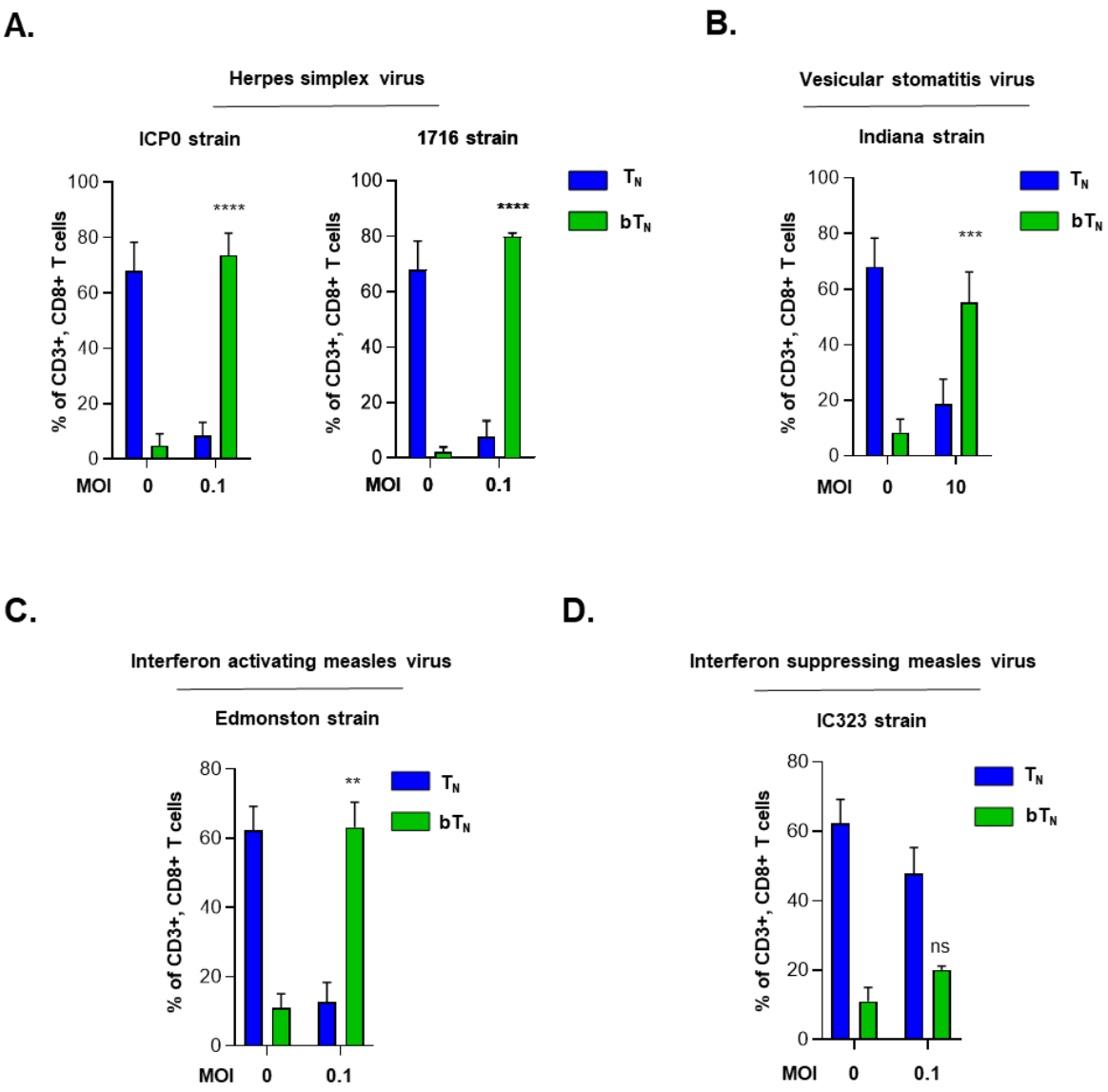

Fig. 3.13: Induction of CD8 bT_N cells *ex vivo* upon exposure to different viruses. Bar graphs showing the induction of CD8 bT_N cells upon exposure of C57BL/6 splenocytes to **A.** two different strains of herpes simplex virus (ICP0 and 1716, n=3 each) at MoI = 0.1, **B.** vesicular stomatitis virus (Indiana strain, n=3) at MoI = 10, **C.** interferon activating strain of measles (Edmonston, n=2) at MoI = 0.1 and **D.** wild type strain of measles (IC323, n=2) at MoI = 0.1 *ex vivo*. Two-way ANOVA with Sidak's multiple comparison test and 95% confidence interval was used for statistical analysis in bar graphs. Significance has

been indicated only for CD8 bT_N cell populations induced within 24 hours in comparison with untreated control population levels. Not significant (ns) = $p > 0.05$; *$p < 0.05$; **$p < 0.01$; ***$p < 0.001$; **** $p < 0.0001$.

3.3.11. NAMPT-mediated NAD^+ biosynthesis through salvage pathway metabolism regulates CD8 bT_N cell induction

Type I interferons have been shown to drive a rewiring of metabolism in a variety of cell types including hepatic cells (Ghazarian et al., 2017) and innate immune cells (Wu, Sanin et al. 2016). In our proteomics analysis, we discovered that proteins related to NAD^+-dependent ADP-ribosyltransferase activity like PARP9 and PARP14 were upregulated in bT_N cells when compared to naïve T cells (Fig.3.16A). Further, many proteins from the OAS family with ATP binding activity were also upregulated (Fig. 3.16B). Consequently, we hypothesized that bT_N cells might be metabolically reprogrammed as compared to T_N cells after reovirus exposure. To test this hypothesis, we employed a semi-targeted approach to study the metabolism of T_N and bT_N cells. T_N cells and bT_N cells (Day 1) were isolated from the spleens of reovirus-injected C57BL/6 mice by flow cytometry and then processed for metabolome analysis (Fig. 3.14A). A heatmap comparing the metabolomic signatures of T_N and bT_N cells clearly showed distinct metabolic rewiring of bT_N cells as compared to T_N cells (Fig. 3.14B). A list of the top upregulated and downregulated metabolites (fold change greater than or equal to 2, $p<0.05$) in bT_N cells as compared to T_N cells is shown in Fig. 3.14C. Enrichment analysis revealed a role for central energy metabolism (glycolysis and oxidative phosphorylation) in bT_N cells (Fig. 3.14D). As glycolysis and oxidative phosphorylation have been extensively studied in T cells (Chang et al., 2013; Menk et al., 2018; van der Windt et al., 2012) and both require NAD^+, we

focused on another pathway- NAD^+ salvage metabolism- that has shown emergent applications within immune cell biology (Cameron et al., 2019; Chatterjee et al., 2018; Gerner et al., 2020) and was discovered in our analysis (Fig. 3.14E). In mammalian cells, the NAD^+ salvage pathway is a major source for NAD^+ synthesis (Revollo et al., 2004) and consists of only 3 metabolites - nicotinamide (NAM), nicotinamide ribotide or nicotinamide mononucleotide (NMN), and NAD^+ (Fig. 3.14F). Using metabolite standards, we conducted a targeted analysis of metabolites involved in the NAD^+ salvage pathway and found higher relative levels of NAM, NMN, and lower levels of NAD^+ normalized to cell number in bT_N cells compared to T_N cells (Fig. 3.15A). Further, our proteomics analysis revealed that NAMPT, which is the rate-limiting enzyme of the NAD^+ salvage pathway, is increased in bT_N cells (Fig. 3.15B). Using qPCR, we determined that transcript levels of *Nampt* were also increased in bT_N cells as compared to T_N cells (Fig. 3.15B). Interestingly, the transcript levels of other enzymes within the NAD^+ salvage pathway like *Nmnats* (Fig. 3.16C) and those involved in other pathways of NAD^+ synthesis (Fig. S4D) like the *de novo* pathway (Fig. 3.16E) and from nicotinamide riboside/ nicotinic acid riboside (Fig. 3.16F) remained unchanged, indicating a possibly preferential reliance of bT_N cells on NAD^+ synthesis via NAMPT.

To further consolidate our understanding of the role of the NAD^+ salvage pathway and NAMPT, we tested the effect of FK866, an inhibitor of NAMPT (Lee et al., 2018; Schuster et al., 2015), on the induction of bT_N cells upon reovirus exposure. As shown in Fig. 3.15C, splenocytes from C57BL/6 mice exposed to reovirus and treated with FK866 showed a reduced induction of bT_N cells compared to those with only reovirus exposure. The robust induction of bT_N cells was rescued when NMN, a metabolite downstream of NAMPT, was

supplemented in the media (Fig. 3.15C). These results showed that FK866 can impair the virus-driven induction of bT_N cells, and further consolidated the role of NAMPT within this phenomenon. One possibility was that the reduced induction of bT_N cells could have occurred via an indirect effect of FK866 treatment like the reduced production of proinflammatory mediators in splenocytes (Al-Shabany et al., 2016; Bruzzone et al., 2009). To elucidate whether FK866 could impair the induction of bT_N cells in the presence of abundant type I interferons, we treated C57BL/6 splenocytes with exogenous IFN-α1 or IFN-β1 along with FK866 and found impaired induction of bT_N cells compared to splenocytes treated with only either interferon (Fig. 3.15D, E respectively). Once again, the impaired induction of bT_N cells upon FK866 treatment was rescued by the supplementation of NMN in the media with both IFN-α1 (Fig. 3.15D) and IFN-β1 (Fig. 3.15E) treatments. In conclusion, these findings suggested that NAD^+ production via the salvage pathway is required for the induction of bT_N cells after reovirus or type I interferon exposure.

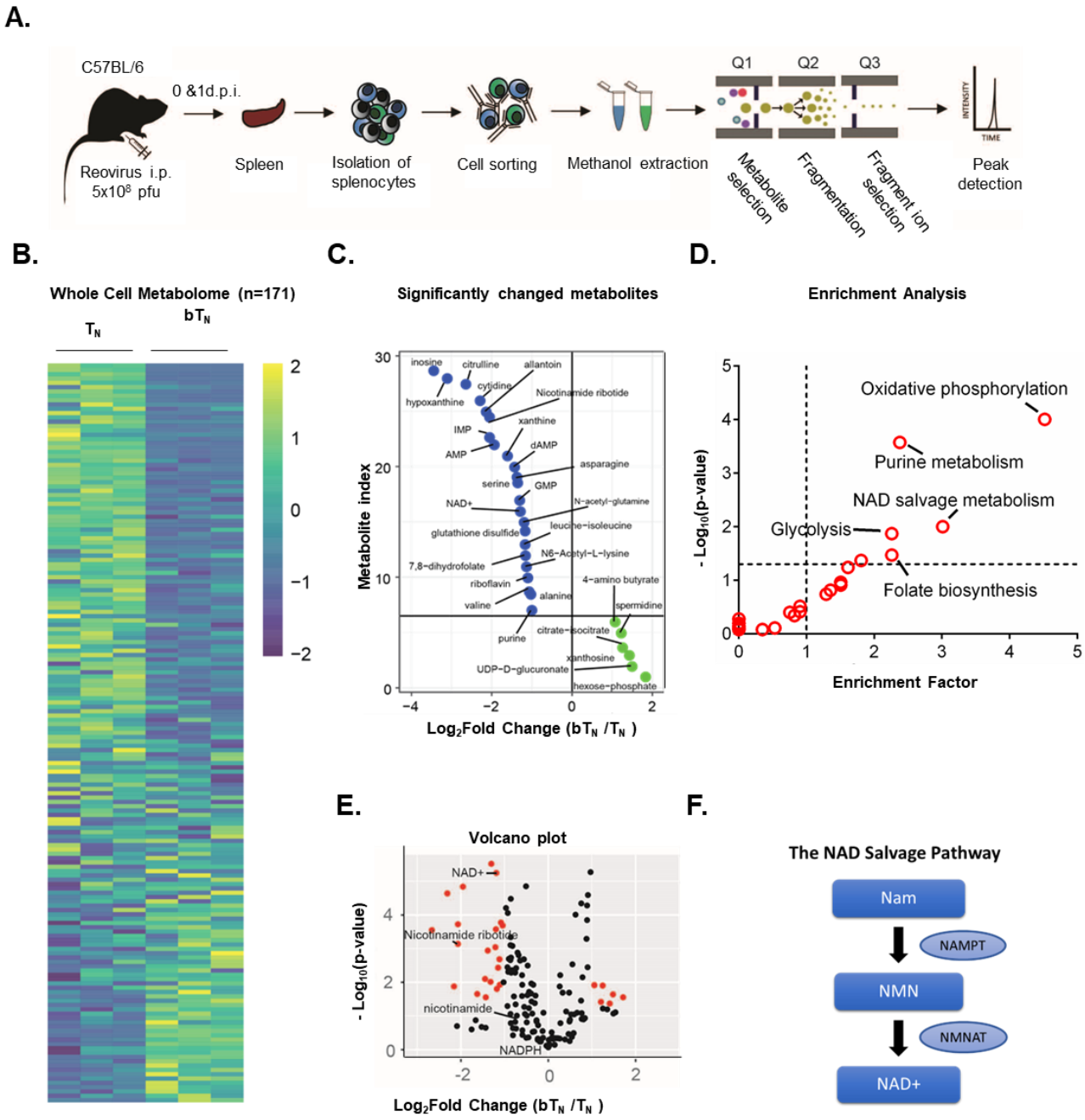

Fig. 3.14: Semi-targeted metabolome analysis of CD8 bT_N cells. A. Schematic for the workflow of metabolome analysis of T cells. **B.** Whole cell metabolome heatmap. **C.** List of significant top upregulated and downregulated metabolites in CD8 bT_N cells. **D.** Significant metabolite Enrichment analysis of significantly changed metabolites.

E. Volcano plot depicting metabolites that are significantly changed in CD8 bT_N cells versus CD8 T_N cells. NAD^+ salvage metabolites are highlighted in red. **F.** NAD^+ salvage pathway. NAM- Nicotinamide, NMN- Nicotinamide mononucleotide, and NAD^+- Nicotinamide adenosine dinucleotide. Two-tailed student's t-test was used for statistical analysis. Not significant (ns) = $p > 0.05$; *$p < 0.05$; **$p < 0.01$; ***$p < 0.001$; **** $p < 0.0001$.

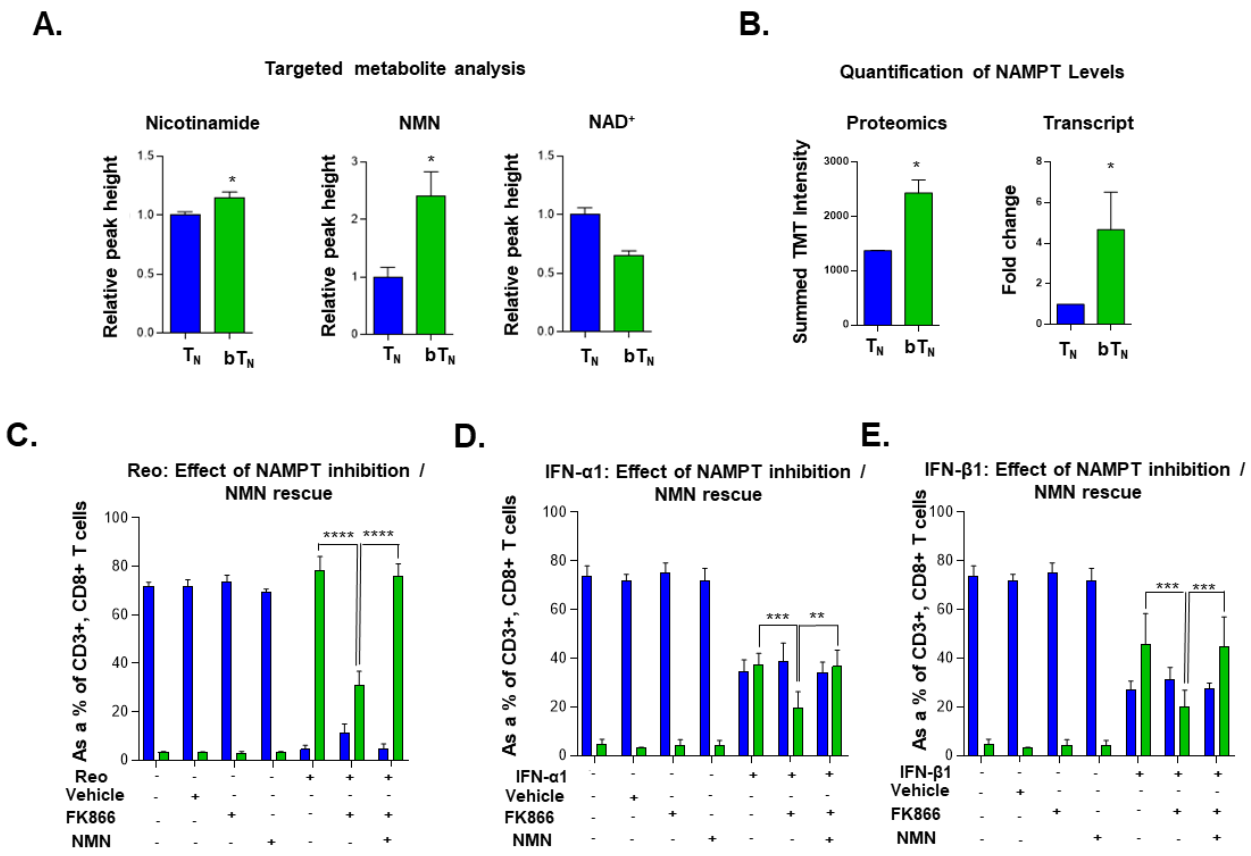

Fig. 3.15: NAD$^+$ salvage metabolism regulates induction of CD8 bT$_N$ cells. A. Bar graphs depicting the relative peak heights o– NAD$^+$ sa–vage metabolit–s - NAM, NMN, and NAD$^+$ - using targeted metabolomics. **B.** Bar graphs for NAMPT levels- proteomics and quantitative PCR analysis. **C, D, & E.** Bar graphs show the induction of CD8 bT$_N$ cells upon *ex vivo* treatment of splenocytes from C57BL/6 miIwith reIrus (MoI = 10) **(C),** IFN-α1 (20 U/I (**D)I**nd IFN-β1 (20 U/mI(**E)** in the presence of FK866 (5nM) and NMN (200µM) (n=3 each, ethanol vehicle control for FK866). Two-tailed student t-test was used for statistical analysis for A. and B. Two-way ANOVA with Tukey's multiple comparisons and 95% confidence interval was used for statistical analysis of C., D., and E. Not significant (ns) = p > 0.05; *p < 0.05; **p < 0.01; ***p < 0.001; **** p <0.0001.

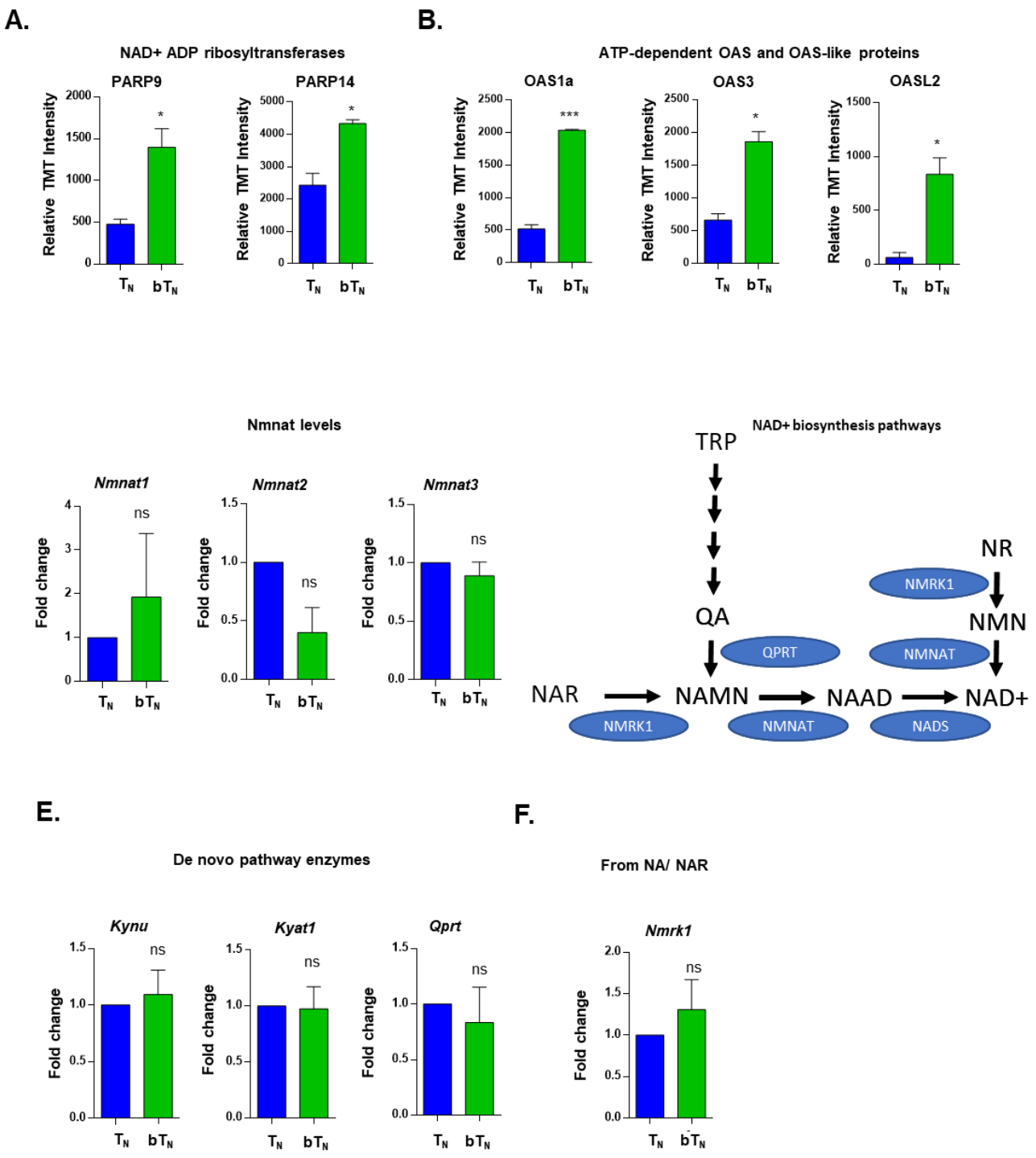

Fig. 3.16: Proteins involved NAD^+ generation or NAD^+ consumption. Bar graphs for protein levels of **A.** NAD^+- dependent ribosyl transferases and **B.** ATP-dependent OAS and OAS-like proteins in CD8 T_N and CD8 bT_N cells (1 d.p.i.) from quantitative *in vivo*

proteomics analysis. **C.** Bar graphs for transcript levels of NMNATs. **D.** NAD^+ biosynthesis pathways. TRP- tryptophan, QA- quinolinic acid, NR- nicotinamide riboside, NMN- nicotinamide mononucleotide, NAD^+- nicotinamide adenine dinucleotide, NAR- nicotinic acid riboside, NAMN- nicotinic acid mononucleotide and NAAD- nicotinic acid adenine dinucleotide. Bar graphs for transcript levels of **E.** *de novo* pathway enzymes and **F.** *Nmrk1* for synthesis from NR/ NAR. Two-tailed student t-test was used for statistical analysis. Not significant (ns) = $p > 0.05$; *$p < 0.05$; **$p < 0.01$; ***$p < 0.001$; **** $p < 0.0001$.

3.4. Discussion

As is being recognized in the context of the SARS-CoV2 pandemic, the understanding of the early immunological events that occur after virus exposure is extremely important. It has become quite clear from various studies on COVID-19 that one of the most important factors determining the clinical outcome of the disease is the early induction of type I interferons (Acharya et al., 2020; Lee and Shin, 2020). Early type I interferon responses are associated with mild COVID whereas delayed tIpe I interferon responses lead to poor viral control, delayed and persistent activation of adaptive immunity, and severe COVID (Moss, 2022). In addition, early bystander activation of T cells has also been shown to be an important characteristic of mild disease compared to delayed bystander activation which has been associated with severe disease (Bergamaschi et al., 2021). Bystander activation is one of the earliest ways in which naïve CD8 T cells are activated even before the cells have had an opportunity to be primed with antigen. Most studies focus on the biology of CD8 T cells after antigenic priming or on the bystander activation of pre-existing memory T cells. In this study, we have delineated the molecular mechanisms that govern the induction of

early naïve bystander-activated CD8 T cells. We demonstrated that CD8 bT_N cells are induced and have an anti-viral, type I interferon signature within 24 hours of reovirus exposure, a timepoint that is not typically studied for CD8 T cells. Not only was this shown to be STAT-1-dependent but also was dependent on the type I interferon activating capacity of different viruses. These findings further highlight the importance of studying early interferon production upon exposure to viruses and provide insight into another avenue through which CD8 T cells can be modulated early on by different viruses.

Recent literature on COVID-19 pathobiology has generated an increased appreciation for the role of immunometabolic reprogramming that occurs during virus exposure (O'Carroll and O'Neill, 2021). Viruses can alter the metabolism of cells directly during their replication or via the effects of type I interferons (Moreno-Altamirano et al., 2019). For example, type I interferons induce important changes in the metabolism of plasmacytoid dendritic cells by acting on them in an autocrine manner, and these changes allow for enhanced immune function. (Wu et al., 2016) Type I interferons can, however, also modulate T cells specifically naïve CD8 T cells which are important during virus exposure. Although some studies have investigated the metabolism of naïve T cells (Mendoza et al., 2017), the impact of metabolism in the context of bystander-activated naïve CD8 T cells remains unexplored. In our study, it is quite intriguing that CD8 bT_N cells, despite being phenotypically similar to prototypic naïve T cells, demonstrate a completely different metabolic signature. In this regard, our findings on the role of the NAD^+ salvage pathway in CD8 bT_N cell induction add a crucial piece to the metabolic puzzle being investigated. Targeting NAD^+ salvage metabolism by inhibiting its rate-limiting enzyme NAMPT has been previously shown to reduce effector T cell function in the tumor microenvironment

(Beier et al., 2018; Chatterjee et al., 2018). In GVHD the functionality of alloreactive T cells was inhibited by targeting NAMPT (Gerner et al., 2020), and similarly, the depletion of NAD^+ in T cells via FK866 treatment reduced demyelination in EAE (Bruzzone et al., 2009; Tullius et al., 2014). The study of metabolism and specifically the NAD^+ metabolic circuitry in naïve T cells following activation in native settings by viral exposure remain few. In this regard, we have demonstrated a clear role for NAD^+ salvage metabolism in the reprogramming of bystander-activated naïve CD8 T cells during the acute phase of the immune response, further underscoring the importance of NAD^+ salvage metabolism in early T cell biology.

Finally, the virus of choice in this study- reovirus- is an oncolytic virus being developed as a cancer immunotherapy agent for the treatment of various tumor types in clinics (Müller et al., 2020). Induction of type I interferons and bystander naïve CD8 T cells upon exposure to oncolytic viruses can have important consequences for cancer immunotherapy. The role of type I interferons in tumor immunology is being widely appreciated (Cao et al., 2021; Zitvogel et al., 2015) and naïve-like T cells with functional capacities have been detected in tumors (Sheng et al., 2017). Further, cancer metabolism can have a direct detrimental impact on naïve T cells (Xia et al., 2017). Understanding the impact of oncolytic viruses like reovirus on naïve T cells via bystander activation and consequent metabolic reprogramming represents an important emerging area of research. We believe that the research in this study provides new avenues for immunometabolism research in T cells, specifically naïve CD8 T cells, and potential therapeutic targets that can be investigated for the reprogramming of T cell immunity. Ultimately, an improved understanding of bystander-activated naïve T cells and immunometabolism following virus exposure will

inform fundamental concepts leading to better development of vaccines/treatments against viral infections and for the effective design and development of oncolytic virotherapy.

Chapter 4. Type I interferon drives metabolically reprogrammed, and functionally enhanced CD44lowCD62Llow CD8 T cells after antigenic stimulation

4.1. Abstract

CD8 T cells are an important part of adaptive immune responses to cancer and viral infections. Early events that drive the activation of CD8 T cells remain poorly understood. Here, we report that CD44lowCD62Llow CD8 T cells (P4), a poorly characterized subset of CD8 T cells, are induced immediately after TCR stimulation *in vitro* and are capable of effector function. P4 cells are also induced *in vivo* during virus infection. We discovered that type I interferons drive increased IFN-γ production in P4 cells, which relies on signaling through the IFNAR1 receptor. Metabolomics analysis of P4 cells revealed that aminoacyl t-RNA metabolism was differentially regulated in P4 cells *ex vivo* and those generated *in vitro* after antigen-specific T cell activation. This report provides, for the first time, a thorough characterization of P4 cells induced very early upon activation, the role of type 1 interferons in modulating their function and provides insight into the metabolic reprogramming that occurs within this cell type.

4.2. Background

As discussed previously, CD8 T cells are an important part of the adaptive immune response and can identify and kill virus-infected cells. Upon antigen encounter, naïve CD8 T cells are activated and differentiate into effector T cells (P3) and memory T cells (P2) (Nakajima et al., 2021). Various models have been proposed for the differentiation of T cells upon being activated (discussed in Chapter 1) (Kaech et al., 2002). The various types of CD8 T cells (naïve, effector, and memory) can be identified in mice based on the expression of adhesion molecules CD44 and CD62L. Naïve T cells are identified as CD44lowCD62L+, memory T cells as CD44hiCD62L+ and effector T cells as CD44hiCD62L-. CD44 expression is commonly thought to be upregulated upon antigen experience in T cells; however, the discovery of cells like stem cell memory T cells which have naïve-like phenotype but are antigen-experienced precursor cells have challenged this dogma (Gattinoni et al., 2009).

CD44lowCD62Llow (P4) CD8 T cells do not fit into any of the classical subsets of differentiated T cells. As a result, the biology of CD44lowCD62Llow T cells remains relatively poorly characterized compared to their counterparts. A recent seminal study by Honjo's group has found that CD44lowCD62Llow CD8 T cells play an important role in the restoration of anti-tumor immunity in aged mice (Nakajima et al., 2021). Specifically, the study investigated the age-related unresponsive to PD-1 therapy for cancer treatment. The authors found that P4 cells are robustly induced in young PD-1 KO mice that can control MC38 tumors whereas they were absent in aged mice which developed tumors. Adoptive transfer of P4 OT-1 CD8 cells into CD8 KO mice with MC38-ova tumors demonstrated the anti-tumor capacity of P4 cells. Further, to study whether P4 cells

differentiated from P1 or P2 cells, the authors isolated P1 and P2 populations and stimulated them with CD3/C28 *in vitro*. They observed that P4 cells were generated on Day 2 post-stimulation only from P1 cells, thus proposing that T cells first transition from P1 to P4 before transitioning to P3. This provides an important additional piece to the current literature wherein one model suggests that T cells transition from naïve to effector to memory (P1 to P3 to P2) (Kaech et al., 2002; Youngblood et al., 2017). The authors in the above study suggest that P4 cells are pre-effector cells and an essential step for the conversion of naïve P1 cells to P3 effectors. To our knowledge, this is the only study that describes the role of P4 cells in a disease context (cancer and PD-1 therapy). The biology of P4 cells in other disease contexts like virus exposure remains to be characterized and this presents an exciting opportunity for current and future research studies.

As discussed in the previous chapter, immunometabolism is a rapidly evolving area of study that describes the metabolic pathways that support the function and differentiation of immune cells like T cells and the consequences of metabolic perturbations on immune function. We have seen how T cells rely on different metabolic pathways at different stages of differentiation to meet the metabolic requirements of the T cells at that stage (Buck et al., 2017). Effector T cells rely heavily on glycolysis to fuel their needs for rapid proliferation and cytotoxic activity (Phan et al., 2016). Memory T cells, which are usually more quiescent until antigen re-encounter, rely on the tricarboxylic acid cycle (TCA cycle) and oxidative phosphorylation for their metabolic needs (Corrado and Pearce, 2022). The study described by Nakajima et al. discussed above also identified an important metabolic pathway that is upregulated in P4 cells using microarray analysis of the cells. The authors demonstrated using that P4 cells rely on one-carbon metabolism for their needs in PD-1

KO mice. Given that metabolites can have context-dependent roles in T cells, it is important to investigate not just the biological function, but also the metabolism of P4 cells in different disease contexts including virus exposure.

We have described in the previous chapter how type 1 interferons can cause bystander activation of naïve CD8 T cells and we have also discussed how the metabolism of these bystander-activated naïve CD8 T cells is completely rewired. Nakajima et al. also question whether any activation/stimulation of naïve CD8 T cells by cytokines can drive differential P4 induction or function. To the best of our knowledge, this has not been investigated in any study so far.

In the present study, we first characterized CD8 T cell activation with different stimulations early after activation (1h) and at later timepoints (upto 24 hours) and reported that P4 cells are induced very early upon TCR-dependent stimulation. Antigen-specific P4 cells induced upon stimulation with cognate peptide have functional capabilities at 6 hours after stimulation and can produce IFN-γ. We further discovered that this IFN-γ production is increased when stimulation occurs in the presence of type I interferons and this increased functional capacity was dependent on type I interferon signaling. Finally, we isolated P4 cells and other T cell subsets by flow cytometry and conducted a metabolomics analysis revealing an important role for aminoacyl tRNA biosynthesis in the induction of P4 cells.

4.3. Results

4.3.1. *In vitro* stimulation drives the induction of CD44lowCD62Llow P4 cells within hours

To investigate the earliest changes that CD8 T cells undergo after *in vitro* stimulation, we treated splenocytes from wild-type (WT) C57Bl/6 mice and OT-1 mice with 3 different

treatments- Concanavalin A (Con A) which leads to T cell activation via crosslinking of the TCR complex, CD3/CD28 antibodies that bind to T cells and activate TCR signaling as well as costimulation, and ova peptide which leads to antigen-specific activation of CD8 T cells- and studied CD8 T cell subsets by flow cytometry. First, we noted that the % of live cells remained unchanged across all the different stimulation conditions (Fig. 4.1A). It was also noted that CD8 T cells comprised a greater % of the lymphocytes in OT-1 mice compared to their C57BL/6 counterparts within the different activation treatment groups (Fig. 4.1B). The % of CD8 T cells was also increased upon CD3/CD28 treatment compared to non-treated splenocytes (NT) in OT-1 splenocytes (Fig. 4.1B).

We noted that without any stimulation majority of the CD8 T cells in WT C57BL/6 mice have a naïve (P1) phenotype (Fig. 4.2). Upon treatment for 6 hours, we observed that ConA and CD3/CD28 stimulation led to the induction of CD44lowCD62Llow P4 cells in WT mice (Fig. 4.2). Since ova peptide does not stimulate T cells from WT mice, no difference was seen in the dot plots compared to NT (Fig. 4.2).

In OT-1 mice, like WT C57BL/6 mice, we observed that without any treatment significant percentagICD8 T cells were also of the naive P1 phenotype (Fig. 4.3). After treatment for 6 hours, stimulation with Con A as well as with TCR stimulation using CD3/CD28 antibodies and ova peptide led to the robust induction of P4 cells (Fig. 4.3).

Quantification of the various T cell subsets after the different treatments revealed that all types of stimulation (except ova for WT) led to the loss of P1 almost completely in both WT and OT-1 mice (Fig. 4.4A). P2 cells were present at lower percentages in OT-1 splenocytes compared to WT C57BL/6 splenocytes and were reduced further in both sets of splenocytes after stimulation (Fig. 4.4B). P3 effector memory T cells were increased in

WT mice after stimulation with CD3/CD28 compared to NT (Fig. 4.4C) while in OT-1 mice, P3 frequencies were seen to be increased significantly only upon treatment with ova peptide (Fig. 4.4C). Finally, the CD44lowCD62Llow P4 populations were robustly induced in both WT and OT-1 mice and made up the majority of CD8 T cells (~70-80%) after all treatment conditions (except ova stimulation for WT mice) (Fig. 4.4D).

Taken together, we observe that all treatments drive a loss of P1 naïve cells and reduction of P2 memory cells within 6 hours of treatment. CD44lowCD62Llow P4 cells are induced robustly by all treatments and a smaller percentage of P3 effector memory cells are induced with all treatments in WT mice but only with ova treatment in OT-1 mice. The early induction of CD44lowCD62Llow P4 cells after stimulation is in line with findings from Honjo's group that suggest that P1 cells transition to P4 cells before transitioning to P3 and P2 cells.

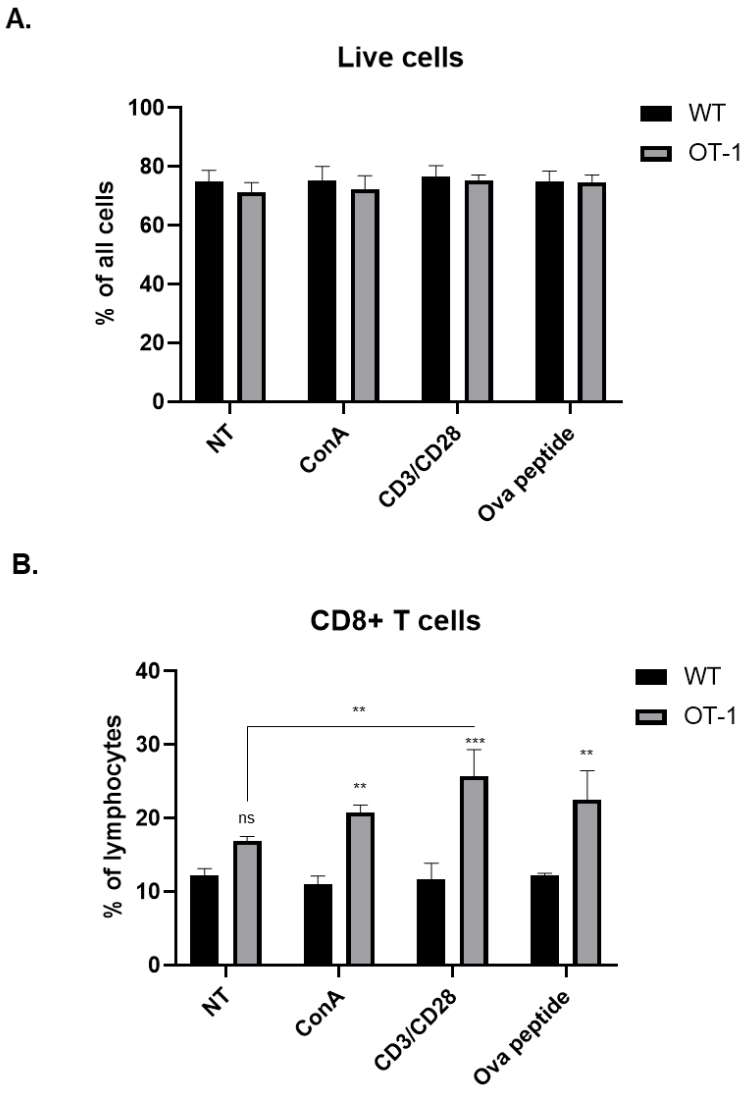

Fig. 4.1: Live cells and CD8 T cells after stimulation for 6h. Bar graphs quantifying the percentage of **A.** Live cells and **B.** CD8+ T cells after stimulation of splenocytes from C57BL/6 and OT-1 transgenic mice with ConA, CD3/CD28 antibodies, or ovalbumin peptide for 6 hours. Two-way ANOVA with Tukey's multiple comparisons and 95% confidence interval was used for statistical analysis. Significance is shown for WT versus OT-1 within each treatment condition unless otherwise indicated. Not significant (ns) = $p > 0.05$; *$p < 0.05$; **$p < 0.01$; ***$p < 0.001$; **** $p < 0.0001$.

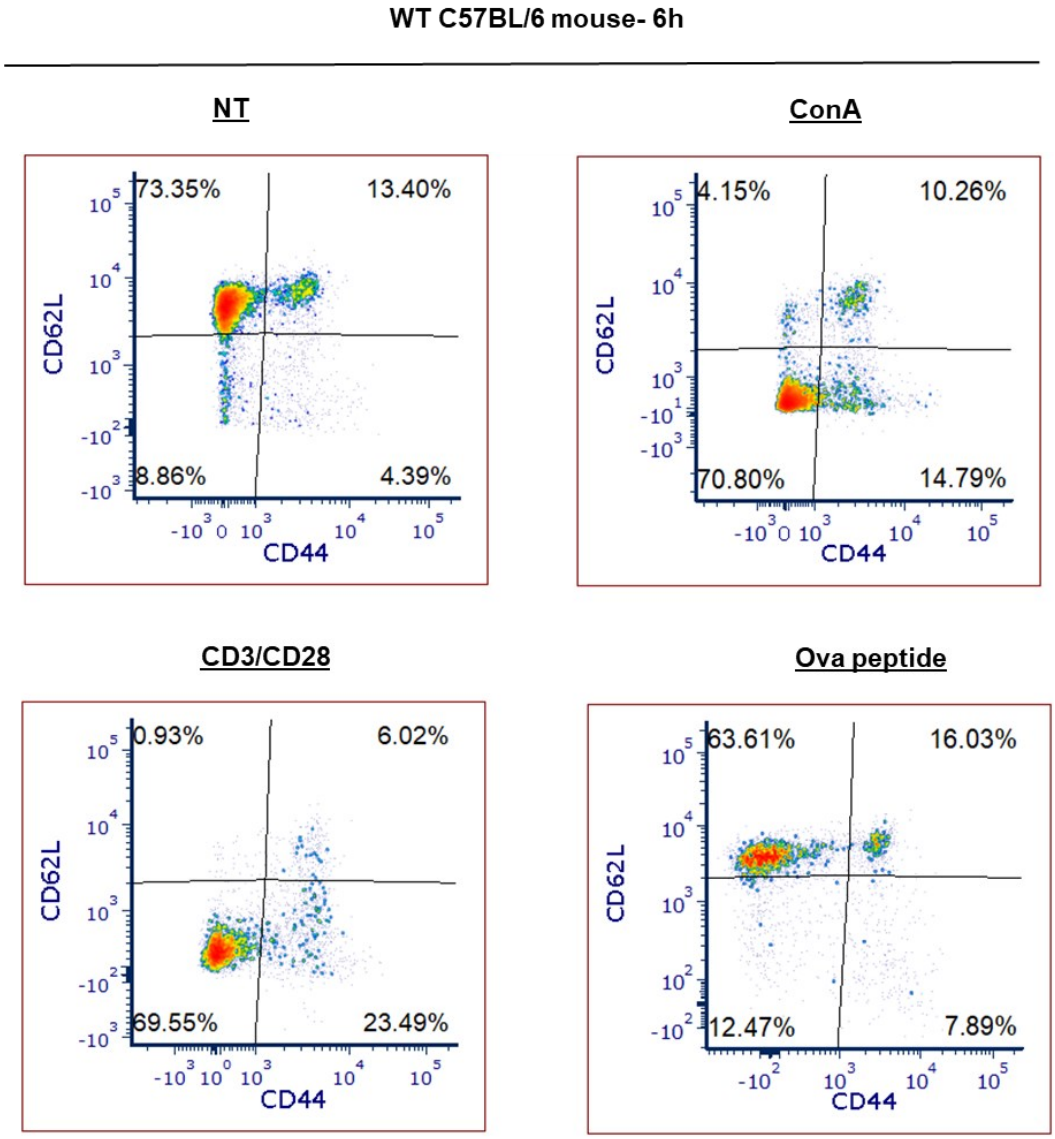

Fig. 4.2: Stimulation of splenocytes from C57BL/6 mice for 6h. Representative dot plots for splenocytes from C57BL/6 mice stimulated with either ConA, CD3/CD28 antibodies, or ovalbumin peptide for 6h in cell culture.

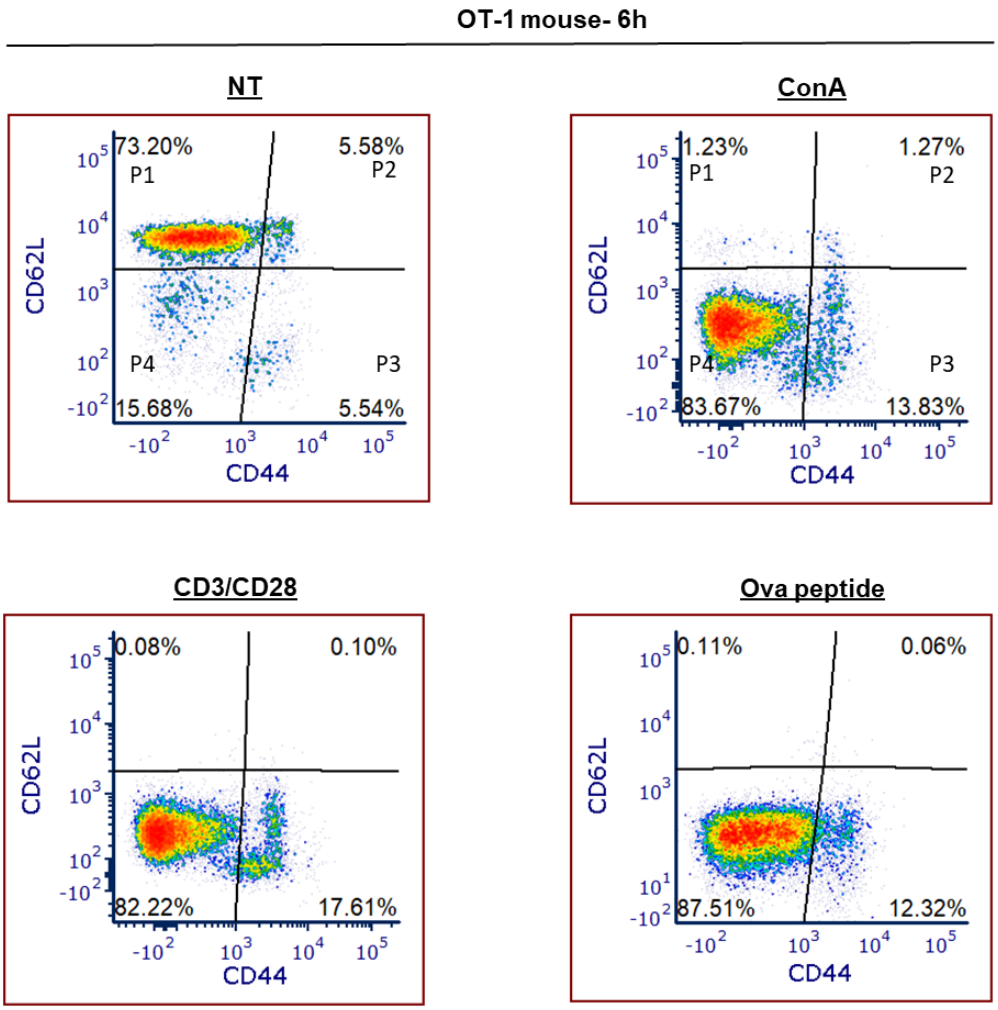

Fig. 4.3: Stimulation of splenocytes from OT-1 transgenic mice for 6h. Representative dot plots for splenocytes from OT-1 mice stimulated with either ConA, CD3/CD28 antibodies, or ovalbumin peptide for 6h in cell culture.

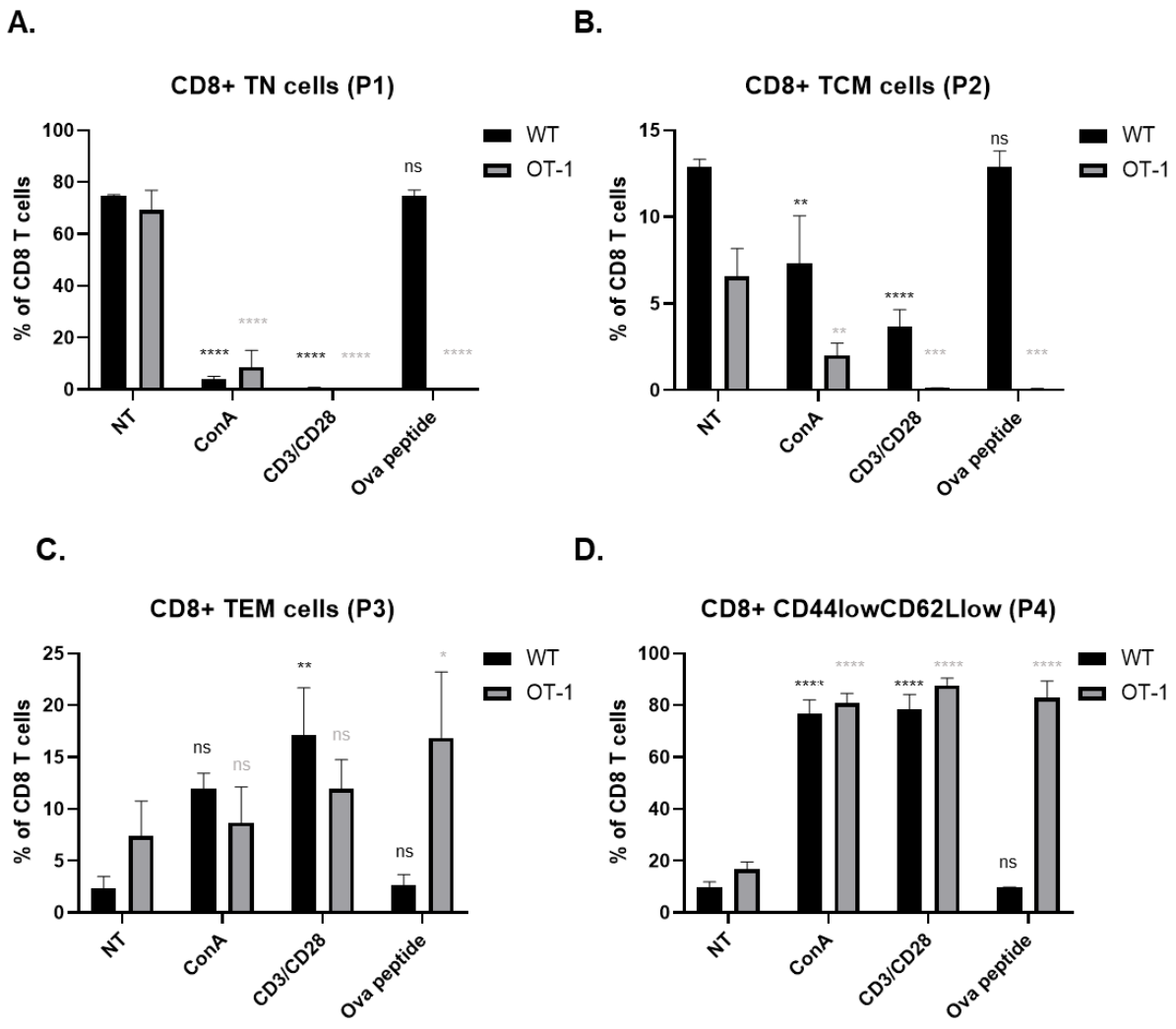

<u>Fig. 4.4:</u> CD8 T cell subsets in C57BL/6 mice and OT-1 mice after stimulation for 6h. Bar graphs quantifying **A.** Naïve P1 cells **B.** Central memory P2 cells **C.** Effector memory P3 cells and **D.** CD44lowCD62Llow P4 cells in both C57BL/6 mice (WT) and OT-1 transgenic mice after 6h of stimulation with ConA, CD3/CD28 antibodies or ovalbumin peptide. Two-way ANOVA with Tukey's multiple comparisons and 95% confidence interval was used for statistical analysis. Significance is shown individually between different treatment groups compared to NT for WT (in black) and different treatment

groups compared to NT for OT-1 (in grey). Not significant (ns) = $p > 0.05$; *$p < 0.05$; **$p < 0.01$; ***$p < 0.001$; **** $p < 0.0001$.

4.3.2. Early induced P4 cells are functionally capable and can produce IFN-γ

To assess whether CD8 T cells are functional after activation at the early time point of 6 hours, we measured the IFN-γ response after the different types of stimulation in WT as well as OT-1 mice. In WT C57Bl/6 mice, a weak IFN-γ response was seen in CD8 T cells upon stimulation with ConA and CD3/CD28 for 6h (Fig. 4.5). In OT-1 mice, similarly, a weak IFN-γ response was observed in CD8 T cells upon stimulation with ConA and CD3/CD28, however, ova peptide stimulation led to the robust production of IFN-γ by CD8 T cells at 6 hours (Fig. 4.6). Further, upon gating on P3 effector memory T cells, we observed that P3 cells were capable of IFN-γ production and almost 70% of P3 cells were IFN-γ+ upon ova treatment (Fig. 4.6). Finally, upon gating on CD44lowCD62Llow P4 cells, we observed that like P3 cells, P4 cells were also capable of IFN-γ production albeit at a lower frequency compared to P3 cells (Fig.4.6).

Quantification of the IFN-γ response showed that in WT mice, IFN-γ+ CD8 T cells were significantly increased only in CD3/CD28 activation compared to NT (Fig. 4.7A). In OT-1 mice, significant increases in IFN-γ+ cells were observed upon CD3/CD28 stimulation as well as ova peptide stimulation (Fig. 4.7A). In the CD44lowCD62Llow P4 population, significantly increased IFN-γ+ T cells were also observed upon stimulation with CD3/CD28 and with ova peptide (Fig. 4.7B). No significant changes to IFN-γ production were observed within this population in WT splenocytes upon any treatment (Fig. 4.7B). It is interesting to note that ova peptide stimulation of OT-1 splenocytes produced the

largest IFN-γ response by CD8 T cells and P4 T cells at 6h of any stimulatory treatment (Fig. 4.7 A and B).

Finally, we also looked at granzyme B production of CD8 T cells and PD-1 expression levels and found these to be unaffected in all the different treatment conditions at this early timepoint of 6h (Fig. 4.8) Taken together, this data suggests that P4 cells are not only induced early after stimulation but also have functional capabilities with the ability to produce IFN-γ after stronger TCR stimulation. This implies that P4 cells may have an important role to play early on after priming with antigen before a strong effector CD8 T cell response has developed.

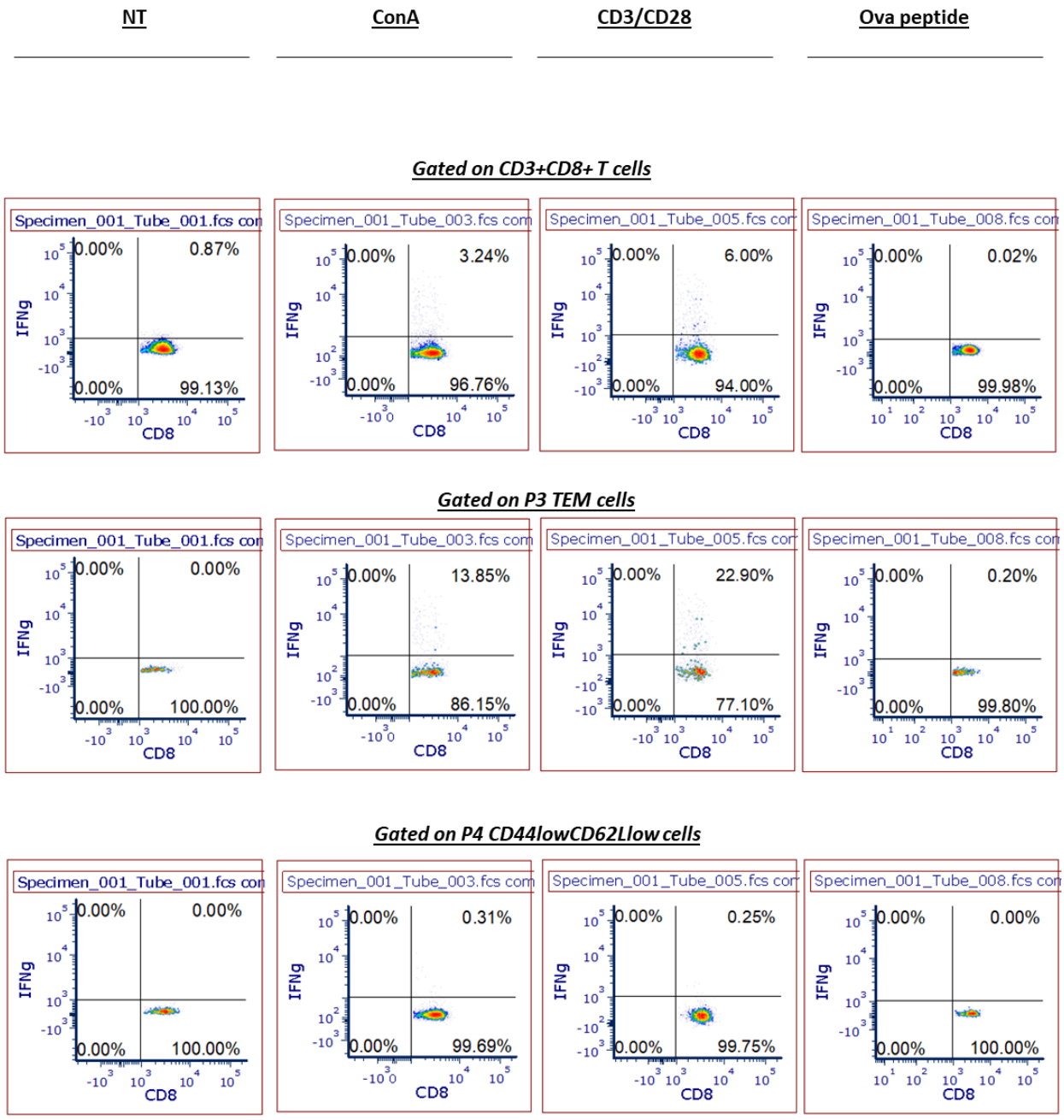

Fig. 4.5: IFN-γ production in C57BL/6 splenocytes upon stimulation for 6h. Representative dot plots showing the production of IFN-γ by **A.** Total CD8 T cells **B.** Effector memory P3 cells and **C.** CD44lowCD62Llow P4 cells upon treatment of WT C57BL/6 splenocytes with ConA, CD3/CD28 antibodies, or ovalbumin peptide for 6h in cell culture.

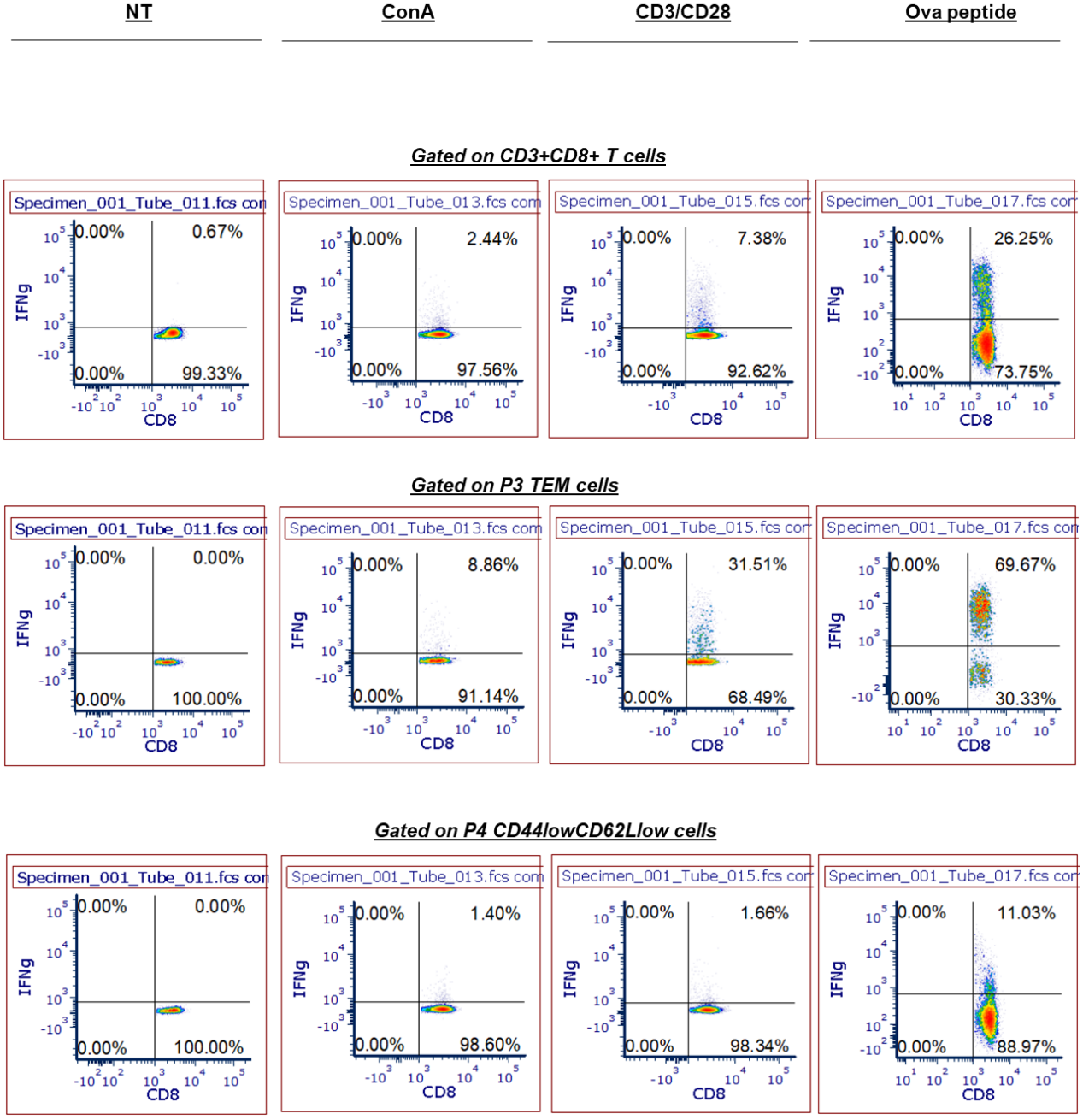

Fig. 4.6: IFN-γ production in OT-1 splenocytes upon stimulation for 6h. Representative dot plots showing the production of IFN-γ by **A.** Total CD8 T cells **B.** Effector memory P3 cells and **C.** CD44lowCD62Llow P4 cells upon treatment of OT-1 splenocytes with ConA, CD3/CD28 antibodies or ovalbumin peptide for 6h in cell culture.

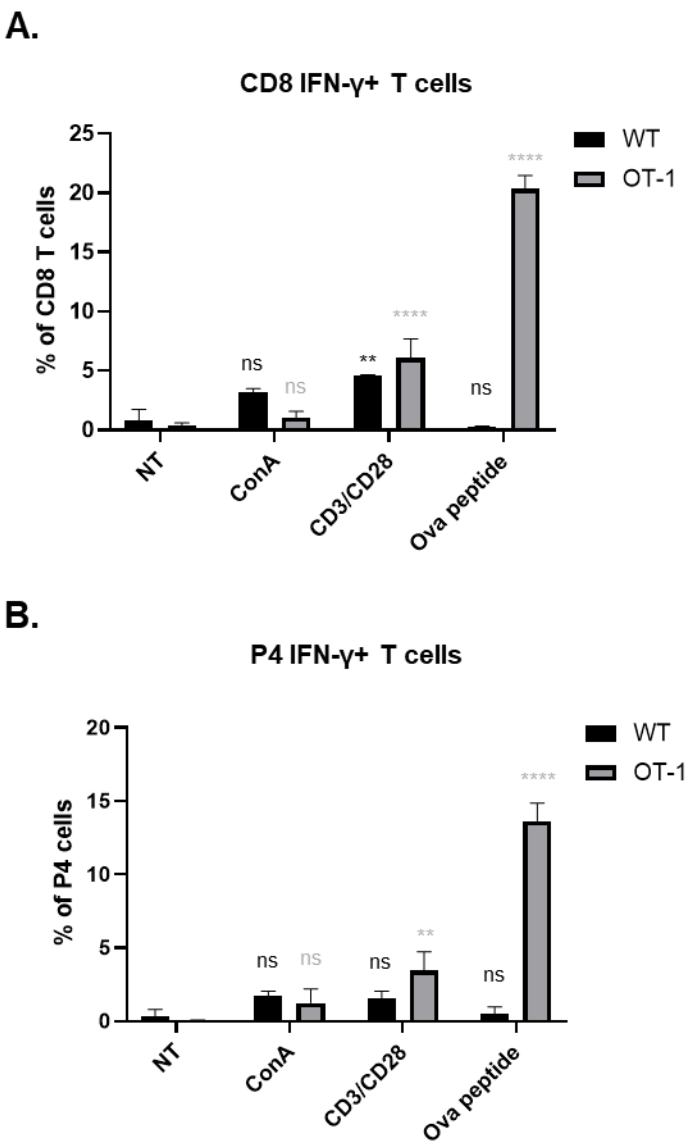

Fig. 4.7: IFN-γ production by CD8 T cells upon stimulation for 6h. Bar graphs depict the percentage of IFN-γ+ cells in **A.** parent CD8 T cells and **B.** CD44lowCD62low P4 cells in both WT C57BL/6 mice (n=2) and OT-1 mice (n=3) after stimulation with ConA, CD3/CD28 and ova peptide for 6h in cell culture. Two-way ANOVA with Tukey's multiple comparisons and 95% confidence interval was used for statistical analysis. Significance is shown individually between different treatment groups compared to NT for

WT (in black) and different treatment groups compared to NT for OT-1 (in grey). Not significant (ns) = $p > 0.05$; *$p < 0.05$; **$p < 0.01$; ***$p < 0.001$; **** $p < 0.0001$.

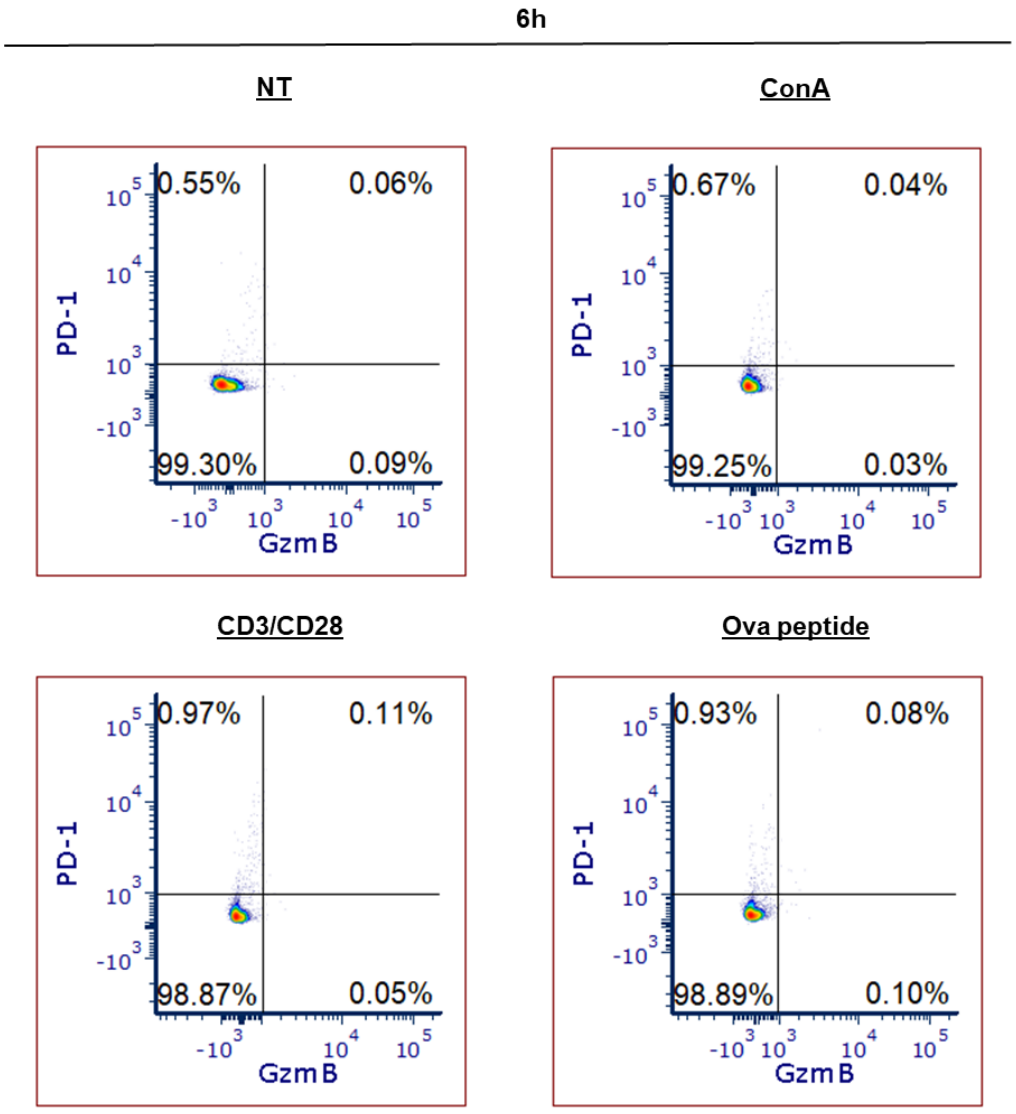

Fig. 4.8: PD-1 expression and GzmB production by P4 cells at 6h. Representative dot plots showing the intracellular production of granzyme B and the cell surface expression of PD-1 on CD8 T cells after stimulation with ConA, CD3/CD28, and ova peptide for 6h in cell culture.

4.3.3. P2 central memory T cells are induced 24 hours after *in vitro* stimulation

Next, to interrogate whether the P4 population of CD8 T cells induced at 6 hours after stimulation is a transitory population, we investigated the CD8 T cell subsets 24 hours after stimulation with ConA, CD3/CD28 antibodies, and ova peptide in C57BL/6 mice as well as OT-1 transgenic mice. At this time point, we noted that, contrary to the 6h timepoint, the percentage of live cells was increased upon stimulation in all cases except stimulation of C57BL/6 mice with ova peptide (Fig. 4.9A) but in line with the 6-hour experiments, CD8 T cells occupied a larger percentage of the lymphocytes in OT-1 mice compared to C57BL/6 mice after all treatments/stimulations (Fig. 4.9B).

Upon treatment with Con A, CD3/CD28, and ova peptide for 24 hours we observed that the P2 cell population was robustly induced (Fig. 4.10). Quantification of the different CD8 T cell subsets at 24 hours showed that in splenocytes from both C57BL/6 mice and OT-1 mice, naïve P1 cells were reduced in all treatment conditions (except ova treatment for WT) (Fig. 4.11A). Next, P2 cells were also significantly increased with all stimulatory treatments in both sets of splenocytes and comprised the majority of CD8 T cells at this timepoint (Fig. 4.11B). In the case of P3 cells, a significant difference was observed only in the case of OT-1 splenocytes activated with ova peptide (Fig. 4.11C). Finally, quantification of the P4 subset revealed that a very small percentage of P4 cells were still observed at 24 hours in both WT and OT-1 splenocytes (Fig. 4.11D). Altogether, this data suggests that the induction of P4 cells is transitory and after the first 24 hours very small percentages of P4 cells are present in the CD8 T cells.

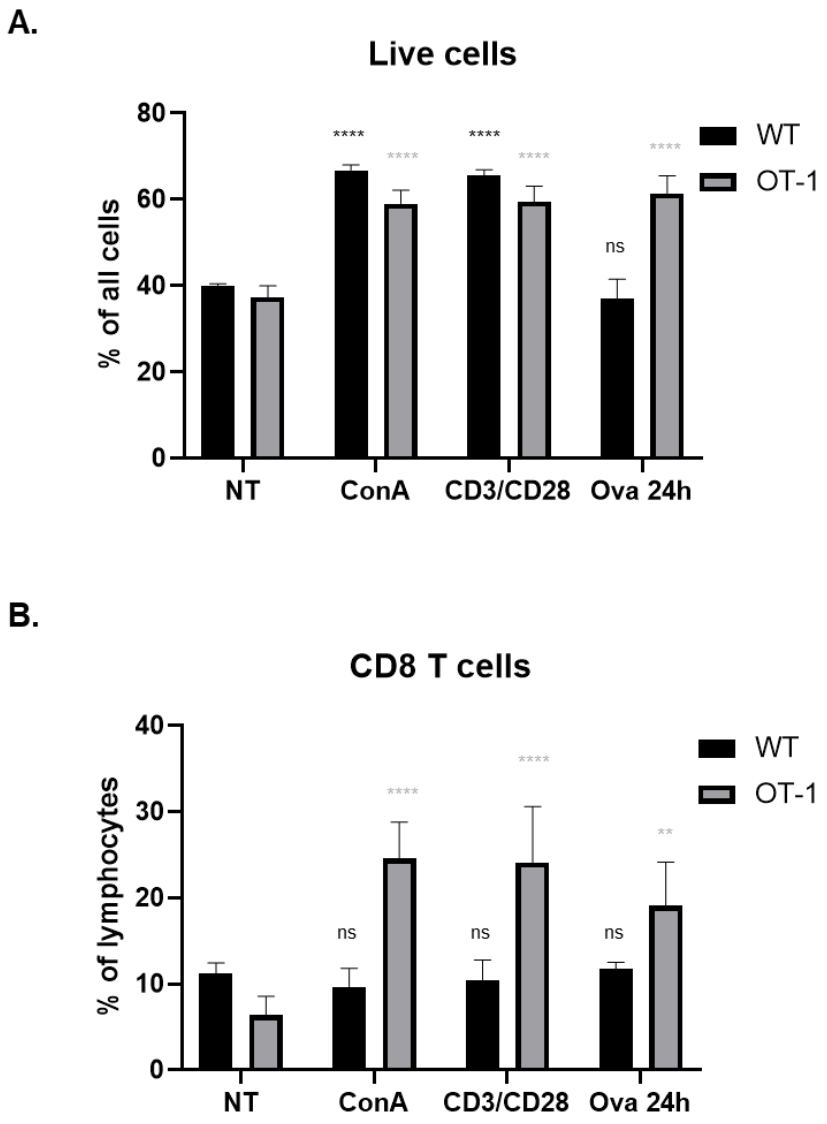

Fig. 4.9: Live cells and CD8 T cells after stimulation for 24h. Bar graphs quantifying the percentage of **A.** Live cells and **B.** CD8+ T cells after stimulation of splenocytes from C57BL/6 and OT-1 transgenic mice with ConA, CD3/CD28 antibodies, or ovalbumin peptide for 24 hours in cell culture (n=3). Two-way ANOVA with Tukey's multiple comparisons and 95% confidence interval was used for statistical analysis. Statistical significance is shown individually between different treatment groups compared to NT for

WT (in black) and different treatment groups compared to NT within OT-1 (in grey). Not significant (ns) = $p > 0.05$; *$p < 0.05$; **$p < 0.01$; ***$p < 0.001$; **** $p < 0.0001$.

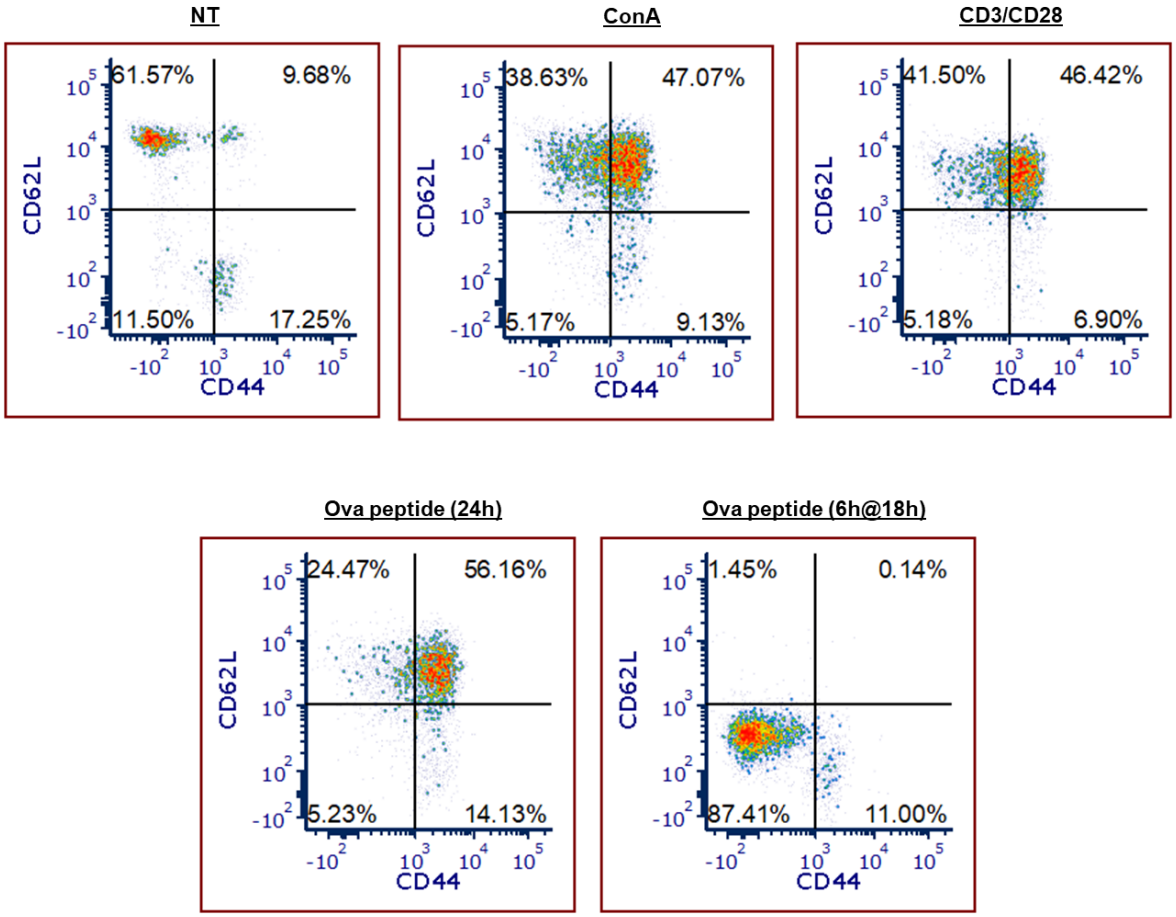

Fig. 4.10: CD8 T cell subsets 24 hours after stimulation. Dot plots showing CD8 T cell subsets after stimulation with ConA, CD3/C28 antibodies, or ova peptide for 24 hours as well as ova peptide stimulation for 6 hours added at the 18-hour timepoint in cell culture.

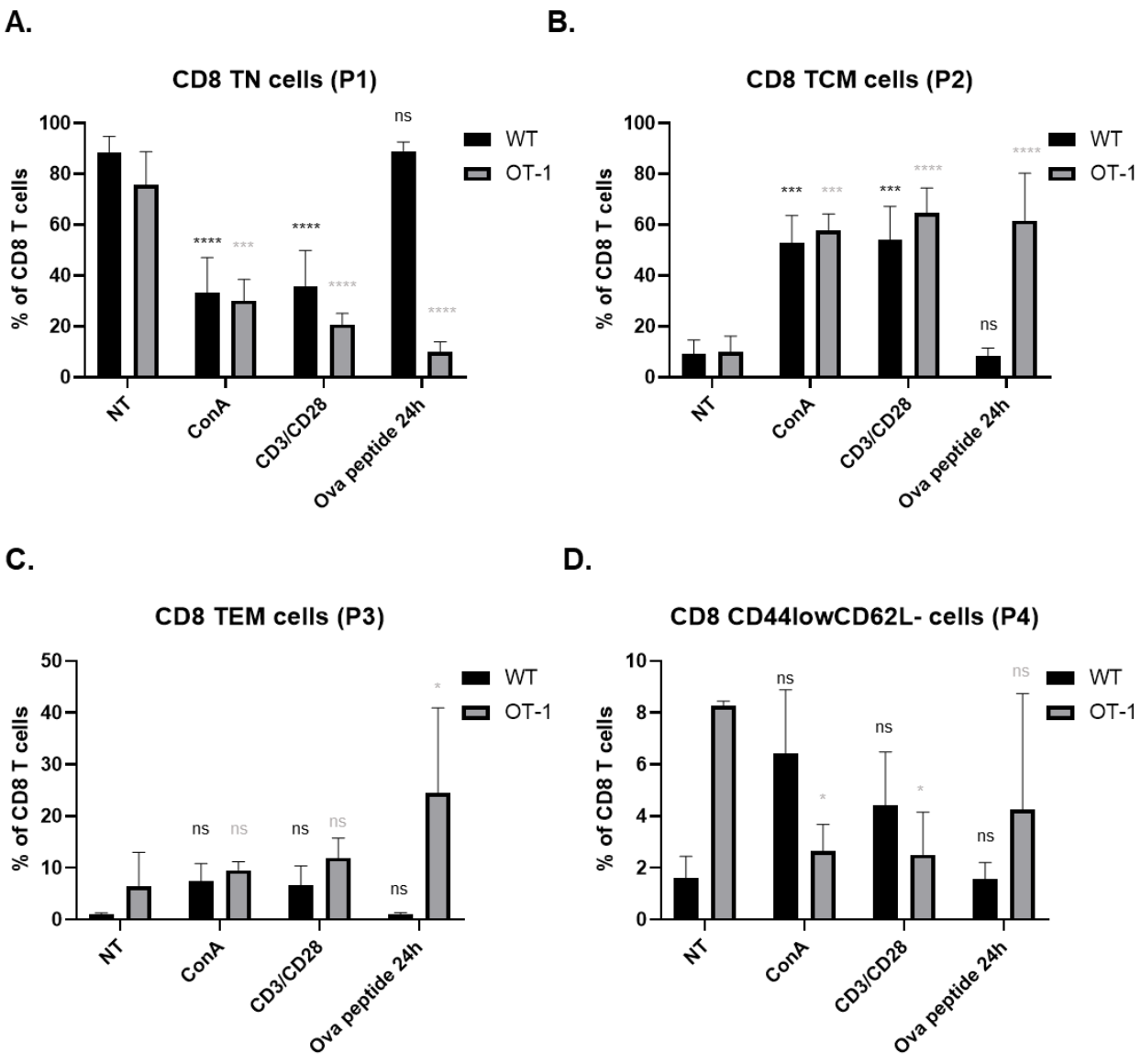

<u>Fig. 4.11:</u> CD8 T cell subsets in C57BL/6 mice and OT-1 mice after stimulation for 24h. Bar graphs quantifying **A.** Naïve P1 cells **B.** Central memory P2 cells **C.** Effector memory P3 cells and **D.** CD44lowCD62Llow P4 cells in both C57BL/6 mice (WT) and OT-1 transgenic mice after 24h of stimulation with ConA, CD3/CD28 antibodies or ovalbumin peptide(n=3). Two-way ANOVA with Tukey's multiple comparisons and 95% confidence interval was used for statistical analysis. Significance is shown individually

between different treatment groups compared to NT for WT (in black) and different treatment groups compared to NT for OT-1 (in grey). Not significant (ns) = $p > 0.05$; *$p < 0.05$; **$p < 0.01$; ***$p < 0.001$; **** $p < 0.0001$.

4.3.4. CD8 T cells are polyfunctional after 24 hours of stimulation

Next, we looked at the ability of CD8 T cells to produce IFN-γ after 24 hours of stimulation with ConA, CD3/CD28, and ova peptide (for OT-1 mice). We observed that in C57BL/6 WT mice CD3/CD28 stimulation led to a significant increase in the production of IFN-γ by CD8 T cells (Fig. 4.12A). In OT-1 mice, CD3/CD28 and ova peptide stimulation led to the increased production of IFN-γ (Fig. 4.12A). We also looked at the GzmB production of CD8 T cells after 24 hours of stimulation and observed that in C57BL/6 mice, both ConA and CD3/CD28 led to similar levels of GzmB expression in CD8 T cells (Fig. 4.12B). In the case of OT-1 mice, GzmB expression was induced by treatment with ConA, CD3/CD28, and with ova peptide (Fig. 4.12B).

To determine whether the CD8 T cells at 24 hours were polyfunctional we looked at the percentage of CD8 T cells positive for both IFN-γ and GzmB. We discovered that in C57BL/6 mice, CD3/CD28 stimulations led to the induction of CD8 T cells with both IFN-γ and GzmB production (Fig. 4.13). In OT-1 mice, CD3/CD28 stimulation and ova peptide led to the induction of polyfunctional CD T cells that were IFN-γ+GzmB+ (Fig. 4.13).

Finally, we also looked at the activation marker PD-1, which is induced early after activation of CD8 T cells and discovered that PD-1 expression was increased in all activation conditions in both WT and OT-1 mice (Fig. 4.14). Stimulation with ova peptide drove the highest increase in PD-1 expression on CD8 T cells in OT-1 splenocytes of all

the different activation conditions (Fig. 4.14). The above data suggest that TCR-based stimulation for 24h leads to CD8 T cell activation and the induction of a strong polyfunctional CD8 T cell response.

From the experiments at 6h and 24h, it is clear that CD8 T cells upon activation with TCR-based stimulation, led to the early induction of P4 cells. Upon stimulation with CD3/CD28 and ova peptide, these P4 cells are capable of IFN-γ production but not GzmB production at 6h. At this time point, they also do not upregulate activation markers like PD-1. By 24 hours, however, P4 cells have disappeared and P2 cells form a majority population within CD8 T cells and demonstrate IFN-γ production, GzmB production as well as upregulation of activation markers like PD-1.

Since P1, P2 and P3 are well characterized as naïve, central memory, and effector memory T cells with many studies focusing on dissecting their biology, we focused on characterizing the P4 subset via further experiments which thus far remains relatively unexplored.

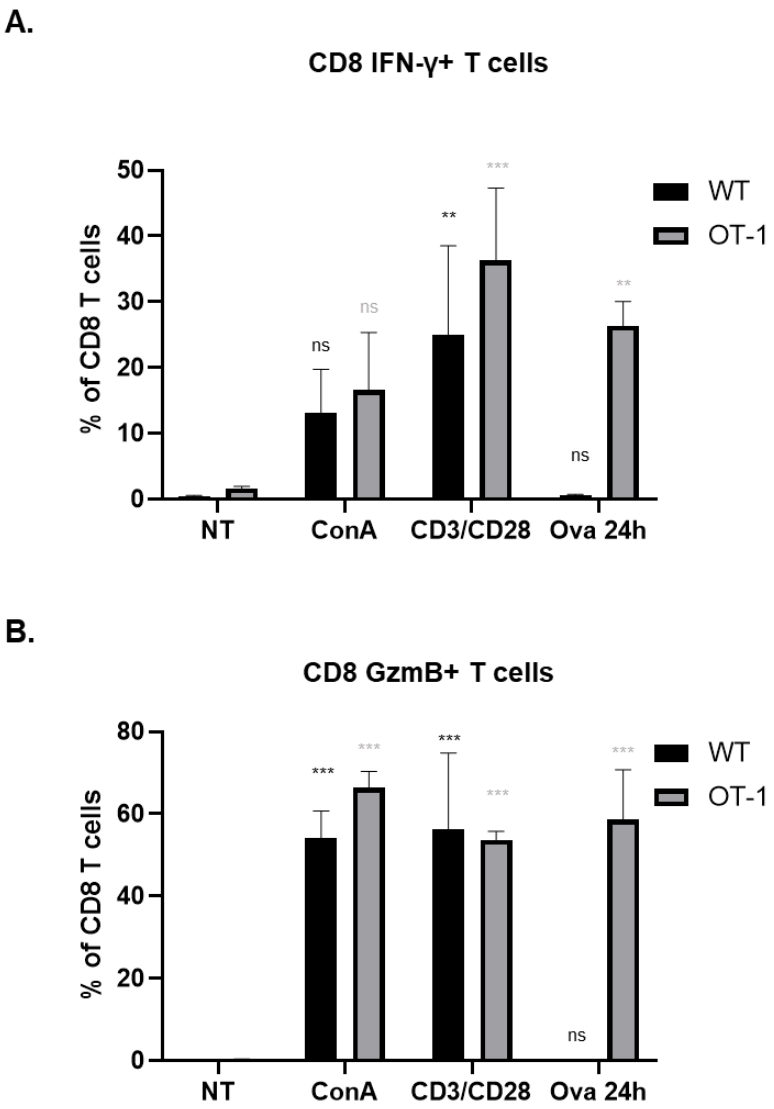

<u>Fig. 4.12:</u> IFN-γ and GzmB production by CD8 T cells upon stimulation for 24h. A. Bar graphs depict the percentage of IFN-γ+ cells in CD8 T cells after 24h of stimulation with ConA, CD3/CD28, and ova peptide in WT and OT-1 mice (n=3). **B.** Bar graphs showing the percentage of GzmB+ CD8 T cells after stimulation of WT and OT-1 splenocytes with ConA, CD3/CD28, and ova peptide for 24 hours in cell culture (n=2). Two-way ANOVA with Tukey's multiple comparisons and 95% confidence interval was

used for statistical analysis. Significance is shown individually between different treatment groups compared to NT for WT (in black) and different treatment groups compared to NT for OT-1 (in grey). Not significant (ns) = $p > 0.05$; *$p < 0.05$; **$p < 0.01$; ***$p < 0.001$; **** $p < 0.0001$.

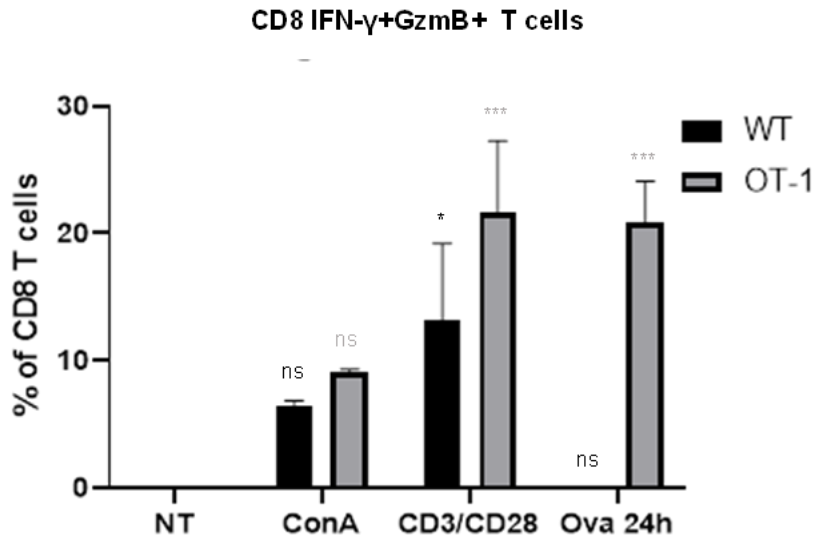

<u>Fig. 4.13:</u> Polyfunctional CD8 T cell response after stimulation for 24h. Bar graphs depicting IFN-γ+GzmB+ CD8 T cells after stimulation of WT C57BL/6 and OT-1 splenocytes with ConA, CD3/CD28, and ova peptide for 24 hours (n=2). Two-way ANOVA with Tukey's multiple comparisons and 95% confidence interval was used for statistical analysis. Significance is shown individually between different treatment groups compared to NT for WT (in black) and different treatment groups compared to NT for OT-1 (in grey). Not significant (ns) = $p > 0.05$; *$p < 0.05$; **$p < 0.01$; ***$p < 0.001$; **** $p < 0.0001$.

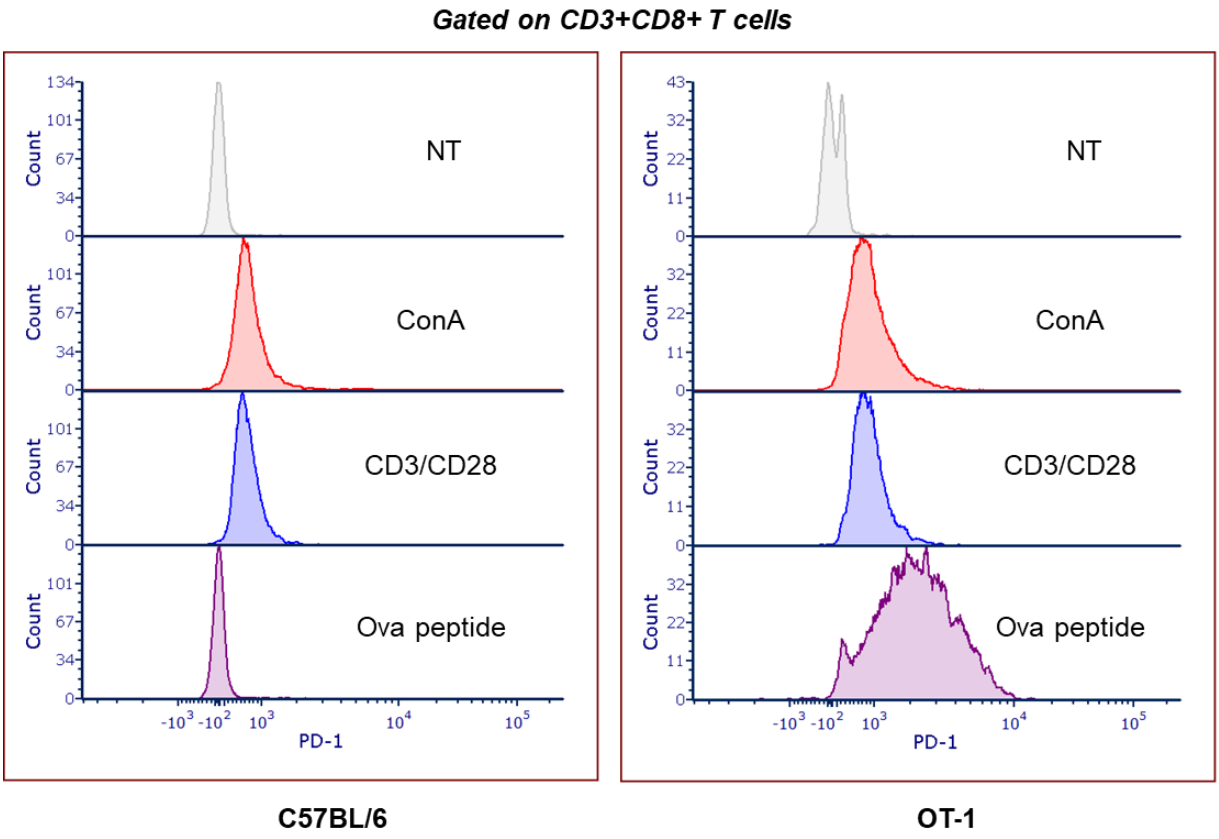

<u>Fig. 4.14:</u> PD-1 expression on CD8 T cells after 24 hours of activation. Representative histograms demonstrate the expression of PD-1 after stimulation of C57BL/6 and OT-1 splenocytes with ConA, CD3/CD28, and ova peptide for 24h in cell culture.

4.3.5. Time course of P4 cell induction and IFN-γ production upon antigenic stimulation

Since P4 cells are induced surprising early at 6h after antigen stimulation and disappear by the 24h time point after activation, we conducted a time course experiment with multiple timepoints within the first 6 hours as well as time points between 6 and 24 hours to delineate the induction of P4 cells and study them over time. For this purpose, we focused on OT-1 mice to study antigen-specific T cells and employed the "OT-1 ova system" to further characterize antigen-specific P4 cells after stimulation with ova peptide. We observed that upon ova stimulation, the percentage of P1 cells was drastically reduced at all time points after stimulation (1, 3, 6, 12, 24h) (Fig. 4.15A). The percentage of P2 cells was quite low in NT OT-1 splenocytes as has been seen previously and was reduced after stimulation even further but was not significant (Fig. 4.15B). At 24h, however, a significant increase in the percentage of P2 cells was observed (Fig. 4.15B) as also been previously noted at this time point. The percentage of P3 cells was not significantly increased at 1h and 3h after ova stimulation but was seen to be significantly increased at 6h, 12h, and 24h (Fig. 4.15C). Finally, and most importantly, the percentage of P4 cells was significantly increased, and P4 cells comprised a majority of the CD8 T cells (~80%) post-stimulation with ova till 6h (Fig. 4.15D). The percentage of P4 cells starts to decrease at 12h, and by 24h, no significant change is seen compared to the NT (Fig. 4.15D).

Considering the change in CD8 populations, we conclude that P1 naïve cells disappear immediately after ova stimulation, and P4 CD44lowCD62Llow cells are induced immediately. P3 cells are increased slowly over time as P4 cells start to reduce in frequency, and P2 cells are only induced at 24h after stimulation. All of these findings

support previously discussed findings from Honjo's group that CD8 T cells may transition from P1 to P4 to P3 cells after activation.

Since we had now seen that the induction of P4 cells happened as early as 1h, it was important to understand whether P4 cells were also functional at this early time point. For this purpose, we investigated the production of IFN-γ by P4 cells at different time points over 24 hours. We discovered that the percentage of IFN-γ+ P4 cells was to be increased with time. At 1h and 3h, the changes in IFN-γ production by P4 cells were not significant however, at 6h, 12h, and 24h after ova stimulation a significant increase in the percentage of IFN-γ+ P4 cells was observed (Fig. 4.16).

It is important to note that by 24 hours, the percentage of P4 cells has reduced to a low level wherein no significant difference is observed against NT (Fig.4.15D). So, although the percentage of IFN-γ+ P4 cells at this timepoint is significantly increased since P4 cells occupy a very small percent of CD8 T cells, the IFN-γ production by these cells at this timepoint may not be substantial overall. Nonetheless, we concluded that P4 cells are induced very early on (1h) after ova stimulation and are functional with significant IFN-γ production by 6h. This suggests that P4 cells may be an important transitory state of CD8 T cells after antigenic stimulation that may have an important role to play in host defense at early time points when a full-scale adaptive immune response has not yet been enabled.

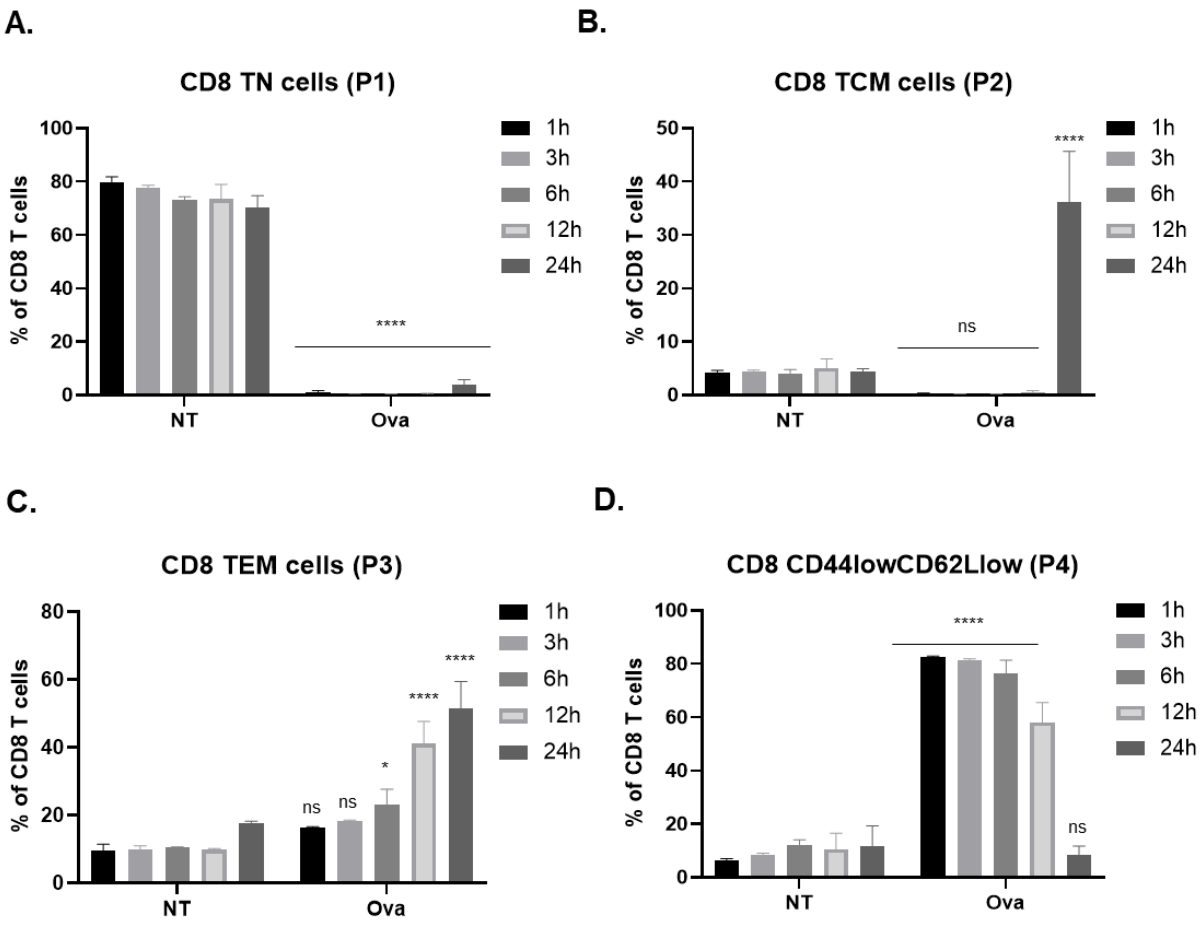

<u>Fig. 4.15:</u> Time course for the loss/induction of P1, P2, P3, and P4 cells after ova peptide stimulation. Bar graphs show the percentage of **A.** naïve P1 cells, **B.** central memory P2 cells, **C.** effector memory P3 cells, and **D.** CD44lowCD62Llow P4 cells after stimulation of OT-1 splenocytes with ova peptide for 1, 3, 6, 12 and 24h in cell culture (n=2). Two-way ANOVA with Tukey's multiple comparisons and 95% confidence interval was used for statistical analysis. Significance is shown for NT vs Ova treatment for each timepoint individually (e.g. NT-1h vs Ova-1h, NT 3h vs Ova 3h, etc.). For P1, P2, and P4, treatments having the same significance range have been grouped with one symbol. Not significant (ns) = $p > 0.05$; *$p < 0.05$; **$p < 0.01$; ***$p < 0.001$; **** $p < 0.0001$.

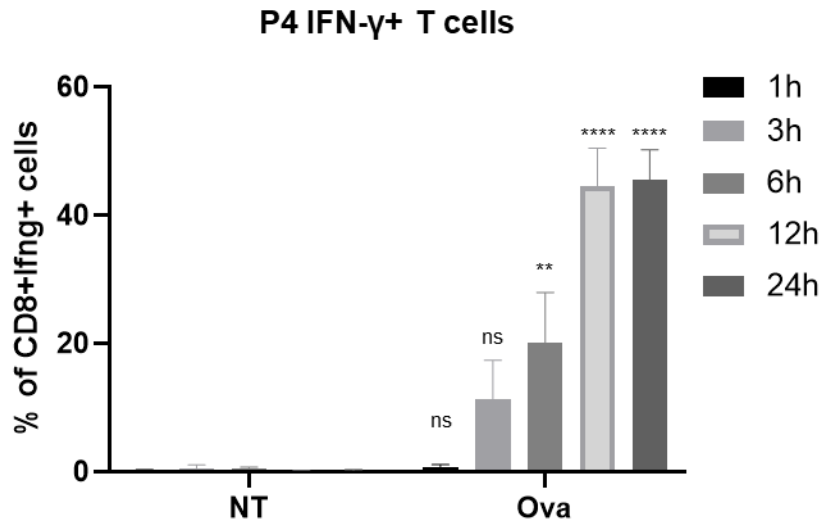

Fig. 4.16: IFN-γ production by CD44lowCD62Llow P4 cells from 1h to 24h. Bar graphs show CD8+IFN-γ+ T cells after stimulation of OT-1 splenocytes with ova peptide for 1, 3, 6, 12, and 24h in cell culture (n=2). Significance is shown for NT vs Ova treatment for each timepoint individually (e.g. NT-1h vs Ova-1h, NT 3h vs Ova 3h, etc.). Not significant (ns) = $p > 0.05$; *$p < 0.05$; **$p < 0.01$; ***$p < 0.001$; **** $p < 0.0001$.

4.3.6. Induction of CD44lowCD62Llow P4 cells *in vivo* after exposure to reovirus

So far, we have demonstrated that P4 cells are induced very early upon priming with antigen and are functionally capable of IFN-γ production. Next, we wanted to investigate whether P4 cells were induced *in vivo* after virus exposure. To this end, we exposed C57BL/6 mice to reovirus and isolated splenocytes, mesenteric lymph nodes, and peritoneal flush from non-treated mice as well as from mice 1,3, and 7 days after injection. Single-cell suspensions were processed for flow cytometry. We observed that, in the spleen, P4 cells were induced early at 3 d.p.i (Fig. 4.17A). The P4 population was reduced on 7 d.p.i. but the percentage of P3 cells was increased (Fig. 4.17A). In the mesenteric lymph node, P4 cells were also induced on 3 d.p.i. and the percentage of P4 cells was maintained at 7 d.p.i. with a slight increase in the P3 population at that timepoint (Fig. 4.17B). In the peritoneal flush obtained from the site of infection (peritoneal cavity) P4 cells were induced very early on 1 d.p.i. along with a large percentage of P3 cells (Fig. 4.17C). Over time, the percentage of the P3 population increased while P4 cells decreased in frequency. P3 cells comprised the majority of CD8 T cells in the peritoneal flush on 7 d.p.i (Fig. 4.17C).

It is interesting to note that even *in vivo*, not only are P4 cells induced early on but the decrease in P4 cells was associated with an increase in P3 cells, similar to what we observed in our *in vitro* time course study over 24h. Once again, these findings further support the model that P1 cells transition to P3 cells via P4 cells as the intermediaries.

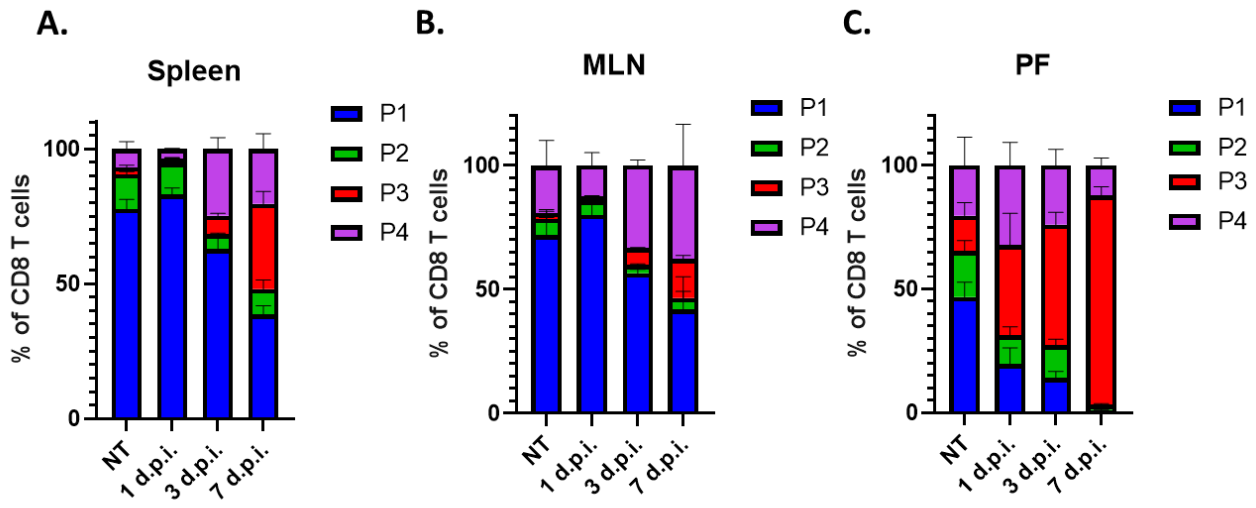

Fig. 4.17: ***In vivo*** **time course for the induction of P1, P2, P3, and P4 cells.** The bar graphs demonstrate the percentage of the different CD8 T cell subsets in the **A.** spleen, **B.** mesenteric lymph node (MLN), and **C.** peritoneal flush (PF) at different time points- 1, 3, and 7 d.p.i.- after intraperitoneal exposure to reovirus *in vivo* (n=3).

4.3.7. Type 1 interferons drive increased functional capabilities of P4 cells

In the previous chapter, we demonstrated that virus exposure drives bystander activation of naïve CD8 T cells via type 1 interferons. As described previously, it is unclear if bystander-activated P1 cells behave like P1 cells in their ability to drive P4 cells induction after stimulation with antigen. We hypothesized that the induction of P4 cells from P1 cells might be different upon stimulation of OT-1 cells with ova peptide in the presence of a virus or type 1 interferon due to the added effect of bystander activation of P1 cells.

Using our reovirus system, we exposed OT-1 splenocytes to reovirus and ova peptide stimulation for 6h and observed T cell subsets using flow cytometry. We discovered that P4 cell induction was not affected by the presence of the virus (Fig. 4.18A). In the presence of type 1 interferon, IFN-β, we found that the P4 cell induction was also not affected by the presence of cytokine during antigen stimulation (Fig. 4.18A). Upon measuring IFN-γ+ P4 cells, however, we discovered that type 1 interferons but not reovirus drove increased frequency of IFN-γ+ P4 cells (Fig. 4.18B). It must be noted that the loss/induction of any of the other CD8 T cell subsets was also unaffected by the presence of reovirus or type 1 interferons during priming with antigen (Fig. 4.19A, B, C).

IFN-γ production was not increased in the presence of the virus possibly because, at 6h, the cells have not had enough time to produce type I interferons that drive increased IFNγ production. To further elucidate the role of type I interferons on P4 IFN-γ production, we treated OT-1 splenocytes with varying concentrations of IFN-β during stimulation with ova peptide for 6h and discovered that the increase in IFN-γ+ P4 cells with type 1 interferon did indeed occur in a dose-dependent manner (Fig. 4.20A). Further, using the IFNAR1

antibody, which blocks the type 1 interferon receptor on the surface of the cell, we observed that the increase in IFN-γ production with the treatment of type 1 interferons was abolished upon treatment with the IFNAR1 antibody (Fig. 4.20B).

Altogether, these data suggest that although the induction of P4 cells after antigen stimulation is not affected by the presence of type 1 interferons during priming, however, the production of IFN-γ by the resulting P4 cells at 6h is directly dependent on the presence of the cytokine. Type 1 interferon signaling initiated by the IFNAR1 receptor is important for the increased IFN-γ production by P4 cells in the presence of type 1 interferons.

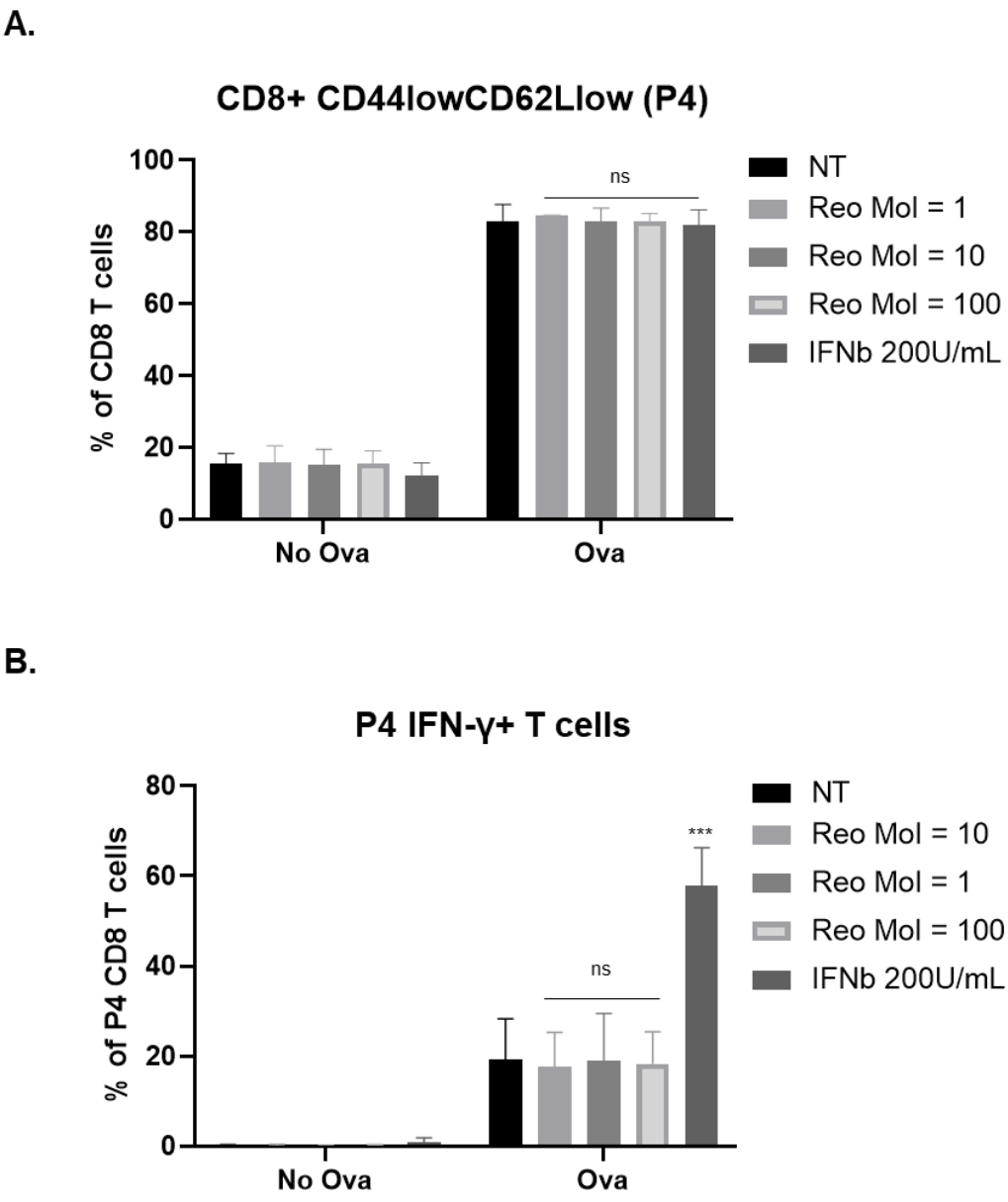

Fig. 4.18: Induction of CD44lowCD62Lloe P4 cells and P4 IFN-γ production with reovirus and type 1 interferon treatment. Bar graphs demonstrate **A.** the induction of CD44lowCD62Llow P4 cells (n=2) and **B.** the percentage of P4 IFN-γ+ CD8 T cells upon treatment with ova peptide in the presence of reovirus or type I interferons for 6h in cell culture (n=2). Two-way ANOVA with Tukey's multiple comparisons and 95% confidence

interval was used for statistical analysis. Significance is shown for all treatment groups compared to NT in the ova treatment group only and treatments having the same significance range have been grouped with one symbol. Not significant (ns) = $p > 0.05$; *$p < 0.05$; **$p < 0.01$; ***$p < 0.001$; **** $p < 0.0001$.

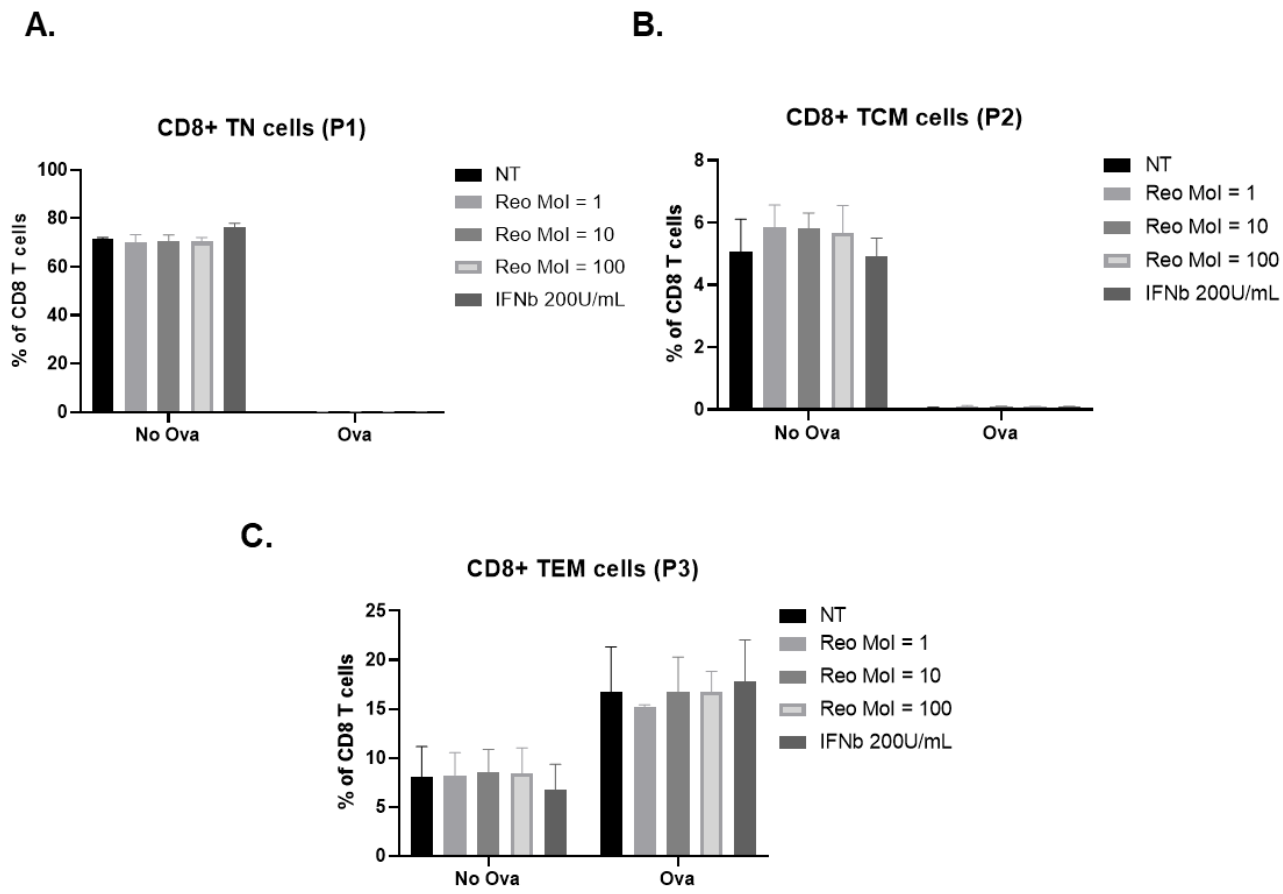

<u>Fig. 4.19:</u> Induction of P1, P2, and cells after ova peptide stimulation in the presence of reovirus or type I interferon. Bar graphs show the percentage of **A.** naïve P1 cells, **B.** central memory P2 cells, and **C.** effector memory P3 cells after stimulation of OT-1 splenocytes with ova peptide in the presence of reovirus or type I interferon for 6h in cell culture (n=2).

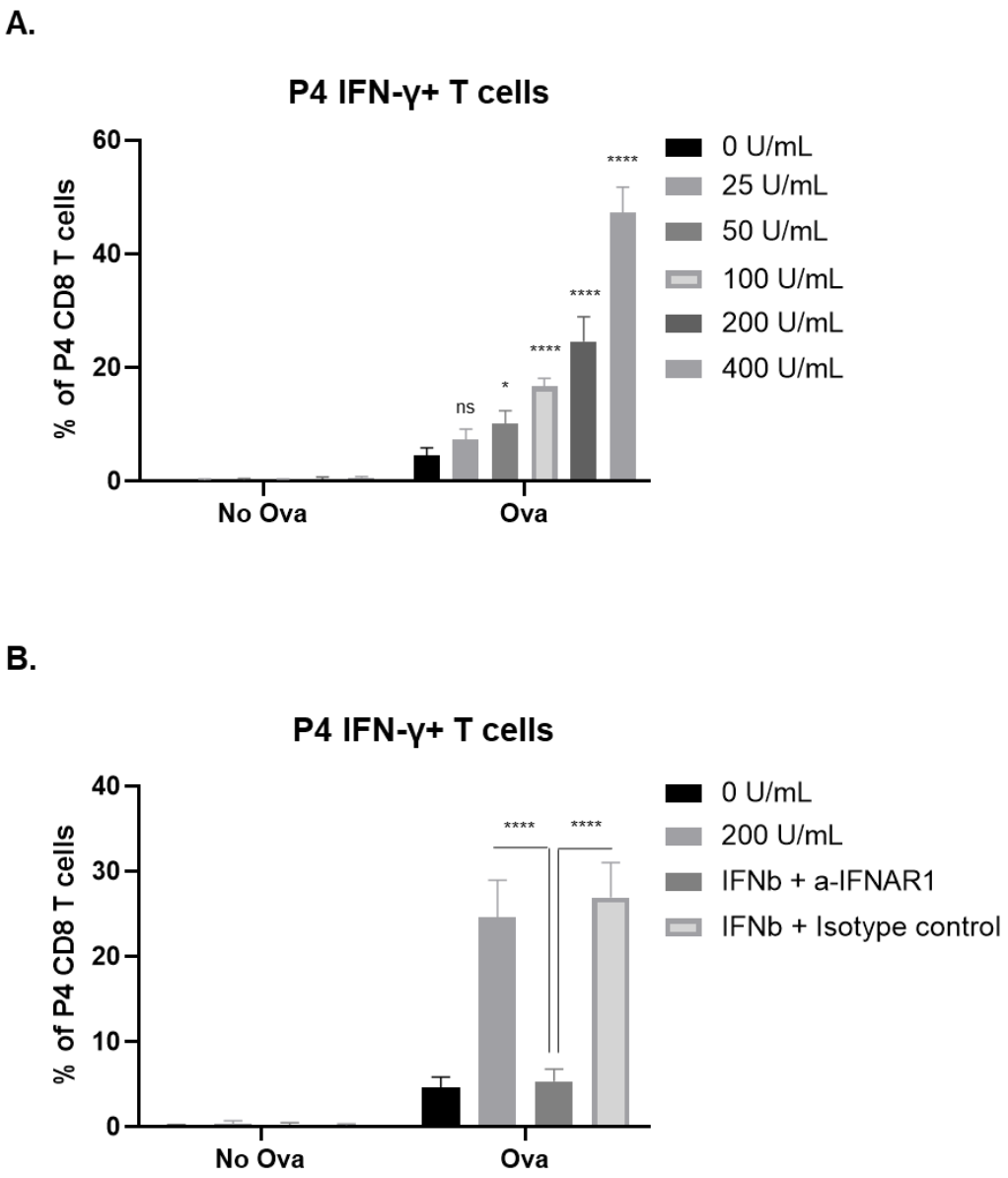

Fig. 4.20: Role of type I interferons in P4 IFN-γ production. Bar graphs depict the percentage of P4 IFN-γ+ cells upon stimulation of OT-1 splenocytes with ova peptide in the presence of **A.** varying doses of type I interferon (n=3) and **B.** IFNAR1 antibody or isotype control (10µg/mL; n=3). Two-way ANOVA with Tukey's multiple comparisons and 95% confidence interval was used for statistical analysis. In **A.** significance has been shown for each dose of type I interferon treatment compared to 0 U/mL in the ova treated group. Not significant (ns) = $p > 0.05$; *$p < 0.05$; **$p < 0.01$; ***$p < 0.001$; **** $p < 0.0001$.

4.3.8. *Ex vivo* and *in vitro* metabolomics analysis of P4 cells

Since the metabolism of CD8 T cells is so closely linked with their function, we wanted to investigate whether the metabolism of P4 cells is rewired compared to P1 cells after activation and elucidate specific differences in metabolic networks between P4 cells and P3 cells as well as P2 cells. To do this, we first isolated P1, P2, P3, and P4 T cell subsets from mice by processing splenocytes directly for flow cytometry after *ex vivo* isolation. This allowed us to generate metabolic signatures of all 4 T cells subsets obtained directly from mice without any activation/stimulation *in vitro*.

Next, we isolated the CD8 T cell subsets after activation of OT-1 splenocytes with ova peptide in cell culture. This was done primarily to study the impact of antigen-specific early T cell activation on the metabolomic profile of newly generated P4 cells. Control populations like P1 cells were isolated after 6h of cell culture without any ova treatment. P2 cells were isolated for comparison to P4 cells generated after 6h of ova priming when they were the predominant population after activation which was at 24h after ova treatment as previously discussed. P3 cells, like P4 cells, were isolated at 6h after ova treatment.

Finally, since type 1 interferons drive increased functional capacity via increased IFN-γ production of P4 cells, we wanted to study the differences in the metabolic signatures of P4 cells generated in the presence and absence of type 1 interferon. To do this, we isolated P4 cells after 6h culture with ova treatment in the presence and absence of IFN-β (100U/mL).

A schematic showing the design for isolation of all the subsets of CD8 T cells *in vitro* and *ex vivo* has been shown in Fig 4.21. Table 7 shows the various samples processed for

metabolomics with sample name, cell number, as well as a normalization factor, along with other sample details. It is important to note that the different samples have varying cell numbers with significant orders of magnitude variation between some samples. For example, all P1 samples have cell numbers in the order of magnitude of 10^6, all P2 samples have cell numbers in the order of magnitude of 10^5, and P4 isolated *ex vivo* directly from OT-1 mice without any stimulation yields cell numbers in the order of magnitude 10^4. This was the case because samples of interest in the case of *ex vivo* sorting were sorted from the same mouse and the inherent frequency of different CD8 T cell subsets vary greatly in these non-treated splenocytes. P1 cells are the most abundant as discussed earlier whereas P3 and P4 populations are the least abundant in non-treated OT-1 mice. As described in detail in Chapter 2, before analyzing comparisons, adjustments for cell numbers were carried out and a representative of the data before and after cell number correction is shown as an example in Fig. 4.22.

Next, when comparing the metabolomics signatures, one of the first questions we asked was whether the metabolic signatures for the starting population- P1- were different when compared between freshly isolated P1 cells and P1 cells from cell culture. Upon plotting all the samples on a PCA plot, we compared P1 *ex vivo* (which was isolated from mice directly and processed for metabolomics) with P1-6h-NT (which was isolated from splenocytes that were in cell culture for 6h but not treated with any stimulation). We observed that both these P1 populations clustered close together in the PCA plot suggesting that they had similar metabolic signatures (Fig. 4.23). *In vitro* and *ex vivo* analyses were conducted separately from this point on.

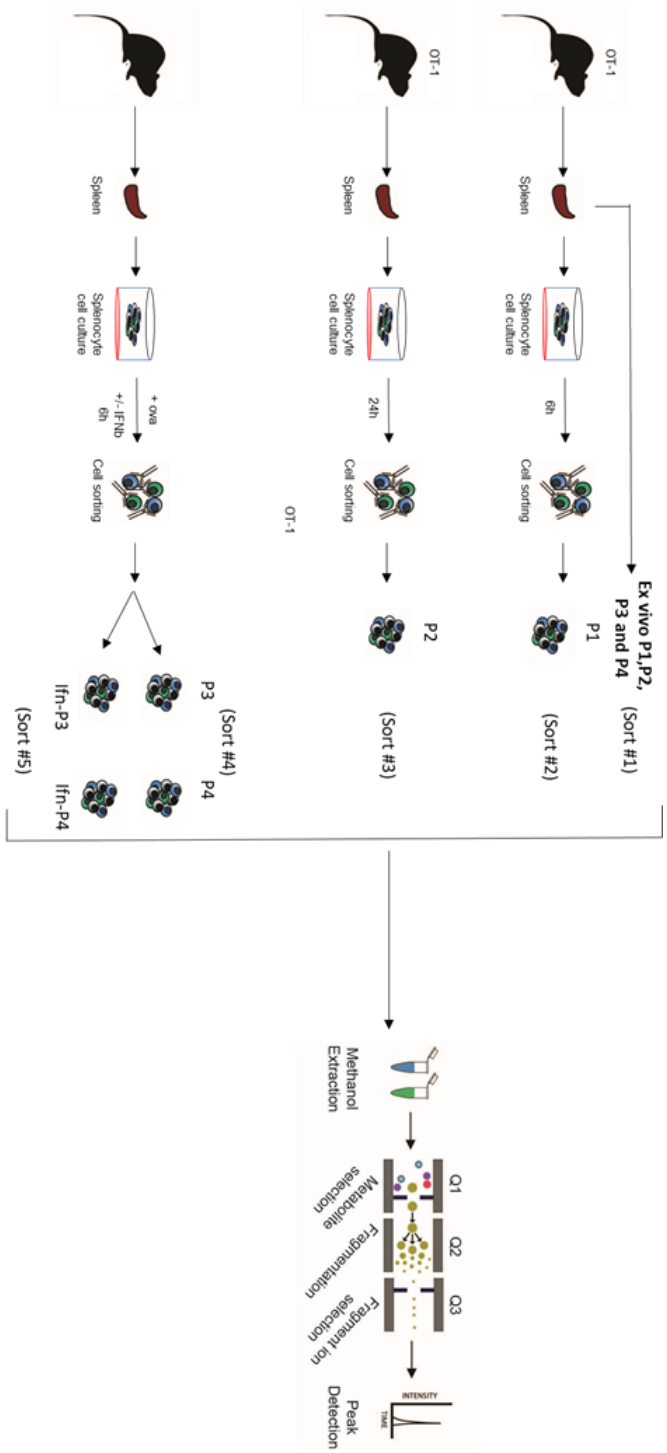

Fig. 4.21: Metabolomics analysis of P4 cells. Schematic depicts the workflow for performing the different sorts to obtain the *ex vivo* as well as *in vitro* samples by flow cytometry followed by methanol extraction and processing for metabolomics analysis.

Sample Name	sample_num	Cell number	P	Group	Rep	NormFactor
P1 6h NT #1	P1-6h-nt-1	3633545	P1	6h-nt	1	112
P1 6h NT #2	P1-6h-nt-2	2486965	P1	6h-nt	2	76
P1 Ex vivo #1	P1-ex-vivo-1	3658433	P1	ex-vivo	1	112
P1 Ex vivo #2	P1-ex-vivo-2	3500000	P1	ex-vivo	2	107
P2 24h ova #1	P2-24h-ova-1	382396	P2	24h-ova	1	12
P2 24h ova #2	P2-24h-ova-2	536916	P2	24h-ova	2	16
P2 Ex vivo #1	P2-ex-vivo-1	173685	P2	ex-vivo	1	5
P2 Ex vivo #2	P2-ex-vivo-2	227023	P2	ex-vivo	2	7
P3 24h ova #1	P3-24h-ova-1	157168	P3	24h-ova	1	5
P3 24h ova #2	P3-24h-ova-2	579181	P3	24h-ova	2	18
P3 6h Ifn ova #1	P3-6h-ifn+ova-1	2520180	P3	6h-ifn+ova	1	77
P3 6h Ifn ova #2	P3-6h-ifn+ova-2	1131689	P3	6h-ifn+ova	2	35
P3 6h ova #1	P3-6h-ova-1	2420863	P3	6h-ova	1	74
P3 6h ova #2	P3-6h-ova-2	1405744	P3	6h-ova	2	43
P3 Ex vivo #1	P3-ex-vivo-1	348081	P3	ex-vivo	1	11
P3 Ex vivo #2	P3-ex-vivo-2	265835	P3	ex-vivo	2	8
P4 6h Ifn ova #1	P4-6h-ifn-ova-1	3313107	P4	6h-ifn+ova	1	102
P4 6h Ifn ova #2	P4-6h-ifn-ova-2	2132916	P4	6h-ifn+ova	2	66
P4 6h NT #1	P4-6h-nt-1	613177	P4	6h-nt	1	19
P4 6h NT #2	P4-6h-nt-2	563243	P4	6h-nt	2	17
P4 6h ova #1	P4-6h-ova-1	2990264	P4	6h-ova	1	92
P4 6h ova #2	P4-6h-ova-2	2976275	P4	6h-ova	2	91
P4 Ex vivo #1	P4-ex-vivo-1	57828	P4	ex-vivo	1	2
P4 Ex vivo #2	P4-ex-vivo-2	32562	P4	ex-vivo	2	1
Pool	Pool	NA	Pool	Pool		

Table 7. Sample information table for metabolomics analysis. The above table provides details of all the samples processed for flow cytometry including sample name, cell number for each sample, population type as well as normalization factor used for analysis.

Before Correction by Cell Count

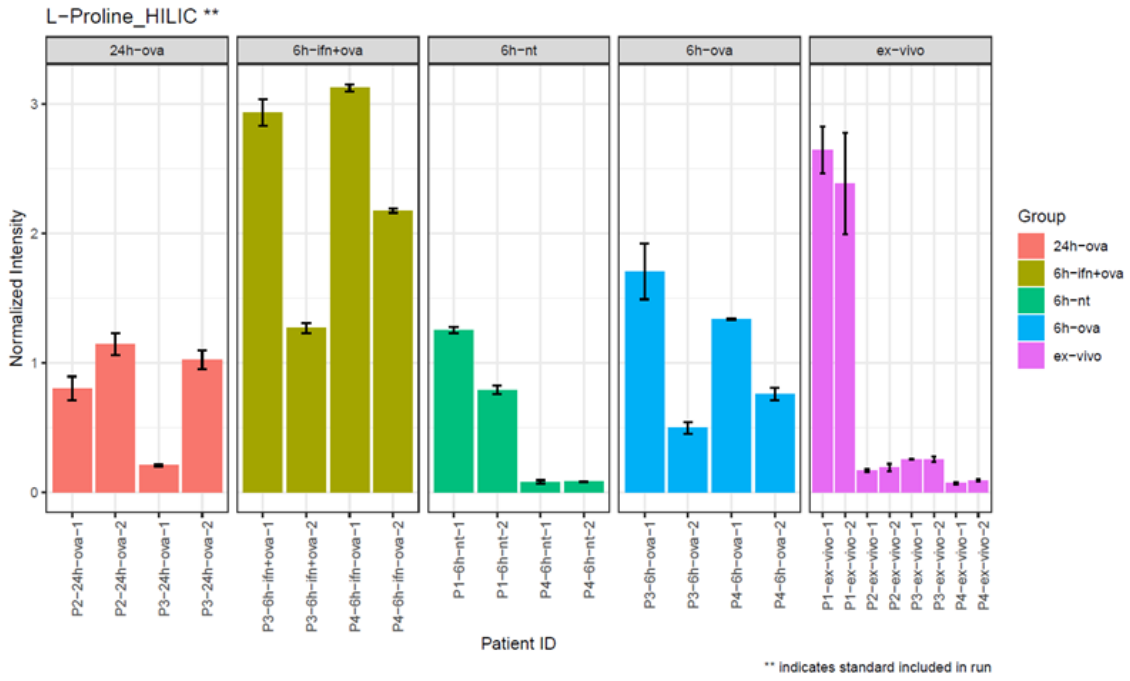

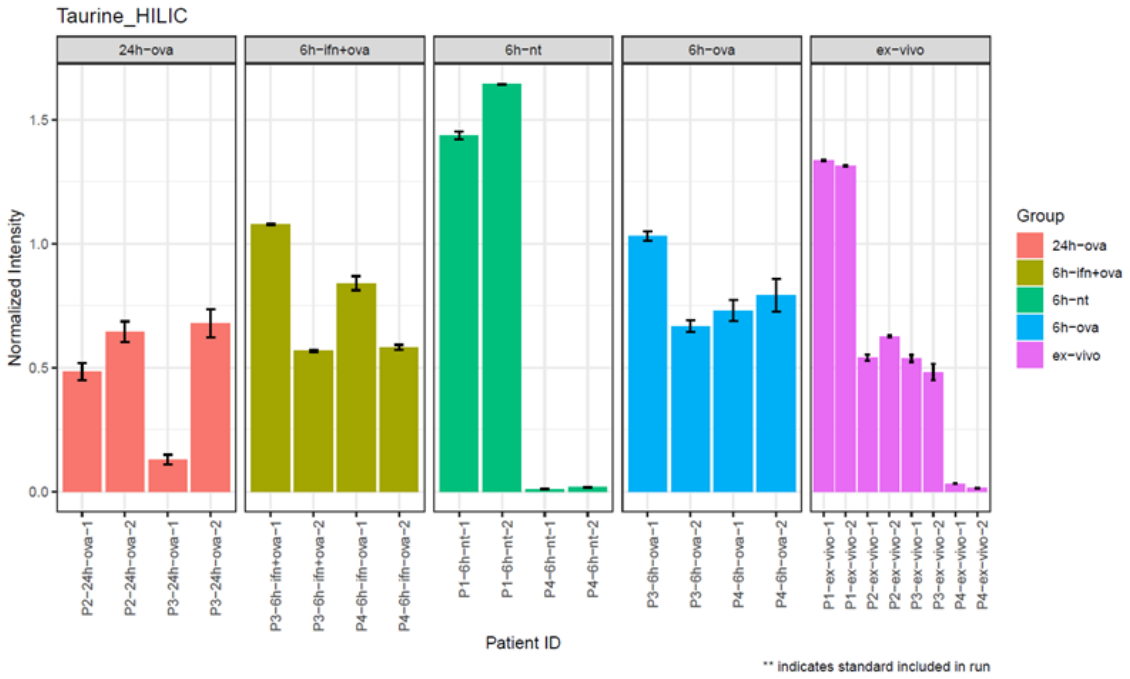

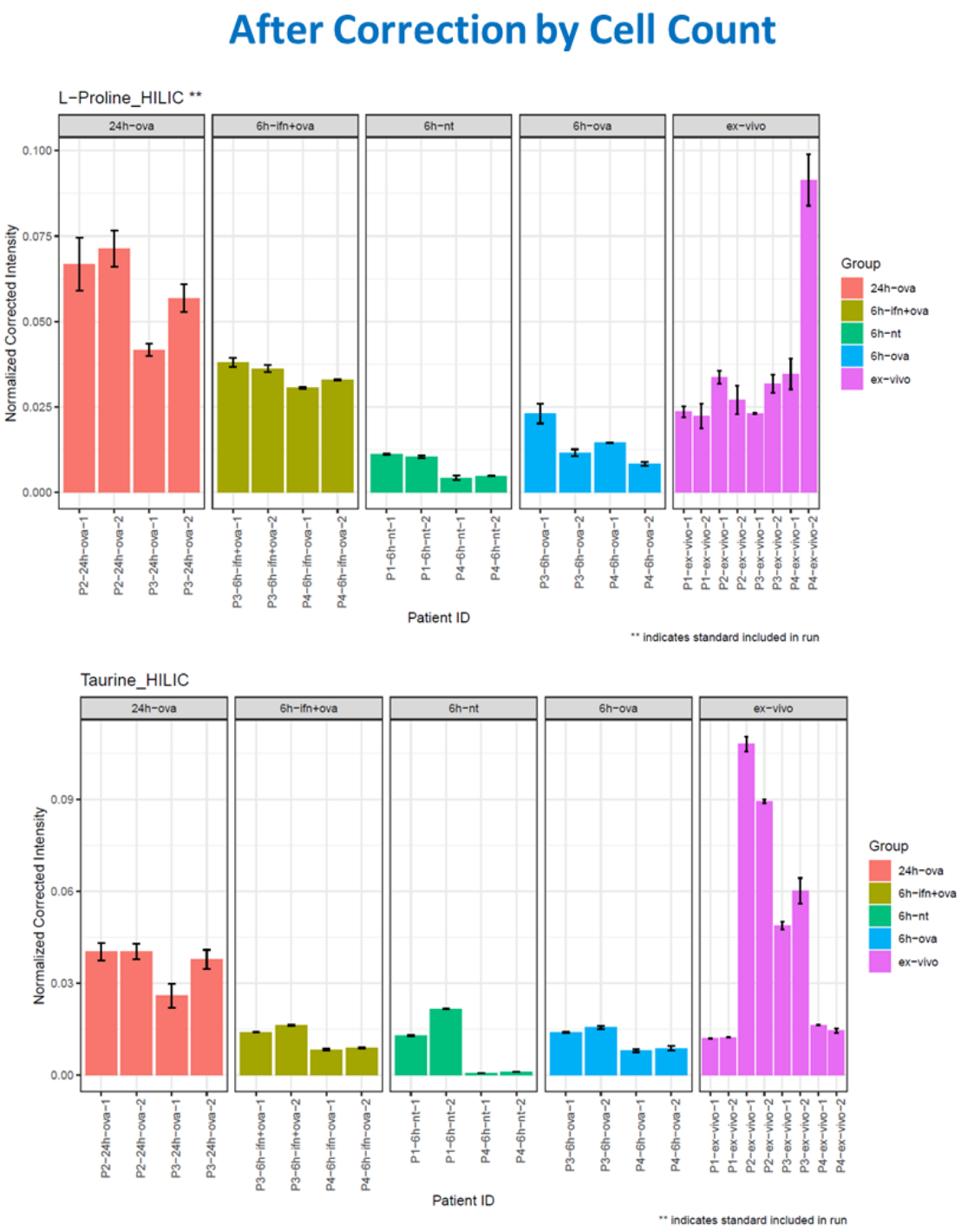

<u>Fig. 4.22:</u> Metabolomics analysis with/without cell number correction. The above bar plots show examples of two different metabolites- L-proline and taurine- to demonstrate the differences in analyses of data with and without cell number correction.

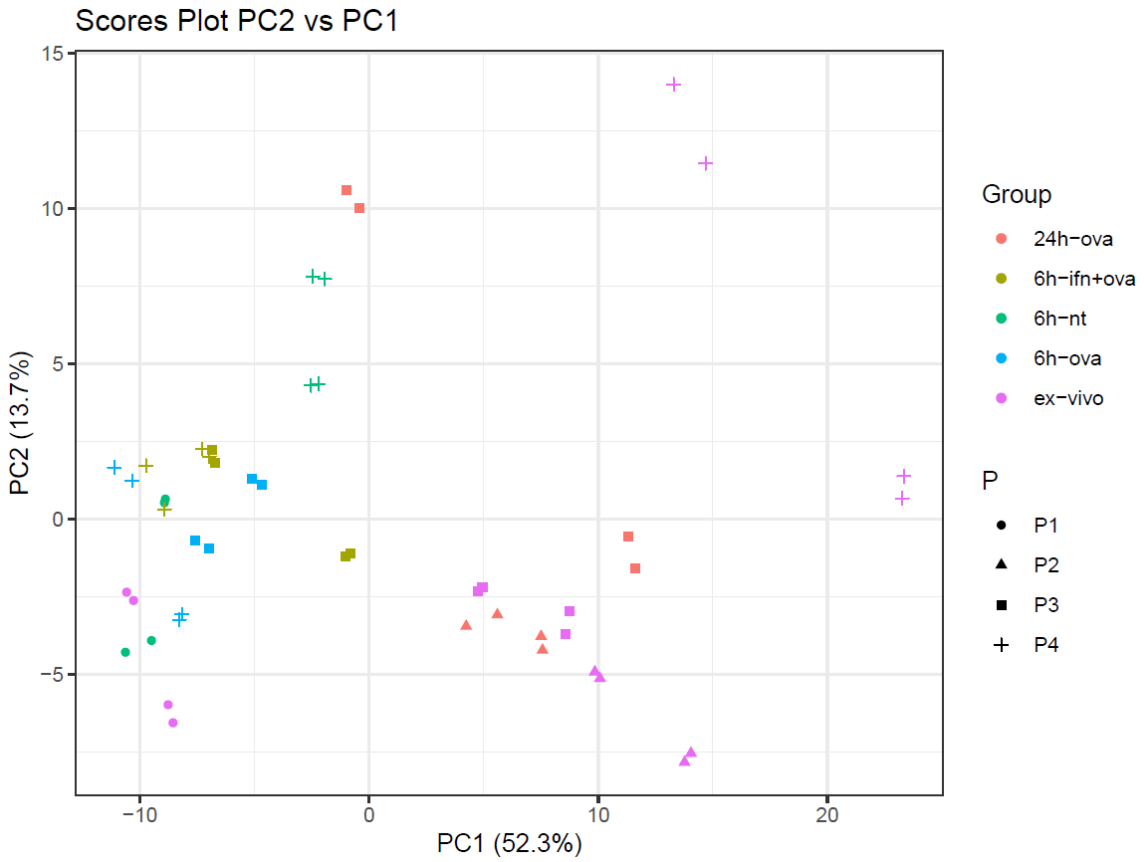

<u>Fig. 4.23:</u> PCA plot for metabolomics analysis of all *ex vivo* and *in vitro* samples. The principal component analysis (PCA) plots show all samples plotted against PC1 and PC2.

4.3.9. The pentose phosphate pathway and aminoacyl-tRNA biosynthesis are differentially regulated in P4 cells compared to other T cell subsets *ex vivo*

Upon plotting all the samples from our *ex vivo* metabolomics analysis on a PCA plot, we discovered that P2 and P3 cells segregated close to each other whereas P1 and P4 samples could be grouped as distinct populations (Fig. 4.24). This is in line with previous literature suggesting that P2 and P3 are both memory T cells- one identified as central memory (P2) with higher memory potential than the other (P3) which is classified as effector memory. This also revealed that metabolically, P4 cells formed a distinct cluster of their own and had different signatures compared to P1, P2, and P3 (Fig. 4.24). A heatmap showing the top 100 metabolites also revealed that P4 cells indeed had completely rewired metabolic signatures compared to P1 cells as well as P3 and P4 cells (Fig. 4.25).

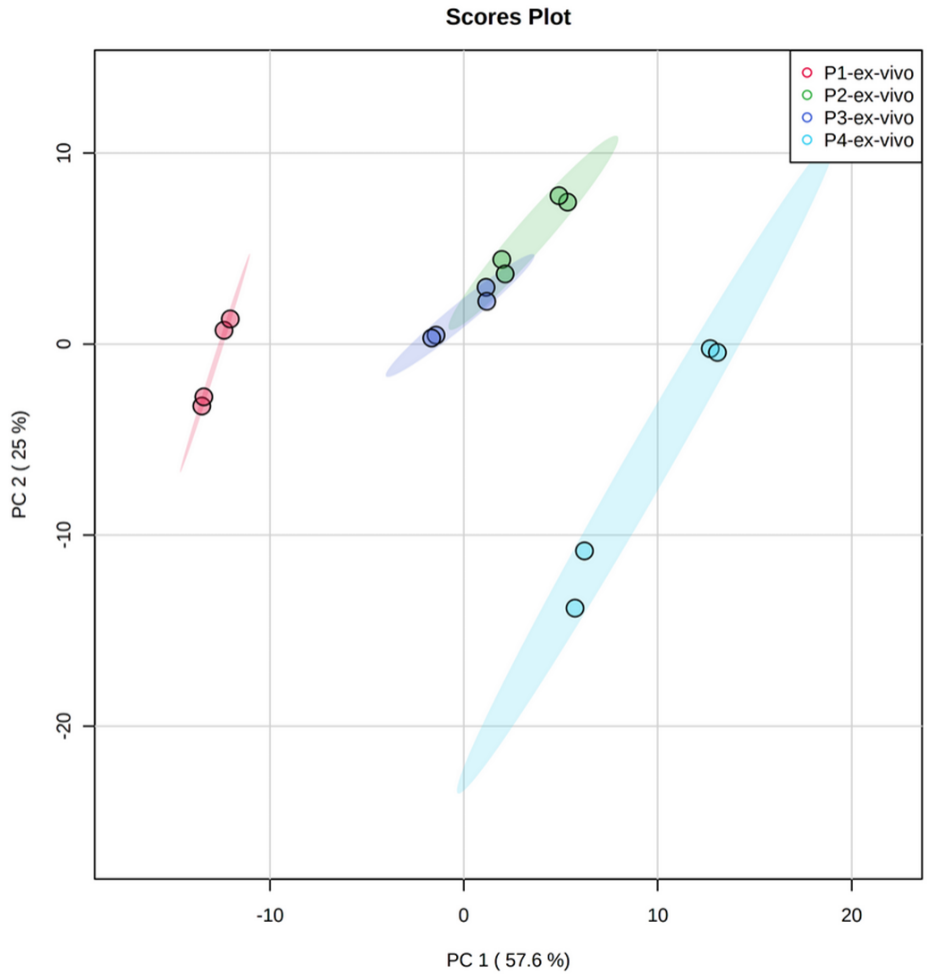

Fig. 4.24: PCA plot for *ex vivo* CD8 T cell metabolomics. PCA plot showing clustering of different samples for P1, P2, P3, and P4 populations isolated from OT-1 mice and processed for metabolomics without cell culture.

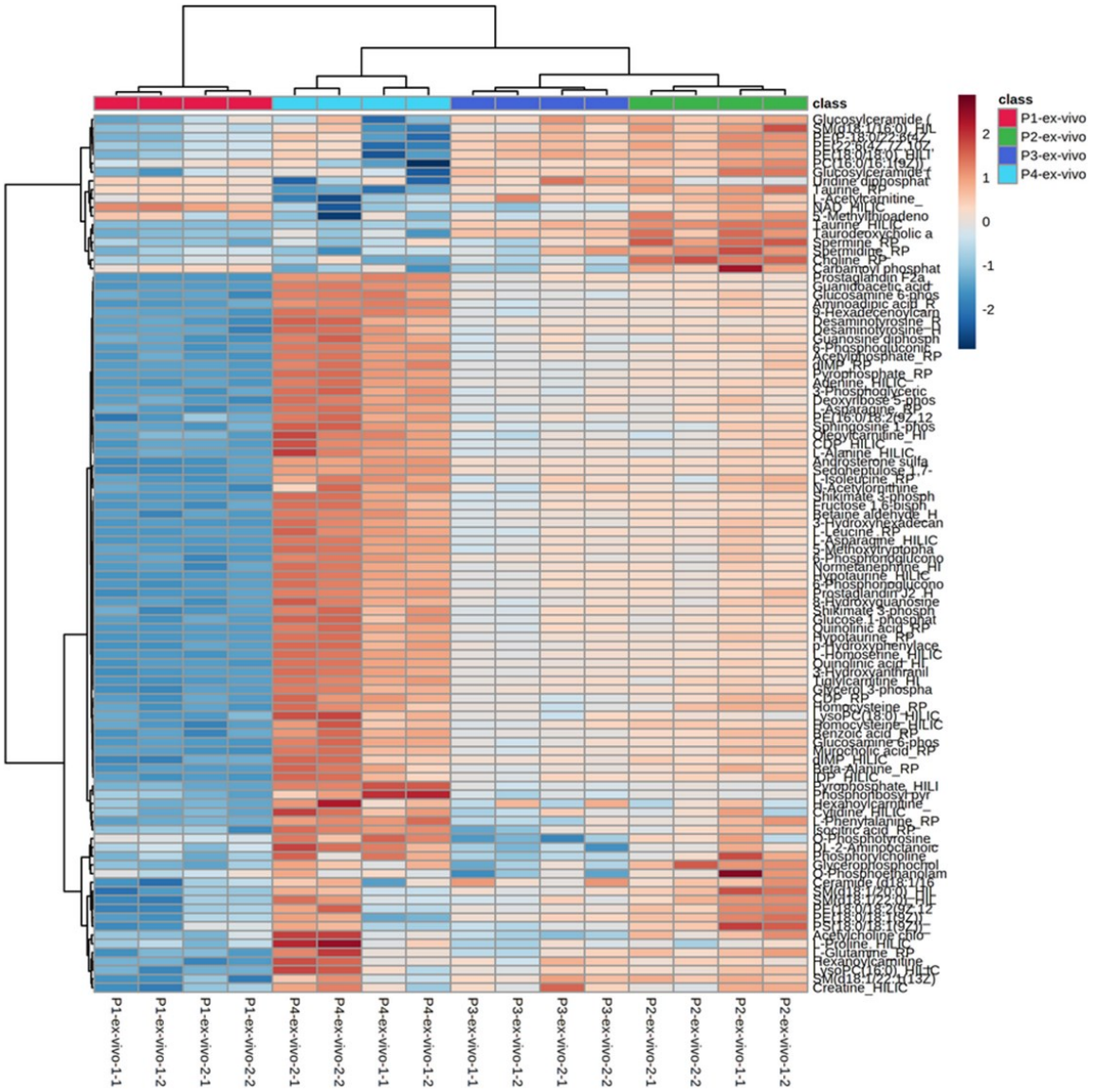

<u>Fig. 4.25:</u> Heatmap for *ex vivo* CD8 T cell metabolomics. Heatmap showing the top 100 significantly changed metabolites by ANOVA in P1, P2, P3, and P4 *ex vivo* samples isolated from T-1 mice and processed for metabolomics without cell culture.

Next, we wanted to investigate how the metabolic signature of P4 cells differed when compared to each of the other CD8 T cell subsets individually. When compared to P1 naïve cells first, we identified 81 significantly changed metabolites that were at least two-fold changed compared to P1 cells. These metabolites have been represented in a volcano plot in Fig 4.26. Enrichment analysis of these metabolites revealed that the aminoacyl tRNA biosynthesis pathway was enriched with metabolites like L-Asparagine, L-Phenylalanine, L-Glutamine, L-Alanine, L-Isoleucine, L-Leucine, and L-Proline as hits within that metabolic set. Other metabolic pathways that were enriched in our enrichment analysis were the pentose phosphate pathway and pyrimidine metabolism, which along with aminoacyl tRNA biosynthesis, made up the top 3 enriched metabolite sets in P4 cells when compared to P1 cells (Fig. 4.27 and 4.28).

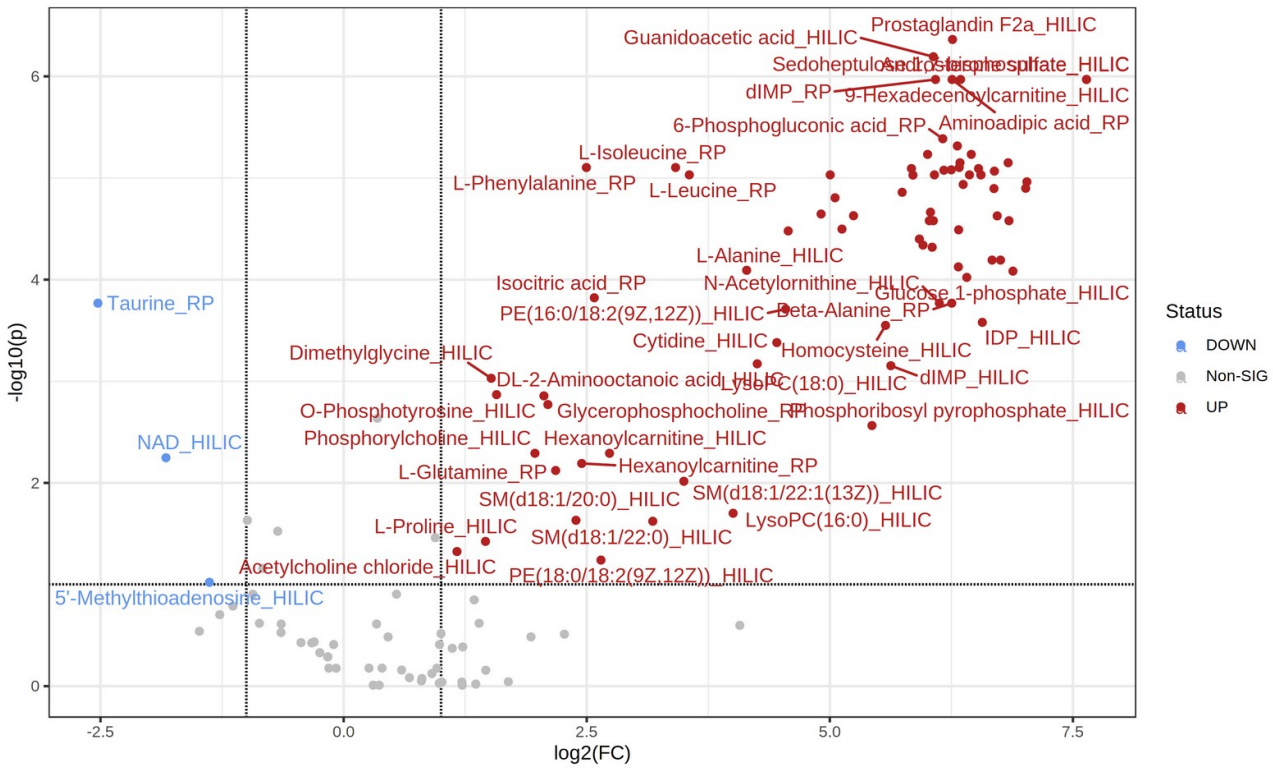

Fig. 4.26: Volcano plot showing significantly changed metabolites (P4 Vs P1). The volcano plot shows significantly changed metabolites (FDR < 0.1 and fold change > 2) for P4 cells compared to P1 cells.

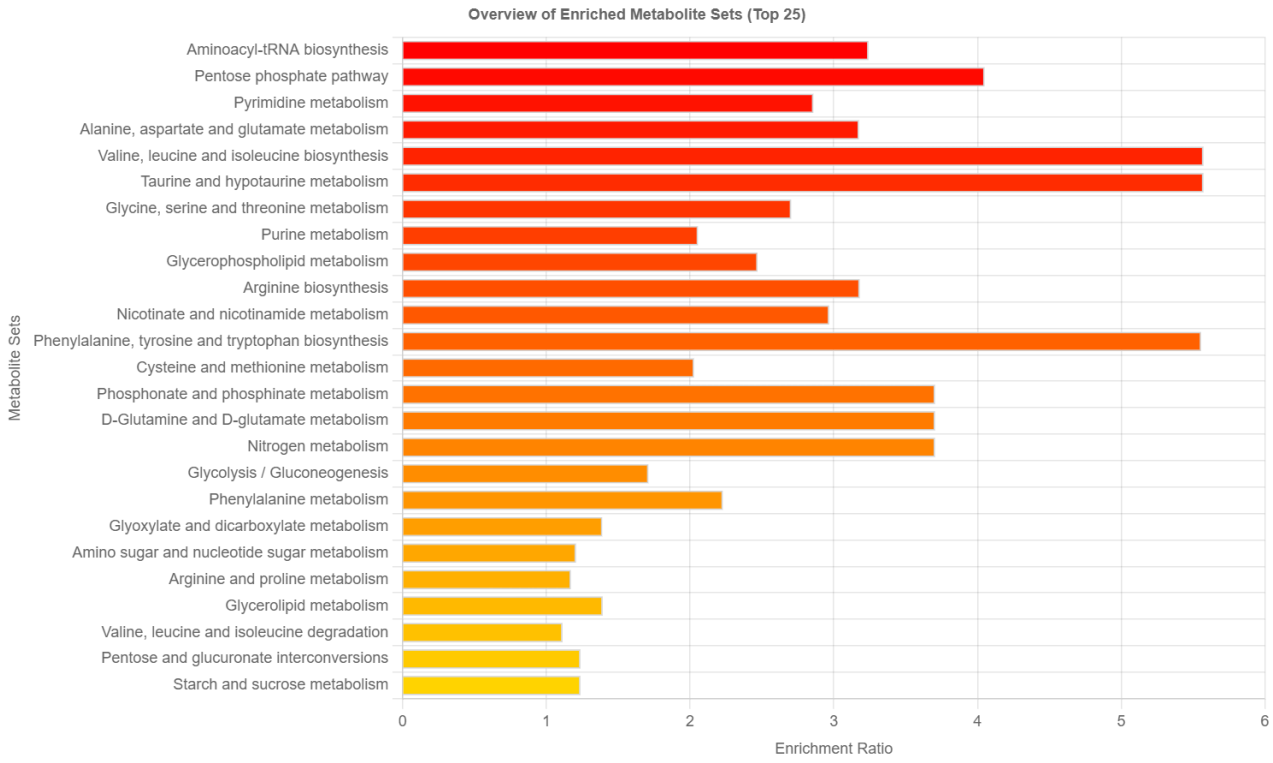

<u>Fig. 4.27:</u> Bar graphs for enrichment analysis P4 vs P1. The bar graphs show the enriched KEGG metabolic pathways when comparing significantly changed metabolites between P4 and P1 cells with the corresponding enrichment score for each pathway. Bar graphs are generated using Metaboanalyst.

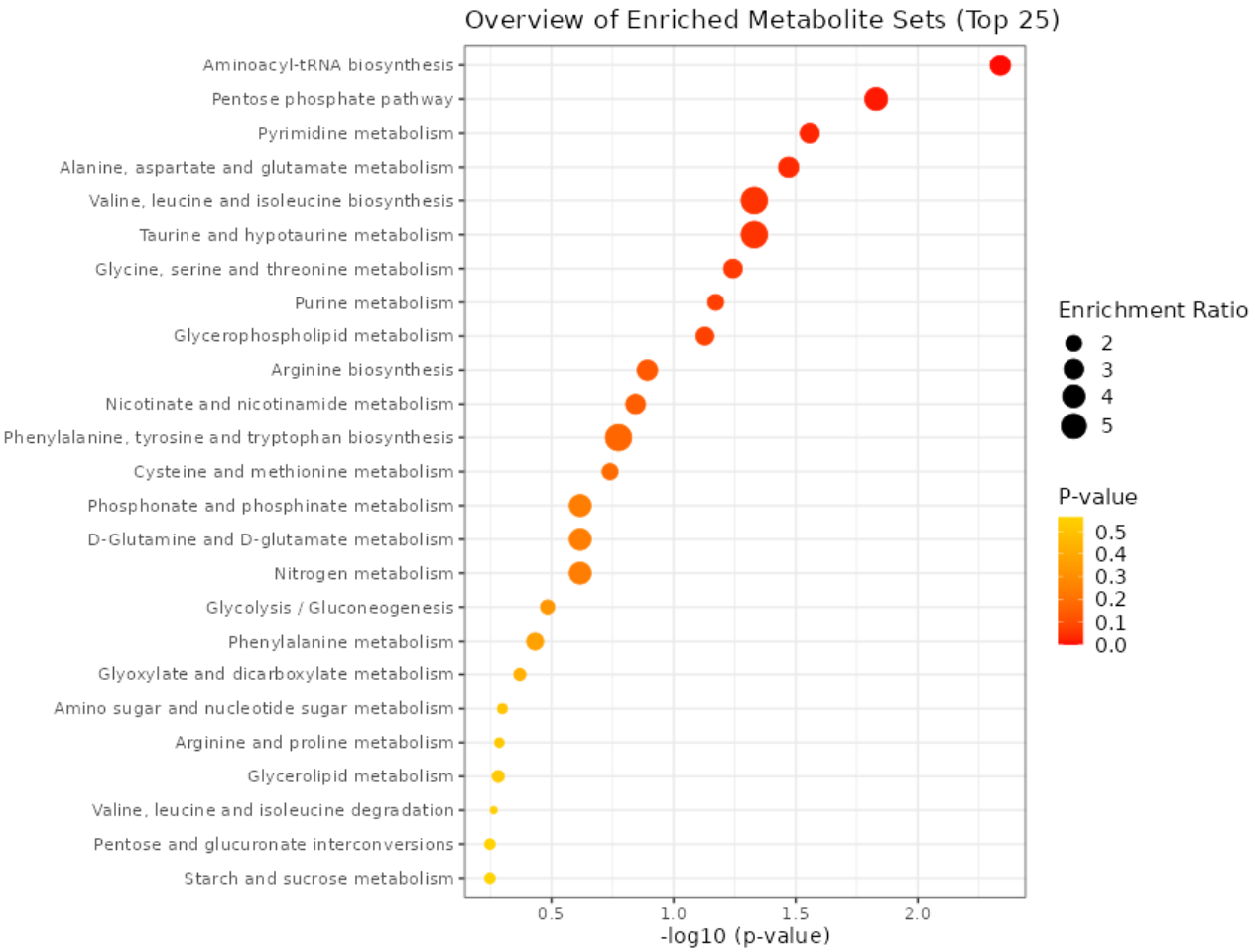

<u>Fig. 4.28:</u> Dot plots for enrichment analysis P4 vs P1. The dot plots show the enriched KEGG metabolic pathways when comparing significantly changed metabolites between P4 and P1 cells with the corresponding enrichment ratio as well as the p-value for each pathway. Dot plots are generated using Metaboanalyst V5.

To investigate the differences in the metabolic networks of P4 cells compared to P2 cells, we focused our analysis on the metabolomics data for these two groups and identified 78 metabolites that were significantly changed at least two-fold (Fig. 4.29). We performed enrichment analysis again using Metaboanalyst on KEGG database metabolite sets and identified glycine, serine, and threonine metabolism, pentose phosphate pathway, and alanine, aspartate, and glutamate metabolism as the top 3 metabolite sets that were found to be significantly enriched for P4 versus P2 cells (Fig. 4.30).

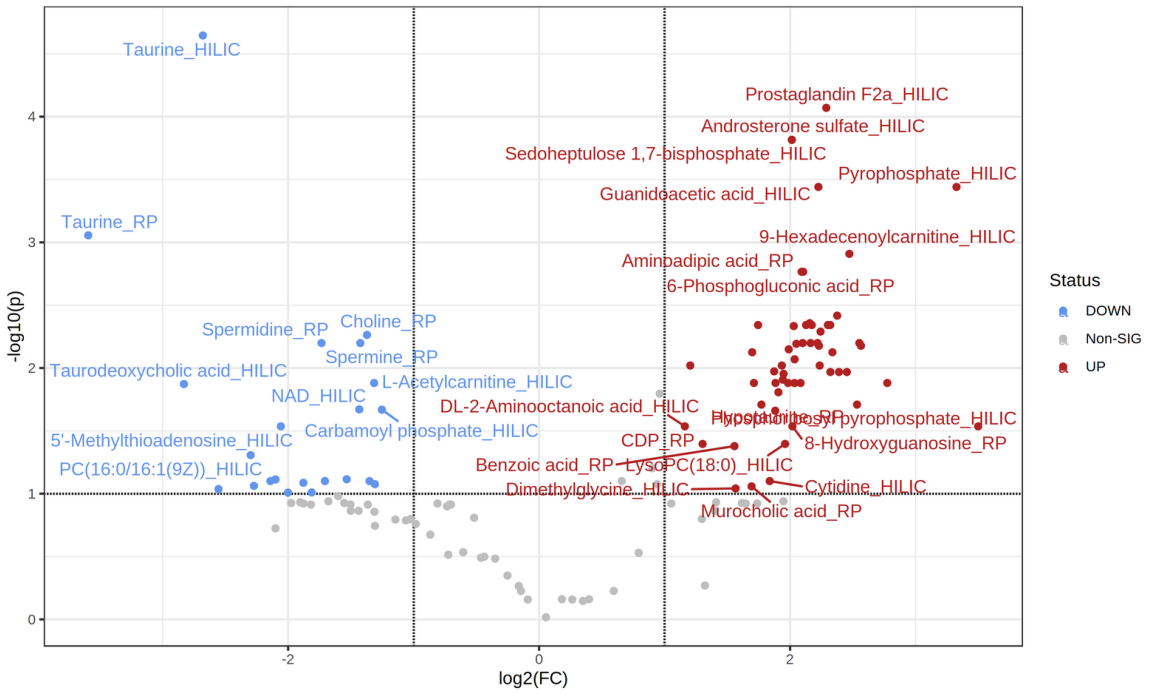

<u>Fig. 4.29:</u> Volcano plot showing significantly changed metabolites (P4 Vs P2). The volcano plot shows significantly changed metabolites (FDR < 0.1 and fold change > 2) for P4 cells compared to P2 cells.

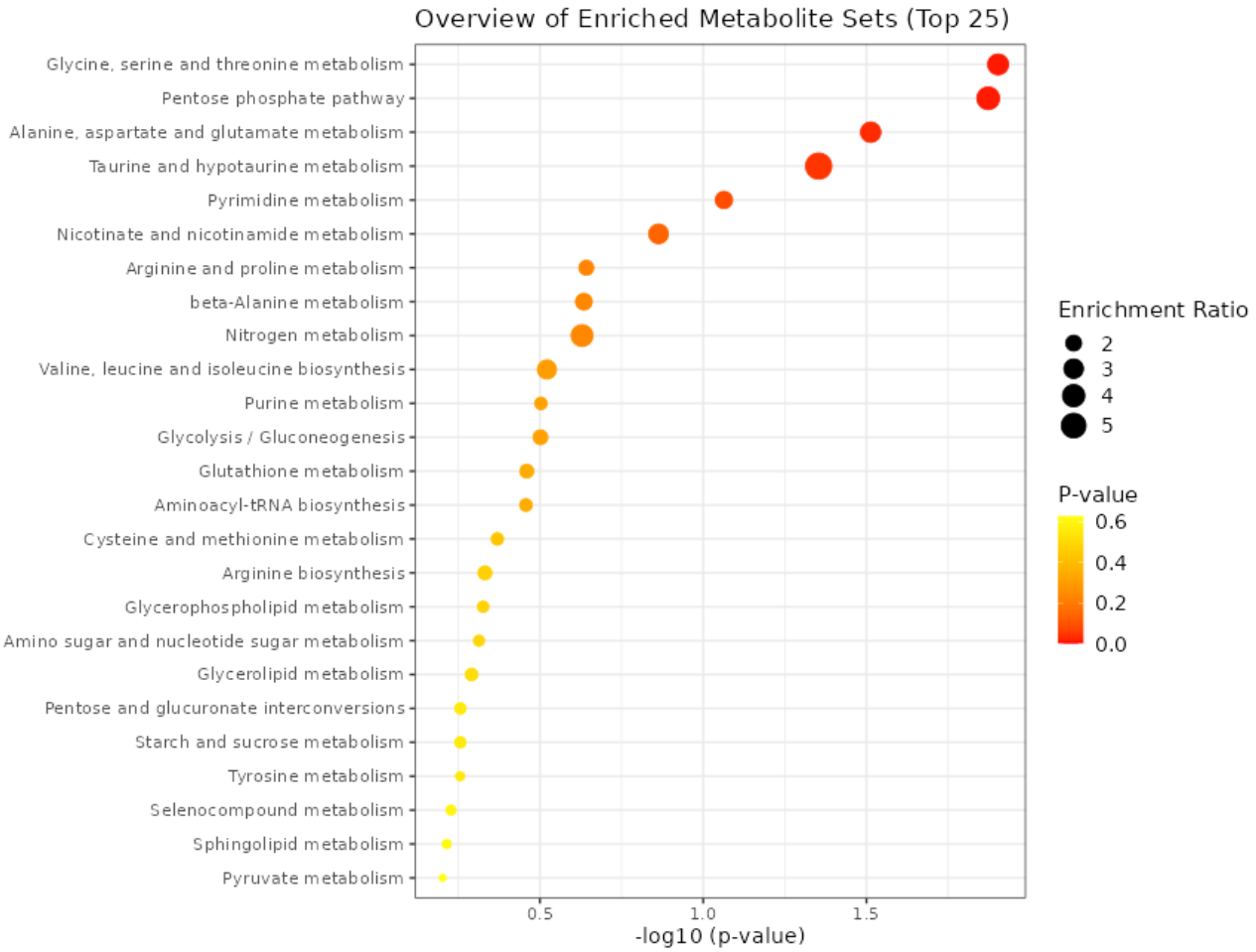

<u>Fig. 4.30:</u> Enrichment analysis for metabolite sets when comparing P4 vs P2. Dot plots show the enriched KEGG metabolic pathways when comparing significantly changed metabolites between P4 and P2 cells with the corresponding enrichment score and p-value for each pathway. Dot plots were generated using Metaboanalyst V5.

Finally, we also compared the metabolic signatures of P4 cells to P3 cells. It has been suggested that P4 cells are the precursors of P3 cells so this was an important comparison to understand the metabolic networks that could drive the differences between these two closely related cell types. We identified 76 significantly changed metabolites in this comparison (Fig. 4.31). Enrichment analysis using Metaboanalyst was carried out again and revealed that the pentose phosphate pathway, aminoacyl tRNA biosynthesis, and valine, leucine, and isoleucine metabolism were the top 3 enriched metabolite sets (Fig. 4.32).

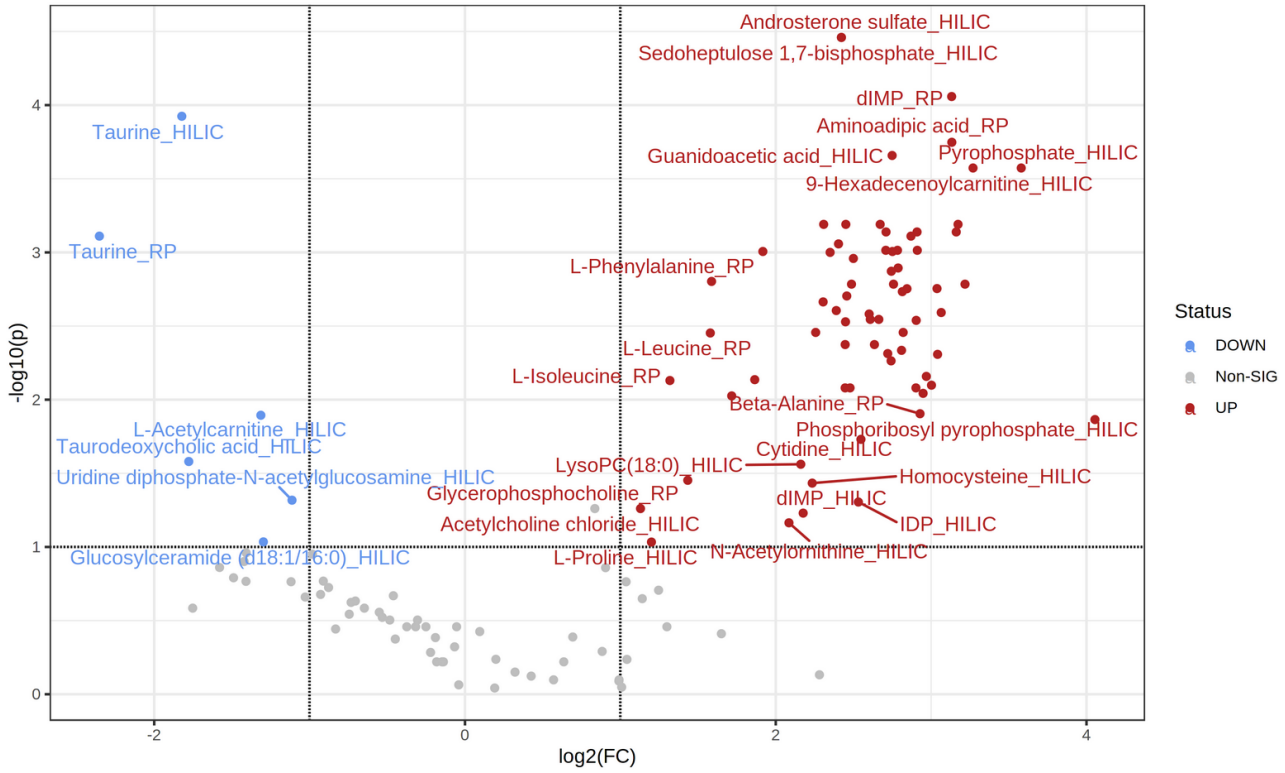

<u>Fig. 4.31:</u> Volcano plot showing significantly changed metabolites (P4 Vs P3). The volcano plot shows significantly changed metabolites (FDR < 0.1 and fold change > 2) for P4 cells compared to P1 cells.

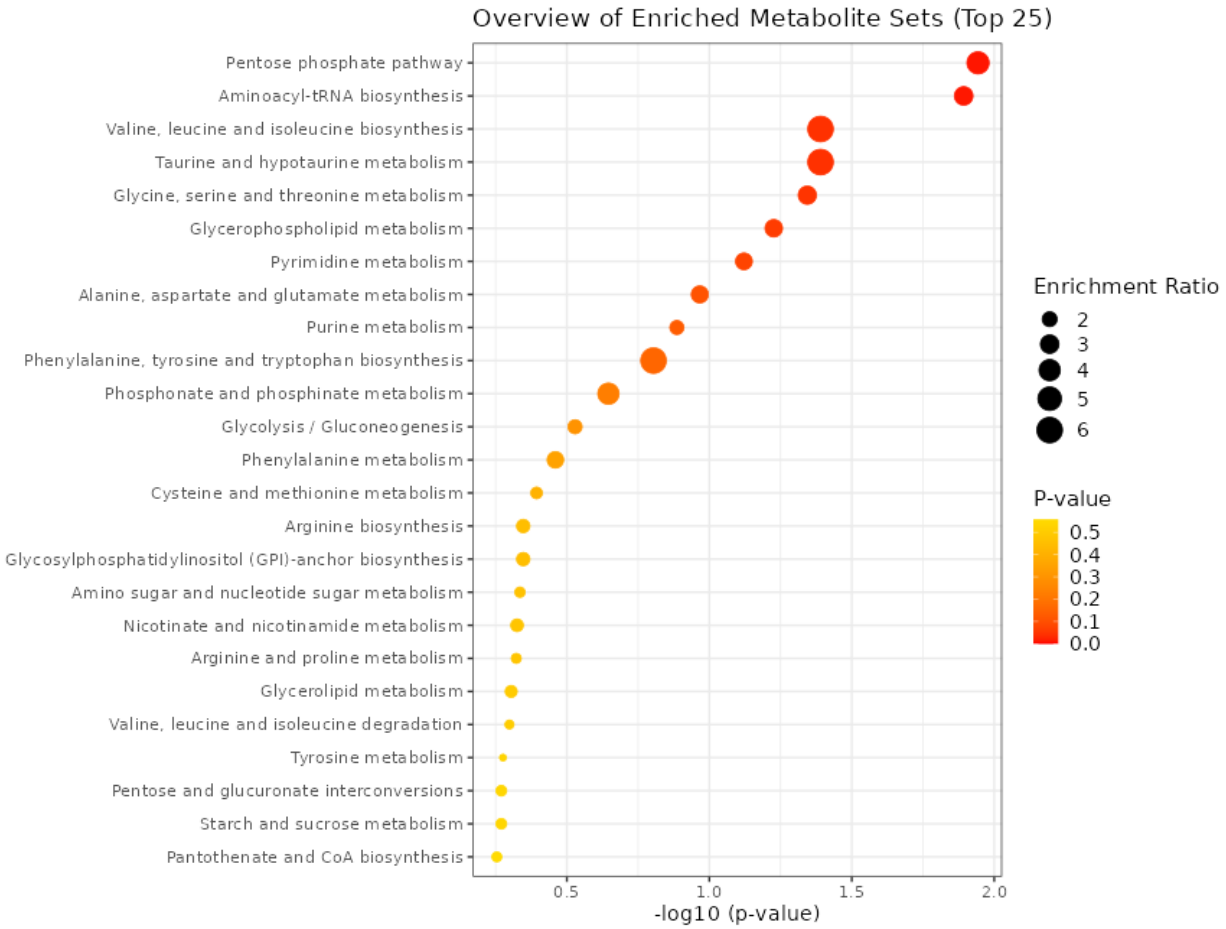

<u>Fig. 4.32:</u> Enrichment analysis for metabolite sets when comparing P4 vs P3. Dot plots show the enriched KEGG metabolic pathways when comparing significantly changed metabolites between P4 and P3 cells with the corresponding enrichment score and p-value for each pathway. Dot plots were generated using Metaboanalyst V5.

Since it has been established that P1 cells lead to the induction of P4 cells, which subsequently lead to P3 cells, we next focused our analysis on comparisons between P4 and immediate neighbors P1 and P3 in the differentiation hierarchy. When comparing the top three enriched pathways in both sets of comparisons, we found that the pentose phosphate pathway and aminoacyl tRNA biosynthesis metabolite sets were common hits. In the pentose phosphate pathway metabolite set, all 4 metabolites identified as hits- Deoxyribose 5-phosphate, 6-Phosphogluconic acid, 6-Phosphonoglucono-D-lactone, and Phosphoribosyl pyrophosphate were seen to be differentially regulated in both comparisons of P4 to P1 as well as P3 (Fig. 4.33). Within the aminoacyl tRNA biosynthesis pathway, L-Asparagine, L-Phenylalanine, L-Alanine, L-Isoleucine, L-Leucine, and L-Proline were common hits in both the P4 vs P1 comparison as well as the P4 vs P3 comparison (Fig. 4.34). L-Glutamine was an additional hit within the same metabolite set that was differentially regulated in the P4 vs P1 comparison only (Fig. 4.34).

Taken together, this data demonstrates that the pentose phosphate pathway and aminoacyl t-RNA metabolism are differentially regulated in P4 cells compared to P1 cells and P3 cells obtained from OT-1 spleens *ex vivo* without any cell culture.

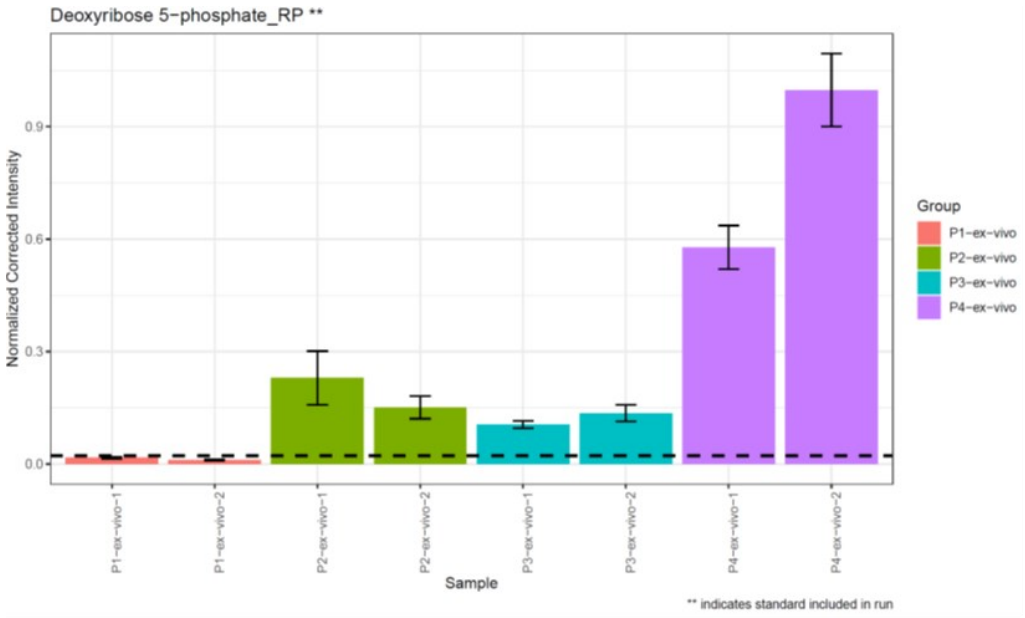
Deoxyribose 5−phosphate_RP **
Normalized Corrected Intensity
0.0
0.3
0.6
0.9
P1−ex−vivo−1
P1−ex−vivo−2
P2−ex−vivo−1
P2−ex−vivo−2
P3−ex−vivo−1
P3−ex−vivo−2
P4−ex−vivo−1
P4−ex−vivo−2
Sample
Group
P1−ex−vivo
P2−ex−vivo
P3−ex−vivo
P4−ex−vivo
** indicates standard included in run

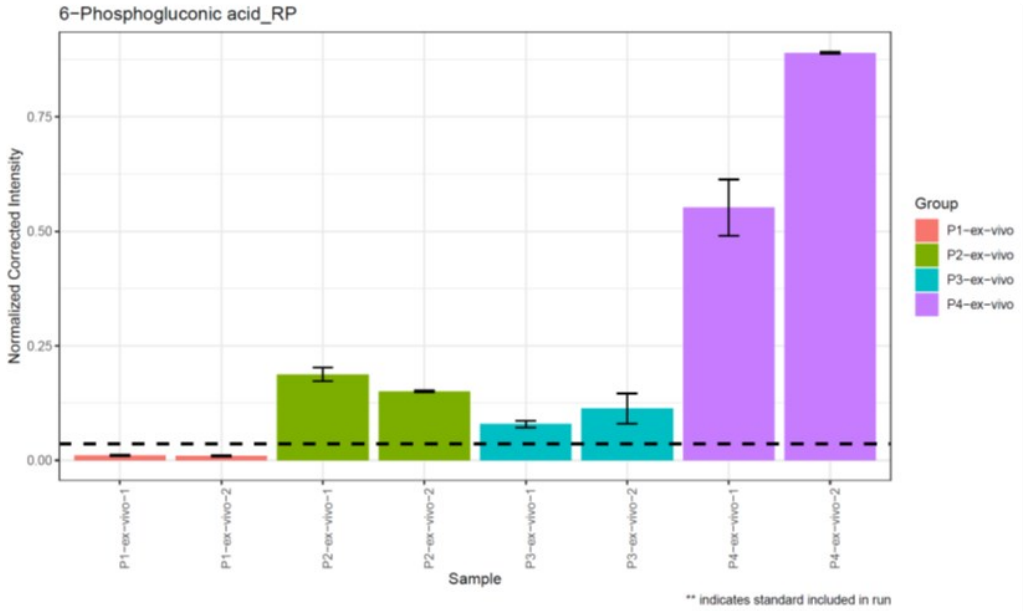
6−Phosphogluconic acid_RP
Normalized Corrected Intensity
0.00
0.25
0.50
0.75
P1−ex−vivo−1
P1−ex−vivo−2
P2−ex−vivo−1
P2−ex−vivo−2
P3−ex−vivo−1
P3−ex−vivo−2
P4−ex−vivo−1
P4−ex−vivo−2
Sample
Group
P1−ex−vivo
P2−ex−vivo
P3−ex−vivo
P4−ex−vivo
** indicates standard included in run

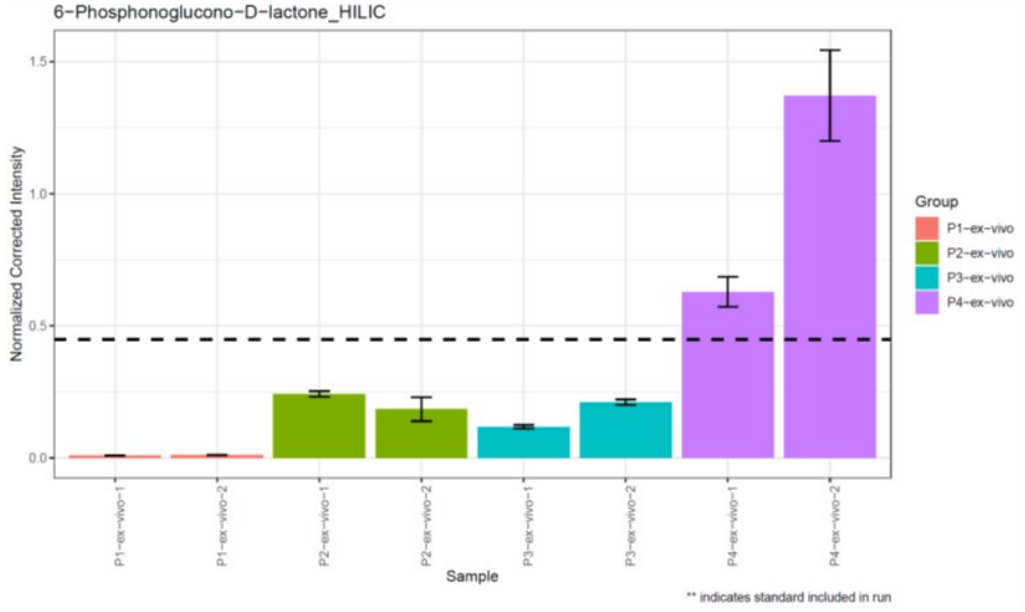
6−Phosphonoglucono−D−lactone_HILIC
Normalized Corrected Intensity
0.0
0.5
1.0
1.5
P1−ex−vivo−1
P1−ex−vivo−2
P2−ex−vivo−1
P2−ex−vivo−2
P3−ex−vivo−1
P3−ex−vivo−2
P4−ex−vivo−1
P4−ex−vivo−2
Sample
Group
P1−ex−vivo
P2−ex−vivo
P3−ex−vivo
P4−ex−vivo
** indicates standard included in run

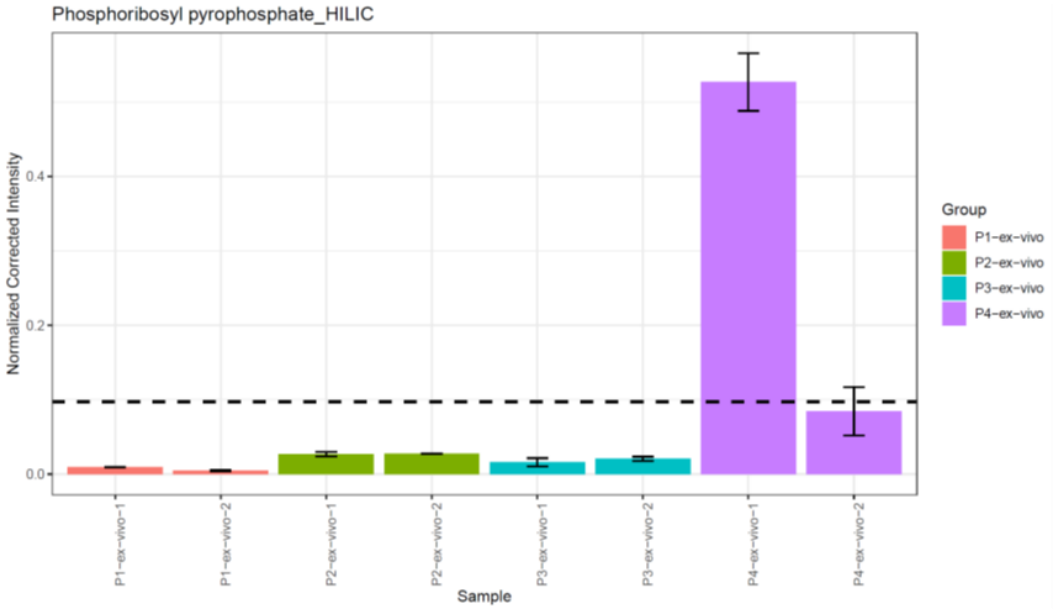

Fig. 4.33: Pentose phosphate pathway in P4 cells. Bar plots show different metabolites identified as hits in the pentose phosphate pathway metabolite set of the KEGG database when comparing P4 to P1 and P3 cells.

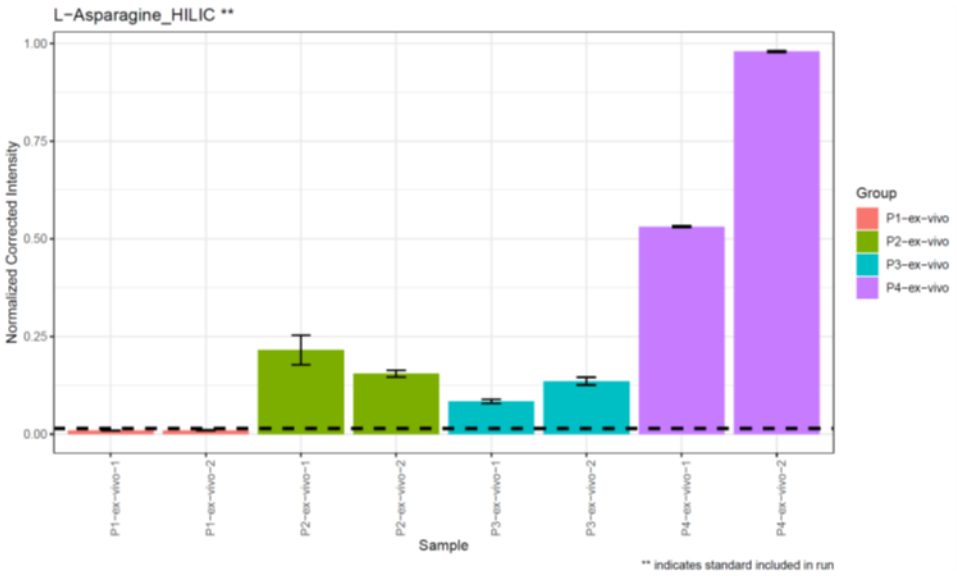
L−Asparagine_HILIC **
Normalized Corrected Intensity
1.00
0.75
0.50
0.25
0.00
P1−ex−vivo−1
P1−ex−vivo−2
P2−ex−vivo−1
P2−ex−vivo−2
P3−ex−vivo−1
P3−ex−vivo−2
P4−ex−vivo−1
P4−ex−vivo−2
Sample
** indicates standard included in run
Group
P1−ex−vivo
P2−ex−vivo
P3−ex−vivo
P4−ex−vivo

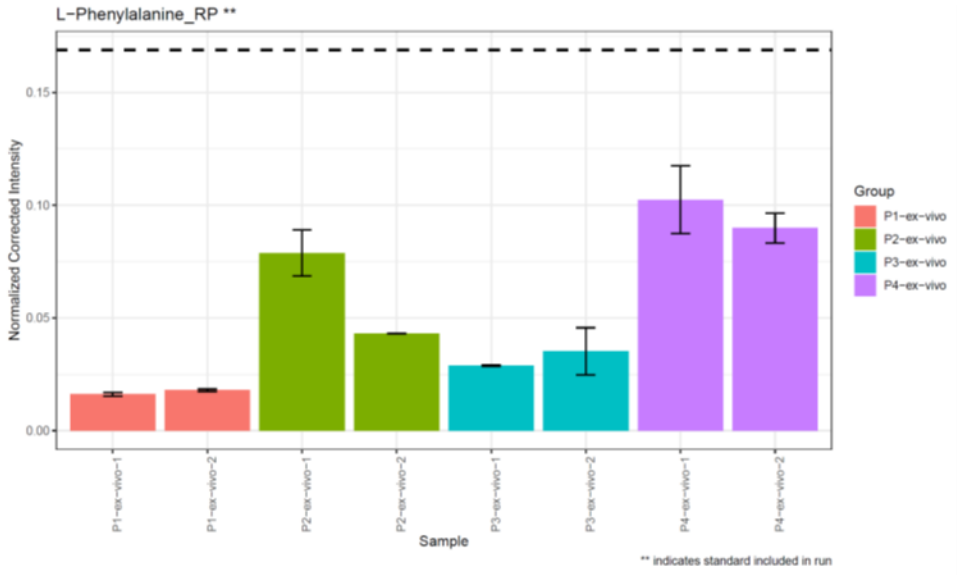
L−Phenylalanine_RP **
Normalized Corrected Intensity
0.15
0.10
0.05
0.00
P1−ex−vivo−1
P1−ex−vivo−2
P2−ex−vivo−1
P2−ex−vivo−2
P3−ex−vivo−1
P3−ex−vivo−2
P4−ex−vivo−1
P4−ex−vivo−2
Sample
** indicates standard included in run
Group
P1−ex−vivo
P2−ex−vivo
P3−ex−vivo
P4−ex−vivo

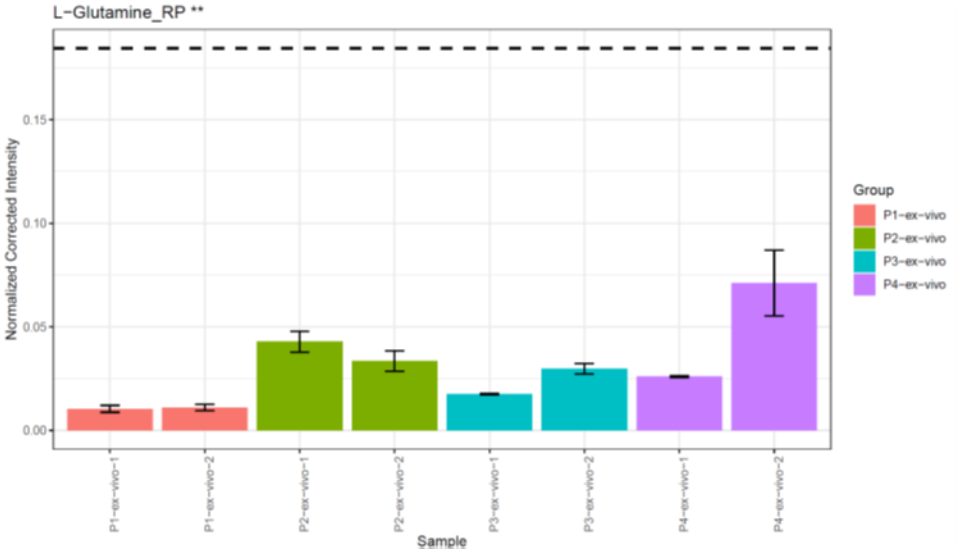
L−Glutamine_RP **
Normalized Corrected Intensity
0.15
0.10
0.05
0.00
P1−ex−vivo−1
P1−ex−vivo−2
P2−ex−vivo−1
P2−ex−vivo−2
P3−ex−vivo−1
P3−ex−vivo−2
P4−ex−vivo−1
P4−ex−vivo−2
Sample
Group
P1−ex−vivo
P2−ex−vivo
P3−ex−vivo
P4−ex−vivo

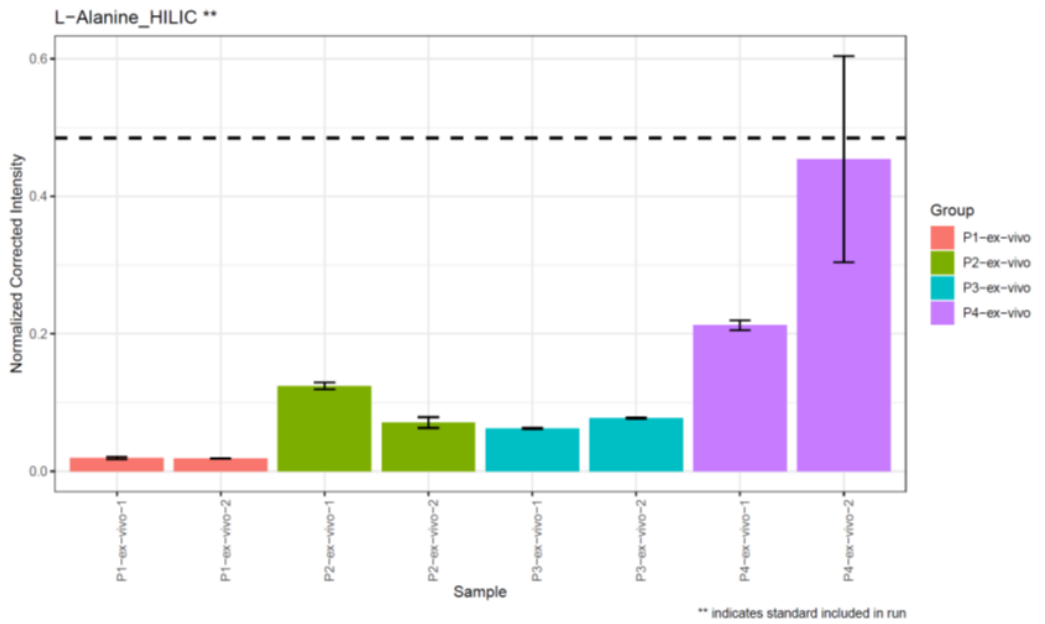
L−Alanine_HILIC **
Normalized Corrected Intensity
0.6
0.4
0.2
0.0
P1−ex−vivo−1
P1−ex−vivo−2
P2−ex−vivo−1
P2−ex−vivo−2
P3−ex−vivo−1
P3−ex−vivo−2
P4−ex−vivo−1
P4−ex−vivo−2
Sample
Group
P1−ex−vivo
P2−ex−vivo
P3−ex−vivo
P4−ex−vivo
** indicates standard included in run

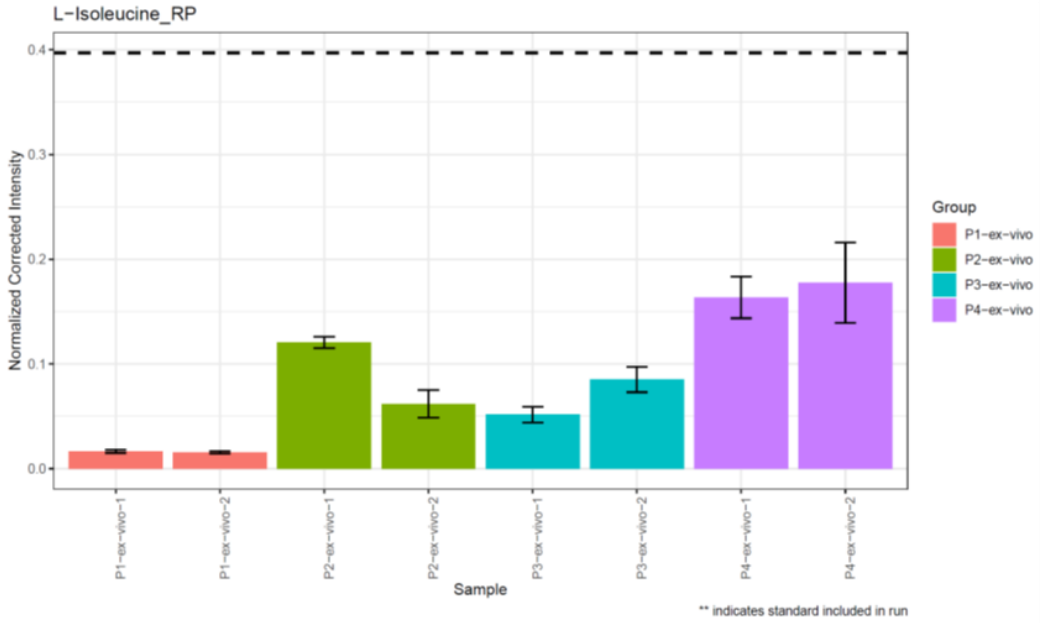
L−Isoleucine_RP
Normalized Corrected Intensity
0.4
0.3
0.2
0.1
0.0
P1−ex−vivo−1
P1−ex−vivo−2
P2−ex−vivo−1
P2−ex−vivo−2
P3−ex−vivo−1
P3−ex−vivo−2
P4−ex−vivo−1
P4−ex−vivo−2
Sample
Group
P1−ex−vivo
P2−ex−vivo
P3−ex−vivo
P4−ex−vivo
** indicates standard included in run

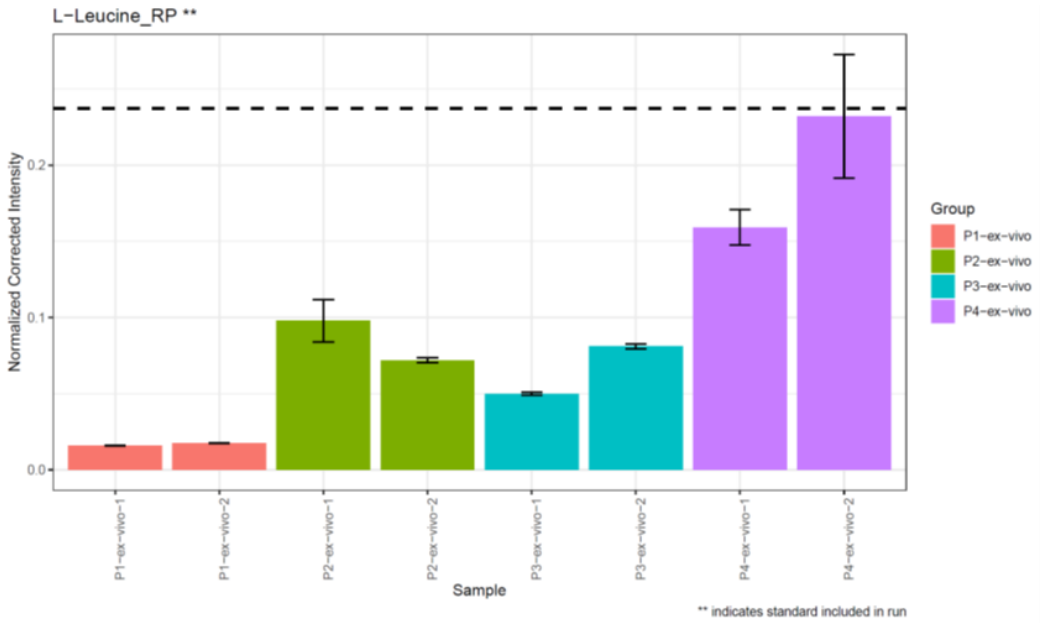
L−Leucine_RP **
Normalized Corrected Intensity
0.2
0.1
0.0
P1−ex−vivo−1
P1−ex−vivo−2
P2−ex−vivo−1
P2−ex−vivo−2
P3−ex−vivo−1
P3−ex−vivo−2
P4−ex−vivo−1
P4−ex−vivo−2
Sample
Group
P1−ex−vivo
P2−ex−vivo
P3−ex−vivo
P4−ex−vivo
** indicates standard included in run

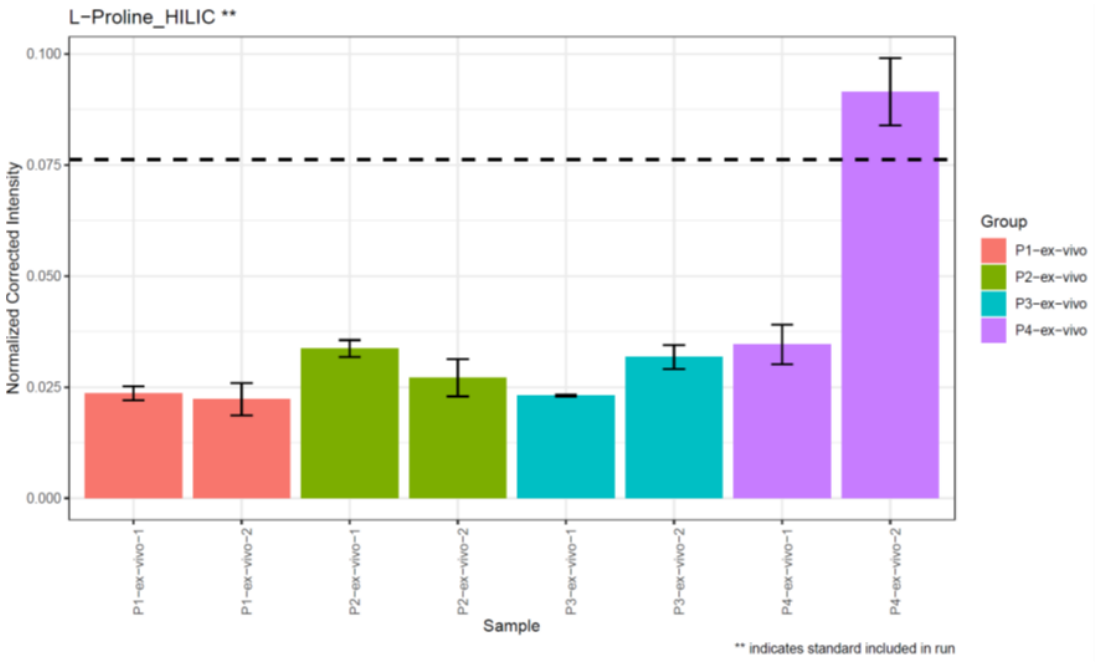

Fig. 4.34: Aminoacyl t-RNA biosynthesis metabolism in P4 cells. Bar plots show the metabolites identified in the t-RNA aminoacyl biosynthesis metabolite set of the KEGG database when comparing P4 cells to P1 and P3 cells.

4.3.10. Aminoacyl t-RNA biosynthesis drives the early induction of P4 cells after antigen-specific activation *in vitro.*

To investigate whether P4 cells induced by antigen priming within 6h were also driven by similar metabolic networks, we next conducted our analysis of the metabolomics samples obtained from cell culture *in vitro*. Heatmap depicts the top 50 metabolites by ANOVA across the different CD8 T cell subsets processed for metabolomics after *in vitro* cell culture (Fig. 4.35). We focused on comparisons of P4 cells and P1 cells as well as comparisons of P4 cells that were generated in the presence and absence of type 1 interferon.

First, comparing P4 cells induced *in vitro* after 6h to P1 cells from cell culture, we identified 27 metabolites that were significantly changed at least two-fold, as represented on the volcano plot (Fig 4.36). Similar to our *ex vivo* analysis, we next conducted an enrichment analysis using Metaboanalyst, focusing on metabolite sets from the KEGG database. Interestingly, we discovered that once again, aminoacyl t-RNA biosynthesis along with glycine, serine, and threonine metabolism and arginine and proline metabolism were the top 3 enriched metabolite sets in this comparison (Fig. 4.37).

Within the aminoacyl t-RNA biosynthesis dataset, 5 metabolites- L-glutamine, L-glutamic acid, L-alanine, L-lysine, and L-isoleucine were significantly changed (Fig. 4.40) between P4 and P1 cells. Altogether, this data shows that aminoacyl tRNA biosynthesis is differentially regulated in P4 cells during the early induction of P4 cells from P1 cells *in vitro* after 6 hours of antigen-specific stimulation in cell culture.

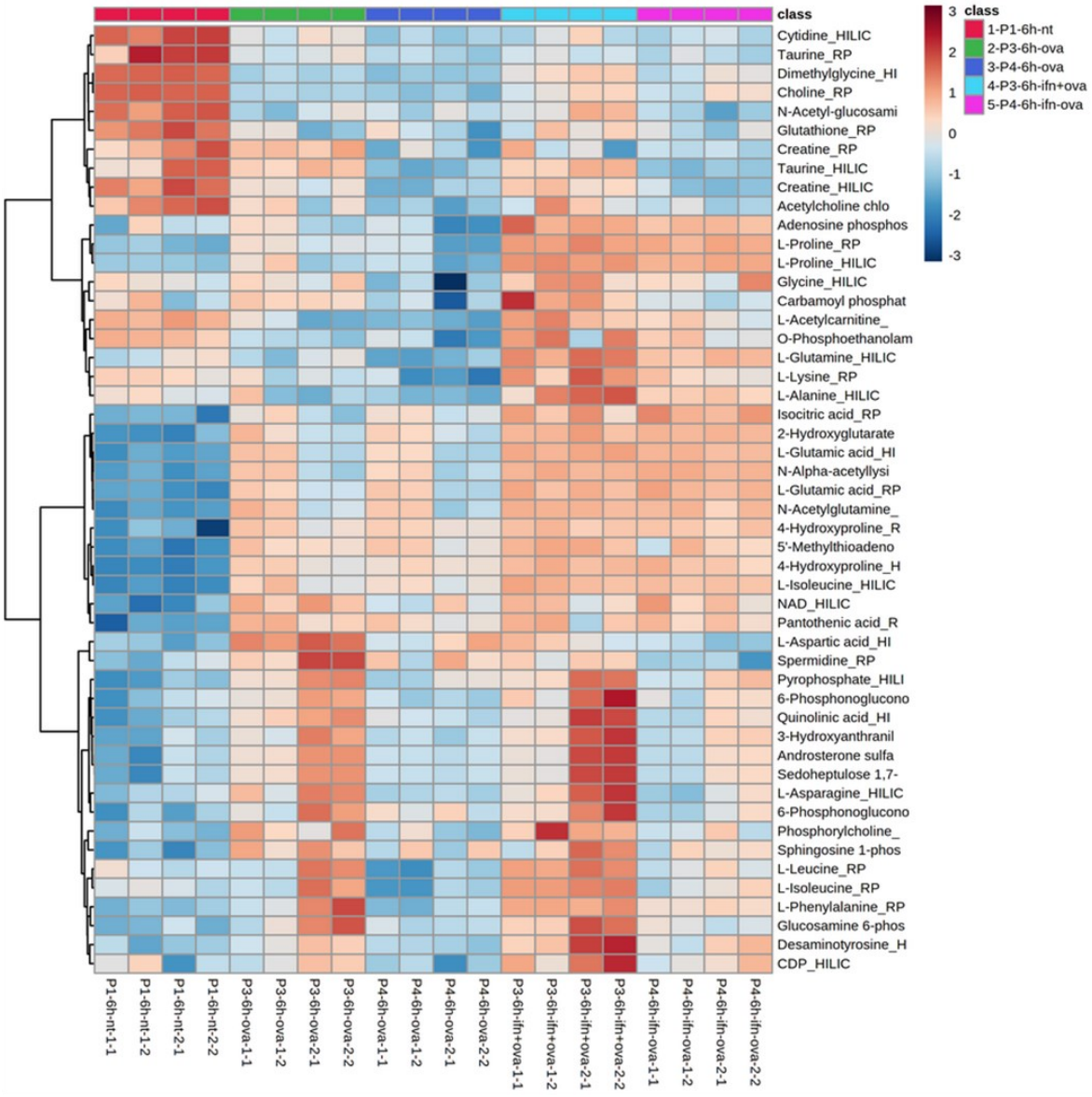

Fig. 4.35: Heatmap for *in vitro* CD8 T cell metabolomics. Heatmap showing the top 50 significantly changed metabolites by ANOVA in P1, P2, P3, and P4 (with and without type 1 interferon) cultured *in vitro*.

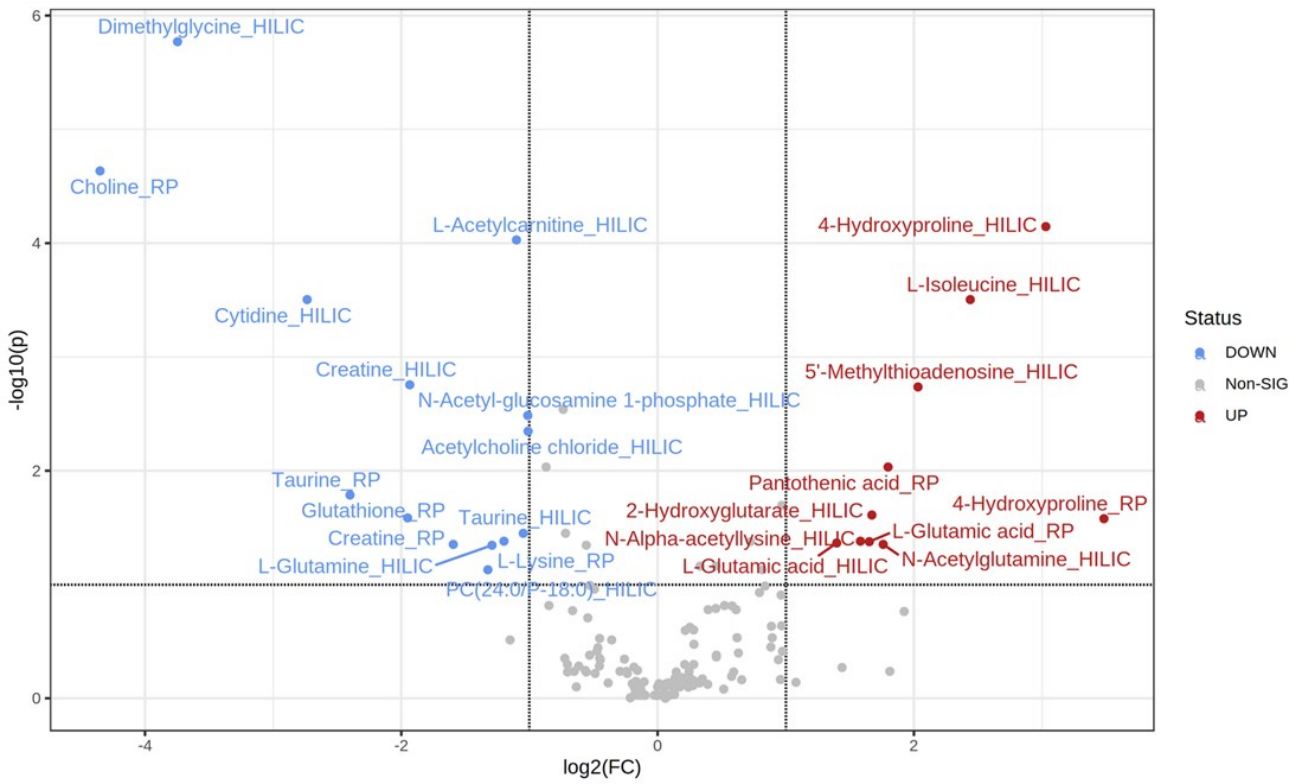

<u>Fig. 4.36:</u> Volcano plot showing significantly changed metabolites (P4 Vs P1). The volcano plot shows significantly changed metabolites (FDR < 0.1 and fold change > 2) for P4 cells compared to P1 cells *in vitro*.

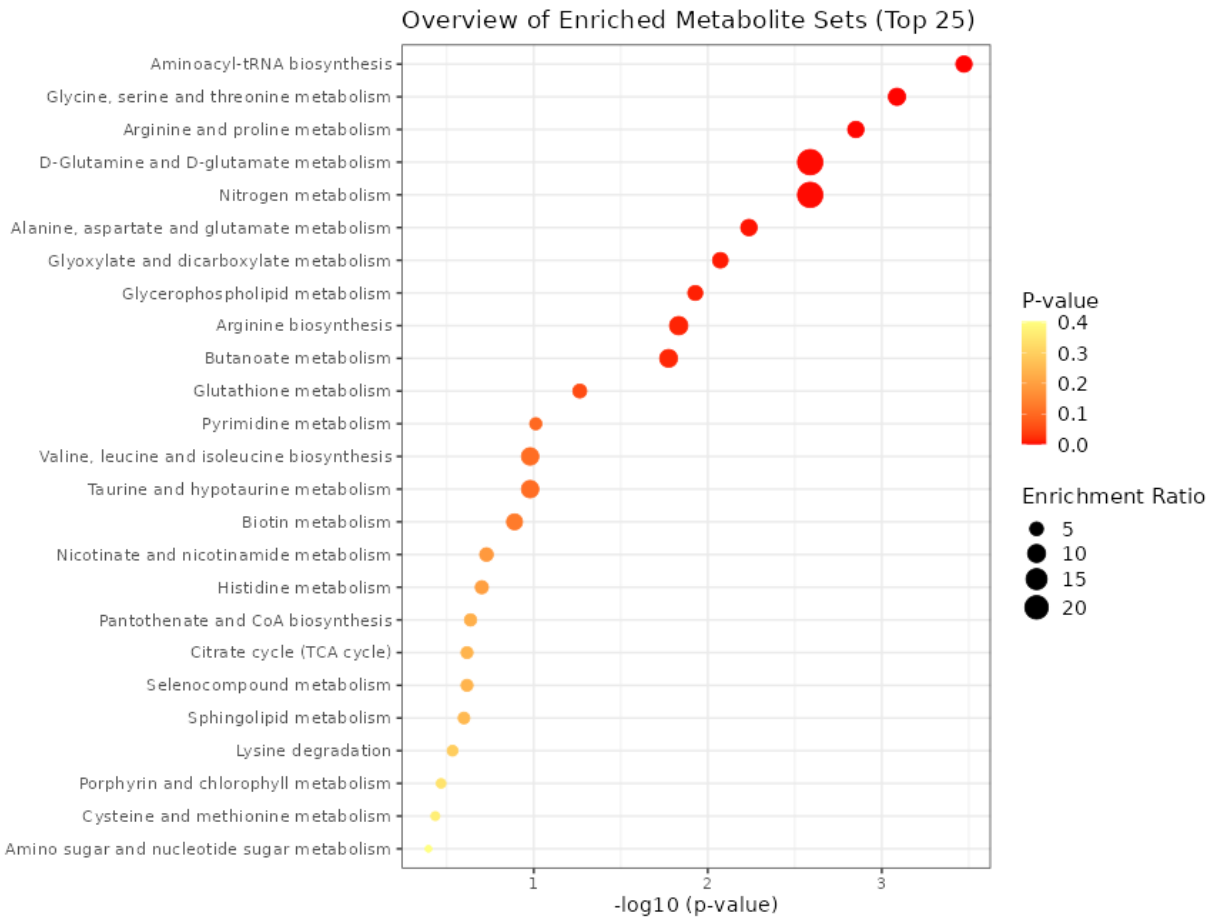

<u>Fig. 4.37:</u> Enrichment analysis for metabolite sets when comparing P4 vs P1 *in vitro*. Dot plots show the enriched KEGG metabolic pathways when comparing significantly changed metabolites between P4 and P1 cells after 6h of cell culture with the corresponding enrichment score and p-value for each pathway. Dot plots were generated using Metaboanalyst V5.

4.3.11. Aminoacyl t-RNA biosynthesis drives increased functional capacity of P4 cells upon activation in the presence of type 1 interferons

Finally, to elucidate the metabolic networks that drove the increased functional capacity of P4 cells upon induction in the presence of type 1 interferons, we also compared the samples of P4 populations induced in the presence and absence of type 1 interferon in cell culture during priming with ova peptide. We discovered that a considerably smaller number of metabolites were significantly changed in this comparison. Only 11 metabolites were observed to be changed at least two-fold and have been represented in the volcano plot (Fig.4.38). Enrichment analysis of these metabolites revealed that, once again, aminoacyl t-RNA biosynthesis along with alanine aspartate and glutamine metabolism as well as glycine, serine, and threonine metabolism were the top three enriched metabolite sets (Fig. 4.39).

Within the aminoacyl t-RNA biosynthesis metabolites, L-glutamine, L-alanine, L-lysine, and L-proline were the 4 metabolites that were significantly changed in the metabolite set when comparing P4 cells primed with antigen in the presence and absence of type I interferons (Fig. 4.40). Given, that aminoacyl tRNA biosynthesis was the only metabolite set that was consistently enriched in P4 cells isolated *ex vivo*, P4 cells when compared to P1 cells after activation for 6h *in vitro* and between P4 cells in the presence and absence of type 1 interferons, we concluded that aminoacyl t-RNA metabolism is not only important for P4 cells *in vivo*, but is also an important pathway that regulates the early induction of P4 cells after antigen-specific activation and drives their increased functional capacity in the presence of type 1 interferons.

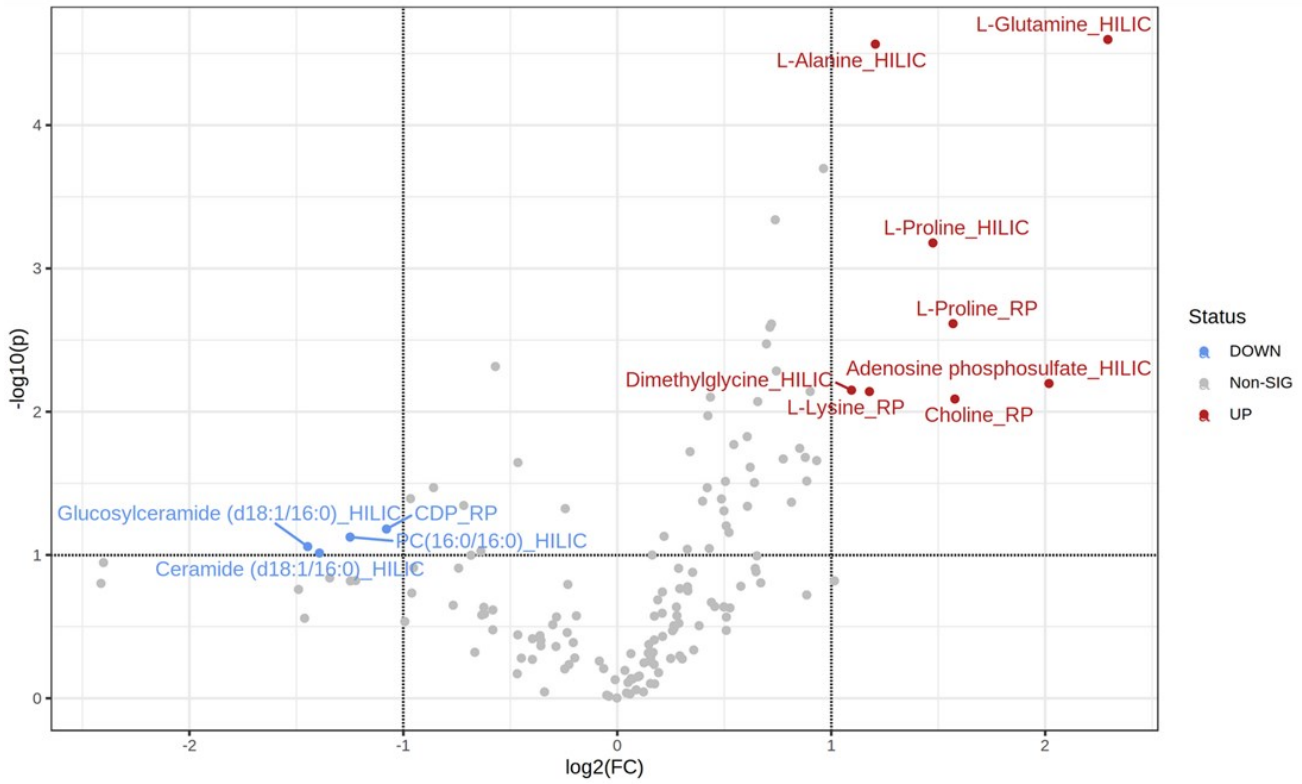

Fig. 4.38: Volcano plot showing significantly changed metabolites (Interferon-P4 Vs P4). The volcano plot shows significantly changed metabolites (FDR < 0.1 and fold change > 2) for P4 cells primed in the presence of type I interferons versus P4 cells primed with antigens in the absence of type I interferons.

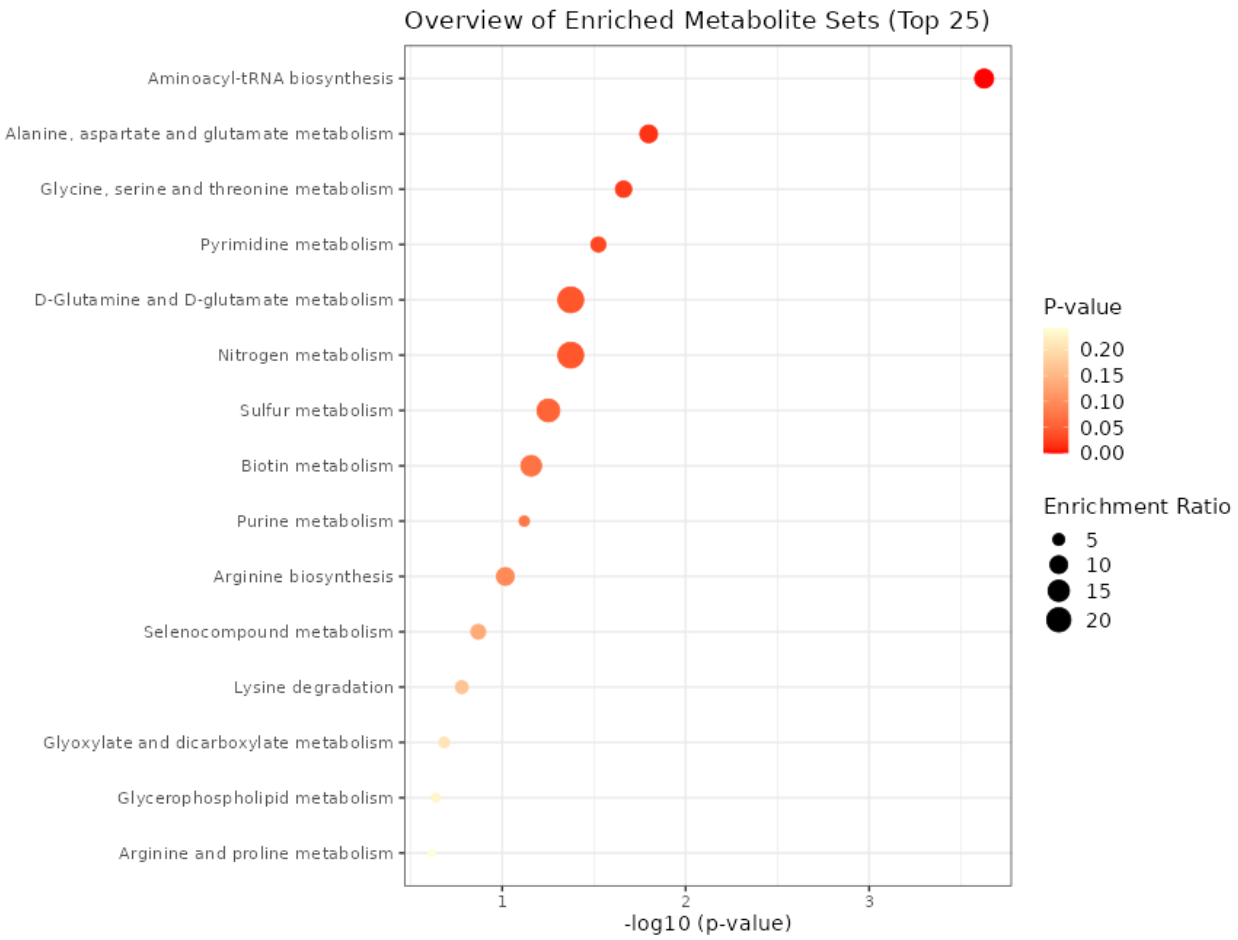

<u>Fig. 4.39:</u> Enrichment analysis for metabolite sets when comparing Interferon-P4 vs P4 *in vitro*. Dot plots show the enriched KEGG metabolic pathways when comparing significantly changed metabolites between P4 cells primed in the presence of type I interferons and P4 cells primed in the absence of type I interferons for 6h in cell culture. Corresponding enrichment score and p-value for each pathway are also depicted in the dot plot. Dot plots were generated using Metaboanalyst V5.

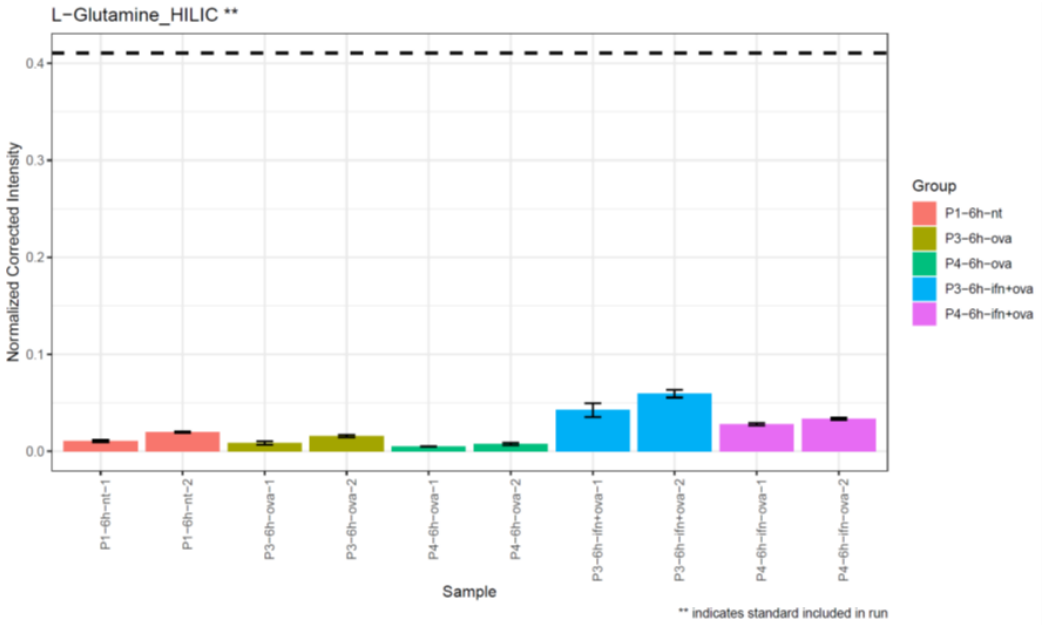
L−Glutamine_HILIC **
Normalized Corrected Intensity
0.4
0.3
0.2
0.1
0.0
P1−6h−nt−1
P1−6h−nt−2
P3−6h−ova−1
P3−6h−ova−2
P4−6h−ova−1
P4−6h−ova−2
P3−6h−ifn+ova−1
P3−6h−ifn+ova−2
P4−6h−ifn−ova−1
P4−6h−ifn−ova−2
Sample
Group
P1−6h−nt
P3−6h−ova
P4−6h−ova
P3−6h−ifn+ova
P4−6h−ifn+ova
** indicates standard included in run

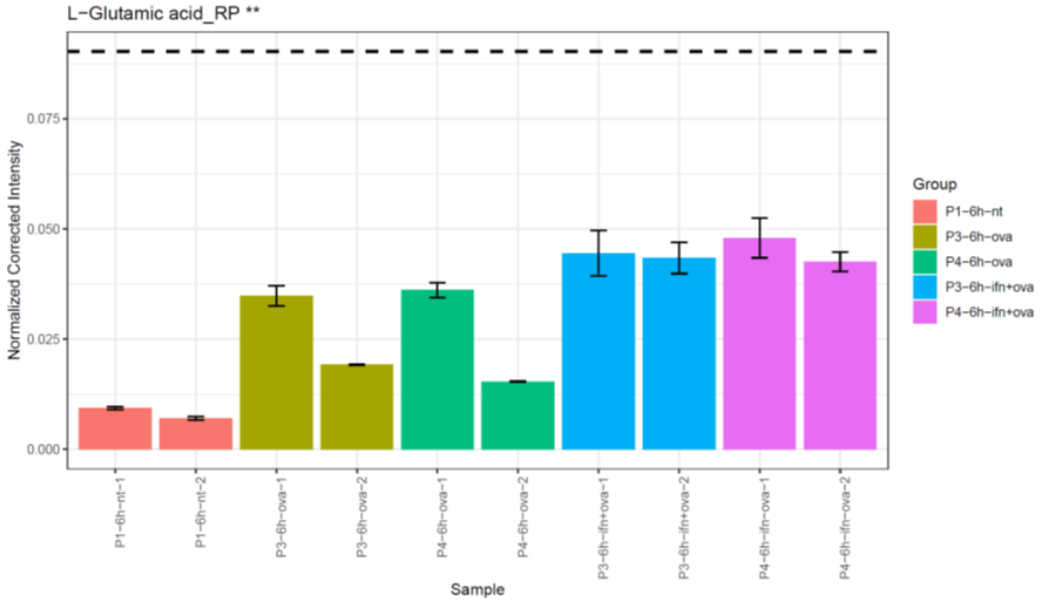
L−Glutamic acid_RP **
Normalized Corrected Intensity
0.075
0.050
0.025
0.000
P1−6h−nt−1
P1−6h−nt−2
P3−6h−ova−1
P3−6h−ova−2
P4−6h−ova−1
P4−6h−ova−2
P3−6h−ifn+ova−1
P3−6h−ifn+ova−2
P4−6h−ifn−ova−1
P4−6h−ifn−ova−2
Sample
Group
P1−6h−nt
P3−6h−ova
P4−6h−ova
P3−6h−ifn+ova
P4−6h−ifn+ova

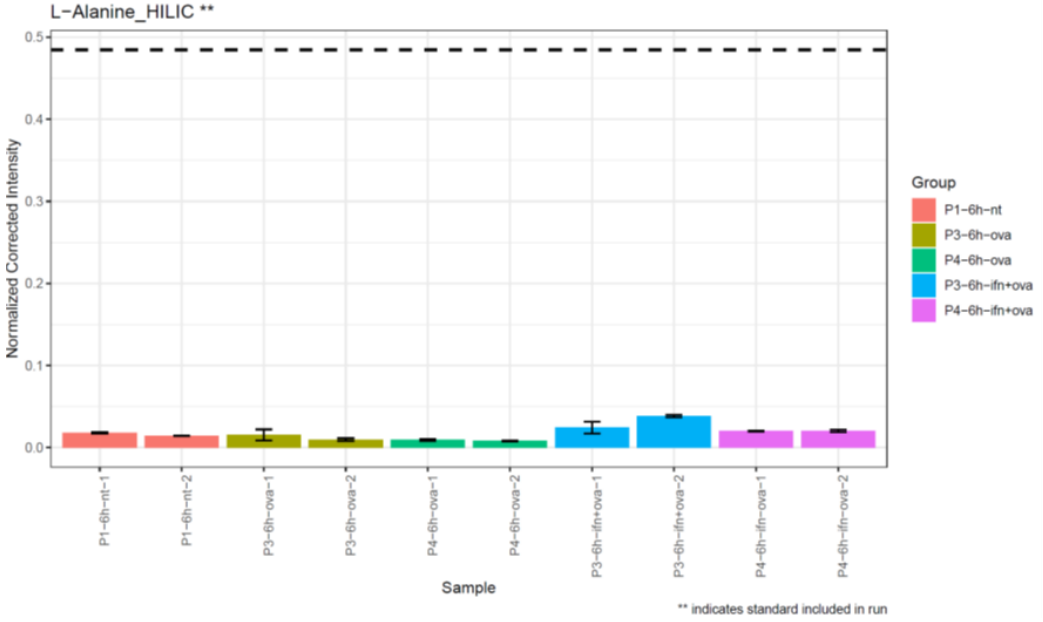
L−Alanine_HILIC **
Normalized Corrected Intensity
0.5
0.4
0.3
0.2
0.1
0.0
P1−6h−nt−1
P1−6h−nt−2
P3−6h−ova−1
P3−6h−ova−2
P4−6h−ova−1
P4−6h−ova−2
P3−6h−ifn+ova−1
P3−6h−ifn+ova−2
P4−6h−ifn−ova−1
P4−6h−ifn−ova−2
Sample
Group
P1−6h−nt
P3−6h−ova
P4−6h−ova
P3−6h−ifn+ova
P4−6h−ifn+ova
** indicates standard included in run

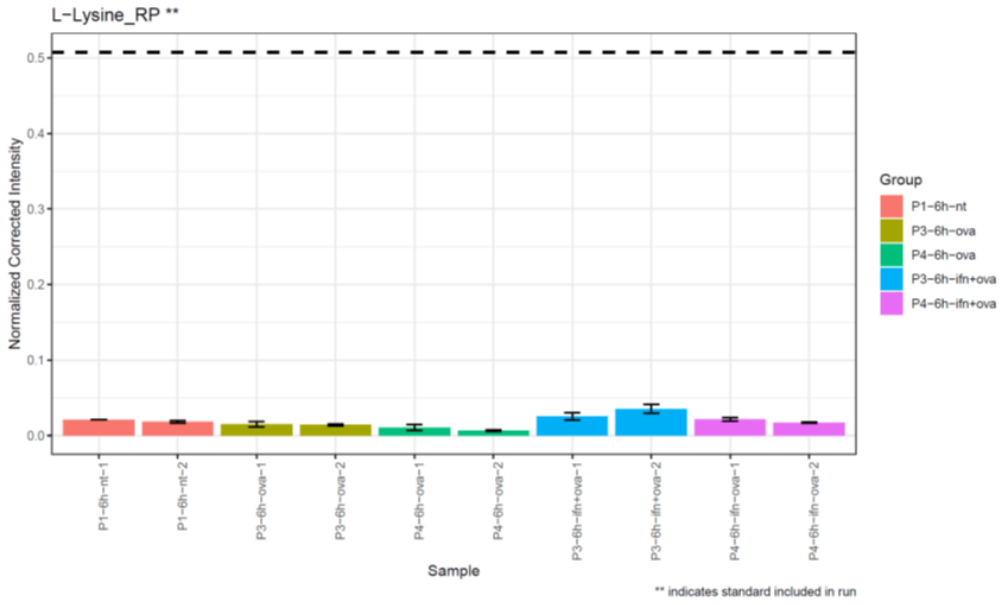
L−Lysine_RP **
Normalized Corrected Intensity
0.5
0.4
0.3
0.2
0.1
0.0
P1−6h−nt−1
P1−6h−nt−2
P3−6h−ova−1
P3−6h−ova−2
P4−6h−ova−1
P4−6h−ova−2
P3−6h−ifn+ova−1
P3−6h−ifn+ova−2
P4−6h−ifn−ova−1
P4−6h−ifn−ova−2
Sample
Group
P1−6h−nt
P3−6h−ova
P4−6h−ova
P3−6h−ifn+ova
P4−6h−ifn+ova
** indicates standard included in run

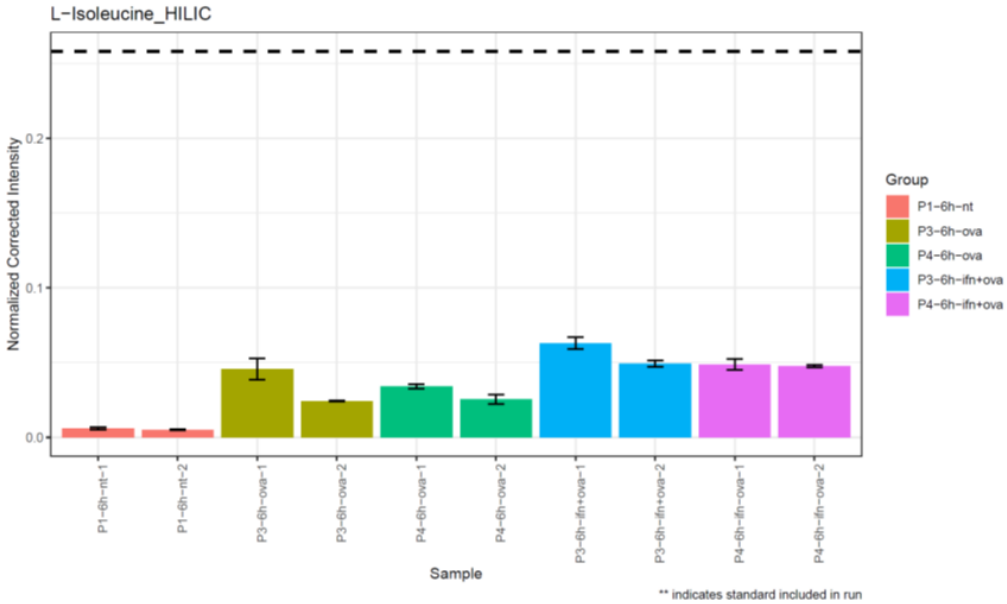
L−Isoleucine_HILIC
Normalized Corrected Intensity
0.2
0.1
0.0
P1−6h−nt−1
P1−6h−nt−2
P3−6h−ova−1
P3−6h−ova−2
P4−6h−ova−1
P4−6h−ova−2
P3−6h−ifn+ova−1
P3−6h−ifn+ova−2
P4−6h−ifn−ova−1
P4−6h−ifn−ova−2
Sample
Group
P1−6h−nt
P3−6h−ova
P4−6h−ova
P3−6h−ifn+ova
P4−6h−ifn+ova
** indicates standard included in run

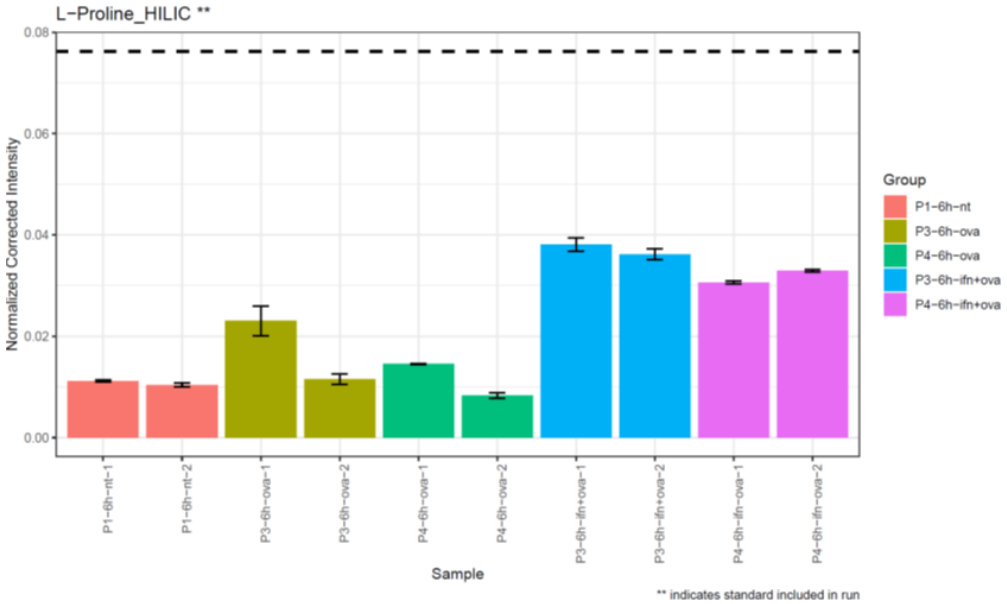
L−Proline_HILIC **
Normalized Corrected Intensity
0.08
0.06
0.04
0.02
0.00
P1−6h−nt−1
P1−6h−nt−2
P3−6h−ova−1
P3−6h−ova−2
P4−6h−ova−1
P4−6h−ova−2
P3−6h−ifn+ova−1
P3−6h−ifn+ova−2
P4−6h−ifn−ova−1
P4−6h−ifn−ova−2
Sample
Group
P1−6h−nt
P3−6h−ova
P4−6h−ova
P3−6h−ifn+ova
P4−6h−ifn+ova
** indicates standard included in run

Fig. 4.40: Aminoacyl t-RNA biosynthesis metabolism in P4 cells activated *in vitro*. Bar plots show the normalized corrected intensity of metabolites identified in the t-RNA aminoacyl biosynthesis metabolite set- L-glutamine, L-glutamic acid, L-alanine, L-lysine- L-Isoleucine and L-proline- in P1, P3, and P4 CD8 T cell subsets.

4.4. Discussion

In light of the recent SARS-CoV2 pandemic, understanding the early determinants of successful CD8 T cell responses has become critical. In this study, we have examined in detail, the early activation of CD8 T cells after TCR-dependent and TCR-independent activation. We demonstrated that, as early as 1h, activation of T cells leads to the induction of CD44lowCD62Llow P4 T cells which have thus far not been investigated thoroughly. We further demonstrated that CD44lowCD62Llow P4 cells were functionally active as early as 6h after stimulation with antigenic peptide and were able to produce IFN-γ. This unique subset of CD8 T cells was also shown to be transitory as its frequency was drastically reduced by 24 hours.

Different models of T cell differentiation have been suggested thus far and have already been discussed in detail in previous sections (Kaech et al., 2002; Restifo and Gattinoni, 2013; Youngblood et al., 2017). Although these models suggest different mechanisms of T cell differentiation, they are aligned in their suggestion of naïve T cells differentiating into either effector or memory T cells. The models diverge on their suggestions for which cells are induced first. Based on our studies, we provide a new piece to this puzzle by suggesting that CD44lowCD62Llow P4 cells arise before either effector or memory T cells and are the earliest T cell type induced after antigen stimulation. We provide data that

supports the model suggested by Honjo's group in their study of P4 cells in the context of cancer immunotherapy (Nakajima et al., 2021). They show that P4 cells are pre-effector cells that arise from P1 cells and transition to P3 cells. Our time course analysis from 1h to 24h after antigen stimulation supports these findings. Together, both studies support the model of dedifferentiation wherein effector T cells can transition to memory T cells (Youngblood et al., 2017).

Type 1 interferons are critical modulators of CD8 T cells as we have discussed (Jergović et al., 2021; Kolumam et al., 2005; Urban et al., 2016, p. 8; Welsh et al., 2012, p. 8). Although Honjo's group had suggested that P4 cells arise from P1 cells, it was unclear if cytokine-driven activation of P1 cells led to any changes in the induction of P4 cells. Since we found in our first study, that virus exposure drives bystander activation of naïve P1 cells via type 1 interferons, we examined whether the presence of type 1 interferons during priming affected P4 cell induction. This led us to another novel finding that type 1 interferons led to the increased functional capacity of P4 cells via enhanced IFN-γ production. The role of CD8 T cells during the early stages of an immune response is gaining appreciation especially due to their ability to exert innate-like cytotoxicity (Kim et al., 2018). Our findings showing the early enhancement in IFN-γ production in the presence of type 1 interferons further suggest that CD8 T cells, specifically P4 cells, may be important for early anti-viral immunity. Further studies are required that will elucidate the role of P4 cells in different contexts of infection and immunity.

Finally, we have also discussed how metabolism is a key driver of immunity (Pearce, 2021; Pearce et al., 2013). In this study, we conducted a global metabolome analysis of P4 cells in comparison to P1, P2, and P3 cells. The previous study discussing P4 cells in the cancer

context (Nakajima et al., 2021, p. 44) discussed one-carbon metabolism as an essential metabolic pathway for P4 cells. This was identified via microarray analysis. So, our study provides an additional investigation of P4 cells, this time with an in-depth analysis of metabolite levels of P1, P2, P3, and P4 cells isolated fresh *ex vivo* as well as after activation with ova peptide for 6h/24h in cell culture. Our metabolomic analysis provided novel insights into the metabolism of P4 cells and revealed a role in aminoacyl t-RNA biosynthesis in these cells. Aminoacyl t-RNA biosynthesis was a consistent hit that was differentially regulated in *ex vivo* and *in vitro* samples. Important amino acids like glutamine, lysine, and alanine were changed in P4 cells and may be important to drive the early phenotype of P4 cells after activation via increased translation. Future studies exploring the role of these amino acids as well as translation in general may reveal important insights into the mechanisms that drive P4 cell induction and their functional capacity early on after antigen priming.

Overall, our study provides a systematic investigation of CD44lowCD62Llow P4 cells induced early after antigen priming and provides new insight into the earliest phenomena that occur during T cell differentiation. We characterized the role of type 1 interferons in this process that are critical for anti-viral immunity and also provided an immunometabolic perspective on these cells. We believe that this study provides immensely valuable insights that can guide further exploration of CD8 T cell biology and help define the earliest factors that drive robust CD8 T cell responses.

Chapter 5. Conclusions and Future Directions

In this thesis, we have discussed various mechanisms by which T cells are activated and highlighted their early consequences. Specifically, we have investigated two separate but interconnected themes of CD8 T cell biology that rely on understanding the *earliest changes* that CD8 T cells undergo with different types of activation. In the first part, we explored bystander antigen-independent activation of naïve CD8 T cells that occurs very early on after exposure to viruses. In the second part of this thesis, we investigated the induction of CD44lowCD62Llow P4 cells from naïve CD8 T cells very early on after TCR-dependent and independent T cell stimulation.

In the first theme, we dissected this virus-driven bystander activation of naïve CD8 T cells and determined that it was the type I interferon and STAT-1 dependent phenomenon. We also investigated the metabolic pathways that drove the induction of these bT_N cells and discovered a novel role for NAD^+ salvage metabolism. Bystander activation is, arguably, one of the earliest changes that naïve CD8 T cells undergo after exposure to the virus. This may occur even before the CD8 T cell has had the opportunity to be exposed to its cognate antigen. As a result, bystander activation of naïve CD8 T cells may have immense consequences when antigen priming does occur. Hence, we believe that bystander activation of naïve CD8 T cells represents one of the earliest events of consequence in adaptive immunity long before this arm of the immune system is thought to be activated. Thus far, this phenomenon has remained relatively unexplored, and our studies have helped shed light on important molecular mechanisms that drive changes in naive CD8 T cells during the early phases of the immune response.

One limitation of this study is that bystander activation was, for the most part, studied on the bulk population of CD8 T cells. We did demonstrate, using the antigen-specific OT-1 model, that bystander activation of naïve CD8 T cells led to increased IFN-γ responses in CD8 T cells; however, the dependence of bT_N cells on type 1 interferons and NAD+ salvage metabolism was shown in the bulk population of naive T cells. Future studies can help assess the inherent heterogeneity in the naïve CD8 T cell subsets in terms of their antigen-specificity and help delineate the role of bystander activation on naïve, antigen-specific CD8 T cells. With the rise in inflammatory disorders and autoimmune conditions, understanding how naïve CD8 T cells are activated in inflammatory settings will prove to be critical in many areas where CD8 T cells are being harnessed for treatment.

Another aspect of bT_N cells that was alluded to in our studies but not followed up in detail is the differential induction of bT_N cells at different sites after virus exposure. At some sites, bT_N cells were induced and maintained for a longer period than at other sites. Given that we observed features like increased Granzyme K production in these cells on day 7 after virus exposure, it will be interesting to explore their role in tissues where they are maintained over the long-term in different disease contexts.

In this thesis, since we have been interested in the theme of the earliest changes that CD8 T cells undergo after activation, it was natural for us to study the earliest changes in antigen-specific CD8 T cells after T cell stimulation with cognate peptide. The finding that CD44lowCD62Llow P4 cells are induced rapidly after T cell stimulation is a critical new insight into T cell differentiation. Most studies on T cell differentiation do not study T cells after a few hours of activation, focusing instead on T cell phenotypes generated a few days after activation treatments. Similar to bystander activation, once again, the induction of

CD44lowCD62Llow P4 cells may be one of the earliest events in T cell differentiation that sets the tone for the development of the adaptive CD8 T cell response.

Most studies on T cell differentiation have dissected effector memory (P3), central memory (P2), and their subsets in detail however, only one study so far has discussed CD44lowCD62Llow P4 cells in a disease context (Nakajima et al., 2021). Future studies can aim to understand the role of various factors like antigen signal strength, duration, and costimulation in the induction of P4 cells since these factors have been demonstrated to have important roles in driving the differentiation of effector and memory T cells, and this may occur through an upstream role in the induction of P4 cells.

Next, as previously mentioned, although our time course analysis after antigen stimulation supported the model that P1 cells transition to P4 cells before transitioning to P3 as proposed by Honjo's group, future studies that can utilize the power of techniques like lineage tracing as well as single cell analysis may provide further substantiative evidence for this model of T cell differentiation.

We have investigated the role of type 1 interferons in P4 cells in this study. Many other cytokines like IL-2, IL-7, IL-12, and IL-15 are known to be important for the differentiation of effector and memory T cells. It will be interesting to investigate how these cytokines can modulate P4 cell induction and their function.

Finally, our metabolome analysis provides many targets to investigate the relationship between metabolic pathways and P4 cells. Supplementation and depletion of key amino acids identified in this study will help determine if these are essential for P4 cell function. There also exist opportunities in the future to conduct flux studies to investigate how

individual metabolites like glutamine are used by P4 cells and identify if these cells utilize these substrates any differently when compared to other CD8 T cell subsets.

Overall, in this thesis, we have sought to provide a thorough characterization of early events that occur during CD8 T cell activation whether it is after cytokine-driven bystander activation, non-specific T cell activation, or TCR receptor-driven activation. We hope that this work will provide important insights for future studies carrying out similar lines of investigation which, given the recent pandemic, have become ever so increasingly important.

Bibliography

Acharya, D., Liu, G., Gack, M.U., 2020. Dysregulation of type I interferon responses in COVID-19. Nat. Rev. Immunol. 20, 397–398. https://doi.org/10.1038/s41577-020-0346-x

Alanio, C., Nicoli, F., Sultanik, P., Flecken, T., Perot, B., Duffy, D., Bianchi, E., Lim, A., Clave, E., van Buuren, M.M., Schnuriger, A., Johnsson, K., Boussier, J., Garbarg-Chenon, A., Bousquet, L., Mottez, E., Schumacher, T.N., Toubert, A., Appay, V., Heshmati, F., Thimme, R., Pol, S., Mallet, V., Albert, M.L., 2015. Bystander hyperactivation of preimmune CD8+ T cells in chronic HCV patients. eLife 4, e07916. https://doi.org/10.7554/eLife.07916

Alizadeh, D., Wong, R.A., Yang, X., Wang, D., Pecoraro, J.R., Kuo, C.-F., Aguilar, B., Qi, Y., Ann, D.K., Starr, R., Urak, R., Wang, X., Forman, S.J., Brown, C.E., 2019. IL15 Enhances CAR-T Cell Antitumor Activity by Reducing mTORC1 Activity and Preserving Their Stem Cell Memory Phenotype. Cancer Immunol. Res. 7, 759–772. https://doi.org/10.1158/2326-6066.CIR-18-0466

Al-Shabany, A.J., Moody, A.J., Foey, A.D., Billington, R.A., 2016. Intracellular NAD+ levels are associated with LPS-induced TNF-α release in pro-inflammatory macrophages. Biosci. Rep. 36. https://doi.org/10.1042/BSR20150247

Alvarez, G.M., Ferretti, E.L., Gutnisky, C., Dalvit, G.C., Cetica, P.D., 2013. Modulation of glycolysis and the pentose phosphate pathway influences porcine oocyte in vitro maturation. Reprod. Domest. Anim. Zuchthyg. 48, 545–553. https://doi.org/10.1111/rda.12123

Anastasiou, D., Poulogiannis, G., Asara, J.M., Boxer, M.B., Jiang, J., Shen, M., Bellinger, G., Sasaki, A.T., Locasale, J.W., Auld, D.S., Thomas, C.J., Vander Heiden, M.G., Cantley, L.C., 2011. Inhibition of pyruvate kinase M2 by reactive oxygen species contributes to cellular antioxidant responses. Science 334, 1278–1283. https://doi.org/10.1126/science.1211485

Arsenio, J., Metz, P.J., Chang, J.T., 2015. Asymmetric Cell Division in T Lymphocyte Fate Diversification. Trends Immunol. 36, 670–683. https://doi.org/10.1016/j.it.2015.09.004

Aulakh, G.K., 2018. Neutrophils in the lung: "the first responders." Cell Tissue Res. 371, 577–588. https://doi.org/10.1007/s00441-017-2748-z

Ayres, J.S., 2020. Immunometabolism of infections. Nat. Rev. Immunol. 20, 79–80. https://doi.org/10.1038/s41577-019-0266-9

Badovinac, V.P., Porter, B.B., Harty, J.T., 2004. CD8+ T cell contraction is controlled by early inflammation. Nat. Immunol. 5, 809–817. https://doi.org/10.1038/ni1098

Bankamp, B., Takeda, M., Zhang, Y., Xu, W., Rota, P.A., 2011. Genetic characterization of measles vaccine strains. J. Infect. Dis. 204 Suppl 1, S533-548. https://doi.org/10.1093/infdis/jir097

Beier, U.H., Quinn, W.J., Jiao, J., TeSlaa, T., Stadanlick, J., Hancock, W.W., Eruslanov, E.B., Rabinowitz, J.D., Baur, J.A., 2018. Nicotinamide adenine dinucleotide (NAD) oxidation preserves T cell function under lactic acidosis characteristic of the tumor microenvironment (TME). J. Immunol. 200, 177.4-177.4.

Belenky, P., Bogan, K.L., Brenner, C., 2007. NAD+ metabolism in health and disease. Trends Biochem. Sci. 32, 12–19. https://doi.org/10.1016/j.tibs.2006.11.006

Belikov, A.V., Schraven, B., Simeoni, L., 2015. T cells and reactive oxygen species. J. Biomed. Sci. 22, 85. https://doi.org/10.1186/s12929-015-0194-3

Belladonna, M.L., Puccetti, P., Orabona, C., Fallarino, F., Vacca, C., Volpi, C., Gizzi, S., Pallotta, M.T., Fioretti, M.C., Grohmann, U., 2007. Immunosuppression via tryptophan catabolism: the role of kynurenine pathway enzymes. Transplantation 84, S17-20. https://doi.org/10.1097/01.tp.0000269199.16209.22

Berg, R.E., Crossley, E., Murray, S., Forman, J., 2003. Memory CD8+ T cells provide innate immune protection against Listeria monocytogenes in the absence of cognate antigen. J. Exp. Med. 198, 1583–1593. https://doi.org/10.1084/jem.20031051

Bergamaschi, L., Mescia, F., Turner, L., Hanson, A.L., Kotagiri, P., Dunmore, B.J., Ruffieux, H., De Sa, A., Huhn, O., Morgan, M.D., Gerber, P.P., Wills, M.R., Baker, S., Calero-Nieto, F.J., Doffinger, R., Dougan, G., Elmer, A., Goodfellow, I.G., Gupta, R.K., Hosmillo, M., Hunter, K., Kingston, N., Lehner, P.J., Matheson, N.J., Nicholson, J.K., Petrunkina, A.M., Richardson, S., Saunders, C., Thaventhiran, J.E.D., Toonen, E.J.M., Weekes, M.P., Cambridge Institute of Therapeutic Immunology and Infectious Disease-National Institute of Health Research (CITIID-NIHR)

COVID BioResource Collaboration, Göttgens, B., Toshner, M., Hess, C., Bradley, J.R., Lyons, P.A., Smith, K.G.C., 2021. Longitudinal analysis reveals that delayed bystander CD8+ T cell activation and early immune pathology distinguish severe COVID-19 from mild disease. Immunity 54, 1257-1275.e8. https://doi.org/10.1016/j.immuni.2021.05.010

Biase, S.D., Ma, X., Wang, X., Yu, J., Wang, Y.-C., Smith, D.J., Zhou, Y., Li, Z., Kim, Y.J., Clarke, N., To, A., Yang, L., 2019. Creatine uptake regulates CD8 T cell antitumor immunity. J. Exp. Med. https://doi.org/10.1084/jem.20182044

Black, A.J., Morris, D.G., 2012. Clinical trials involving the oncolytic virus, reovirus: ready for prime time? Expert Rev. Clin. Pharmacol. 5, 517–520. https://doi.org/10.1586/ecp.12.53

Blanco-Melo, D., Nilsson-Payant, B.E., Liu, W.-C., Uhl, S., Hoagland, D., Møller, R., Jordan, T.X., Oishi, K., Panis, M., Sachs, D., Wang, T.T., Schwartz, R.E., Lim, J.K., Albrecht, R.A., tenOever, B.R., 2020. Imbalanced Host Response to SARS-CoV-2 Drives Development of COVID-19. Cell 181, 1036-1045.e9. https://doi.org/10.1016/j.cell.2020.04.026

Bouziat, R., Hinterleitner, R., Brown, J.J., Stencel-Baerenwald, J.E., Ikizler, M., Mayassi, T., Meisel, M., Kim, S.M., Discepolo, V., Pruijssers, A.J., Ernest, J.D., Iskarpatyoti, J.A., Costes, L.M.M., Lawrence, I., Palanski, B.A., Varma, M., Zurenski, M.A., Khomandiak, S., McAllister, N., Aravamudhan, P., Boehme, K.W., Hu, F., Samsom, J.N., Reinecker, H.-C., Kupfer, S.S., Guandalini, S., Semrad, C.E., Abadie, V., Khosla, C., Barreiro, L.B., Xavier, R.J., Ng, A., Dermody, T.S., Jabri, B., 2017. Reovirus infection triggers inflammatory responses to dietary antigens and development of celiac disease. Science 356, 44–50. https://doi.org/10.1126/science.aah5298

Bruzzone, S., Fruscione, F., Morando, S., Ferrando, T., Poggi, A., Garuti, A., D'Urso, A., Selmo, M., Benvenuto, F., Cea, M., Zoppoli, G., Moran, E., Soncini, D., Ballestrero, A., Sordat, B., Patrone, F., Mostoslavsky, R., Uccelli, A., Nencioni, A., 2009. Catastrophic NAD+ Depletion in Activated T Lymphocytes through Nampt Inhibition Reduces Demyelination and Disability in EAE. PLOS ONE 4, e7897. https://doi.org/10.1371/journal.pone.0007897

Buck, M.D., Sowell, R.T., Kaech, S.M., Pearce, E.L., 2017. Metabolic Instruction of Immunity. Cell 169, 570–586. https://doi.org/10.1016/j.cell.2017.04.004

Burt, R.K., Traynor, A.E., Pope, R., Schroeder, J., Cohen, B., Karlin, K.H., Lobeck, L., Goolsby, C., Rowlings, P., Davis, F.A., Stefoski, D., Terry, C., Keever-Taylor, C., Rosen, S., Vesole, D., Fishman, M., Brush, M., Mujias, S., Villa, M., Burns, W.H., 1998. Treatment of autoimmune disease by intense immunosuppressive conditioning and autologous hematopoietic stem cell transplantation. Blood 92, 3505–3514.

Cameron, A.M., Castoldi, A., Sanin, D.E., Flachsmann, L.J., Field, C.S., Puleston, D.J., Kyle, R.L., Patterson, A.E., Hässler, F., Buescher, J.M., Kelly, B., Pearce, E.L., Pearce, E.J., 2019. Inflammatory macrophage dependence on NAD + salvage is a consequence of reactive oxygen species–mediated DNA damage. Nat. Immunol. 20, 420–432. https://doi.org/10.1038/s41590-019-0336-y

Cao, X., Liang, Y., Hu, Z., Li, H., Yang, J., Hsu, E.J., Zhu, J., Zhou, J., Fu, Y.-X., 2021. Next generation of tumor-activating type I IFN enhances anti-tumor immune responses to overcome therapy resistance. Nat. Commun. 12, 5866. https://doi.org/10.1038/s41467-021-26112-2

Cenerenti, M., Saillard, M., Romero, P., Jandus, C., 2022. The Era of Cytotoxic CD4 T Cells. Front. Immunol. 13, 867189. https://doi.org/10.3389/fimmu.2022.867189

Chamy, L.E., Leclerc, V., Caldelari, I., Reichhart, J.-M., 2008. Sensing of "danger signals" and pathogen-associated molecular patterns defines binary signaling pathways "upstream" of Toll. Nat. Immunol. 9, 1165–1170. https://doi.org/10.1038/ni.1643

Chang, C.-H., Curtis, J.D., Maggi, L.B., Faubert, B., Villarino, A.V., O'Sullivan, D., Huang, S.C.-C., van der Windt, G.J.W., Blagih, J., Qiu, J., Weber, J.D., Pearce, E.J., Jones, R.G., Pearce, E.L., 2013. Posttranscriptional Control of T Cell Effector Function by Aerobic Glycolysis. Cell 153, 1239–1251. https://doi.org/10.1016/j.cell.2013.05.016

Channappanavar, R., Fett, C., Zhao, J., Meyerholz, D.K., Perlman, S., 2014. Virus-specific memory CD8 T cells provide substantial protection from lethal severe acute respiratory syndrome coronavirus infection. J. Virol. 88, 11034–11044. https://doi.org/10.1128/JVI.01505-14

Chatterjee, S., Daenthanasanmak, A., Chakraborty, P., Wyatt, M.W., Dhar, P., Selvam, S.P., Fu, J., Zhang, J., Nguyen, H., Kang, I., Toth, K., Al-Homrani, M., Husain, M., Beeson, G., Ball, L., Helke, K., Husain, S., Garrett-Mayer, E., Hardiman, G., Mehrotra, M., Nishimura, M.I., Beeson, C.C., Bupp,

M.G., Wu, J., Ogretmen, B., Paulos, C.M., Rathmell, J., Yu, X.-Z., Mehrotra, S., 2018. CD38-NAD+Axis Regulates Immunotherapeutic Anti-Tumor T Cell Response. Cell Metab. 27, 85-100.e8. https://doi.org/10.1016/j.cmet.2017.10.006
Chen, K., Liu, J., Cao, X., 2017. Regulation of type I interferon signaling in immunity and inflammation: A comprehensive review. J. Autoimmun. 83, 1–11. https://doi.org/10.1016/j.jaut.2017.03.008
Chng, M.H.Y., Lim, M.Q., Rouers, A., Becht, E., Lee, B., MacAry, P.A., Lye, D.C., Leo, Y.S., Chen, J., Fink, K., Rivino, L., Newell, E.W., 2019. Large-Scale HLA Tetramer Tracking of T Cells during Dengue Infection Reveals Broad Acute Activation and Differentiation into Two Memory Cell Fates. Immunity. https://doi.org/10.1016/j.immuni.2019.10.007
Coffey, M.C., Strong, J.E., Forsyth, P.A., Lee, P.W.K., 1998. Reovirus Therapy of Tumors with Activated Ras Pathway. Science. https://doi.org/10.1126/science.282.5392.1332
Coillard, A., Segura, E., 2019. In vivo Differentiation of Human Monocytes. Front. Immunol. 10, 1907. https://doi.org/10.3389/fimmu.2019.01907
Coombs, K.M., 2006. Reovirus structure and morphogenesis. Curr. Top. Microbiol. Immunol. 309, 117–167. https://doi.org/10.1007/3-540-30773-7_5
Corrado, M., Pearce, E.L., 2022. Targeting memory T cell metabolism to improve immunity. J. Clin. Invest. 132. https://doi.org/10.1172/JCI148546
Correia, M.P., Costa, A.V., Uhrberg, M., Cardoso, E.M., Arosa, F.A., 2011. IL-15 induces CD8+ T cells to acquire functional NK receptors capable of modulating cytotoxicity and cytokine secretion. Immunobiology 216, 604–612. https://doi.org/10.1016/j.imbio.2010.09.012
Costela-Ruiz, V.J., Illescas-Montes, R., Pavón-Martínez, R., Ruiz, C., Melguizo-Rodríguez, L., 2018. Role of mast cells in autoimmunity. Life Sci. 209, 52–56. https://doi.org/10.1016/j.lfs.2018.07.051
Courtney, A.H., Lo, W.-L., Weiss, A., 2018. TCR SIGNALING: MECHANISMS OF INITIATION AND PROPAGATION. Trends Biochem. Sci. 43, 108–123. https://doi.org/10.1016/j.tibs.2017.11.008
Crotty, S., 2015. A brief history of T cell help to B cells. Nat. Rev. Immunol. 15, 185–189. https://doi.org/10.1038/nri3803
Cui, G., Staron, M.M., Gray, S.M., Ho, P.-C., Amezquita, R.A., Wu, J., Kaech, S.M., 2015. IL-7-Induced Glycerol Transport and TAG Synthesis Promotes Memory CD8+ T Cell Longevity. Cell 161, 750–761. https://doi.org/10.1016/j.cell.2015.03.021
Curtsinger, J.M., Mescher, M.F., 2010. Inflammatory cytokines as a third signal for T cell activation. Curr. Opin. Immunol. 22, 333–340. https://doi.org/10.1016/j.coi.2010.02.013
Dalod, M., Dupuis, M., Deschemin, J.C., Goujard, C., Deveau, C., Meyer, L., Ngo, N., Rouzioux, C., Guillet, J.G., Delfraissy, J.F., Sinet, M., Venet, A., 1999. Weak anti-HIV CD8(+) T-cell effector activity in HIV primary infection. J. Clin. Invest. 104, 1431–1439. https://doi.org/10.1172/JCI7162
Deeks, S.G., Kitchen, C.M.R., Liu, L., Guo, H., Gascon, R., Narváez, A.B., Hunt, P., Martin, J.N., Kahn, J.O., Levy, J., McGrath, M.S., Hecht, F.M., 2004. Immune activation set point during early HIV infection predicts subsequent CD4+ T-cell changes independent of viral load. Blood 104, 942–947. https://doi.org/10.1182/blood-2003-09-3333
DeLong, J.H., Hall, A.O., Konradt, C., Coppock, G.M., Park, J., Harms Pritchard, G., Hunter, C.A., 2018. Cytokine- and TCR-Mediated Regulation of T Cell Expression of Ly6C and Sca-1. J. Immunol. Baltim. Md 1950 200, 1761–1770. https://doi.org/10.4049/jimmunol.1701154
Denizot, F., Wilson, A., Battye, F., Berke, G., Shortman, K., 1986. Clonal expansion of T cells: a cytotoxic T-cell response in vivo that involves precursor cell proliferation. Proc. Natl. Acad. Sci. U. S. A. 83, 6089–6092. https://doi.org/10.1073/pnas.83.16.6089
Doisne, J.-M., Urrutia, A., Lacabaratz-Porret, C., Goujard, C., Meyer, L., Chaix, M.-L., Sinet, M., Venet, A., 2004. CD8+ T cells specific for EBV, cytomegalovirus, and influenza virus are activated during primary HIV infection. J. Immunol. Baltim. Md 1950 173, 2410–2418. https://doi.org/10.4049/jimmunol.173.4.2410
DURBIN, E., PILAR GIL, M., SALOMON, R., LOUTEN, J., BIRON, C.A., 2006. Modulation of STAT1 protein levels : a mechanism shaping CD8 T-cell responses invivo. Modul. STAT1 Protein Levels Mech. Shap. CD8 T-Cell Responses Invivo 107, 847–848.
Durek, P., Nordström, K., Gasparoni, G., Salhab, A., Kressler, C., de Almeida, M., Bassler, K., Ulas, T., Schmidt, F., Xiong, J., Glažar, P., Klironomos, F., Sinha, A., Kinkley, S., Yang, X., Arrigoni, L., Amirabad, A.D., Ardakani, F.B., Feuerbach, L., Gorka, O., Ebert, P., Müller, F., Li, N., Frischbutter, S., Schlickeiser, S., Cendon, C., Fröhler, S., Felder, B., Gasparoni, N., Imbusch,

C.D., Hutter, B., Zipprich, G., Tauchmann, Y., Reinke, S., Wassilew, G., Hoffmann, U., Richter, A.S., Sieverling, L., DEEP Consortium, Chang, H.-D., Syrbe, U., Kalus, U., Eils, J., Brors, B., Manke, T., Ruland, J., Lengauer, T., Rajewsky, N., Chen, W., Dong, J., Sawitzki, B., Chung, H.-R., Rosenstiel, P., Schulz, M.H., Schultze, J.L., Radbruch, A., Walter, J., Hamann, A., Polansky, J.K., 2016. Epigenomic Profiling of Human CD4+ T Cells Supports a Linear Differentiation Model and Highlights Molecular Regulators of Memory Development. Immunity 45, 1148–1161. https://doi.org/10.1016/j.immuni.2016.10.022

Ely, K.H., Cauley, L.S., Roberts, A.D., Brennan, J.W., Cookenham, T., Woodland, D.L., 2003. Nonspecific recruitment of memory CD8+ T cells to the lung airways during respiratory virus infections. J. Immunol. Baltim. Md 1950 170, 1423–1429. https://doi.org/10.4049/jimmunol.170.3.1423

Everett, R.D., 2000. ICP0, a regulator of herpes simplex virus during lytic and latent infection. BioEssays 22, 761–770. https://doi.org/10.1002/1521-1878(200008)22:8<761::AID-BIES10>3.0.CO;2-A

Fish, E.N., Uddin, S., Korkmaz, M., Majchrzak, B., Druker, B.J., Platanias, L.C., 1999. Activation of a CrkL-stat5 signaling complex by type I interferons. J. Biol. Chem. 274, 571–573. https://doi.org/10.1074/jbc.274.2.571

Flossdorf, M., Rössler, J., Buchholz, V.R., Busch, D.H., Höfer, T., 2015. CD8+ T cell diversification by asymmetric cell division. Nat. Immunol. 16, 891–893. https://doi.org/10.1038/ni.3235

Frauwirth, K.A., Riley, J.L., Harris, M.H., Parry, R.V., Rathmell, J.C., Plas, D.R., Elstrom, R.L., June, C.H., Thompson, C.B., 2002. The CD28 signaling pathway regulates glucose metabolism. Immunity 16, 769–777. https://doi.org/10.1016/s1074-7613(02)00323-0

Freer, G., Burkhart, C., Ciernik, I., Bachmann, M.F., Hengartner, H., Zinkernagel, R.M., 1994. Vesicular stomatitis virus Indiana glycoprotein as a T-cell-dependent and -independent antigen. J. Virol. 68, 3650–3655.

Fridman, W.H., Zitvogel, L., Sautès-Fridman, C., Kroemer, G., 2017. The immune contexture in cancer prognosis and treatment. Nat. Rev. Clin. Oncol. 14, 717–734. https://doi.org/10.1038/nrclinonc.2017.101

Fu, X.Y., Kessler, D.S., Veals, S.A., Levy, D.E., Darnell, J.E., 1990. ISGF3, the transcriptional activator induced by interferon alpha, consists of multiple interacting polypeptide chains. Proc. Natl. Acad. Sci. U. S. A. 87, 8555–8559.

Gattinoni, L., Speiser, D.E., Lichterfeld, M., Bonini, C., 2017. T memory stem cells in health and disease. Nat. Med. 23, 18–27. https://doi.org/10.1038/nm.4241

Gattinoni, L., Zhong, X.-S., Palmer, D.C., Ji, Y., Hinrichs, C.S., Yu, Z., Wrzesinski, C., Boni, A., Cassard, L., Garvin, L.M., Paulos, C.M., Muranski, P., Restifo, N.P., 2009. Wnt signaling arrests effector T cell differentiation and generates CD8+ memory stem cells. Nat. Med. 15, 808–813. https://doi.org/10.1038/nm.1982

Gc, M., Dp, N., Mp, J., M, W., El, H., Bk, E., R, R., W, H., Sp, G., 2014. MultiNotch MS3 enables accurate, sensitive, and multiplexed detection of differential expression across cancer cell line proteomes. Anal. Chem. 86. https://doi.org/10.1021/ac502040v

Gerner, R.R., Macheiner, S., Reider, S., Siegmund, K., Grabherr, F., Mayr, L., Texler, B., Moser, P., Effenberger, M., Schwaighofer, H., Moschen, A.R., Kircher, B., Oberacher, H., Zeiser, R., Tilg, H., Nachbaur, D., 2020. Targeting NAD immunometabolism limits severe graft-versus-host disease and has potent antileukemic activity. Leukemia 1–13. https://doi.org/10.1038/s41375-020-0709-0

Ghazarian, M., Revelo, X.S., Nøhr, M.K., Luck, H., Zeng, K., Lei, H., Tsai, S., Schroer, S.A., Park, Y.J., Chng, M.H.Y., Shen, L., D'Angelo, J.A., Horton, P., Chapman, W.C., Brockmeier, D., Woo, M., Engleman, E.G., Adeyi, O., Hirano, N., Jin, T., Gehring, A.J., Winer, S., Winer, D.A., 2017. Type I Interferon Responses Drive Intrahepatic T cells to Promote Metabolic Syndrome. Sci. Immunol. 2. https://doi.org/10.1126/sciimmunol.aai7616

Gong, J., Sachdev, E., Mita, A.C., Mita, M.M., 2016. Clinical development of reovirus for cancer therapy: An oncolytic virus with immune-mediated antitumor activity. World J. Methodol. 6, 25–42. https://doi.org/10.5662/wjm.v6.i1.25

Gordon, S., Martinez-Pomares, L., 2017. Physiological roles of macrophages. Pflugers Arch. 469, 365–374. https://doi.org/10.1007/s00424-017-1945-7

Gudgeon, N., Munford, H., Bishop, E.L., Hill, J., Fulton-Ward, T., Bending, D., Roberts, J., Tennant, D.A., Dimeloe, S., 2022. Succinate uptake by T cells suppresses their effector function via inhibition of

mitochondrial glucose oxidation. Cell Rep. 40, 111193. https://doi.org/10.1016/j.celrep.2022.111193
Gujar, S.A., Marcato, P., Pan, D., Lee, P.W.K., 2010. Reovirus Virotherapy Overrides Tumor Antigen Presentation Evasion and Promotes Protective Antitumor Immunity. Mol. Cancer Ther. 9, 2924–2933. https://doi.org/10.1158/1535-7163.MCT-10-0590
Haas, A., Zimmermann, K., Oxenius, A., 2011. Antigen-dependent and -independent mechanisms of T and B cell hyperactivation during chronic HIV-1 infection. J. Virol. 85, 12102–12113. https://doi.org/10.1128/JVI.05607-11
Hardy, G.A.D., Sieg, S., Rodriguez, B., Anthony, D., Asaad, R., Jiang, W., Mudd, J., Schacker, T., Funderburg, N.T., Pilch-Cooper, H.A., Debernardo, R., Rabin, R.L., Lederman, M.M., Harding, C.V., 2013. Interferon-α is the primary plasma type-I IFN in HIV-1 infection and correlates with immune activation and disease markers. PloS One 8, e56527. https://doi.org/10.1371/journal.pone.0056527
Henning, A.N., Roychoudhuri, R., Restifo, N.P., 2018. Epigenetic control of CD8+ T cell differentiation. Nat. Rev. Immunol. 18, 340–356. https://doi.org/10.1038/nri.2017.146
Hiscott, J., Grandvaux, N., Sharma, S., Tenoever, B.R., Servant, M.J., Lin, R., 2003. Convergence of the NF-kappaB and interferon signaling pathways in the regulation of antiviral defense and apoptosis. Ann. N. Y. Acad. Sci. 1010, 237–248. https://doi.org/10.1196/annals.1299.042
Honda, K., Taniguchi, T., 2006. Toll-like receptor signaling and IRF transcription factors. IUBMB Life 58, 290–295. https://doi.org/10.1080/15216540600702206
Howard, C.J., Charleston, B., Stephens, S.A., Sopp, P., Hope, J.C., 2004. The role of dendritic cells in shaping the immune response. Anim. Health Res. Rev. 5, 191–195. https://doi.org/10.1079/ahr200468
Hsu, E.C., Iorio, C., Sarangi, F., Khine, A.A., Richardson, C.D., 2001. CDw150(SLAM) Is a Receptor for a Lymphotropic Strain of Measles Virus and May Account for the Immunosuppressive Properties of This Virus. Virology 279, 9–21. https://doi.org/10.1006/viro.2000.0711
Hubert, S., Rissiek, B., Klages, K., Huehn, J., Sparwasser, T., Haag, F., Koch-Nolte, F., Boyer, O., Seman, M., Adriouch, S., 2010. Extracellular NAD+ shapes the Foxp3+ regulatory T cell compartment through the ART2–P2X7 pathway. J. Exp. Med. 207, 2561–2568. https://doi.org/10.1084/jem.20091154
Hurton, L.V., Singh, H., Najjar, A.M., Switzer, K.C., Mi, T., Maiti, S., Olivares, S., Rabinovich, B., Huls, H., Forget, M.-A., Datar, V., Kebriaei, P., Lee, D.A., Champlin, R.E., Cooper, L.J.N., 2016. Tethered IL-15 augments antitumor activity and promotes a stem-cell memory subset in tumor-specific T cells. Proc. Natl. Acad. Sci. U. S. A. 113, E7788–E7797. https://doi.org/10.1073/pnas.1610544113
Hwang, J.-R., Byeon, Y., Kim, D., Park, S.-G., 2020. Recent insights of T cell receptor-mediated signaling pathways for T cell activation and development. Exp. Mol. Med. 52, 750–761. https://doi.org/10.1038/s12276-020-0435-8
Ivashkiv, L.B., Donlin, L.T., 2014. Regulation of type I interferon responses. Nat. Rev. Immunol. 14, 36–49. https://doi.org/10.1038/nri3581
Jeng, M.Y., Hull, P.A., Fei, M., Kwon, H.-S., Tsou, C.-L., Kasler, H., Ng, C.-P., Gordon, D.E., Johnson, J., Krogan, N., Verdin, E., Ott, M., 2018. Metabolic reprogramming of human CD8+ memory T cells through loss of SIRT1. J. Exp. Med. 215, 51–62. https://doi.org/10.1084/jem.20161066
Jergović, M., Coplen, C.P., Uhrlaub, J.L., Besselsen, D.G., Cheng, S., Smithey, M.J., Nikolich-Žugich, J., 2021. Infection-induced type I interferons critically modulate the homeostasis and function of CD8+ naïve T cells. Nat. Commun. 12, 5303. https://doi.org/10.1038/s41467-021-25645-w
Johnson, S., Imai, S., 2018. NAD + biosynthesis, aging, and disease. F1000Research 7, 132. https://doi.org/10.12688/f1000research.12120.1
Joklik, W.K., 1981. Structure and function of the reovirus genome. Microbiol. Rev. 45, 483–501. https://doi.org/10.1128/mr.45.4.483-501.1981
Joshi, N.S., Cui, W., Chandele, A., Lee, H.K., Urso, D.R., Hagman, J., Gapin, L., Kaech, S.M., 2007. Inflammation directs memory precursor and short-lived effector CD8(+) T cell fates via the graded expression of T-bet transcription factor. Immunity 27, 281–295. https://doi.org/10.1016/j.immuni.2007.07.010
Kaech, S.M., Cui, W., 2012. Transcriptional control of effector and memory CD8+ T cell differentiation. Nat. Rev. Immunol. 12, 749–761. https://doi.org/10.1038/nri3307

Kaech, S.M., Wherry, E.J., Ahmed, R., 2002. Effector and memory T-cell differentiation: implications for vaccine development. Nat. Rev. Immunol. 2, 251–262. https://doi.org/10.1038/nri778
Kalia, V., Sarkar, S., Subramaniam, S., Haining, W.N., Smith, K.A., Ahmed, R., 2010. Prolonged interleukin-2Ralpha expression on virus-specific CD8+ T cells favors terminal-effector differentiation in vivo. Immunity 32, 91–103. https://doi.org/10.1016/j.immuni.2009.11.010
Kambayashi, T., Assarsson, E., Lukacher, A.E., Ljunggren, H.-G., Jensen, P.E., 2003. Memory CD8+ T cells provide an early source of IFN-gamma. J. Immunol. Baltim. Md 1950 170, 2399–2408. https://doi.org/10.4049/jimmunol.170.5.2399
Kawai, T., Akira, S., 2007. Signaling to NF-kappaB by Toll-like receptors. Trends Mol. Med. 13, 460–469. https://doi.org/10.1016/j.molmed.2007.09.002
Keir, M.E., Freeman, G.J., Sharpe, A.H., 2007. PD-1 regulates self-reactive CD8+ T cell responses to antigen in lymph nodes and tissues. J. Immunol. Baltim. Md 1950 179, 5064–5070. https://doi.org/10.4049/jimmunol.179.8.5064
Kennedy, B.E., Giacomantonio, M., Murphy, J.P., Cutler, S., Sadek, M., Konda, P., Paulo, J.A., Pathak, G.P., Renkens, S.H.J., Grieve, S., Pol, J., Gygi, S.P., Richardson, C., Gaston, D., Reiman, A., Kroemer, G., Elnenaei, M.O., Gujar, S.A., 2022. NAD+ depletion enhances reovirus-induced oncolysis in multiple myeloma. Mol. Ther. - Oncolytics 24, 695–706. https://doi.org/10.1016/j.omto.2022.02.017
Kim, J., Chang, D.-Y., Lee, H.W., Lee, H., Kim, J.H., Sung, P.S., Kim, K.H., Hong, S.-H., Kang, W., Lee, J., Shin, S.Y., Yu, H.T., You, S., Choi, Y.S., Oh, I., Lee, Dong Ho, Lee, Dong Hyeon, Jung, M.K., Suh, K.-S., Hwang, S., Kim, W., Park, S.-H., Kim, H.J., Shin, E.-C., 2018. Innate-like Cytotoxic Function of Bystander-Activated CD8+ T Cells Is Associated with Liver Injury in Acute Hepatitis A. Immunity 48, 161-173.e5. https://doi.org/10.1016/j.immuni.2017.11.025
Kim, T.-S., Shin, E.-C., 2019. The activation of bystander CD8+ T cells and their roles in viral infection. Exp. Mol. Med. 51, 1–9. https://doi.org/10.1038/s12276-019-0316-1
Kim, Y.K., Shin, J.S., Nahm, M.H., 2016. NOD-Like Receptors in Infection, Immunity, and Diseases. Yonsei Med. J. 57, 5–14. https://doi.org/10.3349/ymj.2016.57.1.5
Klein Geltink, R.I., Kyle, R.L., Pearce, E.L., 2018. Unraveling the Complex Interplay Between T Cell Metabolism and Function. Annu. Rev. Immunol. 36, 461–488. https://doi.org/10.1146/annurev-immunol-042617-053019
Klein Geltink, R.I., O'Sullivan, D., Corrado, M., Bremser, A., Buck, M.D., Buescher, J.M., Firat, E., Zhu, X., Niedermann, G., Caputa, G., Kelly, B., Warthorst, U., Rensing-Ehl, A., Kyle, R.L., Vandersarren, L., Curtis, J.D., Patterson, A.E., Lawless, S., Grzes, K., Qiu, J., Sanin, D.E., Kretz, O., Huber, T.B., Janssens, S., Lambrecht, B.N., Rambold, A.S., Pearce, E.J., Pearce, E.L., 2017. Mitochondrial Priming by CD28. Cell 171, 385-397.e11. https://doi.org/10.1016/j.cell.2017.08.018
Kolumam, G.A., Thomas, S., Thompson, L.J., Sprent, J., Murali-Krishna, K., 2005. Type I interferons act directly on CD8 T cells to allow clonal expansion and memory formation in response to viral infection. J. Exp. Med. 202, 637–650. https://doi.org/10.1084/jem.20050821
Kumar, V., Barrett, J.E., 2022. Toll-Like Receptors (TLRs) in Health and Disease: An Overview. Handb. Exp. Pharmacol. 276, 1–21. https://doi.org/10.1007/164_2021_568
Kurniawan, H., Kobayashi, T., Brenner, D., 2021. The emerging role of one-carbon metabolism in T cells. Curr. Opin. Biotechnol. 68, 193–201. https://doi.org/10.1016/j.copbio.2020.12.001
Lázár-Molnár, E., Chen, B., Sweeney, K.A., Wang, E.J., Liu, W., Lin, J., Porcelli, S.A., Almo, S.C., Nathenson, S.G., Jacobs, W.R., 2010. Programmed death-1 (PD-1)-deficient mice are extraordinarily sensitive to tuberculosis. Proc. Natl. Acad. Sci. U. S. A. 107, 13402–13407. https://doi.org/10.1073/pnas.1007394107
Lee, C.H., Pinho, M.P., Buckley, P.R., Woodhouse, I.B., Ogg, G., Simmons, A., Napolitani, G., Koohy, H., 2020. Potential CD8+ T Cell Cross-Reactivity Against SARS-CoV-2 Conferred by Other Coronavirus Strains. Front. Immunol. 11, 579480. https://doi.org/10.3389/fimmu.2020.579480
Lee, H., Jeong, S., Shin, E.-C., 2022. Significance of bystander T cell activation in microbial infection. Nat. Immunol. 23, 13–22. https://doi.org/10.1038/s41590-021-00985-3
Lee, J., Kim, Hyosil, Lee, J.E., Shin, S.-J., Oh, S., Kwon, G., Kim, Hakhyun, Choi, Y.Y., White, M.A., Paik, S., Cheong, J.-H., Kim, H.S., 2018. Selective Cytotoxicity of the NAMPT Inhibitor FK866 Toward Gastric Cancer Cells With Markers of the Epithelial-Mesenchymal Transition, Due to Loss of NAPRT. Gastroenterology 155, 799-814.e13. https://doi.org/10.1053/j.gastro.2018.05.024

Lee, J.S., Shin, E.-C., 2020. The type I interferon response in COVID-19: implications for treatment. Nat. Rev. Immunol. 20, 585–586. https://doi.org/10.1038/s41577-020-00429-3
Lee, P.W., Gilmore, R., 1998. Reovirus cell attachment protein sigma 1: structure-function relationships and biogenesis. Curr. Top. Microbiol. Immunol. 233, 137–153. https://doi.org/10.1007/978-3-642-72092-5_6
Lertmemongkolchai, G., Cai, G., Hunter, C.A., Bancroft, G.J., 2001. Bystander activation of CD8+ T cells contributes to the rapid production of IFN-gamma in response to bacterial pathogens. J. Immunol. Baltim. Md 1950 166, 1097–1105. https://doi.org/10.4049/jimmunol.166.2.1097
Levescot, A., Cerf-Bensussan, N., 2022. Regulatory CD8+ T cells suppress disease. Science 376, 243–244. https://doi.org/10.1126/science.abp8243
Lewis, S.A., Sureshchandra, S., Zulu, M.Z., Doratt, B., Jankeel, A., Ibraim, I.C., Pinski, A.N., Rhoades, N.S., Curtis, M., Jiang, X., Tifrea, D., Zaldivar, F., Shen, W., Edwards, R.A., Chow, D., Cooper, D., Amin, A., Messaoudi, I., 2021. Differential dynamics of peripheral immune responses to acute SARS-CoV-2 infection in older adults. Nat. Aging 1, 1038–1052. https://doi.org/10.1038/s43587-021-00127-2
Li, N., Bu, X., Tian, X., Wu, P., Yang, L., Huang, P., 2012. Fatty acid synthase regulates proliferation and migration of colorectal cancer cells via HER2-PI3K/Akt signaling pathway. Nutr. Cancer 64, 864–870. https://doi.org/10.1080/01635581.2012.701704
Liu, K., Catalfamo, M., Li, Y., Henkart, P.A., Weng, N., 2002. IL-15 mimics T cell receptor crosslinking in the induction of cellular proliferation, gene expression, and cytotoxicity in CD8+ memory T cells. Proc. Natl. Acad. Sci. U. S. A. 99, 6192–6197. https://doi.org/10.1073/pnas.092675799
Livak, K.J., Schmittgen, T.D., 2001. Analysis of relative gene expression data using real-time quantitative PCR and the 2(-Delta Delta C(T)) Method. Methods San Diego Calif 25, 402–408. https://doi.org/10.1006/meth.2001.1262
Lukyanova, L.D., Kirova, Y.I., Germanova, E.L., 2018. The Role of Succinate in Regulation of Immediate HIF-1α Expression in Hypoxia. Bull. Exp. Biol. Med. 164, 298–303. https://doi.org/10.1007/s10517-018-3976-2
MacIver, N.J., Michalek, R.D., Rathmell, J.C., 2013. Metabolic Regulation of T Lymphocytes. Annu. Rev. Immunol. 31, 259–283. https://doi.org/10.1146/annurev-immunol-032712-095956
Maini, M.K., Boni, C., Lee, C.K., Larrubia, J.R., Reignat, S., Ogg, G.S., King, A.S., Herberg, J., Gilson, R., Alisa, A., Williams, R., Vergani, D., Naoumov, N.V., Ferrari, C., Bertoletti, A., 2000. The role of virus-specific CD8(+) cells in liver damage and viral control during persistent hepatitis B virus infection. J. Exp. Med. 191, 1269–1280. https://doi.org/10.1084/jem.191.8.1269
Marshall, H.D., Prince, A.L., Berg, L.J., Welsh, R.M., 2010. IFN-αβ and Self-MHC Divert CD8 T Cells into a Distinct Differentiation Pathway Characterized by Rapid Acquisition of Effector Functions. J. Immunol. 185, 1419. https://doi.org/10.4049/jimmunol.1001140
Marshall, J.S., Jawdat, D.M., 2004. Mast cells in innate immunity. J. Allergy Clin. Immunol. 114, 21–27. https://doi.org/10.1016/j.jaci.2004.04.045
McNab, F., Mayer-Barber, K., Sher, A., Wack, A., O'Garra, A., 2015. Type I interferons in infectious disease. Nat. Rev. Immunol. 15, 87–103. https://doi.org/10.1038/nri3787
Mendoza, A., Fang, V., Chen, C., Serasinghe, M., Verma, A., Muller, J., Chaluvadi, V.S., Dustin, M.L., Hla, T., Elemento, O., Chipuk, J.E., Schwab, S.R., 2017. Lymphatic endothelial S1P promotes mitochondrial function and survival in naive T cells. Nature 546, 158–161. https://doi.org/10.1038/nature22352
Menk, A.V., Scharping, N.E., Moreci, R.S., Zeng, X., Guy, C., Salvatore, S., Bae, H., Xie, J., Young, H.A., Wendell, S.G., Delgoffe, G.M., 2018. Early TCR Signaling Induces Rapid Aerobic Glycolysis Enabling Distinct Acute T Cell Effector Functions. Cell Rep. 22, 1509–1521. https://doi.org/10.1016/j.celrep.2018.01.040
Merad, M., Blish, C.A., Sallusto, F., Iwasaki, A., 2022. The immunology and immunopathology of COVID-19. Science 375, 1122–1127. https://doi.org/10.1126/science.abm8108
Mohammad, K., Dakik, P., Medkour, Y., Mitrofanova, D., Titorenko, V.I., 2019. Quiescence Entry, Maintenance, and Exit in Adult Stem Cells. Int. J. Mol. Sci. 20, 2158. https://doi.org/10.3390/ijms20092158
Moreno-Altamirano, M.M.B., Kolstoe, S.E., Sánchez-García, F.J., 2019. Virus Control of Cell Metabolism for Replication and Evasion of Host Immune Responses. Front. Cell. Infect. Microbiol. 9. https://doi.org/10.3389/fcimb.2019.00095

Moss, P., 2022. The T cell immune response against SARS-CoV-2. Nat. Immunol. 23, 186–193. https://doi.org/10.1038/s41590-021-01122-w
Müller, L., Berkeley, R., Barr, T., Ilett, E., Errington-Mais, F., 2020. Past, Present and Future of Oncolytic Reovirus. Cancers 12, 3219. https://doi.org/10.3390/cancers12113219
Murphy, J.P., Stepanova, E., Everley, R.A., Paulo, J.A., Gygi, S.P., 2015. Comprehensive Temporal Protein Dynamics during the Diauxic Shift in Saccharomyces cerevisiae. Mol. Cell. Proteomics MCP 14, 2454–2465. https://doi.org/10.1074/mcp.M114.045849
Murphy, M.P., Siegel, R.M., 2013. Mitochondrial ROS fire up T cell activation. Immunity 38, 201–202. https://doi.org/10.1016/j.immuni.2013.02.005
Murray, P.J., 2017. Macrophage Polarization. Annu. Rev. Physiol. 79, 541–566. https://doi.org/10.1146/annurev-physiol-022516-034339
Nadif, R., Zerimech, F., Bouzigon, E., Matran, R., 2013. The role of eosinophils and basophils in allergic diseases considering genetic findings. Curr. Opin. Allergy Clin. Immunol. 13, 507–513. https://doi.org/10.1097/ACI.0b013e328364e9c0
Nakajima, Y., Chamoto, K., Oura, T., Honjo, T., 2021. Critical role of the CD44lowCD62Llow CD8+ T cell subset in restoring antitumor immunity in aged mice. Proc. Natl. Acad. Sci. 118, e2103730118. https://doi.org/10.1073/pnas.2103730118
Nastasi, C., Willerlev-Olsen, A., Dalhoff, K., Ford, S.L., Gadsbøll, A.-S.Ø., Buus, T.B., Gluud, M., Danielsen, M., Litman, T., Bonefeld, C.M., Geisler, C., Ødum, N., Woetmann, A., 2021. Inhibition of succinate dehydrogenase activity impairs human T cell activation and function. Sci. Rep. 11, 1458. https://doi.org/10.1038/s41598-020-80933-7
Nguyen, N.V., Kato, S., Nagata, K., Takeuchi, K., 2016. Differential induction of type I interferons in macaques by wild-type measles virus alone or with the hemagglutinin protein of the Edmonston vaccine strain. Microbiol. Immunol. 60, 501–505. https://doi.org/10.1111/1348-0421.12392
O'Carroll, S.M., O'Neill, L.A.J., 2021. Targeting immunometabolism to treat COVID-19. Immunother. Adv. 1, ltab013. https://doi.org/10.1093/immadv/ltab013
Odumade, O.A., Knight, J.A., Schmeling, D.O., Masopust, D., Balfour, H.H., Hogquist, K.A., 2012. Primary Epstein-Barr virus infection does not erode preexisting $CD8^+$ T cell memory in humans. J. Exp. Med. 209, 471–478. https://doi.org/10.1084/jem.20112401
Omilusik, K.D., Goldrath, A.W., 2017. The origins of memory T cells. Nature 552, 337–339. https://doi.org/10.1038/d41586-017-08280-8
O'Neill, L.A.J., Kishton, R.J., Rathmell, J., 2016. A guide to immunometabolism for immunologists. Nat. Rev. Immunol. 16, 553–565. https://doi.org/10.1038/nri.2016.70
Oshi, M., Patel, A., Wu, R., Le, L., Tokumaru, Y., Yamada, A., Yan, L., Matsuyama, R., Ishikawa, T., Endo, I., Takabe, K., 2022. Enhanced immune response outperform aggressive cancer biology and is associated with better survival in triple-negative breast cancer. Npj Breast Cancer 8, 1–10. https://doi.org/10.1038/s41523-022-00466-2
O'Sullivan, D., van der Windt, G.J.W., Huang, S.C.-C., Curtis, J.D., Chang, C.-H., Buck, M.D., Qiu, J., Smith, A.M., Lam, W.Y., DiPlato, L.M., Hsu, F.-F., Birnbaum, M.J., Pearce, E.J., Pearce, E.L., 2014. Memory CD8(+) T cells use cell-intrinsic lipolysis to support the metabolic programming necessary for development. Immunity 41, 75–88. https://doi.org/10.1016/j.immuni.2014.06.005
Palm, N.W., Medzhitov, R., 2007. Not so fast: adaptive suppression of innate immunity. Nat. Med. 13, 1142–1144. https://doi.org/10.1038/nm1007-1142b
Pan, Y., Tian, T., Park, C.O., Lofftus, S.Y., Mei, S., Liu, X., Luo, C., O'Malley, J.T., Gehad, A., Teague, J.E., Divito, S.J., Fuhlbrigge, R., Puigserver, P., Krueger, J.G., Hotamisligil, G.S., Clark, R.A., Kupper, T.S., 2017. Survival of tissue-resident memory T cells requires exogenous lipid uptake and metabolism. Nature 543, 252–256. https://doi.org/10.1038/nature21379
Pardigon, N., Bercovici, N., Calbo, S., Santos-Lima, E.C., Liblau, R., Kourilsky, P., Abastado, J.P., 1998. Role of co-stimulation in CD8+ T cell activation. Int. Immunol. 10, 619–630. https://doi.org/10.1093/intimm/10.5.619
Patente, T.A., Pinho, M.P., Oliveira, A.A., Evangelista, G.C.M., Bergami-Santos, P.C., Barbuto, J.A.M., 2019. Human Dendritic Cells: Their Heterogeneity and Clinical Application Potential in Cancer Immunotherapy. Front. Immunol. 9.
Pearce, E.L., 2021. Metabolism as a driver of immunity. Nat. Rev. Immunol. 21, 618–619. https://doi.org/10.1038/s41577-021-00601-3

Pearce, E.L., Poffenberger, M.C., Chang, C.-H., Jones, R.G., 2013. Fueling immunity: insights into metabolism and lymphocyte function. Science 342, 1242454. https://doi.org/10.1126/science.1242454
Phan, A.T., Doedens, A.L., Palazon, A., Tyrakis, P.A., Cheung, K.P., Johnson, R.S., Goldrath, A.W., 2016. Constitutive Glycolytic Metabolism Supports CD8+ T Cell Effector Memory Differentiation during Viral Infection. Immunity 45, 1024–1037. https://doi.org/10.1016/j.immuni.2016.10.017
Raué, H.-P., Beadling, C., Haun, J., Slifka, M.K., 2013. Cytokine-mediated programmed proliferation of virus-specific CD8(+) memory T cells. Immunity 38, 131–139. https://doi.org/10.1016/j.immuni.2012.09.019
Reid, M.A., Allen, A.E., Liu, S., Liberti, M.V., Liu, P., Liu, X., Dai, Z., Gao, X., Wang, Q., Liu, Y., Lai, L., Locasale, J.W., 2018. Serine synthesis through PHGDH coordinates nucleotide levels by maintaining central carbon metabolism. Nat. Commun. 9, 5442. https://doi.org/10.1038/s41467-018-07868-6
Restifo, N.P., Gattinoni, L., 2013. Lineage relationship of effector and memory T cells. Curr. Opin. Immunol. 25, 10.1016/j.coi.2013.09.003. https://doi.org/10.1016/j.coi.2013.09.003
Revollo, J.R., Grimm, A.A., Imai, S., 2004. The NAD Biosynthesis Pathway Mediated by Nicotinamide Phosphoribosyltransferase Regulates Sir2 Activity in Mammalian Cells. J. Biol. Chem. 279, 50754–50763. https://doi.org/10.1074/jbc.M408388200
Richter, F.C., Clarke, A.J., 2021. One carbon (metabolism) to rule T cell identity. Nat. Rev. Immunol. 21, 206–206. https://doi.org/10.1038/s41577-021-00530-1
Rivadeneira, D.B., DePeaux, K., Wang, Y., Kulkarni, A., Tabib, T., Menk, A.V., Sampath, P., Lafyatis, R., Ferris, R.L., Sarkar, S.N., Thorne, S.H., Delgoffe, G.M., 2019. Oncolytic Viruses Engineered to Enforce Leptin Expression Reprogram Tumor-Infiltrating T Cell Metabolism and Promote Tumor Clearance. Immunity 51, 548-560.e4. https://doi.org/10.1016/j.immuni.2019.07.003
Roberts, A.I., Lee, L., Schwarz, E., Groh, V., Spies, T., Ebert, E.C., Jabri, B., 2001. NKG2D receptors induced by IL-15 costimulate CD28-negative effector CTL in the tissue microenvironment. J. Immunol. Baltim. Md 1950 167, 5527–5530. https://doi.org/10.4049/jimmunol.167.10.5527
Saito, T., Hirai, R., Loo, Y.-M., Owen, D., Johnson, C.L., Sinha, S.C., Akira, S., Fujita, T., Gale, M., 2007. Regulation of innate antiviral defenses through a shared repressor domain in RIG-I and LGP2. Proc. Natl. Acad. Sci. U. S. A. 104, 582–587. https://doi.org/10.1073/pnas.0606699104
Sandalova, E., Laccabue, D., Boni, C., Tan, A.T., Fink, K., Ooi, E.E., Chua, R., Shafaeddin Schreve, B., Ferrari, C., Bertoletti, A., 2010. Contribution of herpesvirus specific CD8 T cells to anti-viral T cell response in humans. PLoS Pathog. 6, e1001051. https://doi.org/10.1371/journal.ppat.1001051
Sarkar, S., Kalia, V., Haining, W.N., Konieczny, B.T., Subramaniam, S., Ahmed, R., 2008. Functional and genomic profiling of effector CD8 T cell subsets with distinct memory fates. J. Exp. Med. 205, 625–640. https://doi.org/10.1084/jem.20071641
Schuster, S., Penke, M., Gorski, T., Gebhardt, R., Weiss, T.S., Kiess, W., Garten, A., 2015. FK866-induced NAMPT inhibition activates AMPK and downregulates mTOR signaling in hepatocarcinoma cells. Biochem. Biophys. Res. Commun. 458, 334–340. https://doi.org/10.1016/j.bbrc.2015.01.111
Shakiba, M., Zumbo, P., Espinosa-Carrasco, G., Menocal, L., Dündar, F., Carson, S.E., Bruno, E.M., Sanchez-Rivera, F.J., Lowe, S.W., Camara, S., Koche, R.P., Reuter, V.P., Socci, N.D., Whitlock, B., Tamzalit, F., Huse, M., Hellmann, M.D., Wells, D.K., Defranoux, N.A., Betel, D., Philip, M., Schietinger, A., 2022. TCR signal strength defines distinct mechanisms of T cell dysfunction and cancer evasion. J. Exp. Med. 219, e20201966. https://doi.org/10.1084/jem.20201966
Sheng, S.Y., Gu, Y., Lu, C.G., Tang, Y.Y., Zou, J.Y., Zhang, Y.Q., Wang, R.F., Hong, H., 2017. The Characteristics of Naive-like T Cells in Tumor-infiltrating Lymphocytes From Human Lung Cancer. J. Immunother. 40, 1–10. https://doi.org/10.1097/CJI.0000000000000147
Shin, E.-C., Sung, P.S., Park, S.-H., 2016. Immune responses and immunopathology in acute and chronic viral hepatitis. Nat. Rev. Immunol. 16, 509–523. https://doi.org/10.1038/nri.2016.69
Shingai, M., Ebihara, T., Begum, N.A., Kato, A., Honma, T., Matsumoto, K., Saito, H., Ogura, H., Matsumoto, M., Seya, T., 2007. Differential Type I IFN-Inducing Abilities of Wild-Type versus Vaccine Strains of Measles Virus. J. Immunol. 179, 6123–6133. https://doi.org/10.4049/jimmunol.179.9.6123
Silverstein, S.C., Christman, J.K., Acs, G., 1976. The reovirus replicative cycle. Annu. Rev. Biochem. 45, 375–408. https://doi.org/10.1146/annurev.bi.45.070176.002111

Soudja, S.M., Ruiz, A.L., Marie, J.C., Lauvau, G., 2012. Inflammatory monocytes activate memory CD8(+) T and innate NK lymphocytes independent of cognate antigen during microbial pathogen invasion. Immunity 37, 549–562. https://doi.org/10.1016/j.immuni.2012.05.029

Takeuchi, K., Takeda, M., Miyajima, N., Kobune, F., Tanabayashi, K., Tashiro, M., 2002. Recombinant Wild-Type and Edmonston Strain Measles Viruses Bearing Heterologous H Proteins: Role of H Protein in Cell Fusion and Host Cell Specificity. J. Virol. 76, 4891–4900. https://doi.org/10.1128/JVI.76.10.4891-4900.2002

Tanabe, Y., Nishibori, T., Su, L., Arduini, R.M., Baker, D.P., David, M., 2005. Cutting Edge: Role of STAT1, STAT3, and STAT5 in IFN-αβ Responses in T Lymphocytes. J. Immunol. 174, 609–613. https://doi.org/10.4049/jimmunol.174.2.609

Thirukkumaran, C.M., Nodwell, M.J., Hirasawa, K., Shi, Z.-Q., Diaz, R., Luider, J., Johnston, R.N., Forsyth, P.A., Magliocco, A.M., Lee, P., Nishikawa, S., Donnelly, B., Coffey, M., Trpkov, K., Fonseca, K., Spurrell, J., Morris, D.G., 2010. Oncolytic Viral Therapy for Prostate Cancer: Efficacy of Reovirus as a Biological Therapeutic. Cancer Res. 70, 2435–2444. https://doi.org/10.1158/0008-5472.CAN-09-2408

Thoresen, D., Wang, W., Galls, D., Guo, R., Xu, L., Pyle, A.M., 2021. The molecular mechanism of RIG-I activation and signaling. Immunol. Rev. 304, 154–168. https://doi.org/10.1111/imr.13022

Tough, D.F., Borrow, P., Sprent, J., 1996. Induction of bystander T cell proliferation by viruses and type I interferon in vivo. Science 272, 1947–1950. https://doi.org/10.1126/science.272.5270.1947

Tough, D.F., Sun, S., Sprent, J., 1997. T cell stimulation in vivo by lipopolysaccharide (LPS). J. Exp. Med. 185, 2089–2094. https://doi.org/10.1084/jem.185.12.2089

Trabucchi, E., Radaelli, E., Marazzi, M., Foschi, D., Musazzi, M., Veronesi, A.M., Montorsi, W., 1988. The role of mast cells in wound healing. Int. J. Tissue React. 10, 367–372.

Tullius, S.G., Biefer, H.R.C., Li, S., Trachtenberg, A.J., Edtinger, K., Quante, M., Krenzien, F., Uehara, H., Yang, X., Kissick, H.T., Kuo, W.P., Ghiran, I., de la Fuente, M.A., Arredouani, M.S., Camacho, V., Tigges, J.C., Toxavidis, V., El Fatimy, R., Smith, B.D., Vasudevan, A., ElKhal, A., 2014. NAD + protects against EAE by regulating CD4 + T-cell differentiation. Nat. Commun. 5, 1–17. https://doi.org/10.1038/ncomms6101

Urb, M., Sheppard, D.C., 2012. The Role of Mast Cells in the Defence against Pathogens. PLoS Pathog. 8, e1002619. https://doi.org/10.1371/journal.ppat.1002619

Urban, S.L., Berg, L.J., Welsh, R.M., 2016. Type 1 interferon licenses naïve CD8 T cells to mediate anti-viral cytotoxicity. Virology 493, 52–59. https://doi.org/10.1016/j.virol.2016.03.005

Valyi-Nagy, T., Fareed, M.U., O'Keefe, J.S., Gesser, R.M., MacLean, A.R., Brown, S.M., Spivack, J.G., Fraser, N.W., 1994. The herpes simplex virus type 1 strain 17+ gamma 34.5 deletion mutant 1716 is avirulent in SCID mice. J. Gen. Virol. 75 (Pt 8), 2059–2063. https://doi.org/10.1099/0022-1317-75-8-2059

van Boxel-Dezaire, A.H.H., Rani, M.R.S., Stark, G.R., 2006. Complex Modulation of Cell Type-Specific Signaling in Response to Type I Interferons. Immunity 25, 361–372. https://doi.org/10.1016/j.immuni.2006.08.014

van der Windt, G.J.W., Everts, B., Chang, C.-H., Curtis, J.D., Freitas, T.C., Amiel, E., Pearce, E.J., Pearce, E.L., 2012. Mitochondrial respiratory capacity is a critical regulator of CD8+ T cell memory development. Immunity 36, 68–78. https://doi.org/10.1016/j.immuni.2011.12.007

van der Windt, G.J.W., Pearce, E.L., 2012. Metabolic switching and fuel choice during T-cell differentiation and memory development. Immunol. Rev. 249, 27–42. https://doi.org/10.1111/j.1600-065X.2012.01150.x

Vander Heiden, M.G., Cantley, L.C., Thompson, C.B., 2009. Understanding the Warburg effect: the metabolic requirements of cell proliferation. Science 324, 1029–1033. https://doi.org/10.1126/science.1160809

Veit, S., Jany, S., Fux, R., Sutter, G., Volz, A., 2018. CD8+ T Cells Responding to the Middle East Respiratory Syndrome Coronavirus Nucleocapsid Protein Delivered by Vaccinia Virus MVA in Mice. Viruses 10, 718. https://doi.org/10.3390/v10120718

Verdin, E., 2015. NAD^+ in aging, metabolism, and neurodegeneration. Science 350, 1208–1213. https://doi.org/10.1126/science.aac4854

Vivier, E., Tomasello, E., Baratin, M., Walzer, T., Ugolini, S., 2008. Functions of natural killer cells. Nat. Immunol. 9, 503–510. https://doi.org/10.1038/ni1582

Wang, R., Dillon, C.P., Shi, L.Z., Milasta, S., Carter, R., Finkelstein, D., McCormick, L.L., Fitzgerald, P., Chi, H., Munger, J., Green, D.R., 2011. The transcription factor Myc controls metabolic reprogramming upon T lymphocyte activation. Immunity 35, 871–882. https://doi.org/10.1016/j.immuni.2011.09.021

Wang, T., Yao, W., Li, J., He, Q., Shao, Y., Huang, F., 2018. Acetyl-CoA from inflammation-induced fatty acids oxidation promotes hepatic malate-aspartate shuttle activity and glycolysis. Am. J. Physiol. Endocrinol. Metab. 315, E496–E510. https://doi.org/10.1152/ajpendo.00061.2018

Welsh, R.M., 1984. Natural killer cells and interferon. Crit. Rev. Immunol. 5, 55–93.

Welsh, R.M., Bahl, K., Marshall, H.D., Urban, S.L., 2012. Type 1 Interferons and Antiviral CD8 T-Cell Responses. PLOS Pathog. 8, e1002352. https://doi.org/10.1371/journal.ppat.1002352

Wiertsema, S.P., van Bergenhenegouwen, J., Garssen, J., Knippels, L.M.J., 2021. The Interplay between the Gut Microbiome and the Immune System in the Context of Infectious Diseases throughout Life and the Role of Nutrition in Optimizing Treatment Strategies. Nutrients 13, 886. https://doi.org/10.3390/nu13030886

Wu, D., Sanin, D.E., Everts, B., Chen, Q., Qiu, J., Buck, M.D., Patterson, A., Smith, A.M., Chang, C.-H., Liu, Z., Artyomov, M.N., Pearce, E.L., Cella, M., Pearce, E.J., 2016. Type 1 interferons induce changes in core metabolism that are critical for immune function. Immunity 44, 1325–1336. https://doi.org/10.1016/j.immuni.2016.06.006

Xia, H., Wang, W., Crespo, J., Kryczek, I., Li, W., Wei, S., Bian, Z., Maj, T., He, M., Liu, R.J., He, Y., Rattan, R., Munkarah, A., Guan, J.-L., Zou, W., 2017. Suppression of FIP200 and autophagy by tumor-derived lactate promotes naïve T cell apoptosis and affects tumor immunity. Sci. Immunol. 2, eaan4631. https://doi.org/10.1126/sciimmunol.aan4631

Yoo, J.Y., Groer, M., Dutra, S.V.O., Sarkar, A., McSkimming, D.I., 2020. Gut Microbiota and Immune System Interactions. Microorganisms 8, E1587. https://doi.org/10.3390/microorganisms8101587

Yoshino, J., Baur, J.A., Imai, S.-I., 2018. NAD+ Intermediates: The Biology and Therapeutic Potential of NMN and NR. Cell Metab. 27, 513–528. https://doi.org/10.1016/j.cmet.2017.11.002

Youngblood, B., Hale, J.S., Kissick, H.T., Ahn, E., Xu, X., Wieland, A., Araki, K., West, E.E., Ghoneim, H.E., Fan, Y., Dogra, P., Davis, C.W., Konieczny, B.T., Antia, R., Cheng, X., Ahmed, R., 2017. Effector CD8 T cells dedifferentiate into long-lived memory cells. Nature 552, 404–409. https://doi.org/10.1038/nature25144

Yuan, M., Breitkopf, S.B., Yang, X., Asara, J.M., 2012. A positive/negative ion-switching, targeted mass spectrometry-based metabolomics platform for bodily fluids, cells, and fresh and fixed tissue. Nat. Protoc. 7, 872–881. https://doi.org/10.1038/nprot.2012.024

Zhou, Y., Callendret, B., Xu, D., Brasky, K.M., Feng, Z., Hensley, L.L., Guedj, J., Perelson, A.S., Lemon, S.M., Lanford, R.E., Walker, C.M., 2012. Dominance of the CD4(+) T helper cell response during acute resolving hepatitis A virus infection. J. Exp. Med. 209, 1481–1492. https://doi.org/10.1084/jem.20111906

Zimmermann, P., Curtis, N., 2019. Factors That Influence the Immune Response to Vaccination. Clin. Microbiol. Rev. 32, e00084-18. https://doi.org/10.1128/CMR.00084-18

Zitvogel, L., Galluzzi, L., Kepp, O., Smyth, M.J., Kroemer, G., 2015. Type I interferons in anticancer immunity. Nat. Rev. Immunol. 15, 405–414. https://doi.org/10.1038/nri3845